A geotechnical approach to root anchorage modelling in wheat, oats and oilseed rape

By

Amelia Rouse

A thesis submitted to the University of Birmingham for the degree of DOCTOR OF PHILOSOPHY

Civil Engineering
School of Engineering
College of Engineering and Physical Sciences
University of Birmingham
June 3rd 2019

UNIVERSITY OF BIRMINGHAM

University of Birmingham Research Archive

e-theses repository

Abstract

Lodging is a naturally occurring phenomenon that reduces the yield and quality of cereal and oilseed rape crops, costing farmers millions of pounds in losses. Lodging is the permanent displacement of a plant stem from the vertical position and can occur due to stem failure or root anchorage failure. Understanding mechanisms behind risks of each of these types of lodging could reduce losses to UK and Irish farmers. Mathematical models have been developed to predict the risk of lodging failure in stems and root systems. However, the root anchorage failure model may not be accurately predicting root system failure (root failure moments). The analysis and computation of the root failure of wheat and oilseed rape crops are currently based on the theory of lateral resistance of rigid piles modified by Crook and Ennos, (1993) and Goodman et al., (2001). However, there was uncertainty about the accuracy of the model, the failure mechanism and modifications to the rigid pile analysis. Also, oat root systems had not been included in root anchorage studies.

This research reviewed and evaluated root anchorage models across different plant types and developed methodologies for collecting a dataset to test the models and compared the models for accuracy. It was found that the Crook and Ennos, (1993) and Goodman et al., (2001) models over-predicted root anchorage. These models incorporated soil shear strength, root plate diameter, root diameter and root length. Models by Fourcaud et al., (2008) and Coutts et al., (1999) were more accurate for the wheat and oats dataset collected. These models were suggested for trees, incorporating parameters such as the root plate mass and depth of the roots as well as root plate diameter. In oilseed rape, the results showed a model suggested by Niklas, (1992) was more accurate than the Goodman et al., (2001) model.

A new methodology was developed for laboratory testing of flexible and rigid wheat and oilseed root models in coarse and fine-grained soils. Load-deflection curves for root failure were recorded using a specially created lodging machine. It was found that in coarse-grained soil the root failure moment increased with increased water content. In fine-grained soils, the root anchorage was 4-5 times stronger and closer to the values measured in the field. When the water content was increased in these soils the root failure moment decreases rapidly.

Finally, a model calculating the capacity for under-reamed pile foundations was adapted for root systems of wheat, oats and oilseed rape. The models had options for both fine-grained and coarse-grained soils. It was found that for wheat, the coarse-grained model and an adjusted fine-grained model had the highest accuracy. The coarse-grained model had a normalised root mean squared error (NRMSE) of 0.464 and the fine-grained model had an NRMSE of 0.399 compared to 21.5 for the past model by Crook and Ennos, (1993) . For oats, the same models as wheat had the highest accuracy with the coarse-grained model and fine-grained models having an NRMSE of 0.430 and 0.354 respectively, compared to 63.5 for the model by Crook and Ennos, (1993) . For oilseed rape, it was found that the Niklas, (1992) model was the most accurate model having an NRMSE of 0.282 compared to 10.3 for the past model by Goodman et al., (2001). A sensitivity analysis found that the new models for wheat and oats were sensitive to the adhesion factor; the root length and diameter were important factors. For oilseed rape root length was still the most important factor. Field and laboratory data were used to validate the proposed model. It was found that the new models could reliably predict root anchorage.

This research can be integrated into the lodging risk model to improve the accuracy of root anchorage predictions. A method for farmers to use the information gained from the laboratory testing to understand better the connection between water content, soil characteristics and root anchorage was developed, with the possibility for farmers to either monitor field water content or alter the soil characteristics in their fields.

Dedication

To my family.

Acknowledgements

I would like to acknowledge my supervisors Prof. Nicole Metje, Prof. David Chapman, Prof. Ian Jefferson and Dr. John Spink for their continuous support, advice and guidance throughout my research.

I would also like to thank Teagasc for providing the opportunity and funding for this research. I would like to thank the people working at Teagasc, Eleanor, John Finnan, Eveline, Yuron, Ashook, Mladen and Keith for their help and support.

In the civil engineering lab, I would like to thank, James, Dave, mad Dave, Louis, Jimmy, Nav and Mark. Mainly for their help with my laboratory work and discussing aspects of my testing and life in general.

I would also like to thank Dave, in the Metallurgy and Materials lab, for the great knowledge and advice he gave about fracture mechanics and circuits. But also for his good laughs and lunches.

In the PhD offices, I can't forget to mention, Rachel, Simon, Wendy and Tayo and Richard. And my random friends Iola, Ronald and Umesh, Holly and Holly.

And to Josh and my family, of course, for helping to keep me going.

Table of Contents

List of Figures

List of Tables

1 Introduction

This chapter introduces the research problem, providing background to lodging in cereal and oilseed rape farming and explains the need for lodging risk modelling. The aims and objectives of the research are then stated followed by the structure of the thesis.

1.1 Background

The world relies on cereal crops as a basic food source. There are several diseases and natural phenomena which can reduce the yield of cereal crops thereby putting a secure food supply at risk. One of these phenomena which occur naturally is called lodging (Tams et al., 2004; Berry et al., 2013). Lodging is the response of crops to the interaction of wind, rain and soil (Baker et al., 1998; Berry et al., 2004a) and can be defined as the permanent displacement of a crop stem from the vertical position (Pinthus, 1974) . Lodging (Figure 1.1) occurs in two forms, stem lodging, and root lodging. Stem lodging occurs when the stem of the crop bends or breaks. Root lodging involves the failure of the anchorage system of the plant, with failure occurring in the root, soil or some combination of both (Berry et al., 2004a). Lodging affects the yield and quality of the grain. The yield and quality are dependent on the severity and time of lodging, i.e. the particular time in the growth stage of the plant as well as the weather conditions.

Figure 1.1 (a) Wheat , (b) oilseed rape , (c) oats , (d) lodging in oats.

According to Berry et al., (2004), farmers in the UK and Ireland have lower profits in years of extensive lodging. In 1992, 16% of the UK wheat crop lodged, costing farmers up to £130 million. Widespread lodging occurs on average once every 3 to 4 years, with the summers of 1980, 1985, 1987, 1992 and 1997 known for extensive incidences (Berry et al., 2004a). Similarly, in 2012, an aerial survey of 2000 hectares of oilseed rape grown in England found 35% of the field area had lodged (Berry et al., 2013). This lodging event reduced yield by 20% to 50% and cost the oilseed rape industry £61-£152 million. Farmers and agronomists ranked lodging resistance as the second most important varietal trait after yield potential in the 2007/8 series of oilseed rape conferences (Berry et al., 2013) . Understanding the mechanisms

behind the risk of lodging in wheat and oilseed rape is essential for the reduction of losses worldwide and in particular to the UK and Irish farmers.

1.2 The need for lodging risk modelling

Farmers attempt to mitigate the risk of lodging by introducing special genes to breed lodging-resistant varieties and by using plant growth regulators (PGRs) (Baker et al., 2014).

In the 1970s and 1980s, semi-dwarf genes were introduced to shorten the stems of wheat plants (Pinthus, 1974; Berry et al., 2013) . Wheat varieties recommended by the Agriculture and Horticulture Development Board (AHDB) include JB Diego and Cordiale, which have high rankings for lodging resistance, scoring seven and eight respectively on a scale of 9 (AHDB, 2015) . However, since this innovation, there has been limited success in breeding further lodging resistant varieties of wheat (Baker et al., 2014). Evidence also suggests that increases in yield potential of the crops, i.e. increasing the weight of the ear of the crop, may be contributing to increasing lodging risk as the stem has remained the same height (Berry et al., 2015).

PGRs cost cereal growers £9.9 million in 1994 (Garthwaite, 1995) and were used on 70% of UK cereal fields (Berry et al., 2004a) . In severe lodging years, PGRs do not seem to prevent lodging. Additionally, legislation may restrict the number of products available to farmers (revision of 91/414/EEC (European Union, 1991), and some markets limit PGRs because of the risk of leaving chemical residues in the grains (Baker et al., 2014). Therefore, there is a need for alternative strategies to reduce lodging risk.

One of the strategies is to develop a mathematical model of lodging risk. A model to calculate the risk of both forms of lodging in winter wheat was first proposed by Baker, (1995) and Baker

et al., (1998) and later modified by Berry et al., (2003a), Berry et al., (2003b) and Sterling et al., (2003). The model calculates the risk of lodging by first calculating the wind and rain-induced forces on the crop and the resulting bending moment on the crop stem base. This bending moment was then compared with two bending moments that represent the resistance of the crop: the stem failure moment and the root anchorage failure moment.

Subsequent verification and application of the model found that interaction of crop roots with the soil was the weaker of the two resisting moments (Berry et al., 2003a). A more recent study modelling lodging at large scales by Martinez-Vazquez and Sterling, (2011) found that root lodging was more prevalent than stem lodging, occurring in 35% of the plant population. In addition, when comparing the model predictions to lodging events in the field, early root lodging was under-predicted by Baker's model (Berry et al., 2003b) , suggesting that root anchorage failure could be an even larger percentage of the plant population. Berry et al., (2004) have suggested that the modelling of the root lodging process, especially the soil interactions, needs refinement.

1.3   Aim and Objectives

The study aims to develop new models for the root-soil interaction for wheat, oats and oilseed rape for the prediction of the root failure moment, using simple to measure parameters.

This aim will be achieved by completing the following objectives:

- Critically review the literature concerning root anchorage models for wheat, oats and oilseed rape and other plants that undergo lodging.
  - Assess the root anchorage models found in the literature by the criteria of advantages, disadvantages and applicability to lodging in wheat, oats and oilseed rape.

- Develop a suitable field methodology to carry out lodging experiments in the field and obtain all relevant soil and plant parameters to compare root-anchorage models found in the literature review.
  - Assess the accuracy of existing root anchorage models through comparative analysis of model performance.
- Develop suitable small-scale laboratory experiments to supplement the field trials by testing the lodging resistance of artificial roots in coarse-grained and fine-grained soil types as well as to measure lateral load-deflection curves. This provides information on a wider range of plant and soil characteristics in addition to the field experiments.
  - Assess the failure mechanisms exhibited by the artificial roots and their applicability to real plants.
- Review existing root failure models and if appropriate, improve existing models or develop a new root anchorage model to improve the prediction of root lodging.
- Validate the final model for wheat, oats and oilseed rape.

1.4   Structure of the Thesis

The thesis consists of five chapters. Chapter 2 presents a critical review of the current and relevant research focusing on lodging risk modelling, root anchorage modelling and soil strength modelling. The methodology is described in Chapter 3 focusing on the development of suitable laboratory test procedures as well as field tests to obtain all relevant parameters to test root anchorage models. Chapter 4 describes the results from the field and laboratory tests and includes a discussion on the accuracy of the different root anchorage models. Chapter 4 also includes the results and discussion of the application of a foundation engineering model to root anchorage failure. Chapter 5 contains the conclusions of this research with the original contribution to knowledge, limitations of the research, applications for farmers and recommendations for further work.

2 Literature Review

2.1 Introduction

This chapter presents an overview of root lodging in wheat, oats and oilseed rape. The review begins with a brief background on wheat, oilseed rape and oats, a description of the crop, growth stages, and current varieties and their lodging scores. A more in-depth discussion about the lodging phenomenon, how interrelated factors cause lodging and how these are being combated in agronomy and risk assessment is presented in Section 2.2. This is followed by a brief description of the current mathematical model for calculating lodging risk developed by Baker et al., (1998) in Section 2.3. Section 2.3.1 discusses the soil strength model by Baker et al., (1998). Section 2.3.2 continues with the modelling of the root failure moment by Crook and Ennos, (1993) and Goodman et al., (2001). Finally, root anchorage studies in various species are discussed to better understand parameters that may be relevant to root lodging in wheat, oats and oilseed rape in Section 2.4. Section 2.5 identifies the gaps in the literature which will be addressed in this thesis.

2.2 Background to lodging in wheat, oats and oilseed rape

Wheat and oats, members of the cereal group, are both grasses widely cultivated for their seed. There are many species of wheat which make up the genus Triticum; the most widely grown is Triticum aestivum L. (YARA international, 2019), while for oat it is Avena sativa (Hackett, 2018).

The wheat plant has long slender leaves and stems that are hollow in most varieties. Flowers are borne in groups of two to six in structures known as spikelets, with approximately 20

tightly packed spikelets arranged on alternate sides at the top of the stem forming the spike or ear of the crop (shown in Figure 2.1a). Oats have long leaves with rounded sheaths. The flowering and fruiting structure of the plant is made up of numerous branches bearing florets that produce the one-seeded fruit (Figure 2.1b). Oilseed rape (Brassica napus) also known as rapeseed (or canola), is a bright yellow flowering member of the family Brassicaceae (Figure 2.1c). It is cultivated for its oil-rich seed. All of these crops are susceptible to lodging which can result in significant loss of yield and quality (Berry et al., 2004b).
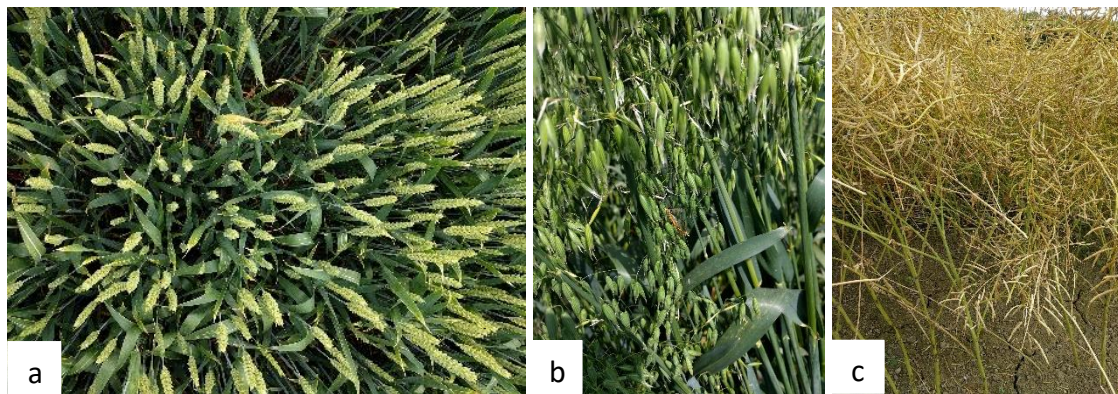
Figure 2.1 (a) wheat, (b) oats and (c) oilseed rape plants in the field.

After a farmer chooses a crop, husbandry decisions such as; sowing date, seeding rate, drilling depth, and the timing and amount of fertilisers, PGRs and pesticides need to be made, each of which can influence the characteristics of the crop including reducing lodging (Berry et al., 2000).

Lodging is the response of crops to the interaction of wind, rain and soil (Baker et al., 1998; Berry et al., 2004). A lodging phenomenon can be defined as the permanent displacement of a crop stem from the vertical position (Pinthus, 1974). It is most likely to occur during the three months preceding harvest when the ear or pods of the crop emerge (Tams et al., 2004). Lodging occurs in two forms, stem lodging, and root lodging (Figure 2.2a, b, c). Stem lodging

occurs when the stem of the crop bends or breaks. Root lodging involves the failure of the anchorage system of the plant, with failure occurring in the root, soil or some combination of both (Berry et al., 2004). (Griffin, 1998) writes that when root lodging occurs "there are normally, straight and intact stems, leaning from the crown, involving disturbance of the soil system". Failure of the anchorage system occurs after heavy, prolonged rainfall which wets the soil and decreases the soil strength to a point where the structural roots lose anchorage strength in the soil (Griffin, 1998).
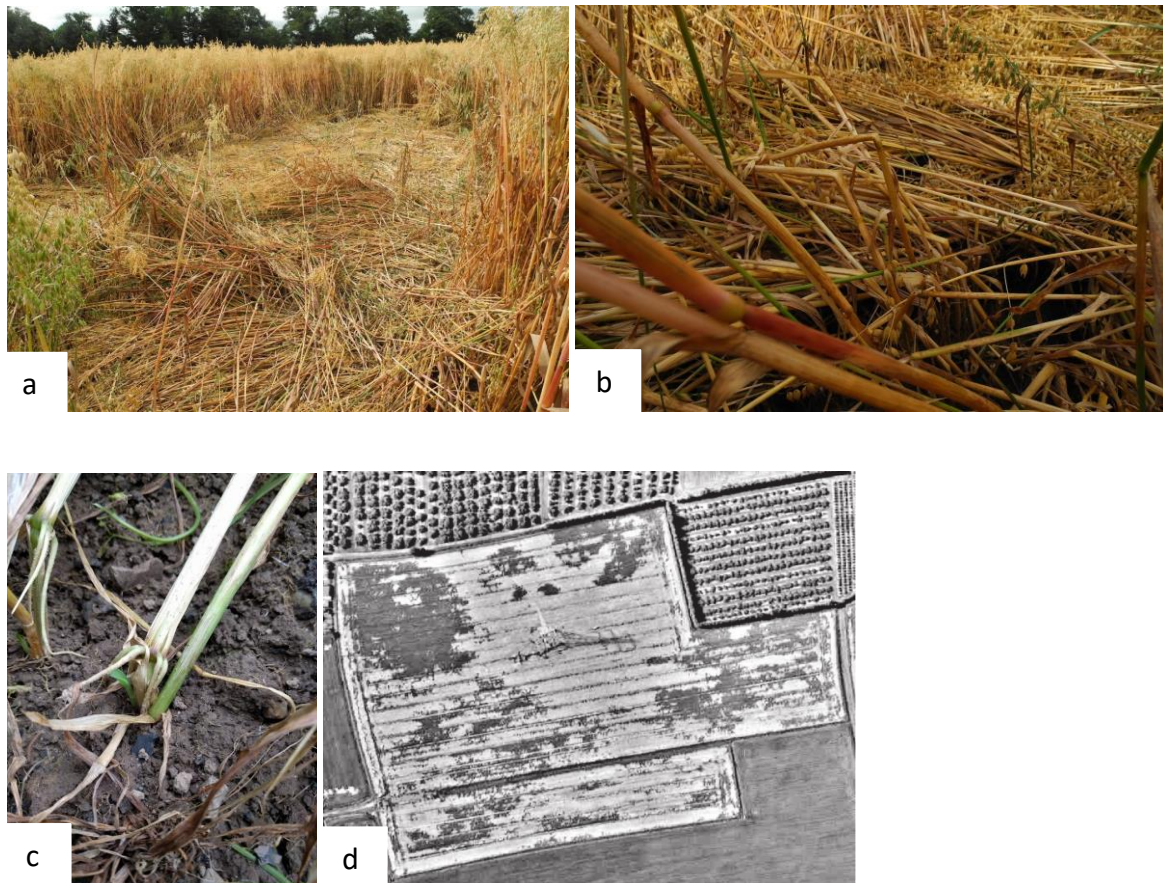
Figure 2.2 (a) Lodging in oats, (b) stem lodging and (c) root lodging (d) aerial photograph of a field with severe lodging adapted from (Berry et al., 2004). Lighter shading shows the lodged area; darker areas are tramline areas and standing crops.

Lodging is the result of a combination of factors including weather conditions and the growth stage of the crop. Lodging occurs during the three months preceding harvest in June, July and

8

August. This period coincides with higher average wind speeds and rainfall in the UK and Ireland, and the crop is at its heaviest weight (Berry et al., 2004). The weather conditions for stem and root lodging were found to occur when the wind speeds were 8-14ms^{-1} and with at least 7mm of rainfall per day. However, for root lodging, wind speeds could be lower, at 6-8ms^{-1} (Berry et al., 2003a).

Lodging at earlier growth stages (GS), such as during stem elongation, may not affect grain yield because the stems often recover to an upright position. Lodging at the end of anthesis (GS67) and the beginning of grain filling (GS73) (likewise at pod development and seed development in oilseed rape) cause the most damage to yields (Griffin, 1998). Stem displacement at this stage of growth causes (Berry et al., 2004, 2013):

- Reduced photosynthesis in the crops (less energy toward growth)
- Incomplete grain and seed filling (grain is not as heavy)
- Grain loss at ear emergence in wheat
- Reduced seed number and weight in oilseed rape
- Higher incidence of disease
- Increased grain drying costs
- Pod shatter
- Extended harvesting times
- Lost revenue to farmers

Lodging has spatial patterns as seen in Figure 2.2d where the lighter shades indicate lodging and the darker shades indicate upright plants. There is some variation within fields associated with the "tramline effect" which describes when fields with widespread lodging have upright plants beside wheel-ways used for agricultural vehicles (Berry et al., 2004). Reasons for this may be greater compaction along tramlines leading to better root anchorage, reduced competition for water, light and nutrients leading to stronger plants and differences in wind

gusting and micro-climate down the tramlines (Easson et al., 1992). Headlands are the areas around the edge of the field where inputs such as fertiliser or seed may be double applied as machinery travelling up and down the main body of the field meet up with the machinery passes around the edge of the field. The passage of the machinery causes the greater soil compaction and these areas tend to be the first area of the field to show lodging (Berry et al., 2003a). Some fields have areas where lodging is a perennial problem. This may be because of fertile soil in these valleys causing tall growth of crops. They may also be particularly wet such as valley bottoms causing poor root anchorage or crops may be more exposed to high winds.

Variation between fields is associated with different varieties, husbandry or soils (Easson et al., 1992). Moreover, the planting history of the field is important as well. If the field was a meadow or used for grass, then the soil might have a very high organic matter content, promoting growth. The field may have also received several applications of manures. There may be shallow soils or hardpan which inhibit good root anchorage or promote root and stem diseases (Easson et al., 1992). Variation between farms is evident and may be a function of different farming or crop management systems (Berry et al., 2004). This depends on the farmer's approach to nitrogen fertilizer application and animal manures. Equally, a farmer may be skilled at selecting varieties and applying growth regulators.

Finally, there are variations in fields within regions of the UK and Ireland. Lodging is associated with Wales, northern and western Britain and Ireland. These are regions with wetter summers and windy weather systems (Easson et al., 1992). The crop develops slowly because of the cooler temperatures and is harvested later. The farming systems involve more livestock, and even without livestock, the soils have higher organic contents. Organic soils of the fens and

peaty soils are lodging prevalent because of the reduced soil strength of peats (Easson et al., 1992).

It should also be noted that field preparation also affects the near surface soil. Farmers use different methods depending on the soil conditions at their farm. However, there needs to be flexibility depending on weather conditions, location of soil compaction and available machinery on the farm. Cultivations aim to:

- Correct compaction
- Maximise seed-soil contact
- Sow seed at 2-3cm depth (maximum 5cm)
- Retain soil water next to seeds to allow germination
- Manage weed populations
- Reduce slug risk
- Bury herbicide residues

Fields are prepared by different cultivation methods such as broadcasting, direct drilling and rolling, sub-cast, non-inversion tillage and ploughing (techniques range from least soil disturbance, broadcasting and direct drilling to most disturbance ploughing). Farmers using sub-cast, non-inversion tillage and ploughing are encouraged to roll the soil afterwards, to increase soil density and this has been found to reduce lodging (Pinthus, (1973); Crook, (1994)). Each method has advantages and disadvantages in terms of pest and weed control. However, each technique affects the soil profile by disturbing the top 0-200mm of soil. Cultivation encourages the formation of a network of soil pores. The pores allow infiltration of water and air to the subsoil, hence, encouraging germination and establishment of crops. However, this also affects the density of the soil, the soil strength and the lodging resistance of the crops.

The minimal cultivations have been shown to reduce lodging compared to more traditional ploughing (to 200mm depth) (Berry et al., 2004). Soil strength was found to increase in the top 80mm of silty loams by 18-49% with direct drilling, but only small increases were seen in sandy soils. Also, the bulk density of the soil when ploughed was 900kg/m^3 compared to the bulk density of 1100kg/m^3 after direct drilling. However, these differences became smaller after 2 or 3 months, but it seems that the increased soil bulk density at the beginning of growth reduced lodging (Berry et al., 2004). Berry et al., (2004) also reported that different cultivation methods did not appear to greatly affect the biomechanical properties of the upper 30 to 50mm of the structural roots. Crook, (1994) found that compacting the seed bed did not affect the length, number and bending strength of wheat roots, suggesting that lodging is reduced due to the increased soil bulk density and not root parameters when considering cultivation.

Table 2.1 A list of interrelated attributes of weather, soils and roots that may cause a particular crop to lodge (Griffin, 1998).

Stem of Crop	Root of Crop
Wind speeds and rainfall	Root pattern
Weather	Root structural integrity
Field exposure	Root depth
Dynamic loading	Sowing depth
Crop canopy structure	Seeding rate
Air movement	Surface layer soil strength
Interception	Pore water suction
Stem length and weight distribution	Particle Size Distribution
Moment at the stem base	Time
Lower stem strength (lower internode)	

The interrelated attributes of the underground crop mentioned by (Griffin, 1998), can be traced back to (Pinthus, 1967) (see Table 2.1). It is these interrelated attributes that were considered when creating the lodging risk model, and each needs to be quantified and integrated to acquire an accurate representation of lodging. The attributes of root-soil

interaction have been split into root and soil characteristics or components. Root characteristics including the number and type of roots, rooting pattern or individual root lengths are known as root architecture, i.e. the spatial configuration of biological units to serve a function (Lynch, 1995). Root strength is another root characteristic. Soil characteristics include the type and shape of individual particles (particle size distribution). The interrelated attributes of the crops have been related to one another in a theoretical model of windthrow of plants created by Baker, (1995) and a method for assessment of risk of wheat lodging was developed by Baker et al., (1998).

2.3 Overview of the lodging risk method for wheat and oilseed rape and its connection to root anchorage

Early research on the windthrow of trees in the UK had concentrated on measuring turning moments required to uproot a tree in a range of soil types (Fraser and Gardiner, 1967). The data turning moments from that study was combined with values of the wind drag forces from wind tunnel studies of crown sections of trees (Fraser, 1964; Mayhead, 1973). When the turning moment required to uproot a tree and the values of wind drag were compared, the windspeeds required to uproot a tree could be predicted (Fraser, 1965). The comparison could determine whether the wind speeds exceeded the moment needed to uproot the tree. Baker, (1995) used the comparison between the base bending moment applied to the plant by the wind and the base bending moments required to cause failure in the plant stem and root system to determine whether a plant would lodge or remain upright.

Baker, (1995) developed the theoretical model for windthrow of plants. The aim was to create a simple model to enable better understanding of the physical processes involved in

windthrow and enable quantitative predictions of failure wind speeds in plants ranging in size from cereals to trees. The model predicted the natural frequencies of trees and cereals using measurements of the full-scale plants. The natural frequencies were then used to determine the stem base bending moments applied to the plant by the wind and then calculate the extreme values of base bending moment. The extreme values could then be compared to stem base and root failure moments to obtain estimates of failure wind speeds.

To be able to predict the natural frequencies of trees and cereals, Baker, (1995) derives a mechanistic model of a plant consisting of two masses. One mass representing the ear of the plant, and one mass representing the root-soil system. The two masses were connected by a weightless elastic stem of length equivalent to the distance from the ground to the plant centre of gravity (Figure 2.3).
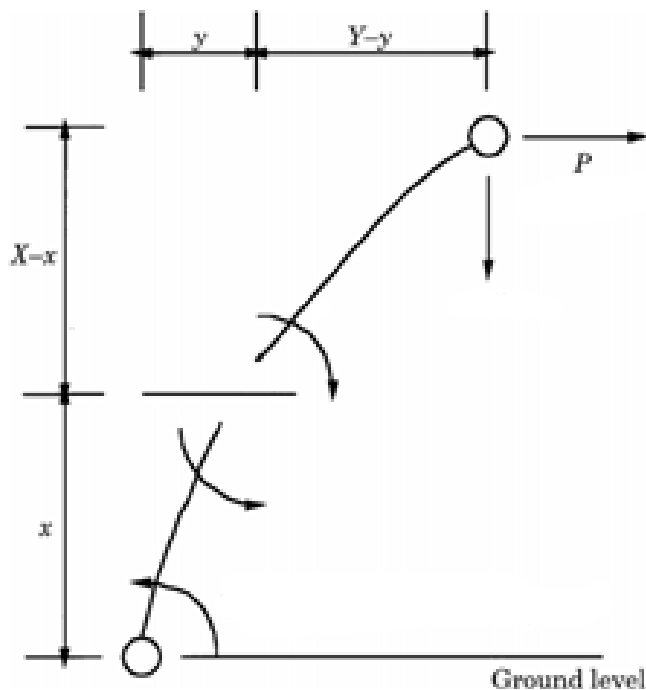
Figure 2.3 The basic mechanical model with the origin of x and y-axes at stem base (Baker, 1995).

The mechanistic model was used to calculate the reaction induced in a structural element (in this case the stem base) when an external force or moment (the wind) is applied to the element causing the element to bend. The forces on the elements of Baker's mechanistic model of the plant were:

- The fluctuating wind force at the top of the stem, P.
- The equivalent weight of the canopy or ear, mg.
- The inertia of the canopy mass,

$$m\frac{d^2Y}{dt^2}$$ 2.1

Where, Y was the instantaneous displacement of the mass.

- The moment in the stem at a height x above the ground where the displacement is y,

$$EI\,\frac{d^2y}{dx^2}$$ 2.2

Where, E was the Youngs modulus of the stem and I was the second moment of area of the stem. The product of EI is the flexural rigidity.

- The rotational inertia of the root ball mass when y = 0,

$$H\frac{d^2\left(\frac{dy}{dx}\right)}{dt^2}$$ 2.3

Where, H is the moment of inertia of the root ball mass.

- The rotational resistance moment of the root ball mass when y = 0,

$$k\left(\frac{dy}{dx}\right)$$ 2.4

Where, k was the resistance moment per radian. The resistance moment of the root ball mass can also be called the root failure moment. The resisting moment was proportional to the base slope as suggested by data from Crook and Ennos, (1993) for cereals and Coutts, (1986) for conifers, which gave a linear root angular displacement relationship with base bending moment.

The mechanical model was dynamic and could relate mean and fluctuating wind velocities to the mean and fluctuating displacements and stem base forces and moments, with the assumption that these forces and moments were the critical parameters for stem failure and uprooting failure.

To compare the stem base bending moment produced by the wind to the failure moments of the stem, Baker, (1995) used structural theory. For a circular trunk, the maximum allowable bending moment was calculated using Equation 2.5.

$$\frac{\sigma \pi a^3}{4} \qquad 2.5$$

Where, σ was the yield strength of the stem material and a, was the base radius, the distance from the neutral axis to the edge of the stem.

To compare the stem base bending moment produced by the wind to the failure moments of the root system, Baker, (1995) used the research by Crook and Ennos, (1993) and Coutts, (1986). Crook and Ennos, (1993) and Coutts, (1986) were both studying root anchorage mechanics in two different species of plants, winter wheat and Sitka spruce. They both provided values of root failure moment that could be used in the model by Baker, (1995).

When tested with data collected from the literature including wind data and structural data for each of the plants, the Baker, (1995) model was able to provide predictions of stem base bending moment and when compared to the failure moments of the stem and root system, root failure was expected to occur at lower wind speeds than stem breakage. Lower wind speeds caused root failure in both isolated plants and plants in canopies for wheat plants. Sitka spruce had the same outcome for isolated trees, however, the stem and root failure

16

moments in canopies were close to each other, which led to both stem breakage and root failure being predicted to occur. Overall, the results suggested root failure would occur more frequently than stem breakage. A result that was found by previous authors in wheat plants specifically (Pinthus, 1973; Graham, 1983; Easson et al., 1992) and was repeated in Baker et al., (1998).

The theoretical model developed in 1995 was then integrated into the method for assessment of risk of wheat lodging, Baker et al., (1998). Figure 2.4, gives an overview of the steps in the method by Baker et al., (1998). The third step, calculating the extreme base bending moment was where the Baker, (1995) mechanistic model was integrated into the research by Baker et al., (1998). The method aimed to predict the probability of stem and root lodging at any one site in a lodging season, in wheat plants only.

Berry, (1998) defines the lodging period as 40 days, centred on July because winter wheat was observed to lodge anytime from the emergence of its ear until the grains had matured (Easson et al., 1992). Baker et al., (1998) took the peak lodging period from June to July similar to work by Griffin, (1998) and Berry, (1998), who collected data used in this study. June to July was the period of time when the ears and panicles of the crops are growing larger and heavier because of grain filling (Berry et al., 2004). At this stage of growth, lodging would severely reduce the yield potential of the crop (Berry et al., 2004). All the data inputs into the model were taken during this high-risk time of the growing season.
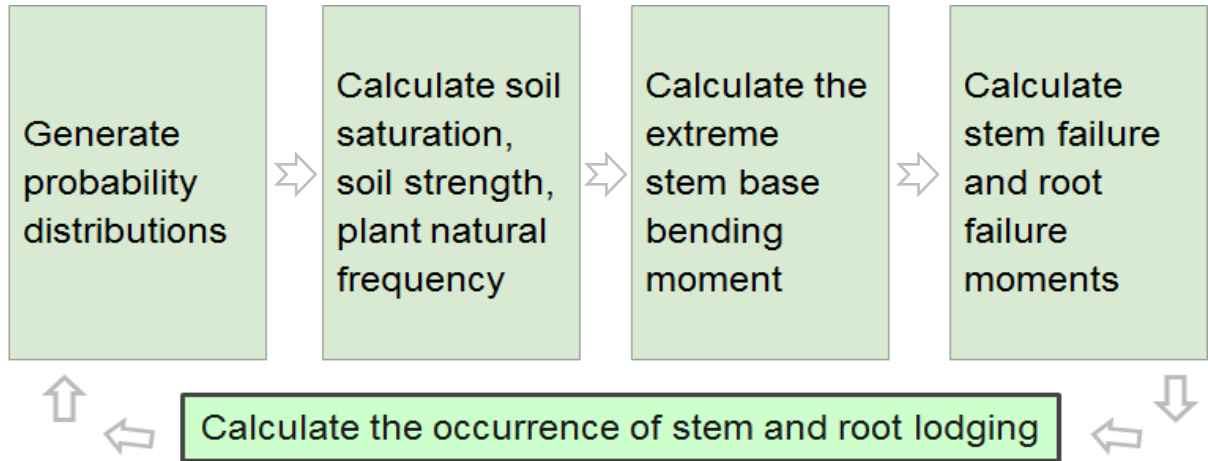
Figure 2.4 A flow diagram of the method for calculating stem and root lodging.

Probability distributions were generated from mean hourly wind speeds and daily average rainfalls obtained from the Meteorological office. The probability distributions were adapted from the Weibull distribution for both wind data and rainfall data. The Monte Carlo simulation technique was used to generate a series of 1000 hourly mean wind speeds and daily rainfalls that were consistent with the calculated probability distributions. This generated wind speed and rainfall data pairs. For each of these pairs, the natural frequencies of the plants were calculated, the degree of saturation of the soil and the soil strength.

2.3.1   Development of a soil strength model

At this stage, the soil strength is predicted by the model created by Baker et al., (1998). Baker et al., (1998) uses relationships between clay content, water content and visual score shown in Equation 2.6, Equation 2.7 and 2.8. These relationships were derived empirically, using principles of soil science, therefore, they need to be applied to different soils than they were derived from to determine their accuracy. The equations are as follows:

$$s_w = \left(1.484x10^3 e^{\frac{-5f}{c}}\right)(2.2 - 0.24v)(4.82c - 0.3) \qquad 2.6$$

$$s_D = \left(1.125x10^3 e^{\frac{-5w}{c}}\right)(2.2 - 0.24v)(4.82c - 0.3) \qquad 2.7$$

$$s = s_D - \frac{i}{\left(\frac{\rho_s}{\rho_w}\right)(f - w)L}(s_D - s_w) \qquad 2.8$$

Where, s is the ground shear strength, s_w is the shear strength at field capacity, f is the water content at field capacity, c is the clay content, v is the visual score, s_D is the shear strength at field capacity, w is the water content at wilting point, i is the average daily rainfall, ρ_s is the density of the soil, ρ_w is the density of water and L is the depth of the roots.

The soil strength model is bounded by an upper and lower limit of soil water content or pore water content (Guérif, 1990). The upper limit is the water content at field capacity and translates to the shear strength at field capacity (FC). In soil science, field capacity is the water content of the soil two to three days after a rain or irrigation event when the downward forces of gravity have removed the remainder of the water. This assumes that the water removed from the soil profile is only removed by gravity, not through the plants or through evapotranspiration. The soil is considered to be at field capacity when the water potential in the soil is at -33 kPa (Twarakavi et al., 2009). The model of soil strength for root lodging describes the shear strength of wet soil at field capacity, s_w (Baker et al., 1998).

The lower limit is the water content of the soil at the wilting point and translates to the shear strength at the wilting point. Permanent plant wilting occurs when the volumetric water content in the soil is too low for the plant roots to extract water. The soil is at the permanent wilting point when the water potential, i.e. soil water content, in the soil is at or below -1.5 MPa (Twarakavi et al., 2009). For a dry soil at the permanent wilting point (PWP), the soil strength s_D is given by Equation (2.7).

In geotechnical engineering, the shear strength can be separated into saturated and unsaturated soil mechanics, with the ground water presenting the boundary. Soil above ground water table is unsaturated, whereas soil below the ground water table is saturated.
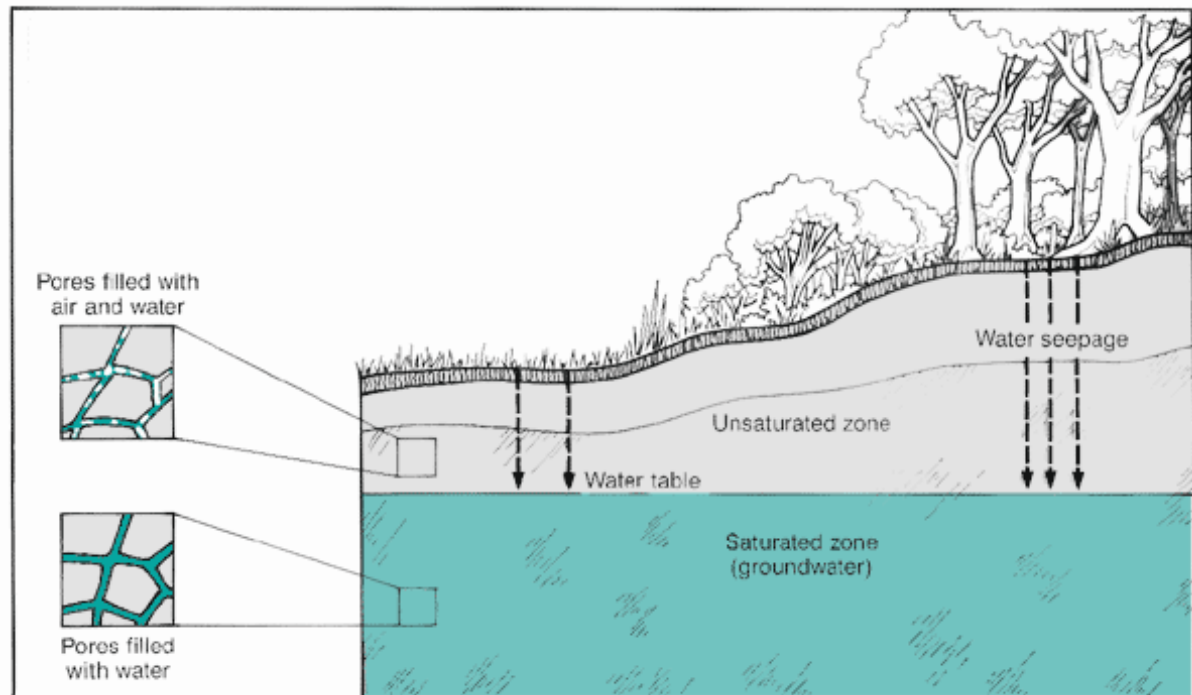
Figure 2.5 A diagram showing the unsaturated and saturated zones in a cross-section of soil (Oram, 2014)

Subsurface water, suction, and stress profiles depend on the soil and pore water properties as well as the prevalent environmental or atmospheric conditions (Likos and Lu, 2004). Soil type, particle size distribution and pore size distribution all influence the distribution and flow of pore water within the soil profile. Atmospheric conditions, which include relative humidity, temperature, wind speed and precipitation, all act to influence transient changes in the flow and distribution of the subsurface pore water (Likos and Lu, 2004).

The mechanical stability of any point in the subsurface depends on the strength parameters of the soil and the state of stress at that point. In saturated soils, the state of stress can be

described by the total stress and pore pressure, unified under the concept of effective stress. Effective stress, which is the difference between the total stress and the pore water pressure, is the stress experienced by the soil skeleton or the solids in the soil (Equation 2.9).

$$\sigma' = (\sigma - u_w) \qquad\qquad 2.9$$

Where σ is the total stress, u_w is the pore water pressure and σ' is the effective stress. The state of the effective stress controls whether or not a given soil mass is under a state of stability or a state of failure. Soil strength is an intrinsic material property that generally depends on the soil mineralogy, particle shape and size (morphology), and interparticle arrangement. A macroscopic description of these controlling factors often leads to empirical material parameters, most notably cohesion and internal angle of friction. These material parameters, together with the stress state variable (effective stress and matric suction), define the boundaries controlling whether soils are stable or in a failure condition (Likos and Lu, 2004).

The shear strength of an unsaturated soil can be defined by an extended Mohr-Coulomb failure envelope given by Equation 2.10 (Fredlund et al., 1978).

$$\tau' = c' + (\sigma - u_a)tan\varphi' + (u_a - u_w)tan\varphi^b \qquad 2.10$$

Where, τ is the shear stress on the failure plane at failure in kPa, c' is the intercept of the extended Mohr-Coulomb failure envelope on the shear stress axis where the net normal stress and the matric suction at failure are equal to zero; it is also referred to as the effective cohesion (kPa), $(\sigma-u_a)$ is the net normal stress on the failure plane at failure (kPa), φ' is the effective angle of internal friction associated with the net normal stress state variable $(\sigma-u_a)(°)$,

(u_a-u_w) is the matric suction on the failure plane at failure (kPa), and ϕ^b is the angle indicating the rate of change in shear strength relative to the change in matric suction (u_a-u_w)(°).

As the soil approaches saturation, the pore-water pressure, u_w approaches the pore-air pressure, u_a, and the matric suction, (u_a-u_w) goes to zero (Fredlund and Rahardjo, 1993) and Equation 2.10 can be modified to Equation 2.11.

$$\tau' = c' + (\sigma - u_a)tan\varphi' \qquad\qquad 2.11$$

Where (σ-u_a) is the effective normal stress on the failure plane at failure (kPa) (Rahardjo et al., 2008).

Equations (2.6) and (2.7) are composed of three separate bracketed equations. The term in the first bracket relating soil strength to water content at field capacity (exponential) was derived using a relationship described by (Guérif, 1990):

$$T_w = T e^{\frac{-5w}{CLAY}} \qquad\qquad 2.12$$

Where, T_w is the mean textural tensile strength of soil at a given water content. T is the dry textural tensile strength (kPa); CLAY is the clay content (gg^{-1}), where 1 gg^{-1} is 100% clay content. Textural tensile strength is a measurement used in tillage and agriculture. The textural tensile strength measures the strength needed to break down large soil aggregates into smaller fragments without destroying the soil microstructure focusing of the strength due to the soil skeleton and the cementing effect of clay. The textural tensile strength is measured on spherical aggregates of soil, under compressive forces. The textural tensile strength is not commonly used in geotechnical engineering, instead the soil shear strength is used. The shear strength is measured on a sample of soil under shearing forces causing sliding failure along a

plane. Instruments to measure soil strength in the field like the shear vane measure shear strength and not tensile strength. Berry et al., (2000) used the shear vane to measure soil strength for comparison with the soil strength model by Baker et al., (1998). The differences in the textural strength used for the model derivation and shear strength used for the measurement may result in the model making inaccurate predictions. Ideally, if shear strength is measured then the soil shear strength parameters could be used to derive the soil strength model.

Berry, (1996) refers to the data collection for Equations (2.6) an (2.7). The water content was measured using time domain reflectometry (TDR) probes and the soil strength measured with a shear vane from data collected at ADAS Rosemaund. This data was all obtained for a clay content of 20%-35%, water content 7-27% and the soil strength ranged from 15-80kPa. The relationship between shear strength and the ratio of water content to clay content showed similar results to those by Guérif, (1990) in the range of 0.4-0.6 w/CLAY. The range of values 0.4-0.6 from ADAS Rosemaund (Figure 2.6), shows a linear relationship. However, the range of values by (Guérif, 1990) suggests an exponential relationship (Figure 2.7).
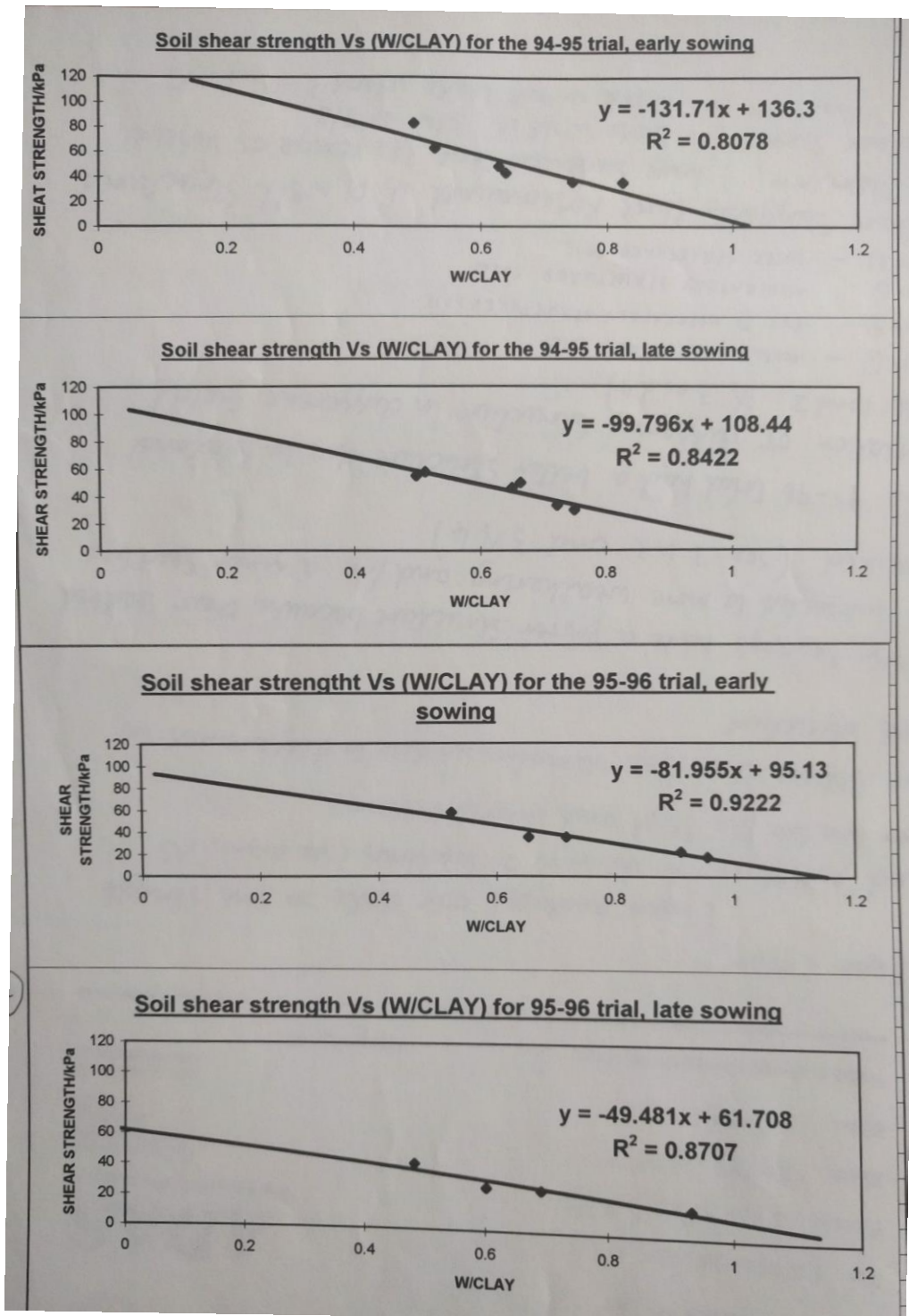
Figure 2.6 Shear strength versus (water content/clay) for trials in at ADAS Raosemaud, (Berry, 1996).
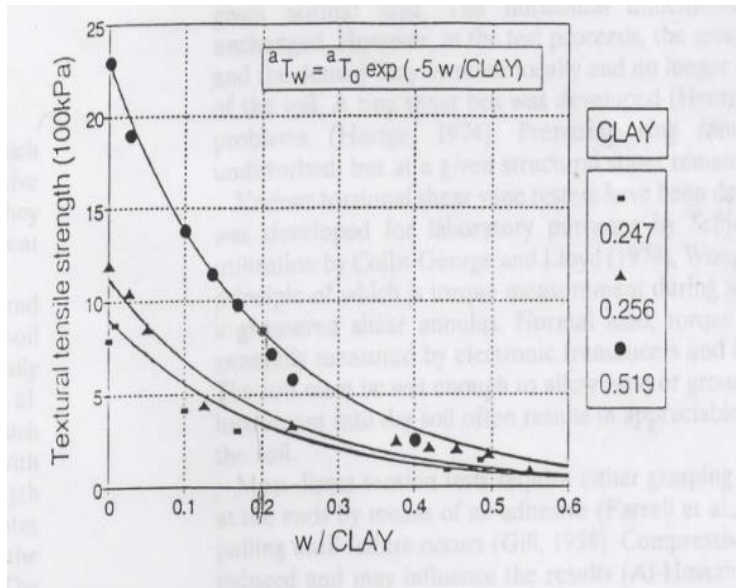
Figure 2.7 (a) Relationship between textural tensile strength and relative water content of the clay fabric, for three clay contents (Guérif, 1990).

Equation (2.12) was derived for calcic soils (Guérif, 1990), which have calcium carbonate as part of their mineralogy. As soils found in agricultural context in the UK and Ireland are not mainly calcic soils, the equations need to be tested on soils relevant to the UK and Ireland, to determine whether they can predict soil strength accurately. Also, Equation (2.12) makes several assumptions about the theoretical mechanisms behind soil strength such as the textural tensile strength, which is no longer widely used in soil mechanics or geotechnical engineering.

In geotechnical engineering, the relationship between the soil water content and the pore water pressure (water potential) is given by the soil water characteristic curve. The curve changes for different soils and is therefore not specific to one soil type. Typical soil water characteristic curves are presented in Figure 2.8 for sands (course grained) and silty clays (fine grained).

25
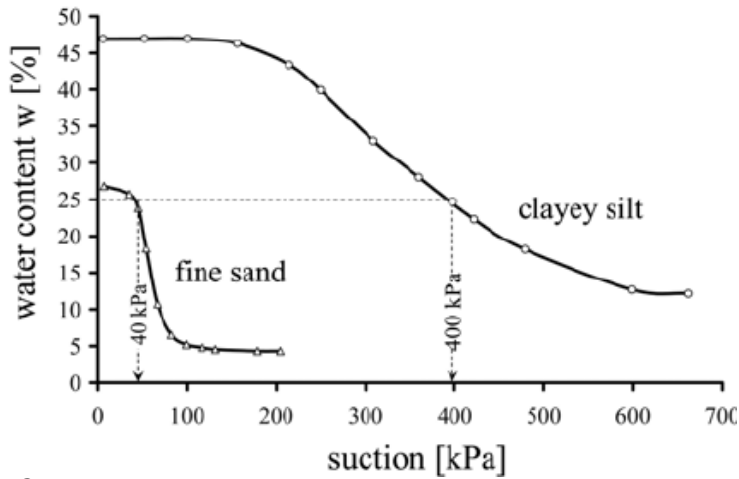
a
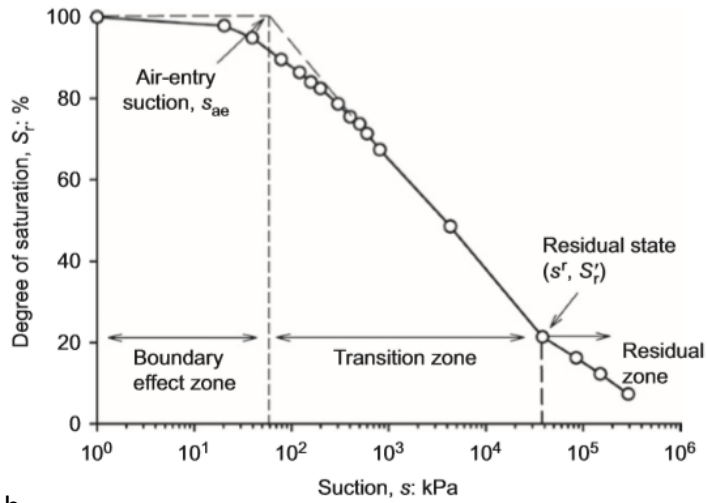
b
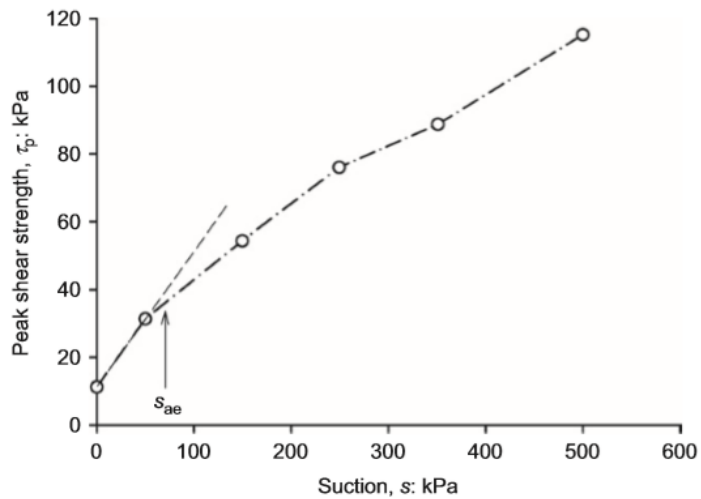
c

Figure 2.8 (a) The soil water characteristic curve for a fine sand and a clayey silt (Abed and Vermeer, 2006), (b) soil water characteristic curve for compacted glacial till and (c) peak shear strength – suction relationship for compacted glacial till (Han and Vanapalli, 2016).

26

Figure 2.8a and b show the relationship between water content and suction for a fine sand, a clayey silt and a glacial till (Han and Vanapalli, 2016). The difference is due to the capillary water under suction in the soil pores. In a sand (course grained soil), the soil pores are larger, which leads to water being held in the pores for a smaller range of suctions compared to the clayey silt during the boundary effect zone (degree of saturation is 100% and decreasing). As the air-entry suction is reached, the capillary water drains and in sands, this occurs rapidly compared to clayey silts. Finally, when the suction exceeds the residual suction, the amount of capillary water and the contribution of the capillary effect and suction towards the soil skeleton becomes negligible. The water at this stage is retreating into the micropores, which are present in clayey silts and not in the sands (Han and Vanapalli, 2016).

Figure 2.8c shows the peak shear strength versus suction relationship for a compacted glacial till, and demonstrates the non-linear relationship between soil water content, suction and shear strength. This behaviour is related to the variation of the capillary water and its associated capillary effect and suction. The suction contributes to the effective stress and hence the shear strength properties. In the saturated stage (boundary effect zone) the soil and capillary water can be considered a continuum. However, as the capillary water drains, the suction contributes to the effective stress resulting in an increase in shear strength properties, therefore, there is a slower increase in strength. The contribution of suction is less in the transition zone and when the soil passes the residual suction. These relationships would not have been considered when the model presented by Baker et al., (1998), was being developed, the effect of water content is contained within the effective stress and therefore could be incorporated into the new model of anchorage.

The second term in Equations (2.6) and (2.7), relating soil strength to visual score is taken from MAFF, (1982). Visual score is a measure of the macro-porosity of the soil, i.e. soil compaction and structure. This is usually done by observation of the overall structure and feel of soil by a knowledgeable individual. This is not common in geotechnical engineering. It is measured on a scale of 1-10, 1 being poor structure and 10 being a good structure. The relationship between soil strength and visual score were given by:

$$\text{Soil strength} = 76.7 - 8.39(\text{VisualScore}) \qquad 2.13$$

Where, soil strength is measured in kPa. This relationship was derived via empirical fiiting of visual scores and soil strength measured using a shear vane for a sandy clay loam topsoil (at a depth of 0-20cm) containing approximately 20% clay (NAS, 1976). The relationship assumed that the soil strength to visual score relationship for soils with greater clay content was also linear, with a similar gradient. Using Equation (2.13), the soil strength at a visual score of 2 would be predicted to be 60kPa and at 8 would be 9.6kPa. Berry et al., (2000) measured the soil strength and recorded the visual scores in well-drained silt clay loam. Berry et al., (2000) found that the visual score of 2 corresponded to 51kPa and visual score of 8 corresponded to 6kPa. Which were similar values to those predicted by Equation 2.13, suggesting the relationship was close to field measurements at ADAS Rosemaud (Figure 2.9). However, the measurement of the visual score will depend on the judgement of the practitioner completing the measuring, which, could lead to large variations in visual score values, leading to inaccurate readings.

The third term in Equations (2.6) and (2.7) relates soil strength to clay content and is taken from Guérif et al., (1994) (Figure 2.10). Clay content refers to the percentage of clay in the

particle size distribution. Soil particle size distributions describe the composition of the soil and reflect the percentages of different soil particles, e.g. boulders, pebbles, sands, silts and clay minerals within the soil.
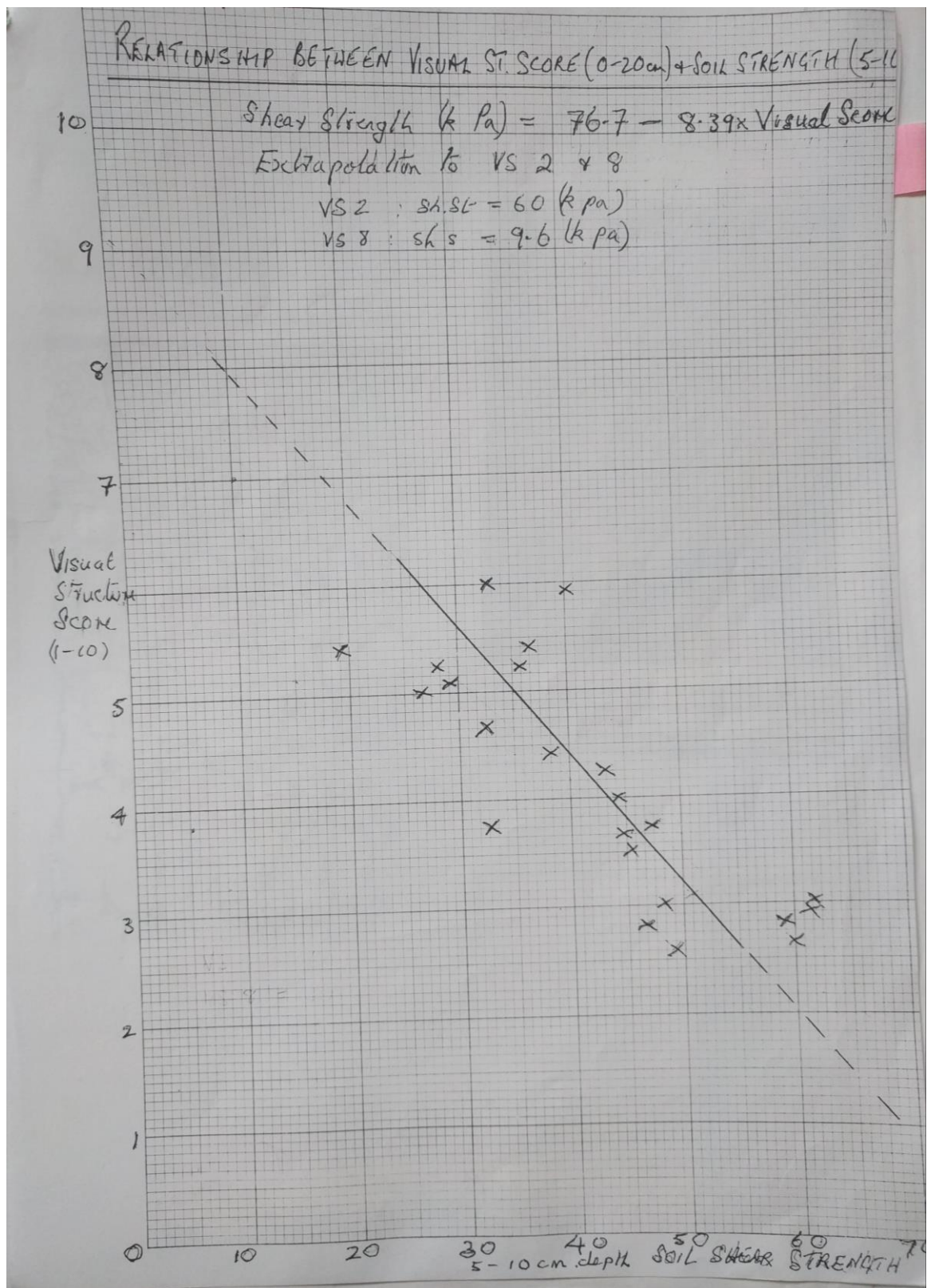
Figure 2.9 Relationship between visual score and soil strength, (Berry, 1996).
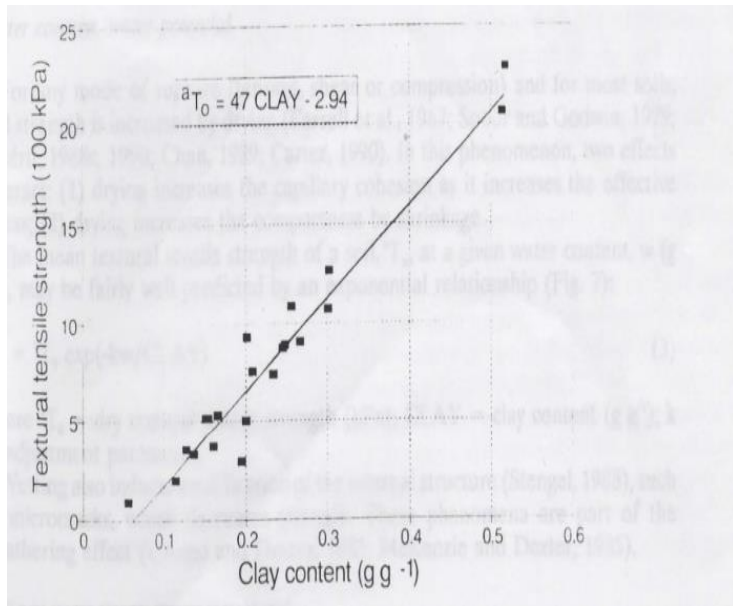
Figure 2.10 Relationship between textural tensile strength and clay content Guérif et al.,(1994).

Guérif et al., (1994) found that there was a statistical correlation between soil textural tensile strength and clay content. Specifically, they found that the textural tensile strength of calcic soils from temperate regions was highly correlated with clay content. The empirical relationship could be represented by:

$$T_w = pCLAY + q \qquad\qquad 2.14$$

Where, T_w is the mean textural tensile strength of dry spherical aggregates of 2-3 mm diameter; CLAY is the clay content (gg^{-1}); q is a constant. The coefficient p can be interpreted as the mean tensile strength of an ideal clay, representative of the different soils involved in the regression analysis (Guérif et al., 1995). Again, the textural tensile strength is used in the equation and the relationship shown in Equation 2.14.

Equations 2.12, 2.13 and 2.14 were all empirical and may not be applicable to a wide range of soil particle size distributions. When Baker et al., (1998), included the equations in the soil strength model, the relationships needed to be tested to determine whether they could

31

predict soil strength. Baker et al., (1998) acknowledged there was lack of data to validate the soil strength model, therefore they completed a sensitivity analysis.

A sensitivity analysis by Baker et al., (1998) consisted of using real data ranges from the UK to generate wind speed and rainfall probability distributions to simulate the behaviour of the soil under different degrees of saturation. Increasing the clay content decreased the probability of lodging, as the clay content is assumed to have a strengthening effect on the soil (Baker et al., 1998). In Equations 2.6, 2.7 and 2.8, clay content is seen as the parameter that controls strength and water retention.
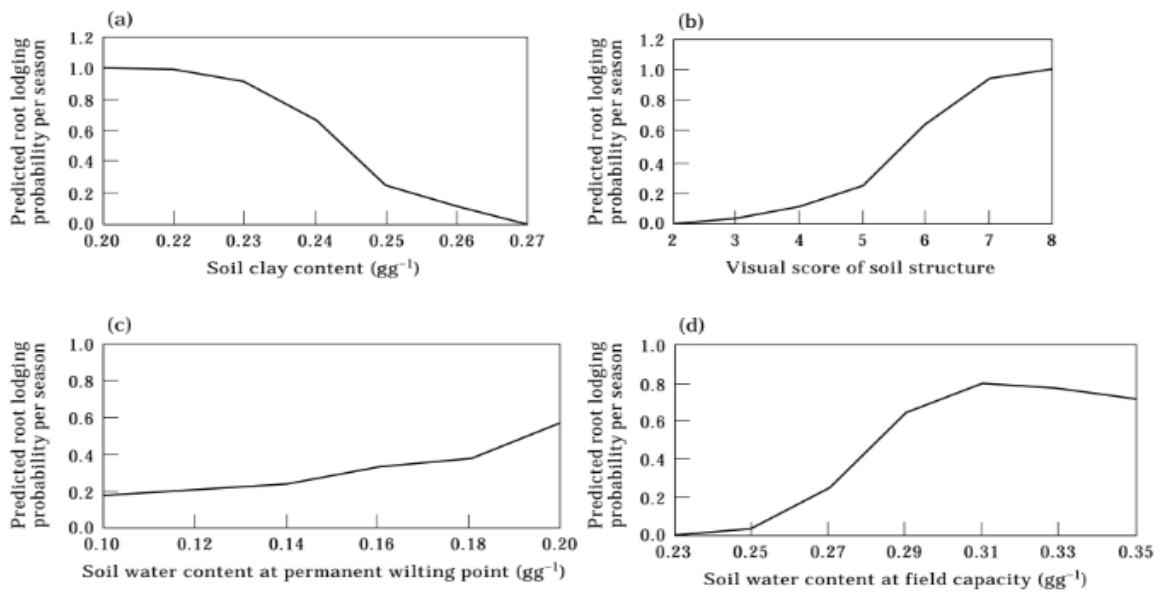
Figure 2.11 Variations in seasonal root lodging risk for variations in soil parameters (Baker et al., 1998).

Figure 2.11 shows that increasing the visual score (decreasing the density of the soil or decreasing the soil strength) increased the probability of lodging. The soil water content at the permanent wilting point did not increase the probability of lodging by a large amount. This is because the permanent wilting point is the lower bound of the soil model. Soil water content at field capacity showed more of a difference, as this was the water content that changed the

soil strength by a greater amount. Field capacity would be closer to completely saturates soil, which is the worst-case scenario for lodging. The soil water content at field capacity and permanent wilting point are separate bounds that are different for different soil particle size distributions. Equations 2.6, 2.7 and 2.8 show that, as the soil becomes wetter, it will become weaker. The results from the equations also suggest that a soil that rapidly decreases in strength from wilting point to field capacity could be more prone to lodging than one that has a slower decrease in strength between wilting point and field capacity. A similar result was found by Rahardjo et al., (2009) the soil with the largest rate of change in shear strength also had the highest rate of change of lodging resistance.

The soil strength model was only tested using root measurements from the field and the lab, soil parameters were assumed. Berry et al., (2000), completed measurements of structural rooting depth and the root plate diameter for winter wheat were collected in three growing seasons from 1994 to 1996. The soil (a well-drained silty clay loam, a sand, silt and clay mixture with a larger proportion of silt and clay compared to sand, no precise soil fractions were given) was assumed to be at permanent wilting point for rainfall equal to zero and it was assumed that the water content did not exceed field capacity (at 7mm of rainfall). The most commonly occurring daily rainfall value was estimated to be 0mm from 30-year weather records for July at ADAS Rosemaund. The measurements and rainfall data were supplemented with assumed values for the remaining soil strength parameters. The values are shown in Table 2.2. Calculations were completed using the equations Baker et al., (1998) derived. The values in Table 2.2, plus the measurements, led to the prediction of soil strength at the permanent wilting point of 51kPa and a field capacity of 6kPa.

Table 2.2 Assumed values used in the model by Berry et al., (2000).

Soil Property	Value	Value in Soil Mechanics
Field Capacity	0.27gg^{-1}	27%
Permanent Wilting Point	0.15gg^{-1}	15%
Soil density	1.4gcm^{-3}	1400kgm^{-3}
Water density	1gcm^{-3}	1000kgm^{-3}
Clay content	0.25gg^{-1}	25%
Visual Score	5	

Berry et al., (2000) assumed that the permanent wilting point for the soil was when there was 0mm of daily rainfall. Soil strength was measured using a shear vane at the permanent wilting point. The mean measured soil strength in 1994-1995 was above the expected maximum at 97kPa compared to 50kPa in 1995-1996. The 50kPa result agreed with the prediction of 51kPa by the model. However, 97kPa was significantly higher. This was because ground conditions were drier in 1994-1995 (soil water content 0.09gg^{-1} or 9%) than in 1995-1996 (0.14gg^{-1} or 14%) because hot, dry periods during 1994-1995 reduced the water content in the top 50 mm of soil to below permanent wilting point (PWP).

Gance, (2015) tested the effect of increasing the silt or fine sand content on root anchorage failure. The results are summarised in Table 2.3. The clay content was maintained at 0.30gg^{-1} for three soil samples. The silt content was varied using values of 0.35, 0.55 and 0.65gg^{-1}. The shear strength was measured using a shear vane and varied between 22-35kPa. The shear strength was also predicted using Baker et al., (1998) model and was predicted as 106kPa. The difference in measured and predicted soil strengths could be due to silt and fine sand fractions of soil. The equations only include clay content, not other soil fractions. Soil strength is influenced by the interactions of the different soil particles and soil water content. The model

needs to be tested on a range of soil types outside the ranges the equations were created for. Also, both Berry et al., (2000) and Gance, (2015) assumed values for the soil water content and visual score. Soil measurements for from the field or the laboratory has not been used to test the accuracy of the soil strength model.

Table 2.3 Results of the anchorage resistance study by Gance, (2015).

Measured shear strength	Shear strength predicted using Baker et al., (1998)
22 - 35kPa	106kPa (For w = 0.15gg^{-1}, v = 5, c=0.3gg^{-1})

As noted by Baker et al., (1998), the relationships for soil strength are empirical and rely on correlations developed for particular soils in the Agricultural, Development and Advisory Service (ADAS). Equations 2.6, 2.7 and 2.8 were only developed with specific values of water and clay contents as well, further restricting the use of the model. This indicates the limitations of the existing model. Therefore, a useful, unifiable model should be able to predict the soil strength for larger variations in soil variables. This could be achieved by using models and relationships found in soil mechanics, related to effective stress and shear strength, rather than relying on empirical fit equations which are very specific to the soil parameters they are based on.

Rahardjo et al., (2009) proposed a different approach, incorporating models for the soil strength derived from geotechnical engineering and soil mechanics for the stability of trees. This model is based on an engineering method of analysis called the limit equilibrium method. The limit equilibrium model is then applied to the ordinary method of slices (proposed by

Fellenius, (1936) referenced in Barnes, (2010)). This method was adapted to calculate the soil strength for tree anchorage and is discussed further in Section 2.4.

Soil strength calculation is only one step in the lodging risk model. After, the soil strength was calculated, the calculation of the stem base bending moment and the stem failure moment and root anchorage failure moments were completed. The soil strength is part of the root anchorage failure moment. The calculation of the root anchorage model will be discussed in the following sections.

2.3.2   Development of root anchorage models for wheat and oilseed rape

As mentioned in Section 2.3, Baker et al., (1995) used work done by Crook and Ennos, (1993) and Coutts, (1986) to compare the stem base bending moments and stem failure and root failure moments. Baker et al., (1998) used the model by Crook and Ennos, (1993) to predict root failure moments of wheat. However, there had been development of relationships between root failure moment and wheat parameters before Crook and Ennos, (1993).

Pinthus, (1967) investigated the relationship between the spread of the root system and the anchorage of 10 varieties of wheat root structures grown in the field (sandy loam soil, particle size distribution not given) and in gravel cultures (beds were prepared with gravel and nutrient solutions for plants to grow in). Pinthus, (1967) found that the lodging proof varieties had larger angles of spread, measured by removing the plants form the soil, washing the roots and placing them on graph paper with crowns on a marked line and the contours of the roots sketched onto the graph paper. The correlation between lodging rate and spreading angle was reported as (linear correlation coefficient, -0.814, r^2 0.662 and regression coefficient -.2762). Pinthus, (1967) also reasoned that the angle of root spread could be used to estimate the

anchorage strength of wheat. However, no model for predicting root anchorage was suggested.

Ennos, (1991), while modelling lodging of spring wheat and wheat seedlings, suggested that a single structural root will resist lodging both because of its resistance to being bent and its resistance to being moved axially through the soil. Therefore, the total lodging resistance of the root system is the sum of all the coronal (structural lignified) roots in relation to these separate components. The model is shown in Equation 2.15.

$$M_a = \sum_{i=1}^{N} k_i R_i^2 \, \alpha \qquad\qquad 2.15$$

Where, M_a is the total anchorage component for the whole root system, k is a constant for the root (the root is resisting axial motion, which means k is the bending stiffness), R is the perpendicular distance from the base of the root to the axis of rotation, α is the stem angle to vertical during lodging and N is the number of roots.

Bending resistance is modelled by considering a coronal root emerging from the base of the stem (Figure 2.12). It has an orientation with the vertical stem and an angle from the plane of the lodging force (horizontal). The root projects a perpendicular distance from the lodging plane and a parallel distance from the vertical. The total anchorage component of the root bending stiffness is the sum of all the coronal roots. The bending component of the anchorage depends on the direction in which the lodging force is applied. However, this method requires measurement of the root stiffness, which is a difficult parameter to obtain. The root stiffness was measured by bending the coronal roots of average diameter 1mm to a 45° angle and the resistance to bending was recorded using an Instron machine. Ennos, (1991) tested 8 plants

with 10-15 coronal roots each and acknowledged there was large variability between roots, with the moment required to cause bending of 45°being 7.6±4.8x 10^{-3}Nm.
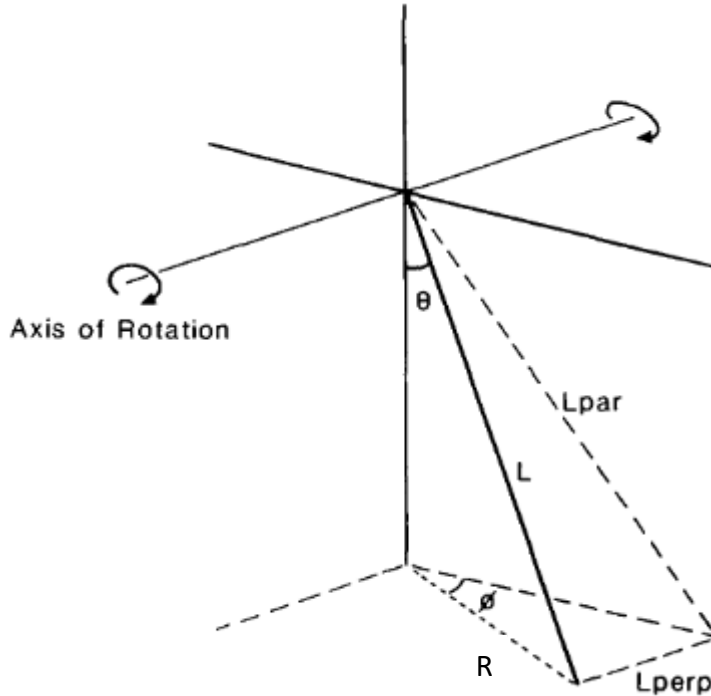
Figure 2.12 Diagram showing how the projected length of a root along the parallel plane can be calculated. The root length, L and angle, θ to the vertical and at an angle, ɸ, to the plane of lodging (Ennos, 1991).

The resistance to axial motion of a root depends on its surface area and the strength of the root-soil interface. Long, thick roots will resist motion more strongly than short, thin ones (Ennos, 1990, 1991). The extent to which this resistance contributes to the anchorage will depend on the position and orientation of the root, which is sometimes referred to as root tortuosity. Axial movement was measured by pulling entire root systems from the soil (not described). For 6 plants measurements ranged from 0.064±0.027Nm. Root failure moment was also measured for comparison with the semi-empirical model proposed. The setup shown in Figure 2.13 was used to push plants over at a rate of 42°min^{-1} using the Instron machine in the laboratory. For 14 plants the range of failure moment was 0.124±0.029Nm. When the

predictions of Ennos, (1991) model were compared to the lodging tests, the results were reported to be "roughly equal", no accuracy data were provided.
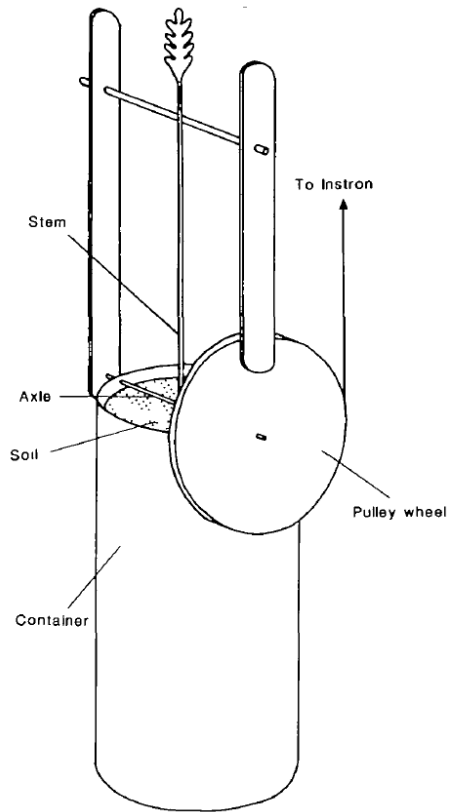
Figure 2.13 A pulley system connected to the an Instron machine (Ennos, 1991).

Easson et al., (1992) conducted experiments on vertically pulling of 41 wheat roots out of soil (sandy clay loam, 48% sand, 30% silt, 21% clay, 5.94% organic matter and sandy loam, 65% sand, 20%, silt, 15% clay, 5.32% organic matter). Plants were pulled in a similar manner to the axial strength tests by Ennos, (1991) (Figure 2.14 and Figure 2.15). They suggest that the root anchorage of wheat could be represented as a fibre bundle because of the root pullout behaviour. When testing the strengths of the wheat roots, it was found that they have a similar extraction curve to that of fibre-reinforced composites (Figure 2.16). The stress-strain curve was linear until the root-soil complex failed. From there, the load was carried by the roots,

which continue to stretch elastically until failure. The stress gradually drops to the yield strength of the matrix in stages as the fibres break. When the root-soil complex fractures the composite fails. Equation 2.16 and 2.17 were proposed.

$$Epll = Vf\ Ef + (1 - Vf)Em \qquad\qquad 2.16$$

$$Erta\ = \left\{ \frac{Vf}{Ef} + \frac{1 - Vf}{Em} \right\}^{-1} \qquad\qquad 2.17$$

Where, Epll is the modulus of composite with fibres parallel to the load, Erta is the modulus of composite with fibres at right angles to direction of the load, Vf is the volume fraction of fibres, modulus of matrix, Ef is the modulus of the fibre. The model was never validated with data from the field. Easson et al., (1992), model requires measurements of the root strength and the outer diameter of the roots, both of which require pulling tests on the wheat plants as well as individual roots which might be difficult for farmers and practitioners to measure easily.
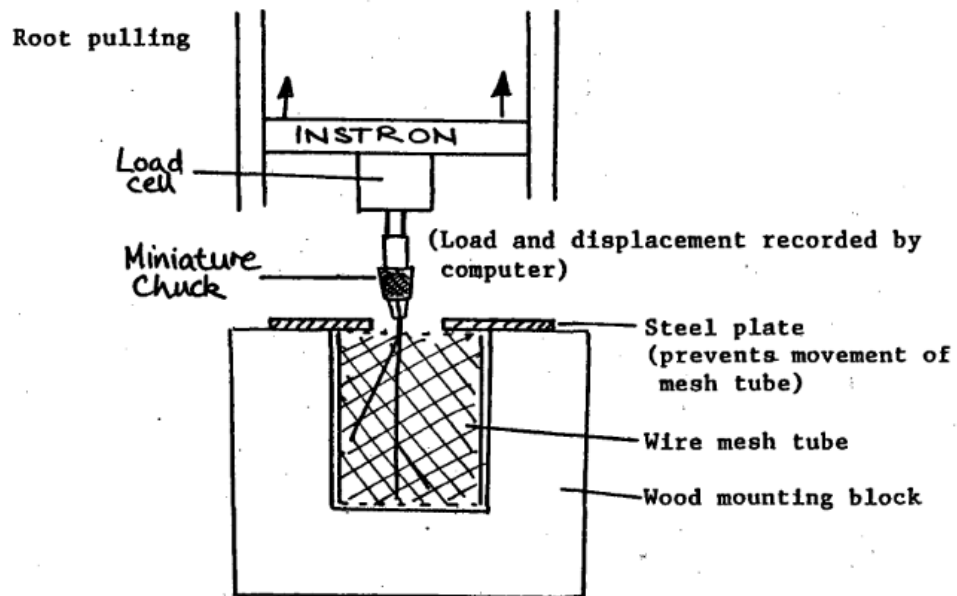
Figure 2.14 Setup for the pulling experiment Easson et al., (1992).
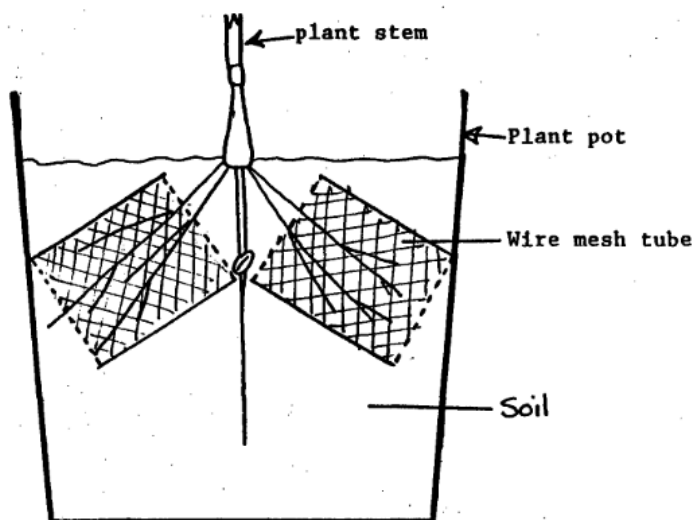
Figure 2.15 Growing material for root pulling experiment Easson et al., (1992).
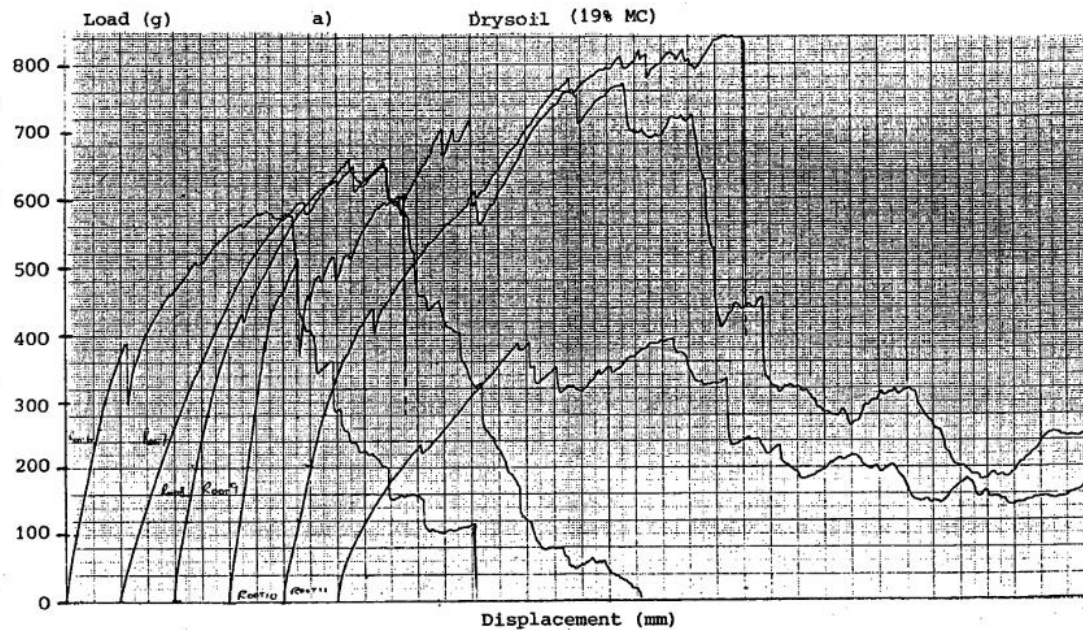
Figure 2.16 Typical load vs displacements for root pulling from dry soil Easson et al., (1992).

Crook and Ennos, (1993) combined observational study with the geotechnical model created by Broms, (1964a, 1964b) to create a semi-empirical model. Crook and Ennos, (1993) conducted the observational lodging study on mature winter wheat plants (Figure 2.17a), grown in soil cores of saturated, remoulded agricultural soil. The soil was described as a sandy loam (loam is a soil composed of sand, silt and clay); the specific particle size distribution was not provided. Before testing a trench was dug next to the roots so that direct observations of the roots could be made. Lodging was simulated by applying a static, horizontal load to the stems of the plant. The height of the applied load was not given. However, in subsequent experiments, the height of the applied load was 17cm from the stem base. The results for this experiment were described qualitatively.

Under small lateral displacements, the root movement was the same as observed by Ennos, (1991). When the lateral displacement of the stems of winter wheat was increased, Crook and Ennos, (1993) observed that the roots began to act as a root-soil plate or cone instead of

individual roots. Easson et al., (1992), defined the root-soil plate as the volume of soil entrapped by roots as it is uprooted. It is related to the root-soil plate diameter or angle of root spread (the angle of the widest roots to the stem). The centre of rotation changed from directly below the stem to the edge of the root-soil cone (20-30mm below the soil surface). The centre of rotation is shown as a dot in Figure 2.17b. Crook and Ennos, (1993) suggested this was because the windward roots were held still by the fine seminal regions which were loaded in tension and strong enough not to break or slip out of the soil. The cone of soil that the coronal roots surround was rotated deeper into the ground, compressing the soil beneath (Figure 2.17b). When they removed the lateral force, the plant had lodged. They suggested that this was because the soil under the root-soil plate had been compressed and plastically deformed.

Therefore, the anchorage failure of winter wheat depended on the dimensions of the root-soil cone, the rigidity of the roots and the resistance of the soil to compression (Crook and Ennos, 1993). The main contrast between Ennos, (1991) and Easson et al., (1992) was the root-soil plate and the removal of the influence of root strengths in either tension or compression or bending.
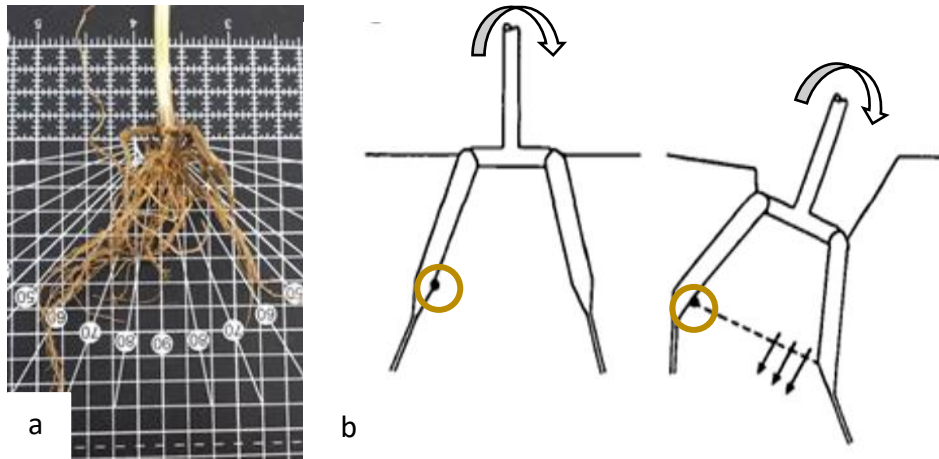
Figure 2.17(a) An image of wheat roots (b) Schematic depicting root lodging in winter wheat, as the stem rotates, a cone of soil contained by the coronal roots rotates in a clockwise direction down through the soil compressing the soil below the cone. The dot represents the centre of rotation (Crook and Ennos, 1993).

Considering the root architecture and the movement observed, Crook and Ennos, (1993) derived a model for root anchorage in wheat. Crook and Ennos, (1993) adapted the ultimate lateral resistance for short piles in fine-grained soils by Broms, (1964a) for pile foundations and given by Equation (2.18).

$$P_u = c_u d^2 \qquad\qquad 2.18$$

Where, P_u is the resistance of the pile to lateral loading, c_u is the undrained shear strength of the soil and d is the diameter of the pile.

Broms, (1964a and b) derived equations for lateral deflections for piles under working loads (the maximum load that a structure is designed to bear) and the ultimate lateral resistance, (i.e. the load a pile can take) of piles under lateral loads. When a lateral load is applied to the pile, the pile deflects. The amount of deflection increases linearly with the applied load. As the ultimate capacity of the soil is approached the lateral deflections increase rapidly with

increasing load. Failure of the pile may occur as shown in Figure 2.18a, b and c, where, the pile rotates through the soil.

A similar behaviour can be observed for root lodging, as lodging is defined as the permanent displacement of the stem from the vertical position of the root system, in other words when rotational failure has occurred. While the load is applied at the top of the pile, the soil is reacting by distributing the lateral earth pressures along the length of the pile. When the pile fails, the soil located at the front of the pile is pushed upwards in the direction of least resistance. The soil at the back of the pile separates from the pile to a certain depth (Broms, 1964a).

Figure 2.18a and Figure 2.18b represent the failure mechanism and the resulting soil reaction distribution of short, rigid piles in fine-grained soil. Piles can be divided into two groups; short, rigid or long, flexible. A short pile is one that is rigid enough to move in the direction the load is tending by rotation or translation. A long pile is one that the top will rotate or translate without moving the bottom of the foundation Figure 2.18c. Broms, (1964a, 1964b), developed lateral resistance equations for both short and long piles in fine-grained and coarse-grained soil. Fine and coarse-grained refer to the soil particle size distribution.

a

b

c
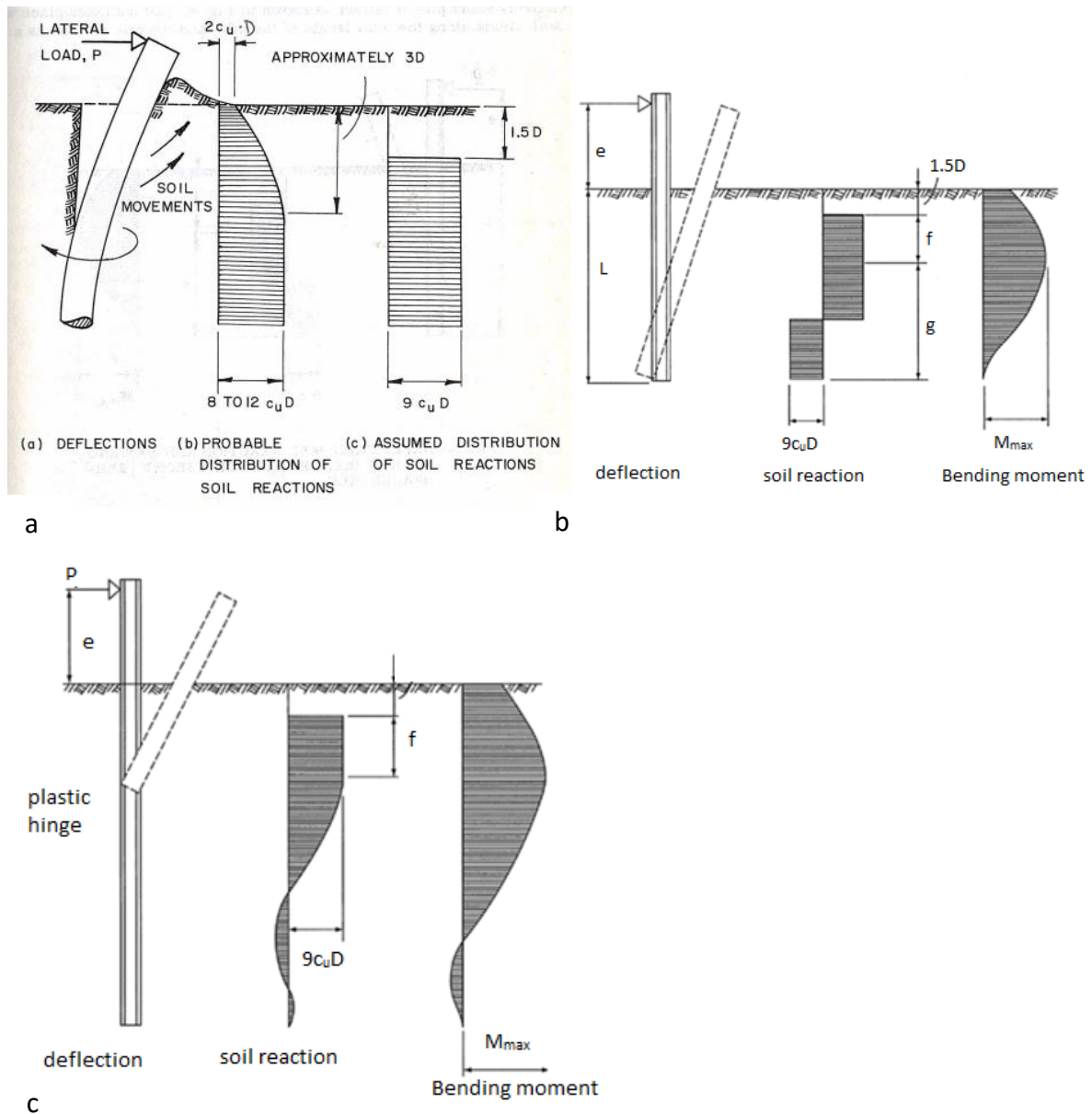
Figure 2.18 (a) Shows the deflection of the pile as well as the probable and assumed soil reactions for rigid piles (image from Broms (c_u is the undrained shear strength, D is the diameter of the pile, P is the lateral load), (1964a). Distribution of lateral earth pressures and bending moments for (b) Short rigid piles in fine-grained soils with a point of rotation (D is the diameter of the pile, e is the height of the lateral load, f and g are lengths along the pile) (c) long piles with a plastic hinge in fine-grained soil by Broms, (1964a), (P is the lateral force, e is the height to the lateral force, f is a length along the pile, cu is the undrained shear strength and D is the diameter).

The ultimate soil reaction against a laterally loaded pile is related to the soil resistance (c_u, the unconfined compressive strength) and the pile dimensions (d, diameter of the pile) which is similar to those parameters identified for root anchorage in wheat. The probable distribution of the soil reaction is shown in Figure 2.18a. The soil reactions were reduced to a rectangular

46

distribution of lateral earth pressures which was larger than the corresponding lateral pressure distribution at failure. Therefore, the model produces higher resistances than may occur in reality which means the model is overestimating the resistances. The soil resistance was used as part of the equations to find the point of rotation below the ground surface and the maximum bending moment. The parameters needed for the lateral resistance of piles were the soil resistance, the pile diameter and the depth of the point of rotation.

Crook and Ennos, (1993) adapted the original equation proposed by Broms, (1964a, 1964b) to include the area of the root-soil plate (the area of a plate) because of the observed movement of root-soil plate downwards into the soil. It was then multiplied by the distance from the centre of the cone to the centre of rotation ($\frac{1}{2}d$) (see Figure 2.17) to obtain the moment resisting overturning. This resulted in Equation (2.19):

$$R_{fm} = \frac{9}{8}\tau\pi d^3 \qquad\qquad 2.19$$

Where, R_{fm} is the root failure moment (Nm), τ is the soil shear strength (kPa), and d is the root-soil plate diameter (m).
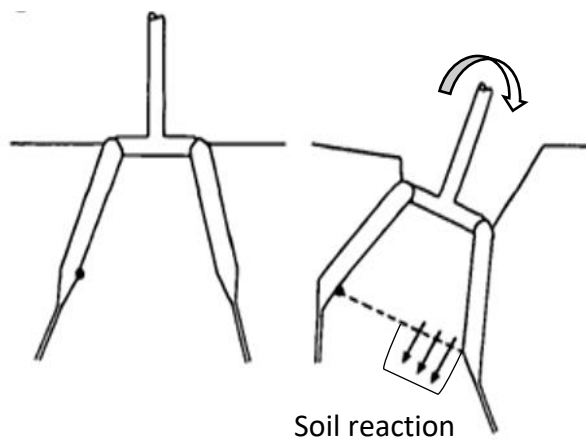
Soil reaction

Figure 2.19 Diagram of the pressure distribution by Crook and Ennos, (1993).

Examining the Equation 2.19, Crook and Ennos, (1993) modelled the root anchorage resistance by considering the soil reaction beneath the root-soil plate (Figure 2.19). This soil distribution is different from the distribution by Broms, (1964a) (Figure 2.19) because the soil distribution is below the circular plate of the root-soil cone and not distributed along the root depth. This difference is significant because the difference in distributions and hence failure mechanisms could impact the accuracy of the root anchorage model for wheat and oats.

According to Stokes and Mattheck, (2007), there are three basic types of root form. The heart root system with many deep branches, the plate system with shallow spread roots, and tap root system with a large central vertical root and smaller lateral roots. It should be noted that wheat and oats have root structures that are considered a plate root system. For the purposes of this study, they are considered to have the same mechanism of failure. Oilseed rape has a tap rooted system and would have a different failure mechanism.

Crook and Ennos, (1993) collected data on the anchorage resistance of four different varieties of wheat in the field and measurements of the root cone diameter and the soil strength. The research included four different species with 20 samples of each. The root failure moment (restoring moment) was correlated with the cone diameter. Crook and Ennos, (1993) stated a coefficient of determination, R^2 of 0.41 for a sample size of 80 plants, which suggests that there was a significant variance between the measured anchorage resistance and the root cone diameter (Figure 2.20). They stated that this result supported the model (Equation 2.19). The low R^2 values could be a result of using crops in the field, where there could have been variations in the plant growth conditions accompanied by the natural variation between plants. The R^2 value could also indicate that other variables might be important to anchorage.

These could include those suggested by (Griffin, 1998) including root patterns, soil particle density or point of rotation and length suggested by Broms, (1964a) in the pile model. The R^2 value can also indicate that a linear model may not provide the best fit for the data.
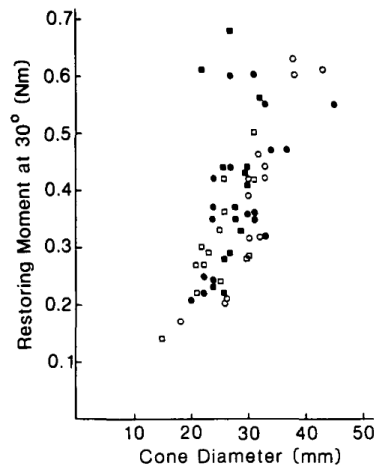
Figure 2.20 (a) Relationship between the diameter of the root-soil cone and the restoring moment (anchorage resistance) at a displacement of 30° during simulated lodging of four winter wheat varieties (R^2 0.41, P<0.001) ((Crook and Ennos, 1993).

Interestingly, in the work by Crook and Ennos, (1993) there was a variety of wheat that contradicted the established relationship (Equation 2.19). The variety Hereward had small root cone diameters but produced large anchorage resistance. The researchers suggested that this may be because of the resistance of the coronal roots to bending. Closer observation of Figure 2.20 showed that, as the cone diameter increases, there is increasing scatter of the data. This also suggests that there may not be a linear relationship between anchorage resistance and cone diameter.

Crook and Ennos, (1993) completed a second experiment (simulated lodging tests) using artificial roots of wheat plants. This experiment was conducted to investigate the effect of changing the root cone diameter and soil shear strength on the anchorage resistance. This part of the research was limited to three soil strengths (4.4, 6.5, 10.2kPa) (using sandy loam,

no particle size distribution given) and three cone diameters (22, 28, 34mm) made from polythene, 6mm thick. There were nine different tests. Each test was repeated three times. A sandy loam, was collected from the field trial, air-dried and sieved through 6mm sieve. Soil was placed in containers 11cm height and 10.4cm diameter. The containers were shaken to promote soil settlement and water was added until it started to drain. The containers were then brought to zero matrix potential (pore water pressure) by submerging in water for 24 hours. The soil strength was manipulated by using a sand table. Sand tables were set a three different water suctions, 0cm, 30cm, 54cm suction, producing soil strengths of 4.4±0.44, 6.5±0.98 and 10.2±0.26kPa, respectively. The plastic models were then placed on the sand table for rotation (Figure 2.21).
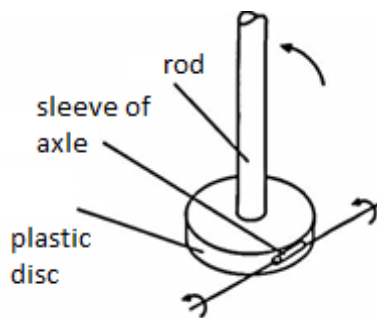
Figure 2.21 A plastic lodging disc. The disc represents the base of the root-soil cone during lodging in wheat, the rod is the stem of the plant and the hollow tube allows the centre of rotation to be on the windward side when a steel axle is threaded through both it and the soil container.

One of the limitations of the experiments was the placement of the models on top of the soil and rotating the samples into the soil. This form of testing was not representative of the crop roots being in the ground and rotating within the soil. The artificial roots were 6mm plastic discs, which do not represent the geometry (morphology) or strength of real root systems.

This study found results to similar Crook and Ennos, (1993) in that the anchorage resistance increased with increasing cone diameter (Figure 2.22). Gance, (2015), used similar shaped

plastic models placed into the ground at a depth of 50mm and a similar relationship between anchorage and cone diameter was found. This was supported in later studies by (Berry et al., 2003) who looked at the same relationships between root cone diameter and anchorage strength for 15 varieties of wheat. Also, (Berry et al., 2006) found that the relationship was similar for wheat and barley, suggesting that barley would have a similar failure mechanism to that of wheat.

Crook and Ennos, (1993) stated that the root anchorage moment was proportional to the cube of the disc diameter, thus this result supported the model (Equation 2.19). The model in Equation 2.19 was used to predict anchorage for one measurement in Crook and Ennos, (1993) study, the model predicted a value of 0.73Nm while the measured value was 0.6Nm. The model was not validated beyond this prediciton.
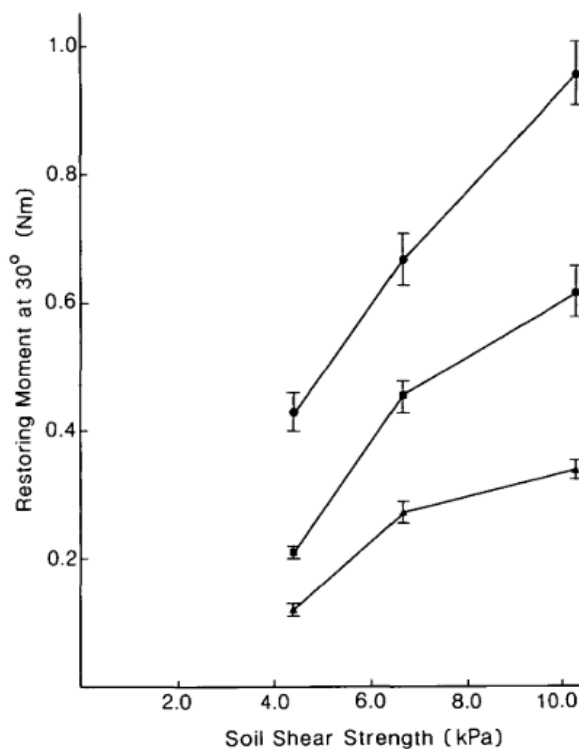
Figure 2.22 Results of model tests: 22mm, 28mm and 34mm diameter discs.

Equation 2.19 was then used by Baker et al., (1998) with the constant values of $\frac{9}{8}$ and π, replaced to give:

$$R_{fm} = k\tau d^3 \qquad\qquad 2.20$$

Where k is a constant. Griffin, (1998) completed testing where on mechanically lodged wheat plants that gives a k value of 0.43 (Figure 2.23).
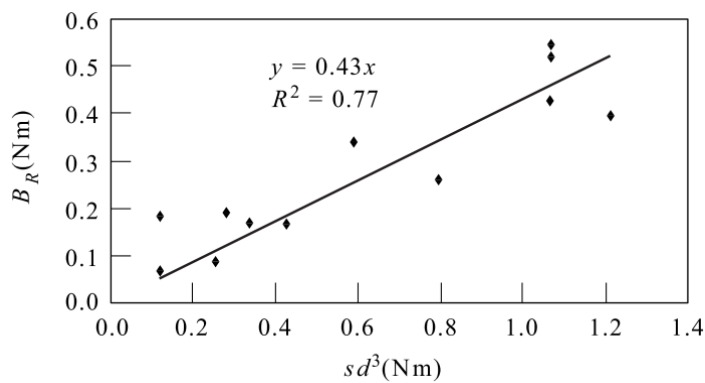
Figure 2.23 The product of soil shear strength (s) and root plate diameter cubed plotted against root failure moment (B_R).

Berry et al., (2003) found that by applying the lodging risk model to new datasets (Baker et al., 1998), the root lodging model under-predicted early root lodging compared with field measurements. This meant that the root strength model was overestimating the actual strength of the crop in the field. They suggested that the constant k may be a factor that needs more investigation. Both Baker et al., (2014) and Berry et al., (2003) have agreed that the anchorage model needed refinement. Research into the components of the model such as slippage between roots and root strength and using simulations that reflect the dynamic nature of wind forces on the root system were suggested.

During their simulated lodging tests, (Crook and Ennos, 1993) used a universal materials testing machine fitted with a lodging attachment, which was similar to Figure 2.13. The

apparatus applied a rotational force to the plant and measured the restoring anchorage moment supplied by the root system. The force was applied at the height of 17cm from the stem base, and the rotational velocity or strain rate was 60° min^{-1} in one direction. It should be noted that the method for testing root anchorage testing varies considerably in the literature (Figure 2.24). Methods are manual and automatic, resulting in maximum values of anchorage or continuous curves of anchorage moment versus time. Manual testing included pushing the plant over to failure (giving the maximum moment) (Berry et al., 2006), pushing and stopping at specific angles (Goodman et al., 2001), or adding weights to a container connected to the model (Gance, 2015). Ideally, continuous curves would be useful to analyse the behaviour of the root system as the rotation angle increases and also to see how these curves develop for different soil conditions. However, the Instron machine is not portable, therefore an instrument that could be used both in the field and the laboratory that was capable of measuring continuous values of root failure moment and rotation would be suitable.
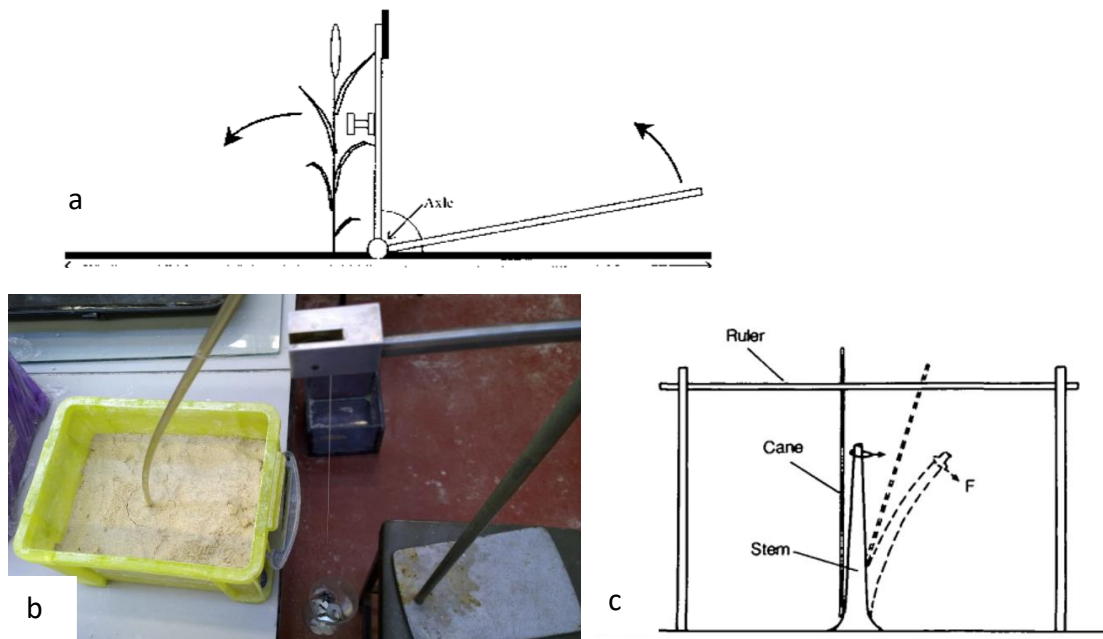
Figure 2.24 Images of previous lodging devices (a) an adjustable pushing plate connected to a rotating handle and base frame (Sterling et al., 2003),(b) pulley system connected to a small container with weights, (Gance, 2015) (c) pulling measurement system used in Goodman et al., (2001)

There have been various anchorage studies between the wheat model by Crook and Ennos, (1993) and the Goodman et al., (2001) model for oilseed rape, including sunflower (Ennos et al., 1993), balsam (Ennos et al., 1993), maize (Ennos et al., 1993) and deep rooted larch (Crook and Ennos, 1996). However, there seems to be a lack of research on the anchorage mechanics of oats. This is an area that could be investigated in this research.

The oilseed rape root system could simply be classified as a tap root system (Stokes, 2002). Oilseed rape roots consist of a main tap root and lateral roots (Figure 2.25a). The tap root is significantly larger than the lateral roots and is usually orientated downward. The lateral roots are arranged at an angle to the tap root (Figure 2.25a). In oilseed rape, both the lateral roots and the tap root have structural roles. There is a significant difference in size and strength between the wheat (and oat) roots and oilseed rape roots. The root morphology described for oilseed rape would mean that the root failure mechanism was different to that of wheat and oats. Crook and Ennos, (1993) found that the wheat root system had a bending strength of

0.011±3.00Nm compared with Goodman et al., (2001) found the tap rooted system had a bending resistance of 2.4±0.22Nm (there is no previous data on the lodging resistance of oats)
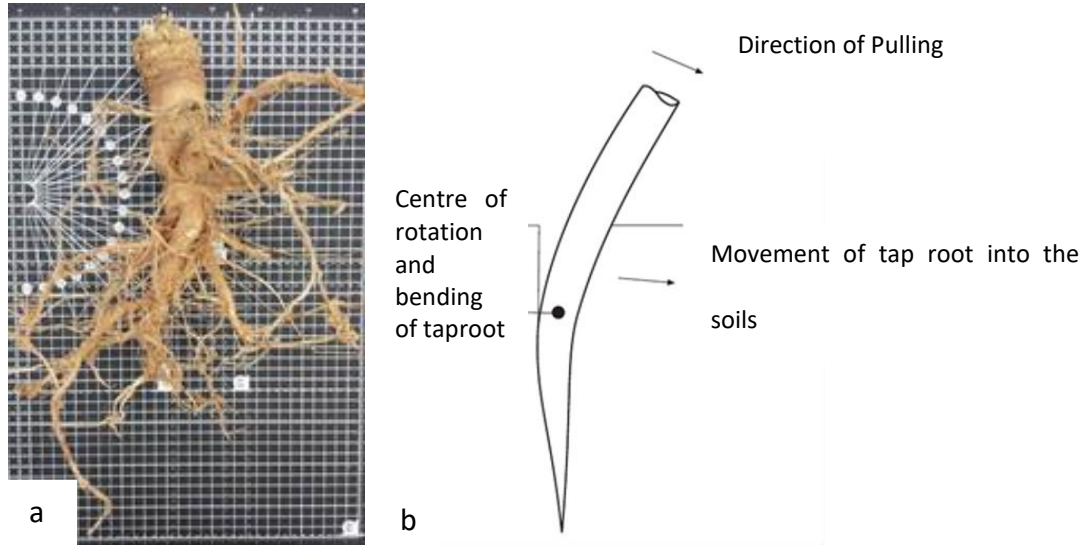
Figure 2.25 (a) An image of oilseed rape root systems. (b) Diagram depicting root lodging in winter oilseed rape. (Goodman et al., 2001).

Similar to Crook and Ennos, (1993), preliminary observations were completed before derivation of the model. Contrasting with the observations for wheat, anchorage failure in oilseed rape was a result of compression of the soil on the nearside and bending of the tap root (Figure 2.25b). As plants were pulled over, the top 30 mm (approximately) of the tap root bent and the soil was compressed, leaving a crack in the soils surface on the opposite side. Though this description is different from the failure of wheat, the model was based on the same engineering theory of lateral resistance of piles to loads (Broms, 1964a). Assuming the tap root is a rigid rod of length, L and it rotates about its base, the final expression is as follows:

$$P_u = c_u d^2 \qquad\qquad 2.21$$

$$R_{fm} = \frac{9}{2} c_u dl^2 \qquad\qquad 2.22$$

Where, R_{fm} is the root failure moment, d and l are the diameter and length of the tap root respectively and c_u is the shear strength. Goodman et al., (2001) completed anchorage testing on oilseed rape plants and artificial roots made of steel (using the method shown in Figure 2.24). The correlation between the anchorage moment and tap root diameter is shown in Figure 2.26. Again, similar to the Crook and Ennos, (1993) the linear relationship may not be ideal, also the data is clustered into two specific areas. The artificial root tests found that increasing root diameter increased root failure moment. However, the artificial roots were constructed from steel and this material does not represent root strength. The plastic roots in the wheat anchorage study were also not representative of root strengths. The model proposed in Equation 2.21 was not used to predict anchorage.
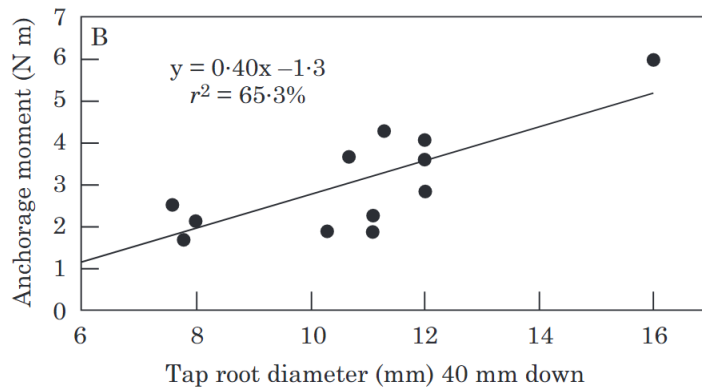
Figure 2.26 Maximum anchorage moment (anchorage resistance) against the diameter of the tap root at 40 mm down (R^2 0.65, P<0.001) during simulated lodging of oilseed rape. Results for 13 crops (Goodman et al., 2001)

Equation 2.22 was then used by Baker, Sterling and Berry, (2014) to yield Equation 2.23:

$$R_{fm} = k\tau dl^2 \qquad\qquad 2.23$$

Where, k is a constant, where k was given as 4.0. This model was not validated with a new dataset.

(Farquhar and Meyer-Phillips, 2001) and (Oladokun and Ennos, 2006) used safety factors to quantify the margin of safety against lodging of wheat. In Farquhar and Meyer-Philips, (2001), the relative safety factor quantifies the risk of anchorage rotation, which can occur if the imposed bending moment, M exceeds the anchorage strength M_m. The moment applied to the ground uses the height of the plant, L_e and the lateral force, F associated with the lateral displacement, x. The lateral force is determined from the k and x given in Equation (2.24).

$$M = F L_e = kx L_e \qquad\qquad 2.24$$

k is the effective stiffness and is derived from the stem mass, the spike mass (mass of the grain or head of the wheat), empirical parameters derived from the force of gravity and the resonant frequency. The resonant frequency was determined by using a linear shaker motor. The excitation frequency was varied to find the resonant frequency of vibration. This method found that the safety factor could be calculated for different breeding lines. However, the research was geared towards comparing safety factors, not towards predicting anchorage failure. The models derived by Crook and Ennos, (1993) and Goodman et al., (2001) are integrated into the lodging risk model (Baker et al., 2014) as Equation 2.17 and 2.20. There is some uncertainty around the accuracy of the models, the oilseed rape model has not been validated. This is an area that could be addressed in this research. The lack of certainty around root anchorage prediction in these two species led to a review of theoretical and semi-empirical models for root anchorage in other plant species.

2.4   Development of root anchorage models in other plant species

Table 2.4 shows the root anchorage models found in the literature which modelled lodging or rotation (overturning).

Table 2.4 Models related to root anchorage.

Model Reference	Model Technique	Main Advantages	Parameters needed	Applica bility
Baker et al., (1998) Crook and Ennos, (1993)	Theoretical	Simple formula, Lodging model	Considers root plate diameter and undrained soil strength, root depth	Wheat
Farquhar and Meyer-Philips, (2001)	Theoretical	Simple formula	Considers above plant measurements, stem mass and spike mass	Wheat
Baker et al., (1998) Goodman, et al., (2001)	Theoretical	Simple formula, Lodging model	Considers root diameter, root length and root depth.	Oilseed Rape
Schutten et al., (2005)	Empirical Regression Analysis	Simple formula	Uses sediment cohesion, instead of shear strength, difficult parameter to measure	Submer ged Plants
Schutten et al., (2005)	Empirical Regression Analysis	Simple formula	Considers root area, cohesion and difficult parameter to measure	Submer ged Plants
Coutts et al., (1999)	Empirical Regression Analysis	Simple formula, uprooting model	Considers root plate mass, root plate radius, wind load, the height of the centre of gravity	Trees
Moore, (2000)	Empirical Regression Analysis	Simple formula, uprooting	Considers stem volume, tree height, diameter and root plate width	Trees
Fourcaud et al., (2008)	Empirical Regression Analysis	Simple formula, uprooting	Considers root plate volume or mass and hinge distance from stem base	Trees
Peltola and Kellomaki, (1993)	Empirical Regression Analysis	Simple formula. uprooting	Considers gravitational constant, the mass of the root-soil plate, depth and proportion of weight to the root-soil anchorage.	Trees
Rahardjo et al., (2009)	Limit Equilibrium Analysis	Includes soil shear strength, root shear, tensile and slippage strength	Difficult to measure parameters, the ordinary method of slices required	Trees
Yan et al., (2016)	Bayesian Inference	Predictive model	Only used for shrubs, difficult calculations	Shrubs, trees
Blackwell et al., (1990)	Theoretical	Complex	Complex formula, difficult to measure parameters	Trees

Blackwell et al., (1990) modelled the anchorage of Sitka spruce trees by analysing experiments

conducted by (Coutts, 1986). These experiments involved pulling or winching Sitka spruce

trees in peaty gley soil. Sitka spruce is a tree with a shallow root system (mean height of 19.2m and root plate depth of 46cm). Peaty gley soil occurs in Scotland and is a soil with a high organic content (peat) and a distinct blue-grey colour (Coutts, 1986).
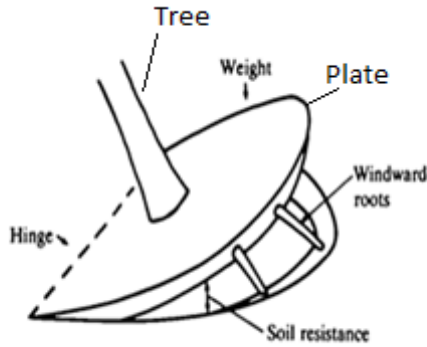
a

Figure 2.27 (a) A diagram showing the main parts of the root system model, (Blackwell et al., 1990).

The model calculates the disturbing moment of the tree with changing angle. The system of equations changes with angular momentum (Figure 2.27). It tries to calculate the changing strength of the tree based on the angle to horizontal. Since the assumption is made that the system moves by rotating about a hinge or pivot, the equation of angular motion (Equation 2.25) is used by (Coutts, 1986).

$$\frac{d^2 a}{dt^2} = \frac{T}{I}$$
2.25

Where, a is the angle of displacement of the system from the vertical, t is time, T is the net disturbing moment on the system (total of the applied disturbing moments and the damping disturbing moment), I is the moment of inertia of the system about the same axis as that used to determine the disturbing moments. The model calculates the resistance of the tree root systems as the angle of the tree changes with time. The model simulates the motion of a tree as snapshots of time incorporating dynamic failure into the plant anchorage process. They

found that the model could predict root failure moments within the range of measured data for Sitka spruce. Prediction were done using data collected by Coutts, (1986), where Sitka spruce trees were pulled over, using winching. A sensitivity analysis changing different root parameters was completed but a new dataset was not used to validate the model.

Similar to Crook and Ennos, (1993), a number of simplifications were applied to the problem of uprooting Sitka spruce trees to simplify the modelling process (Blackwell et al., 1990). The root-soil plate, stem and crown were considered rigid bodies, able to rotate about a fixed horizontal axis touching the edge of the plate. This enables the position of the tree at any time to be described by a single variable, i.e. the angle of tilt. The plate is assumed to be of uniform thickness and density and comprises semi ellipses. The stem and crown are represented by a rod of negligible radius, whose mass is distributed along its length. At the end of all these simplifications, the tree looks like a disk with a rod; very similar to Crook and Ennos, (1993) simplification used in their model for wheat lodging. For further detail, refer to Blackwell et al., (1990) and Coutts, (1986).

The net disturbing moment of the root-soil system is a function of the disturbing moments of each of the four components according to Coutts, (1986):

- the resistance caused by the weight of the root-soil plate;

- the resistance to failure of the soil underneath the plate;

- the resistance offered by roots subjected to tensile forces as the plate topples;

- the resistance of roots on the lee side (opposite side of the windward side or the side of the plant where the force is applied) as the plate hinges.

Applying this type of equation to cereal and oilseed rape roots would be interesting but would require collecting continuous data on their anchorage resistance over time for each component of anchorage. Another drawback of applying this research to wheat roots is the difference in size between trees and wheat plants. Trees are larger, and have stronger roots, than wheat and oilseed root systems. More extensive root systems with stronger material properties may not exhibit the same pattern of root anchorage failure as smaller plants due to size, strength and scale (Coutts et al., 1999). In contrast, (Dupuy et al., 2005) suggested that the larger the root system, the less it is influenced by the root architecture and the more uprooting is limited by the soil characteristics and the root-soil interface. However, at smaller scales root architecture becomes more important than the soil characteristics.

The concept of soil resistance was noted in by Niklas, (1992). Casada et al., (1980 cited in (Niklas, 1992), conducted a study on lodging in tobacco plants. This study showed that the force required causing the tobacco plants to overturn related to the same concept of lateral earth pressure along the length of the portion of the plant below the soil. In this case, the force above the ground multiplied by the height of the stem was plotted against the depth of the plant. The gradient of the resulting line (Equation 2.26) was the soil pressure.

$$F_w h = M_R + \frac{P_s A L_s}{2} \qquad\qquad 2.26$$

Where, F_w is the force of the wind, h is the distance of application of the wind force above the pivot point which was taken at the depth of the root plate. M_R is the moment of resistance provided by the root, P_s is the soil pressure, A is the projected area of the stem (which could be changed to the projected area of the root) acting against the soil and L_s is the distance of

the pivot point below the soil, which was determined by measuring the length of the root plate.

Interestingly, Niklas, (1992) equation is similar to the method of evaluating the resistance of a cantilever sheet pile (Figure 2.28). The cantilever sheet pile design method (Equation 2.27 and 2.28) uses Rankine's theory of lateral earth pressure and mechanics to find the forces and moments being experienced by the cantilever sheet pile system (Das, 2011).

$$P(L + z) = \frac{\gamma z^3 \left(k_p - k_a \right)}{6} \qquad \text{2.27}$$

$$z = \sqrt{\frac{2P}{\gamma (K_p - K_a)}} \qquad \text{2.28}$$

Where, P is the wind force, L is the height of the wall above ground, z is the depth to the pivot point, γ is the unit weight of soil, K_p is the Rankine passive pressure and K_a is the Rankine active pressure. This model assumes that the soil has failed and is in the process of shearing and that the sheet pile is rigid.
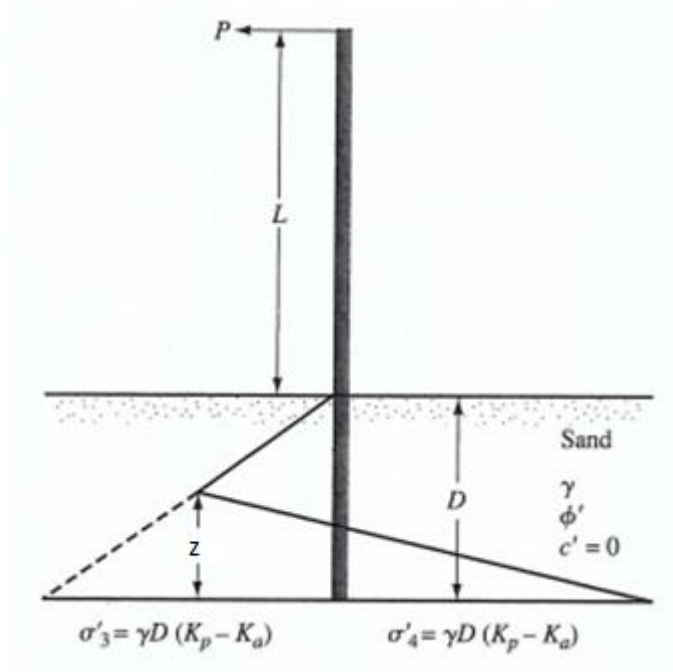
Figure 2.28 A diagram showing the free cantilever sheet pile penetrating a layer of sand. P is the wind force, L is the height of the wall above ground, z is the depth to the pivot point, γ is the unit weight of soil, K_p is the Rankine passive pressure and K_a is the Rankine active pressure. This model assumes that the soil has failed and is in the process of shearing and that the sheet pile is rigid.

However, this model has not been adapted to predict anchorage of plant roots and therefore will not be used in the comparison with root anchorage models.

Rahardjo et al., (2009) used the engineering theory of limit equilibrium used to analyse the stability of soil slopes to model root anchorage in trees. Limit equilibrium methods investigate the equilibrium of a soil mass tending to slide under the influence of gravity (Rahardjo et al., 2009). This method is based on the comparison of forces resisting the movement of the mass with forces causing the movement of the mass. The method is split into four parts each evaluating different aspects of tree root anchorage as shown in Figure 2.29. The comparison is used to see which of the four parts of the system has the lowest value of forces at failure and hence is the limiting factor.
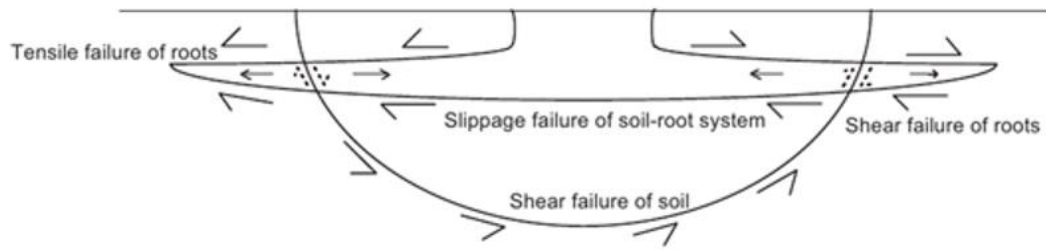
Figure 2.29 A diagram showing the principle of the modified limit equilibrium method used by Rahardjo et al., (2009) with the four considerations, tensile failure of roots, slippage failure of the root-soil system, shear failure of roots and shear failure of soil.

Part one of the method describes the soil shear strength and is modelled by using the ordinary method of slices proposed by Fellenius, (1936) in a computer model to find the most vulnerable slip surface. This slip surface is assumed to be within the root-soil plate, and this means that the root strengths have to be incorporated into the analysis. Part two of the method is to find the sum of the shear strength of the roots. The third step is to find the sum of the slippage strength of the roots, and in the fourth step, the tensile strength of the roots must be determined. The equations are presented in Equations 2.29-2.32.

$$F_{soil} = \Sigma \frac{c_u b \ sec \ \alpha}{W \ sin \ \alpha} \qquad \qquad 2.29$$

$$F_{shear} = \sum_{i=1}^{n} A \, \tau_{shear} \qquad \qquad 2.30$$

$$F_{slip} = \sum_{i=1}^{n} K L_{slip} \tau_{slip} \qquad \qquad 2.31$$

$$F_{tensile} = \sum_{i=1}^{n} A \, \tau_{tensile} \qquad \qquad 2.32$$

Where, F_{soil} is the resisting shear force induced by the soil (N), c_u is the undrained shear strength of the soil (kPa), b is the width of the slice (m), a is the angle of the slice to the centre

of rotation (°). F_{shear} is the resisting shear force induced by the root (N), n is the number of roots, A is the surface area of each root (m^2) and τ_{shear} is the shear strength of the root. F_{slip} is the resisting slippage force induced by the root (N), k is the circumference of each root, L_{slip} is the length of the horizontal root providing the slippage resistance, and τ_{slip} is the slippage strength between the soil and the roots. $F_{tensile}$ is the resisting tensile force of the root (N) and $\tau_{tensile}$ is the average tensile strength of the roots.

This model takes into account the soil and roots as separate entities with their inherent strength. However, the mechanism of failure of the soil portion of the analysis is a slip surface. This uses the circumference of the circle produced by the root system and the undrained shear strength as the soil resistance. It is not clear whether a slip surface forms completely during the lodging of wheat, oats and oilseed rape or the shape of the slip surface.

Rahardjo et al., (2009) completed predictions using dimensions of a typical tropical tree from Singapore and four soil types: topsoil, 50% top soil and 50% granite chip, 20% top soil and 80% granite chip, and 100% granite chip. The predictions of each of their proposed models was compared with predictions from Crook and Ennos, (1993) model and Peltola and Karrameki, (1993) model. The predictions by Equation 2.30 F_{shear} (45, 45, 53, 45kN) was the closest to the Crook and Ennos, (1993) model (21, 27, 76, 28kN). Peltola and Karrameki, (1993) predicted the highest values of the three models (73, 81, 93,77kN). However, the model has not been validated using a dataset of real plant parameters.

Coder, (2010) completed a review of root strength and tree anchorage investigating several models on tree anchorage. Coder, (2010) discusses factors affecting tree root anchorage such as soil resistance, root strength, root resistance, root density and distribution and root plate.

Most of the models used regression analysis to correlate the variables. This resulted in correlations to the height and weight of the tree, and the root plate radius. One example of this is Coutts et al., (1999) who wrote about the tree root plate mass and the root plate radius to tree anchorage (Equation 2.33). Another example is Fourcaud et al., (2008) who reported on a possible relationship between root plate volume or mass and hinge distance for trees rotating about the edge of the root-soil plate (Equation 2.34). Neither of these models has been tested with data to understand whether they can make accurate predictions.

$$Coutts \ = \ (PlantWeight(kg))X \ (Root \ Plate \ Diameter(m)) \qquad 2.33$$

$$Fourcaud \ = \ (Root - Soil \ Mass \ (kg))X(Root \ Plate \ Diameter \ (m)) \qquad 2.34$$

Yan et al., (2016) used a probabilistic approach based on Bayesian inference to modelling (Zhang et al., 2004). Yan et al. (2016) used this technique to create a model that could use past measurements of anchorage strength combined with current measurements of important parameters to be able to predict anchorage strength. The method comprised:

- A database of vertical uproot resistance of shrubs was compiled using non-destructive techniques with above ground size parameters;
- Multiple regression analysis was used to find empirical models with different complexities;
- The Bayesian model class selection method was used to find the most plausible regression model;
- The uncertainty of the regression model coefficients and the credibility of the predictions were qualified;
- The selected models were used to predict the maximum vertical uproot resistance, P_{max} by only using the basal diameter and the height of the plant.

Yan et al., (2016) suggested that this approach could be a possible non-destructive method of predicting plant anchorage. Bayesian model class selection can be used to identify the most suitable empirical equation in a complicated system. This is because the model tries to balance the model complexity (robustness) and fitting ability (goodness-of-fit). Over-complicated models are penalised.

Finally, there is a need to review all the root anchorage models discussed previously in order to determine the parameters, which needed to be collected in the field and laboratory tests to allow a comparison of the accuracy of the different models. Model comparisons have been carried out in many studies, for example, Zhang and Wang, (2017) and Dong et al., (2015), where they investigated thermal conductivity in soils. Root anchorage models for trees have been reviewed by Coder (2010). However, this did not include determining the accuracy of the models for real plants.

The models were grouped based on the model technique, main advantages and disadvantages and the applicability (which plant root system the models were originally created for). This type of grouping gave an indication of the models that could be compared and the ease with which the variables could be measured. Concerning the modelling of root anchorage in wheat, oats and oilseed rape, the tree models may not be applicable because of the scale differences between the material properties and the root architecture. The models for submerged plants may also be difficult to apply due to the model requiring parameters that were difficult to measure, such as, species specific attachment coefficients for the surface of a root ball, and the difference in forces on submerged plants, for example, tidal currents. Finally, the model proposed by Yan et al., (2016) was not considered appropriate as the statistical approach

utilized in their work is outside the scope of the current research. Peltola and Kellomaki, (1993) and Moore, (2000) were not compared because the model required the maximum root anchorage force measured as part of the calculation. This would mean that the maximum root anchorage would have to be known prior to predicting anchorage.

Therefore, for wheat and oats, the models to be compared were the Crook and Ennos, (1993), Goodman, Crook and Ennos, (2001), Niklas, (1992), Rahardjo et al., (2009), Fourcaud et al., (2008) and Coutts et al., (1999) (Table 2.5). These models were chosen because they were developed for the plate root system, which represents wheat and oats and because the parameters were easy to obtain.

For oilseed rape, the tap rooted system was taken into consideration meaning that the Goodman et al., (2001) and Niklas, (1992) models were appropriate because the model assumes a correlation between root length, root diameter and soil resistance. Crook and Ennos, (1993) was also used even though it was only relating root diameter to anchorage resistance.

Table 2.5 Models to be compared in the present research.

Prediction	Model based on lodging risk model by Baker et al., (2015)	Comparison Models
Wheat and Oat Anchorage	Crook and Ennos, (1993)	Rahardjo et al., (2009) Goodman et al., (2001) Niklas, (1992) Fourcaud et al., (2008) Coutts et al., (1999)
Oilseed Rape Anchorage	Goodman et al., (2001)	Crook and Ennos, (1993) Niklas, (1992)
Soil Strength	Baker et al., (1998)	

2.5 Summary and Identified Gaps in the Literature Review

This section discussed in-depth the background to the lodging risk method and equations used within different models to predict soil strength and root failure moments in wheat and oilseed rape. It was noted that wheat and oats are considered to have the same failure mechanism while oilseed rape has a different failure mechanism. The section also discussed research into root anchorage mechanics of other plants, which provided relationships and equations that could be compared to the Crook and Ennos, (1993) model used by Baker et al., (2014) to understand its accuracy. A dataset would need to be collected to carry out the test. Finally, this section discussed some of the advantages and disadvantages of methods used to measure lodging resistance in the laboratory and it was discovered that there is very little research on the root anchorage of oats.

- There is uncertainty around the accuracy of the prediction of the current root failure models developed for wheat and oilseed rape. Models were not validated, or the used datasets were small.
- It is unclear whether other root anchorage models developed for non-crop plants could be applied to wheat, oats and oilseed rape.
  - Models have been developed before and after the model by Crook and Ennos, (1993) that could be used to predict lodging resistance; however, no dataset exist that contains all the measurements needed for all of these models to be tested.
  - Some of the parameters for these root failure models may be difficult to measure considering these models are to be used by practitioners and farmers, who will need to be able to measure the parameters themselves, essentially creating their own datasets to predict root and stem lodging.
- Research has been limited on the load-displacement curves for wheat and oilseed rape.
  - However, the curves were not recorded for different soil types and different artificial root types, thus providing limited information.
- Field lodging testing was conducted using different methods and different configurations of equipment, producing only maximum values of lodging resistance.

- Laboratory testing requires a large Instron machine. Ideally, a machine should be used which could be used both in the laboratory and in the field.
- Artificial roots used by researchers were not representative of real roots because they were polythene or steel artificial root models. Materials and architectures closer to the root strengths could be used as well as different artificial root configurations.
- The soil strength models were only validated using two very small datasets in which some data was estimated and only a few data were actually measured, thus providing limitations with respect to the validation of the models.

3 Methodology: Development of field investigation, laboratory experiments and preliminary results.

3.1 Introduction

As identified in the literature review, to date several relationships have been suggested to determine the risk of lodging based on root anchorage failure. Many of these models have not been validated in practice, only validated on small samples or been developed for non-cereal crops. Thus, there is a need to evaluate existing models and potentially develop new models. This is done using data collected both from the field and also controlled laboratory experiments.

This chapter outlines the methods of investigation and test procedures used in this research for assessing the current root anchorage models. This includes standard geotechnical techniques for collecting soil samples for detailed soil characterisation. Methods for root measurements were related to past studies, as standard methods were not available.

This chapter begins with the selection of the root anchorage parameters used in the root anchorage models that will be compared in the Results chapter. Section 2.2 describes the field investigation, including site selection and descriptions (Section 3.2.1), field soil characterisations including results over two years of soil investigations (Section 3.2.2), field anchorage failure measurements including the development of the method for testing anchorage failure, development of a new lodging instrument and results of the plant measurements (Section 3.2.3). This is followed by the laboratory experiments on artificial roots which includes the determination of the properties of soils to be tested, development

of artificial root structures to represent wheat and oilseed rape, the method for testing the anchorage failure of the artificial roots and finally a section is dedicated to assessing the failure mechanisms observed in the laboratory experiments.

3.2 Selection of root anchorage parameters from the root anchorage models that will be compared

A survey of the literature found that a dataset containing measurements for the crops of interest, i.e. wheat, oats and oilseed rape, was not available; therefore, a dataset had to be collected. A method of measurement was planned for each variable identified in Table 3.1 involving either field or laboratory measurements.

Table 3.1 The input variables required for the selected anchorage models.

Soil	Plant	Root	Weather
Clay Content	Height of Centre of Gravity	Anchorage Resistance	Rainfall Data
Sand Content	Plant Height	Root Area	Wind Speed Data
Silt Content	Stem Diameter	Root Circumference	Soil Moisture Deficit
Unit Weight of Soil	Plant Wet Weight	Root Diameter	Evaporation Rate
Internal Friction Angle		Root Length	
Particle Density of Soil		Root Number	
Water Content at Field Capacity		Root Plate Diameter	
Water Content at Permanent Wilting Point		Root Plate Volume	
Shear Strength		Root Surface Area	
Bulk Density		Root Shear Strength	
Visual Score		Root Slip Strength	
		Root Tensile Strength	
		Root-Soil Plate Mass	
		Root Plate Depth	

3.3   Field Investigation

In this section, a suitable field methodology to obtain all soil and plant parameters (Table 3.1) for the root-anchorage models is developed. This was done because there was no suitable dataset of root failure moments and corresponding plant, root and soil measurements available. Where appropriate, standard geotechnical testing according to BSI, (2016) was employed to ensure repeatability.

3.3.1   Field Site Selection and Description

Field data was collected at Teagasc (Agriculture and Food Development Authority) in Oak Park, Carlow, Ireland (Figure 3.1) as they funded the research. Data was collected over three periods in the summer of 2016, the summer of 2017 and the summer of 2018.
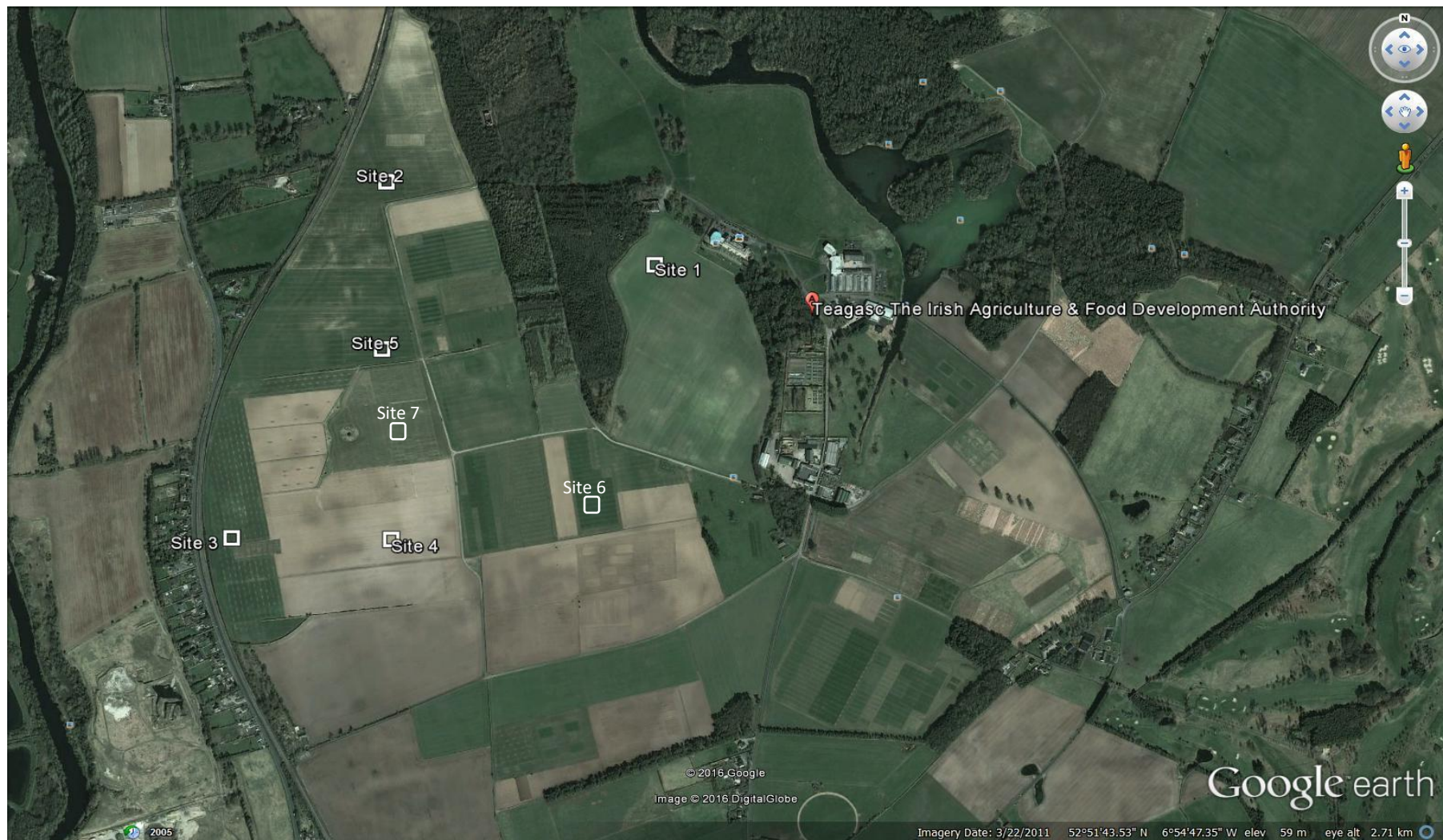
Figure 3.1 A Google Earth image of site locations at Teagasc, Oak Park research (Google Earth, 2016).

In 2016, the purpose of the field experiment was to complete preliminary soil descriptions of different fields, determine the differences in lodging resistance or anchorage failure of different varieties of winter wheat and winter oat crops present in Oak Park. Moreover, it provided an opportunity to test and evaluate the repeatability of the lodging instrument.

The Oak Park site is split into several fields. Every year these fields are allocated to different crop trials by the Teagasc researchers. The following year the trials are rotated onto different fields. The different agronomic treatments used on the plots dictated which plots were chosen for the field experiments in 2016. Seeding rate, sowing date, PGR application and nitrogen application are agronomic treatments that affect lodging resistance (Berry et al., 2000; Berry et al., 2003), therefore, plots were chosen where these treatments had been used to manipulate the winter wheat and winter oat crops. The crops, varieties and plots selected for testing in the 2016 study are described in Table 3.2. All of the wheat varieties were semi-dwarf, which are regularly used by farmers. Lodging resistance testing was completed on winter wheat and winter oats (Figure 3.1: Sites 2, 3 and 4).

Table 3.2 Plots chosen for investigation in the wheat and oat fields in 2017

Crop Type	Variety	Agronomic Treatments
Winter Wheat	Rockefeller	Seeding rates, Sowing dates
	Cordiale	Seeding rates, Sowing dates
	JB Diego	PGR application, nitrogen application
	Cordiale	PGR application, nitrogen application
	Stigg	PGR application, nitrogen application
Winter Oats	Bara	Seeding rates, nitrogen application, PGR application

In 2017, the purpose of the field data collection was to collect measurements and samples for the variables of the models selected to be compared in this research. Plant sampling, soil sampling and anchorage testing were completed between 7th June and the 15th of July 2017,

which is the period of grain filling, the time period the crop is most likely to lodge (Berry et al., 2000, Berry et al., 2005, Baker et al., 2014). Four varieties of wheat were planted specifically for this research, on the Coach House field (Figure 3.1: Site 1). Four wheat cultivars were chosen based on the varieties sampled in 2016. Oats were grown at a new site in Knockbeg, for Teagasc research, not specifically for this research project. However, sampling was allowed at this site. The Knockbeg site was planted with 2 varieties of oats, Husky and Barra. Barra was chosen for the plant and soil characterizations and lodging experiments as this was used in 2016 as well. Oilseed rape was grown at Site 5 (Figure 3.1). Two plots were chosen. There was no variation in treatments.

It should be noted that all of the crops are grown in randomized block designs. Randomized block design is an experimental technique used, to investigate the results of different crop husbandry treatments (Berry et al., 2000). For example, the wheat crop was separated into three blocks. Block 1 was separated into 16 unique plots with different agronomic treatments. Blocks 2 and 3 contain repeats of the 16 plots arranged randomly. Of the 16 plots, 8 were chosen because of the combination of treatments applied to wheat in each of these plots. Plots 3, 4, had a variety of wheat called Cordiale planted. Plot 3 had a low seeding rate (160g/plot) and Plot 4 had a high seeding rate (480g/plot). The difference in seeding would produce a difference in plant root growth and hence a difference in lodging resistance. Berry et al., (2000) found that seeding rate caused the largest difference in lodging resistance as higher seeding rates reduce the amount of space each plant has to grow and spread the root system, therefore limiting the anchorage resistance. Treatments used in the 2017 study are shown in Table 3.3.

Table 3.3 Plot numbers and treatments for each of the plots.

Crop Type	Variety	Plot Number	Treatments
Wheat (W)	Cordiale	3	Low seeding rate
	Cordiale	4	High seeding rate
	JB Diego	7	Low seeding rate
	JB Diego	8	High seeding rate
	Rockerfeller	11	Low seeding rate
	Rockerfeller	12	High seeding rate
	Stigg	15	Low seeding rate
	Stigg	16	High seeding rate
Oats (KB)	Barra	1	High seeding rate, low nitrogen
	Barra	2	High seeding rate, high nitrogen
	Barra	3	Low seeding rate, low nitrogen
	Barra	4	Low seeding rate, high nitrogen

In 2018, a small dataset was collected to test the newly created root anchorage model. Two new sites were added, Figure 3.1: Site 6 and Site 7. Wheat, oats and oilseed rape were sampled from Site 4, Site 6 and Site 7 respectively. The same variety and treatment were chosen for this dataset, to limit variability of plant measurements.

3.3.2   Field Soil Characterisation

After choosing the sites in 2016, the soils at each site were investigated. According to the Irish Soils Information System (Environmental Protection Agency, 2014), the Oak Park site is situated on the Elton soil association, which is described as fine loamy drift with limestones. This falls within the subgroup of typical luvisols. Within the Elton soil association, two soil series are in the Carlow County, which are the Kellistown and Newtown series. The Kellistown series is described as a coarse loamy drift with limestones. The top 18cm is described as a sandy loam (57% sand, 29% silt and 14% clay), granular, fine structure and friable consistency.

It also contains 0.23% nitrogen, 2.2% organic carbon and has a pH of 5.60 (Environmental Protection Agency, 2014). The Newtown series has a similar description. The top 18 cm is described as an organic sandy loam (57% sand, 29% silt and 14% clay) with a weak granular, fine structure and friable consistency. It also contains 0.23% nitrogen, 2.2% organic carbon and has a pH of 5.60 (Environmental Protection Agency, 2014).

The records from the Irish Soils Information System (Environmental Protection Agency, 2014), give a background into the parent material of the soils. However, the soil map was designed to be used at a scale of 1:250,000, which was too large to derive specific information about the soil properties at Oak Park. Also, although the Kellistown and Newtown soil series are different, they have almost the same description. Therefore, an in-depth investigation into the soil at the near surface (top 100mm corresponding to the depth of the roots) was undertaken in specific fields and plots in order to get more accurate information.

Soil descriptions were completed on site using the BS5930 method for soil and rock description (BSI, 2016). They suggest large particles such as pebbles and cobbles (1 mm-100 mm) were present in the soil matrix. Some of the roots of the crops were growing around these larger particles. The presence of pebbles and cobbles proved to be a limiting factor later in the soil characterisation when measuring the bulk density and shear strength using the shear vane. The presence of particle sizes as large as pebbles caused difficulty when extracting cores for bulk density.

When small areas were dug, the soil matrix could be described as humus according to engineering soil descriptions as provided by Barnes, (2016). Humus is described as having plant remains and living organisms combined with inorganic constituents (Barnes, 2016). It is

also called topsoil. However, the soil classification was focused on the inorganic components of the topsoil as the proportion of organic to inorganic was low. The description can be seen in Table 3.4.

Site No.	Field Name and Location	Crop Type	Soil Description (BSI, 2016)	Picture
1	Church Field 52°51'55.35"N 6°54'55.51"W	Oilseed Rape	Firm, low to medium strength, low plasticity, light yellowish brown, clayey, very sandy, SILT, with sub-rounded gravel	
2	Malone's Field 52°52'1.32"N 6°55'26.14"W	Winter Oats	Firm, low strength, low plasticity, dark reddish brown grey, clayey, SILT with angular and sub-rounded gravel and cobbles	
3	Big Bull Park (top) 52°51'35.21"N 6°55'43.70"W	Winter Wheat	Soft, low strength, low plasticity, light yellowish brown, clayey SILT with angular to sub-rounded gravel and cobbles	
4	Big Bull Park (bottom) 52°51'35.09"N 6°55'25.56"W	Winter Wheat	Firm, low to medium strength, low plasticity, yellowish brown, sandy SILT with rounded to angular, fine to coarse gravel	
5	Big Bull Park (right) 52°51'49.04"N 6°55'26.59"W	Winter Barley	Soft, low strength, low plasticity greyish brown sandy, clayey SILT with angular to sub-rounded, fine to coarse gravel	

Table 3.4 Soil description completed during the field investigation in 2016. Descriptions completed according to the BS 5930 (BSI, 2016).

In 2016, three soil samples per site were taken at this initial stage to understand the density of the soil as well as accompanying characteristics like the void ratio, porosity, degree of saturation and air content. These characteristics were calculated using the phase equations from (Knappett and Craig, 2012) (shown in Table 3.5). These results show that the soil was partially saturated at the time of sampling. Also, the low density and high porosity indicate that the soil may not have a high shear strength as there is a large number of voids between the soil particles.

Table 3.5 Average of three samples, water content and bulk density measurements with additional calculations. The bulk density was calculated using the BSI, (2016), completed in 2016

Site No.	Water Content (%)	Bulk Density (kg/m³)	Dry Density (kg/m³)	Void Ratio	Porosity (%)	Degree of Saturation (%)	Air Content (%)
1	21	1632	1349	0.991	50	58	21
2	22	1422	1169	0.966	49	12	43
3	19	1601	1342	1.00	50	52	24
4	16	1562	1343	0.995	50	44	28
5	19	1619	1360	0.972	49	53	23

Although, the soil investigation in 2016 gave some ideas about the soil formations and possible soil fractions, specific values were needed to be able to compare the root anchorage models. This required a more detailed soil characterisation to obtain these values. In 2017, soils at the three sites chosen for the wheat, oat and oilseed crops, were sampled. These crops were situated on the Coach House (Site 1), Big Bull Park (Site 5) and Knockbeg fields. Two samples were taken from the wheat and oilseed fields (Site 1 and Site 5) because the areas in which the crops needed for plant sampling were in two separate areas of the field (Table 3.6). In 2018, 1 soil sample was taken from each site; Sites 4, 6 and 7.

Table 3.6 The sites, crops and number of samples for the 2017 and 2018 field investigations.

Site	Crop	Sampling	Year
1	Wheat (W)	2 soil sample pits (W1 and W2)	2017
5	Oilseed rape (O)	2 soil sample pits (O1 and O2)	
Knockbeg	Oats (KB)	1 soil sample pit (KB)	
4	Wheat	1 soil sample pit	2018
6	Oats	1 soil sample pit	
7	Oilseed	1 soil sample pit	

Table 3.7 shows the soil test, number of samples per site, amounts and procedure used for each test. The number of soil samples per site was in line with the standard volume of soil required by BSI, (2016). However, the number of samples was restricted by transporting soils from Ireland to the UK.

Soil testing included particle size distribution, soil water characteristic curve for drying, x-ray diffraction, the plasticity index and the undrained shear strength using a 100mm shear box using a modified method from the BSI, (2016). All samples were taken at a depth of 50-100mm below the soil surface, reflecting the rooting depth for the cereal crops.

In 2018, all of the tests were completed except compaction and soil water characteristic curve.

Table 3.7 Soil Sampling and testing in 2017 and 2018.

Soil Test	Number of Samples per site	Amount of soil needed per test, Testing Depth	Procedure
Particle Size Distribution	2	1kg, 50mm	Wet Sieving (BS 1377: Part 2: 2016) Dry Sieving (BS1377: Part 2: 2016: 9.3)
Compaction	1	6kg, 50mm	Light Compaction Test (2.5kg rammer method) (BS 1377: Part 4: 2016: 3.3)
Soil Water Characteristic Curve	Two cores for Hyprop apparatus + 1 core for WP4	-	Procedure taken from the Hyprop Manual
Plasticity Index	2	500g, 50mm	Liquid and Plastic Limit (BS1377: Part 2: 2016: 4.3, 5.3)
Shear strength	3	500g, 50mm	Small Shear box: Rapid test (BS1377: Part 7: 2016: 4)

3.3.2.1 Particle size distribution

The particle size distribution, compaction and plasticity index, were all completed according to the British Standard for soil testing, BSI, (2016) to ensure repeatability. After inspecting the samples, it was found that they were composed of fine soil fractions. This meant that before the dry sieving procedure could be used, the samples had to be prepared for wet sieving according to BSI, (2016). After separation via the wet sieving method, any particles greater than 63 µm were dried in the oven in preparation for the dry sieving procedure. The remaining sample passing through the 63µm sieve was tested using the sedimentation procedure using the Hydrometer method. This method requires the sample passing the 63µm sieve to be mixed with a dispersant to help separate the clay and silt particles.

The particle size distributions for all the samples in the present research were very similar as shown in Figure 3.2a. Figure 3.2b shows the sedimentation tests. The sedimentation test was

repeated twice as the results of the tests were very similar (within 5% of each other). From the particle size distribution and the sedimentation analyses, the soils from 2017 and 2018 were classified as sandy Silts, which agrees with the descriptions in 2016. The clay content for all of the samples was significantly lower than the values given in Baker et al., (1998), who reported the lowest clay content at 20% compared to this study, where the lowest clay content was 6.7%. This is not surprising as the samples were taken from different sites, but this difference might be important when assessing the lodging model developed by Baker et al., (1998).

X-ray diffraction was also completed on the samples by the Chemistry department of the University of Birmingham in order to measure the mineralogy of the soil. The mineralogy of the soil was found to consist of quartz (silicate mineral), SiO_4. Silicate is quartz, therefore, the particle density was taken to be 2.65 for the soils at Oak Park (Barnes, 2016).
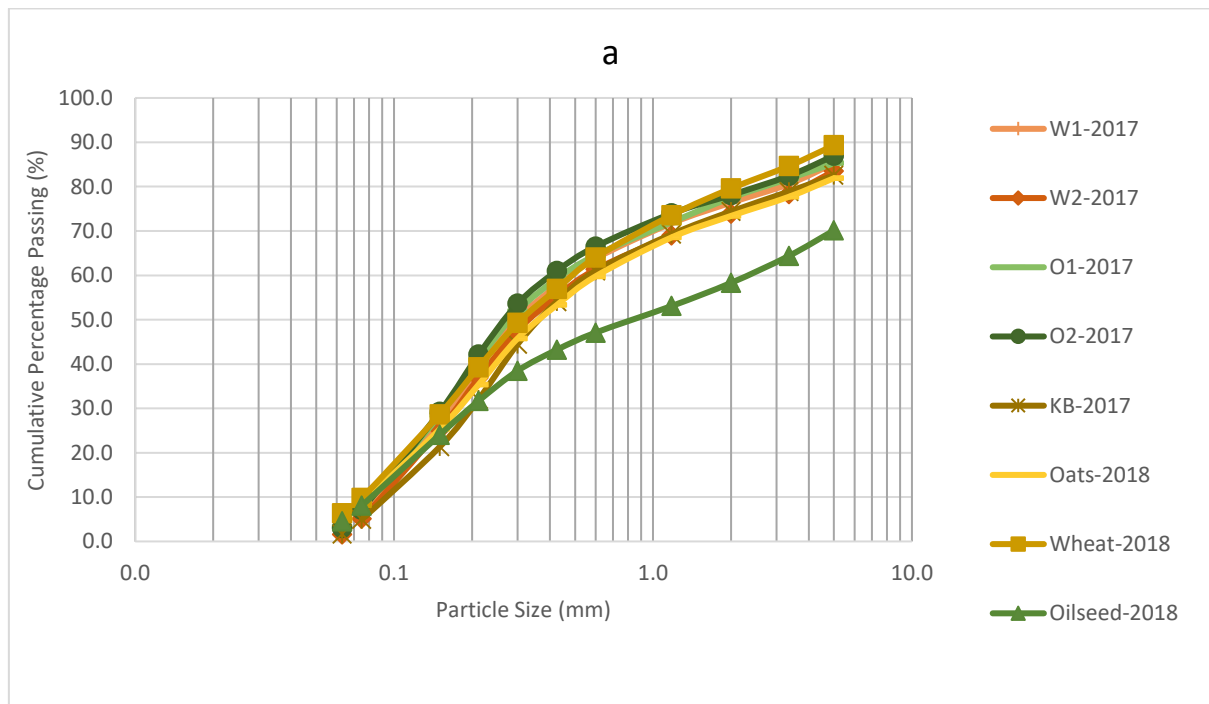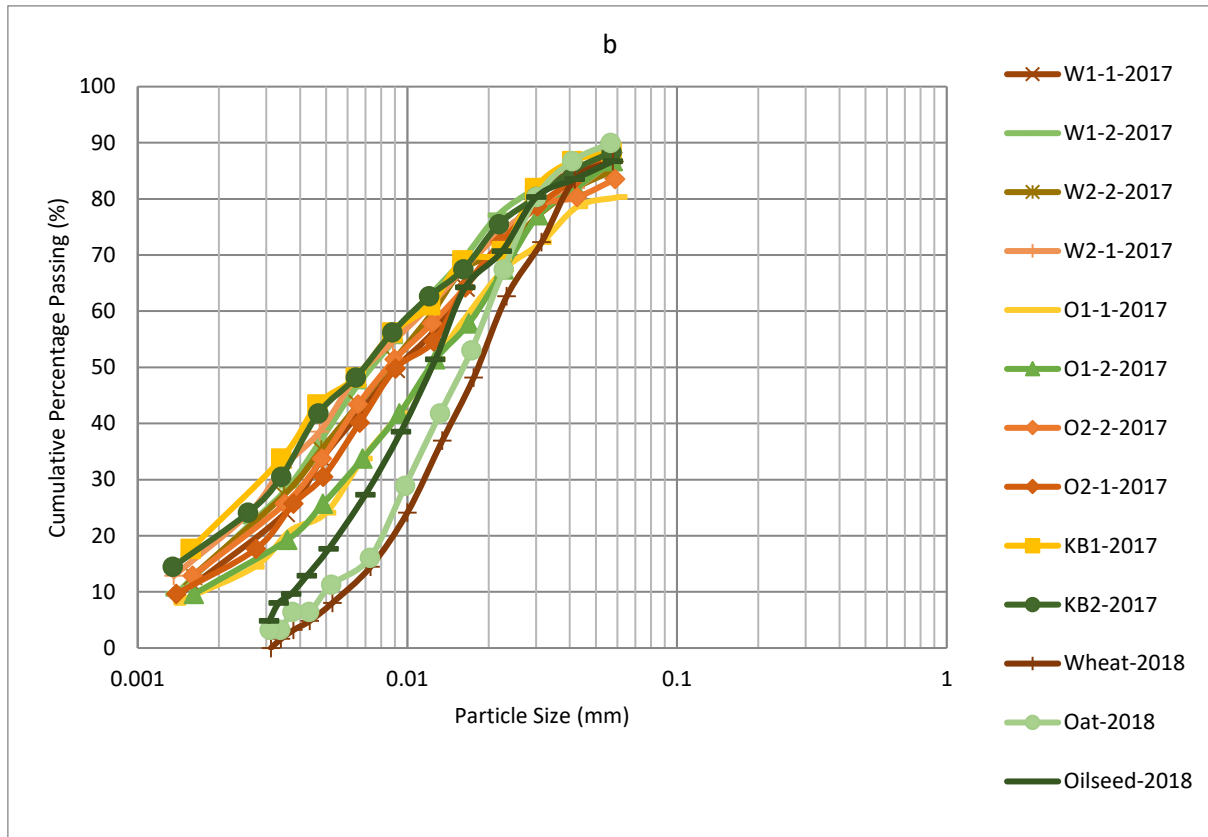
Figure 3.2 (a) The particle size distribution for 2017 (Wheat field W1, W2, Oilseed rape field-O1, O2, Oats field-KB1, KB2)) and Wheat, Oats and Oilseed were samples from 2018 (b) sedimentation results for the soils collected from Oak Park, 1-1 and 1-2 are repeated tests of the same sample.

3.3.2.2 Compaction

The test was completed according to BSI, (2016). The light compaction procedure was used on the five soil samples collected. The light compaction test produces lower densities than heavy compaction tests by reducing the compaction energy used on the soil samples. Number of soil layers is reduced from 5 layers to 3 layers, the weight of the compaction hammer is reduced from 5kg to 2.5 kg and the height the hammer is dropped is reduced from 450mm to 310mm. The number of blows was reduced from the standard 27 blows to 10 blows per layer in order to achieve a lower density closer to the density encountered in the field (dry densities measured in 2017 for wheat ranged between 1013-1489kg/m^3, for oats ranged between 893-1528 kg/m^3 and for oilseed rape ranged between 1066-1299 kg/m^3).

The results for the compaction tests of all sites are shown in Figure 3.3. The optimum water contents were between 20.5% and 25.7%. It found that the soil from the oats field at Knockbeg (KB) had the highest optimum density and the lowest optimum water content (Figure 3.3). The compaction test was used as a comparison for the field density tests. The bulk density and dry density measured in the field were calculated using BSI, (2016) and the results are shown in Figure 3.3, Table 3.12 and Table 3.13. The dry density was higher using the modified compaction methodology but still within the range of the densities measured in the field mentioned above.
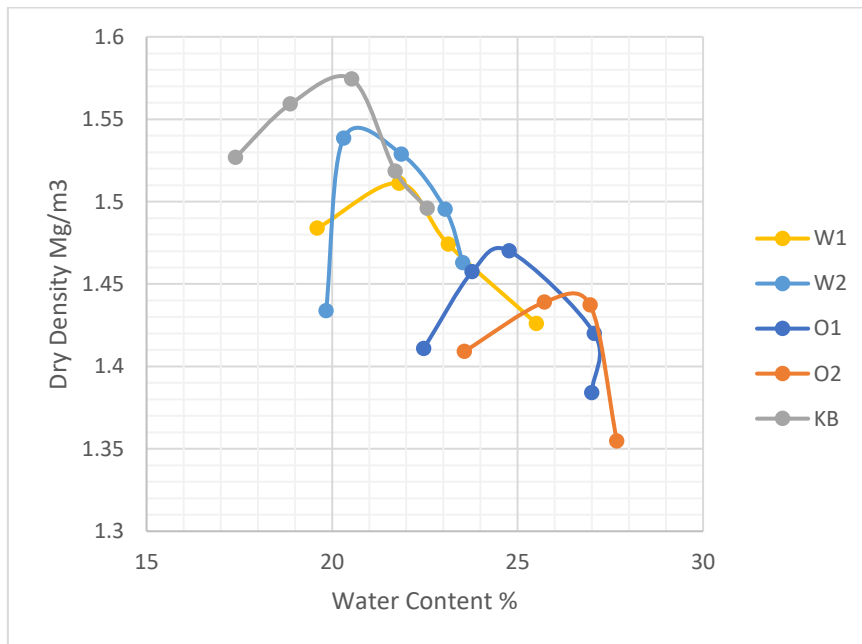
Figure 3.3 The optimum density of the soil from the five sites in 2017.

3.3.2.3 Plasticity Index

The liquid and plastic limits were measured using BSI, (2016). Samples were prepared in the same method as the wet sieved samples in the particle size distribution methodology. The soil was dried to a point where it could be manipulated easily with a spatula. The liquid limit test was completed while a small sample was allowed to dry further for the plastic limit tests. After

testing the samples were dried in an oven at 105° for 24 hours. The water contents were recorded for the liquid and plastic limits and the plasticity index was calculated. A plasticity chart was plotted.
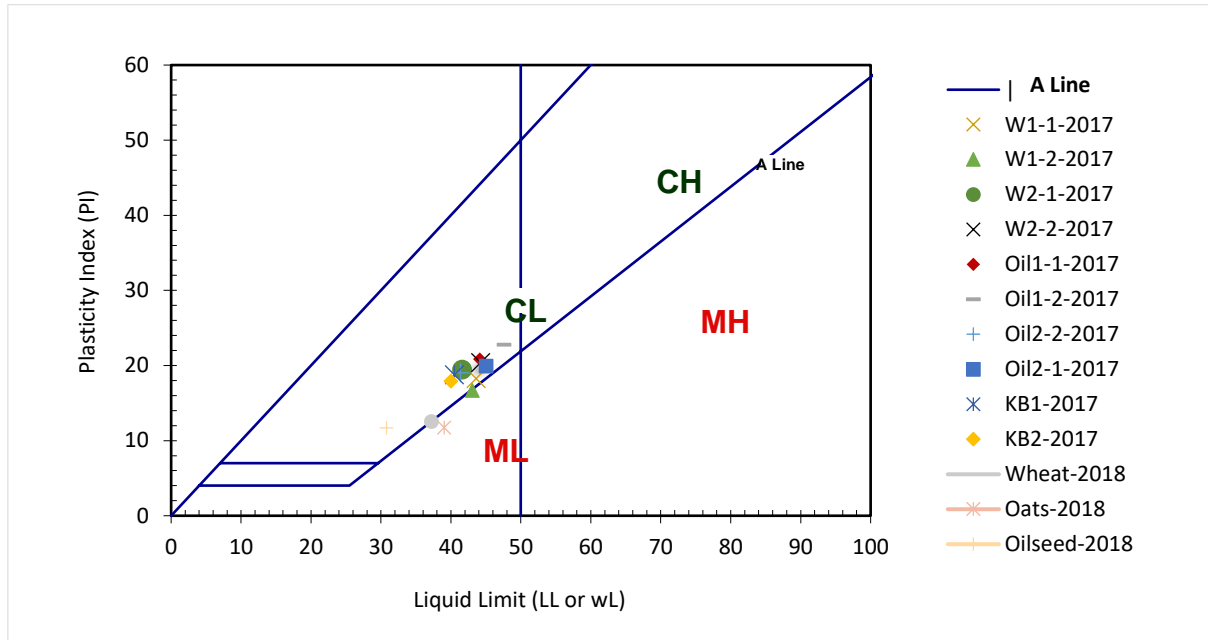
Figure 3.4. The classification of the soils using the plasticity chart.

Figure 3.4 shows the results for the plasticity index test. The fine fractions of the soil samples from 2017, can be classified as intermediate plasticity clays. Wheat, Oats and Oilseed samples from 2018 had slightly lower plastcity indices than the 2017 samples. The Oat sample could be classified as intermediate plasticity silt. Plasticity describes the extent to which a soil can be permanently deformed without rupturing (Barnes, 2016). The plasticity of soil can affect its behaviour when being deformed, as occurs during lodging. It is useful to know the plastic and liquid limits because they give an indication of the water content at which the behaviour and the strength of the soil change. The plastic limit is the point at which a soil goes from solid to mouldable and there is an accompanying reduction in stiffness. This limit may be the most important as lodging may occur at this water content. The soils at the three sites in 2017 had

plastic limits that ranged from 21.7% to 26.4%, so at this water content the soil becomes softer, beginning to show plastic behaviour. This water content was also close to the optimum water contents for the density of the soil shown in Section 3.3.2.2.

3.3.2.4 Soil Water Characteristic Curve

The soil water characteristic curve is defined as the relationship between the water content and the suction of the soil. The soil water characteristic curve was used to determine the water content at wilting point and field capacity. The curve was measured using the Hyprop apparatus for matric suctions between 0.001kPa and 10kPa. The Hyprop is a fully automated measuring and evaluation system to determine the hydraulic properties of soil samples. A ring with an 80mm inside diameter was inserted into the soil in the field. The ring and soil were excavated and the cylindrical soil sample sealed on both sides. On returning to the laboratory the Hyprop apparatus (Figure 3.5) and samples were prepared.
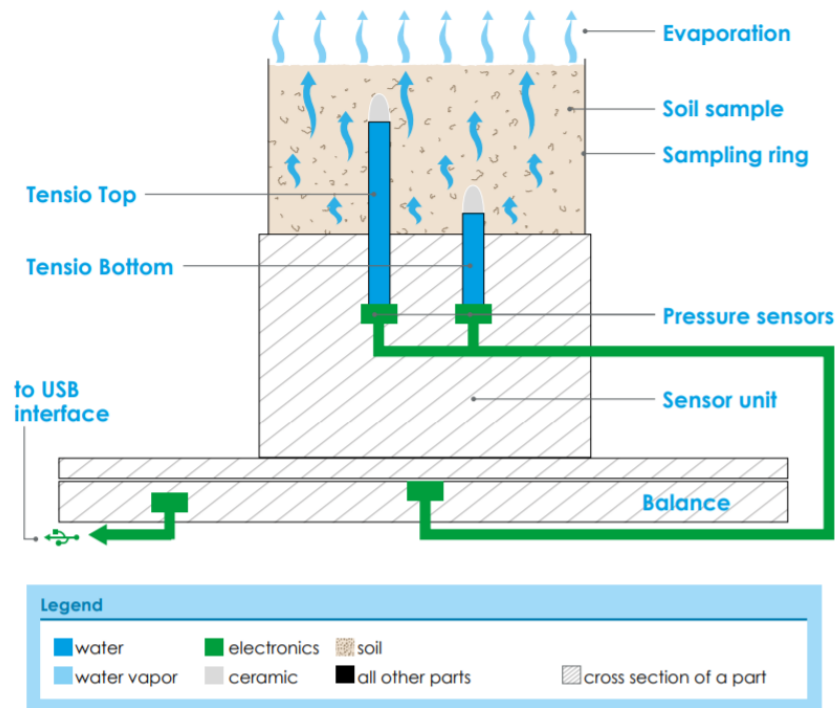
Figure 3.5 A diagram showing the Hyprop testing unit (image taken from the Hyprop Manual, (2015)).

The Hyprop measures the water tension at two levels of a sample using tension shafts by transducing the matrix potentials of the soil samples through porous ceramic tips. The shafts are like capillaries in the soil sample and are connected to pressure sensors in the main unit of the Hyprop. The ceramic tips have contact with soil water, and as the water dries and the matrix potential increases the pressure sensors respond. For this to work the water-filled shafts cannot have any air bubbles or dissolved air within them. Therefore, the tension shafts and the sensor unit need to be degassed completely before the testing begins by filling them with deaired water. After the Hyprop sensor unit and the tension shafts were deaired, the tension shafts were carefully connected to the Hyprop sensor and tested for correct connections. Once this was completed the soil samples had to be added. 3mm holes (the same size as each tension shaft) were drilled into the saturated soil sample using the tension shaft auger. The soil sample was then fitted onto the shafts by lining up the respective holes and

the perforated plastic cap removed. More deaired water was added to the sample to ensure it was saturated. The completely assembled Hyprop was then placed on the scale and connected to a computer. Initial measurements on the sample (ring weight) and sample identifiers were recorded in the software before commencing the measurements. These were completed when the readings had dropped to zero. The sample was removed from the Hyprop, and the dry weight was determined after drying in the oven at 105°C for 24 hours.

The WP4C is a soil water potential lab apparatus used to measure matric suctions between 10kPa and 100,000kPa in this research. The WP4C measures the driest values of the soil water characteristic curve. Samples for the WP4C testing were collected in 38 mm x 150mm cylinders because the instrument uses sample cups 38mm in diameter. The cylinders were pressed into the ground, in a similar way to the bulk density and Hyprop samples. The entire sample was then extruded in the laboratory. 16 soil samples were weighed. The samples were then lightly compacted with a miniature tamp diameter 36mm from a height of 2cm above the sample to 4 mm in height to achieve the average density of the soil measured in the fields (1444, 1485, 1579kg/m^3). This procedure was used to ensure repeatability of the sample preparation process. Water was added to saturate the samples. They were then placed in an incubator at 25°C. Before each test, the samples were allowed to dry sequentially so that the first sample was the wettest and the final sample was driest, so each sample was left in the incubator for 5 minutes more than the last (5, 10, 15, 20, 25, 30, 35, 40 until 75 minutes). This method was repeated for each of the five soil cores taken from the field during sampling.

The WP4C was calibrated before each use. The samples were measured by simply removing one from the incubator, placing the tin in the WP4C and waiting for a reading. All readings were recorded by the WP4C software.
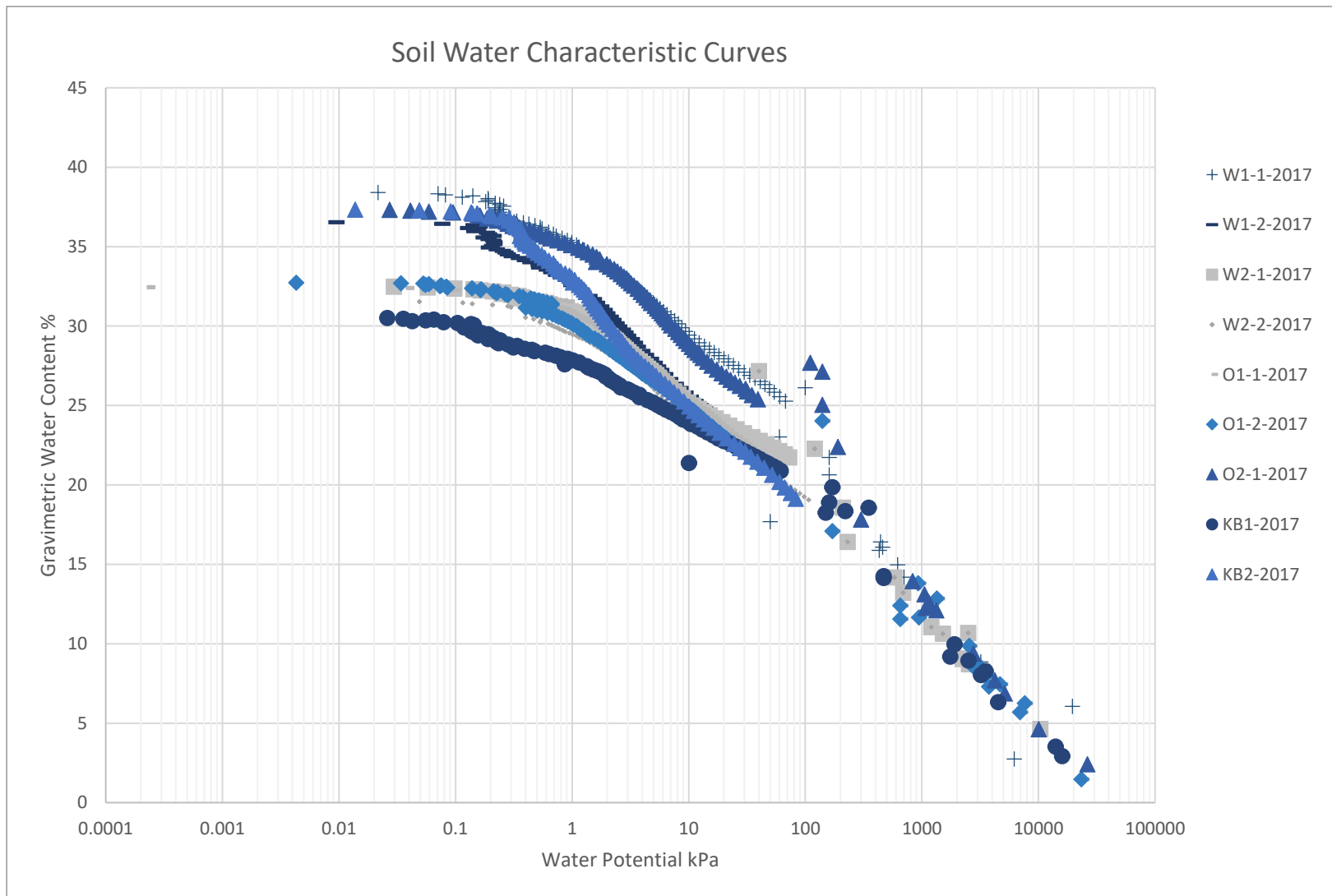
Figure 3.6 The Soil Water Characteristic curves for the sites studied in 2017, showing combined results from the Hyprop and the WP4C apparatus.

Figure 3.6 shows the soil water characteristic curves. The curves fall between silty and sandy

soils in the idealised curves suggested by Fredlund and Xing, (1994) (Figure 3.7), which agrees

with the soil particle size distribution and plasticity index testing discussed previously.
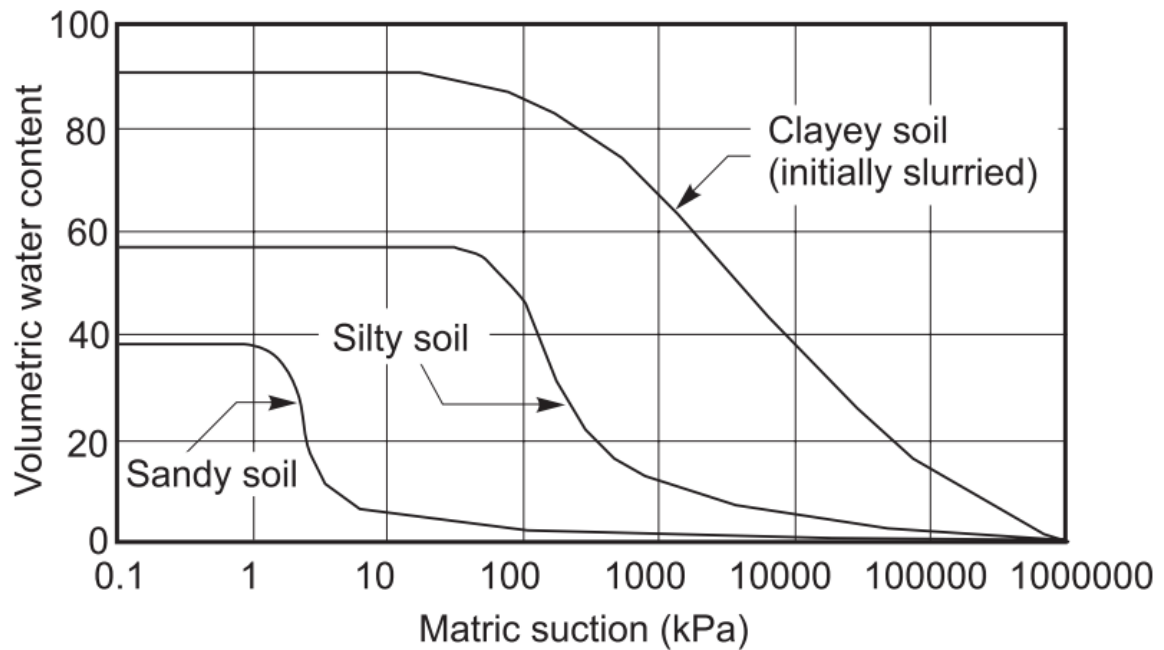
Figure 3.7 Soil water characteristic curves for a sandy soil, a silty soil and a clayey soil (Fredlund and Xing, 1994).

For the soils collected in the field, the water contents at field capacity and wilting point were

23% and 12%, while the plastic limit was 25% and the liquid limit was 44.1%. This means that

at field capacity when the soil is supposed to be at its weakest point according to the soil

strength model (Baker et., 1998), the soil is in a softer, plastic state. In terms of soil mechanics,

the increasing degree of saturation of the soil would correspond to a decrease in matric

suction. As the matric suction decreases, the shear strength of the soil also decreases. This

reduction in strength could be associated with a reduction in anchorage strength.

3.3.2.5 Soil Shear Strength

The purpose of this experiment was to determine the undrained shear strength for the soils associated with the three agricultural fields at the Oak Park site. Two series of measurements were used, the hand vane shear tests in the field and the quick direct shear test. The hand vane shear test was used as part of the field anchorage failure measurements, detailed in Section 3.3.3, where, shear strength was tested around the roots being lodged. The quick direct shear test was completed in the laboratory on soil samples collected from each of the three fields in 2017 and 2018.

The quick direct shear test was used for ease of setup and the nature of the soil sample being tested (Head, 2006). Approximately 10kg soil samples were collected from Oak Park from the three sites previously described, i.e. the wheat field, the oat field and the oilseed rape field. The wheat field and oilseed rape fields were split into W1 and W2 and O1 and O2 because of the different locations of these fields. The oat field was labelled as KB and was not split because this field was considered more uniform according to Teagasc. 1.5kg of disturbed soil samples were used for this experiment. The samples were split into three soil samples, one for each normal stress in this test. After the sample had been tested, the soil was removed and retested. The weight of each sample for the test was calculated from the average bulk density measured in the field and the volume of the shear box (100 mm square), i.e. 144.4g for wheat, 157.9g for oats and 148.5g for oilseed rape. Samples were prepared at 10% water content at wilting point. The water content was increased to 15% to understand the change in strength at water contents between wilting point and field capacity. Preparing partially saturated samples, at 10% and 15% water content, will affect the final shear strength

properties, giving the effective internal friction angles at the given water content. Therefore, this will provide the effective angle of friction at field capacity and wilting point.

The 100mm shear box was chosen because this allowed a sample thickness of 1 cm, which was suitable for the maximum particle size within the samples (2mm) (Head, 2006). The normal stress was chosen to simulate the stress near the surface of the soil (less than 1m depth), and so reflect the rooting depth of the plants. The normal stress levels were therefore relatively small in these tests, i.e. $1.4kN/m^2$, $11.4kN/m^2$ and $22.4kN/m^2$. These normal stresses were used for all of the samples. The unit weights for all of the field varied from $10.72kN/m^3$ to $18.88kN/m^3$ at a depth of 50mm. Therefore, this was an acceptable range of normal stresses. These stresses are much lower than the stress levels normally used in this type of test for geotechnical projects and hence the lowest normal stress was achieved by modifying the test. The test was conducted without any weight hanger, although the vertical dial gauge was placed on the top platen as normal.

The samples were prepared according to BSI (2016). The samples were prepared in the shear box at the chosen water content by separating a sample into three even layers. One-third of the sample was poured into the assembled shear box and compacted using a tamper (600g-50mm falling height) with ten blows and the subsequent layers added and compacted in the same way. The height of the final sample in the shear box was measured and the final stages of assembly completed. The fixing screws were removed and the platen placed on top of the soil sample, the top section of the box was raised off of the sample using the adjustment screws, the dial gauges were adjusted, and the machine was started.

Measurements were taken at intervals of 0.002 divisions on the load ring dial gauge. The tests were completed in 7-10mins. Five initial tests were completed to understand better aspects of the methodology (i.e. the shear rate and the normal stress) and the subsequent analysis (i.e. selecting the failure point, the residual stress and observing the shape of the graph).

Initial tests were completed at different rates, 0.5mm/min, 1mm/min and 2mm/min based on Head, (2006) (Appendix A1). However, 0.5mm/min was chosen because it was closer to the rate of testing for the lodging instrument. Initial tests were difficult to interpret, as there was no clear failure point in the data (change from linear elastic behaviour to plastic behaviour). The shear stress was found to continue increasing until the end of the test. The shear strength was determined by observing the vertical displacement. The vertical displacement measurements of the top platen, i.e. an indication of volumetric strain, indicated a change in shear strength (as the maximum shear strength is associated with the maximum rate of expansion or dilation of the sample (Barnes, 2016)). If this proved difficult (for example, the 1.4kN/m^2 tests), then a horizontal displacement of 1.5mm was chosen as this was the point where change in volumetric strain was observed in multiple samples. Although the vertical movements had variable magnitudes in the tests, the point of change was similar in each test. Overall, this testing aimed to gain values of the shear strength parameters for low-density soils under low stress levels for use in the subsequent predictive models of root anchorage.

Figure 3.8, Figure 3.9 show the results of the shear box testing on samples in taken in the 2017 soil collection. The samples did not show brittle failure but showed two phases of elastic behaviour; an initial steep section followed by a shallow section. The vertical displacement curves showed whether the sample was expanding (dilation) or contracting. Samples at lower

normal stress ($1.4kN/m^2$) showed no vertical movement or very small vertical movement 0.046mm (kb 15% water content). This may be because of the low confining stress and the density of the sample when it was sheared. When under low confining stress the soil particles would be allowed to move or collapse over each other and reduce the volumetric size if the soil was loosely packed in the shear box apparatus. This did not happen because the density of the sample was high enough for the samples to show no volume change. Therefore, the shear strength required to shear the sample was only the shear strength required to overcome small inter-particle friction and the apparent cohesion effects (the surface tension effects in partially saturated materials).

Samples under higher vertical stresses ($11.4kN/m^2$) showed dilatancy. Some of the abnormalities in the results may be a result of larger particles in the particle size distribution having a disproportionate effect on the soil behaviour. The internal friction angles and apparent cohesion values are shown in Table 3.8 and Table 3.9. Appendix B1 shows the results for soil samples W2 and O2. Figure 3.11 and Figure 3.12 show the results for the shear box testing in 2018 with similar behaviour as 2017.
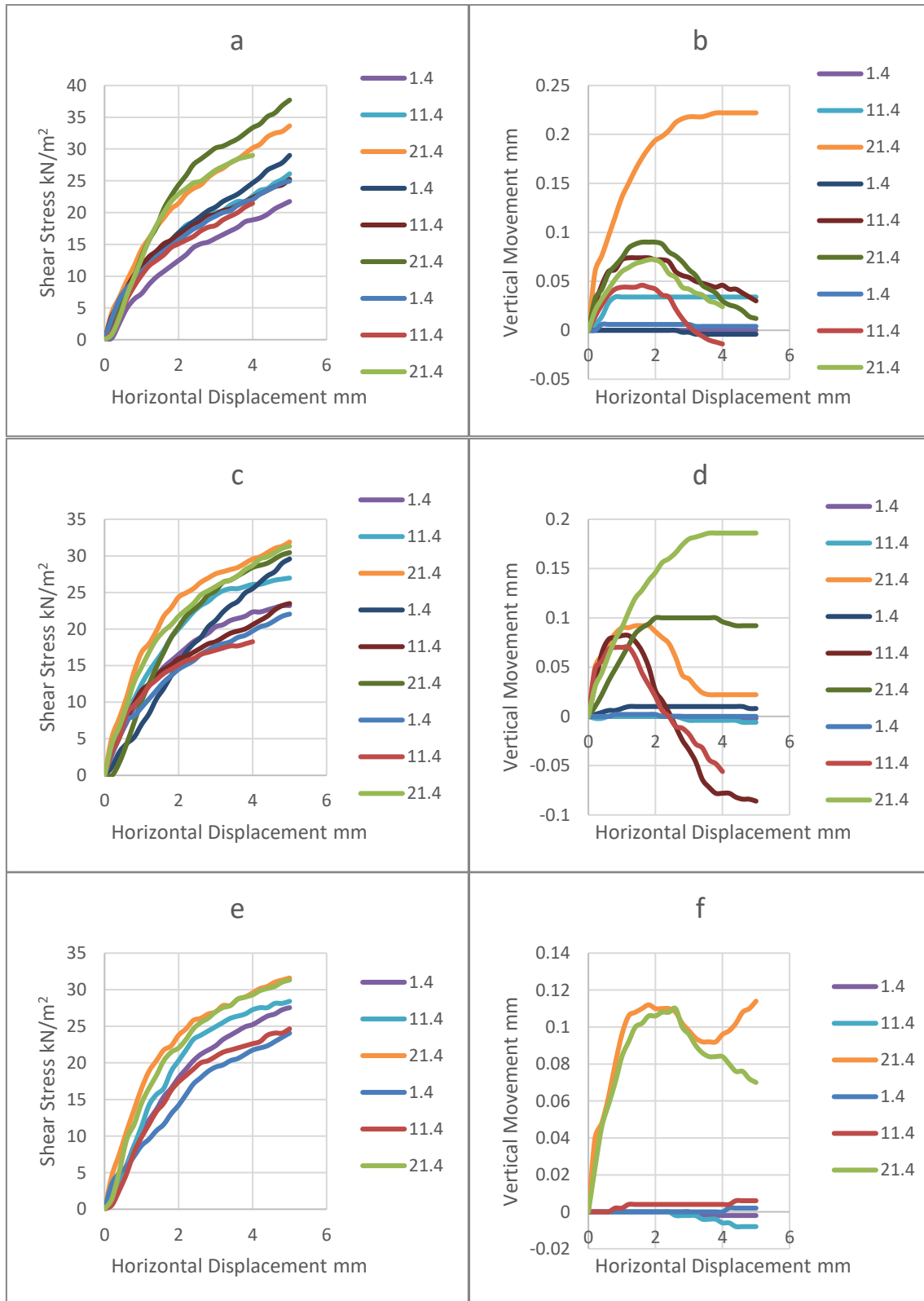
Figure 3.8 Shear box test results for the 2017 soils samples related to the (a,b) wheat (W1), (c,d) oilseed (O1) and (e,f) oats (KB) sites at 10% water content. The legend shows the stress levels of each test, 1.4, 11.4, 21.4kN/m².

98
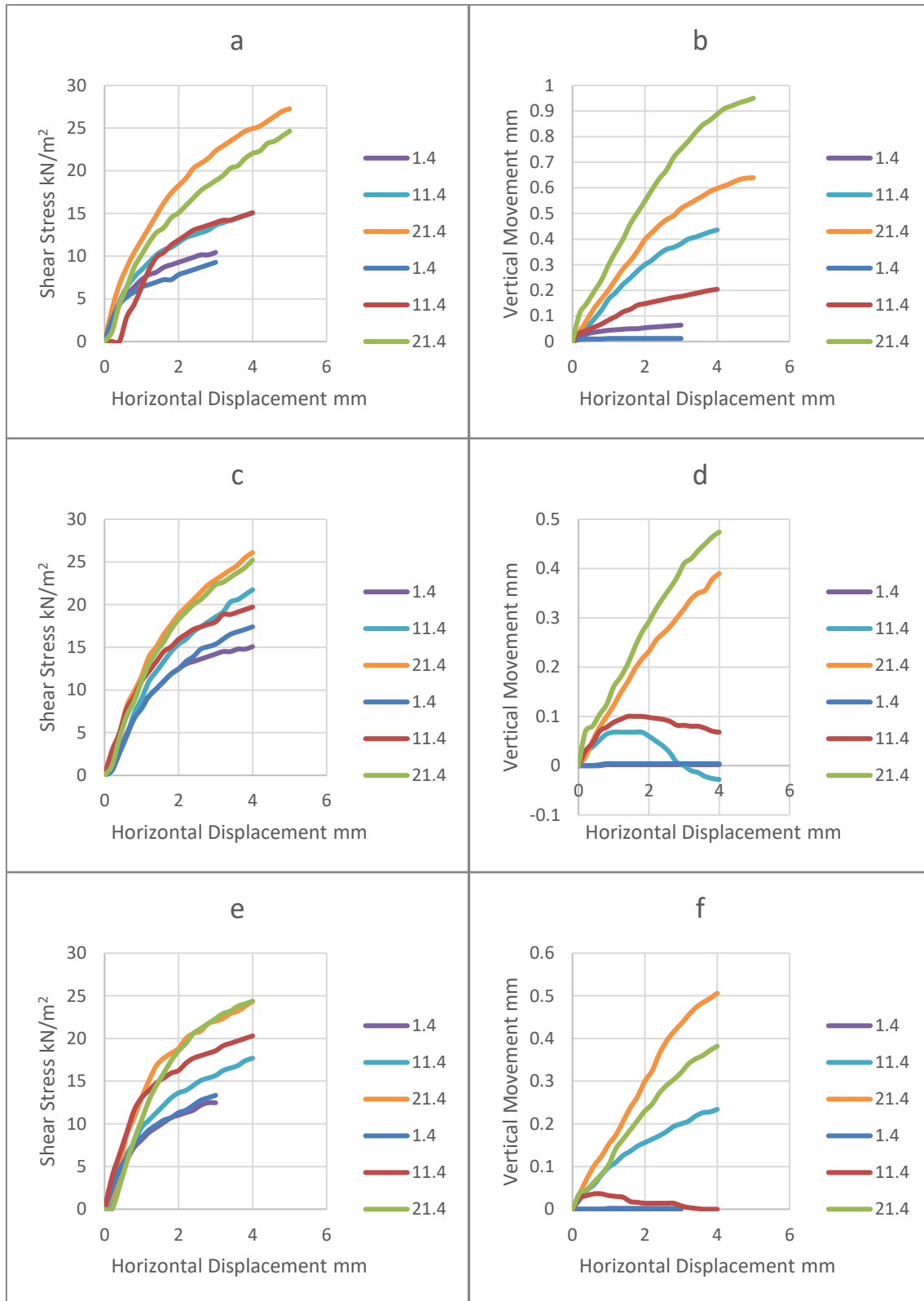
Figure 3.9 Shear box test results for the 2017 soils samples related to the (a,b) wheat (W1), (c,d) oilseed (O1) and (e,f) Knockbeg (KB) sites at 15% water content. The legend shows the stress levels of each test, 1.4, 11.4, 21.4kN/m².
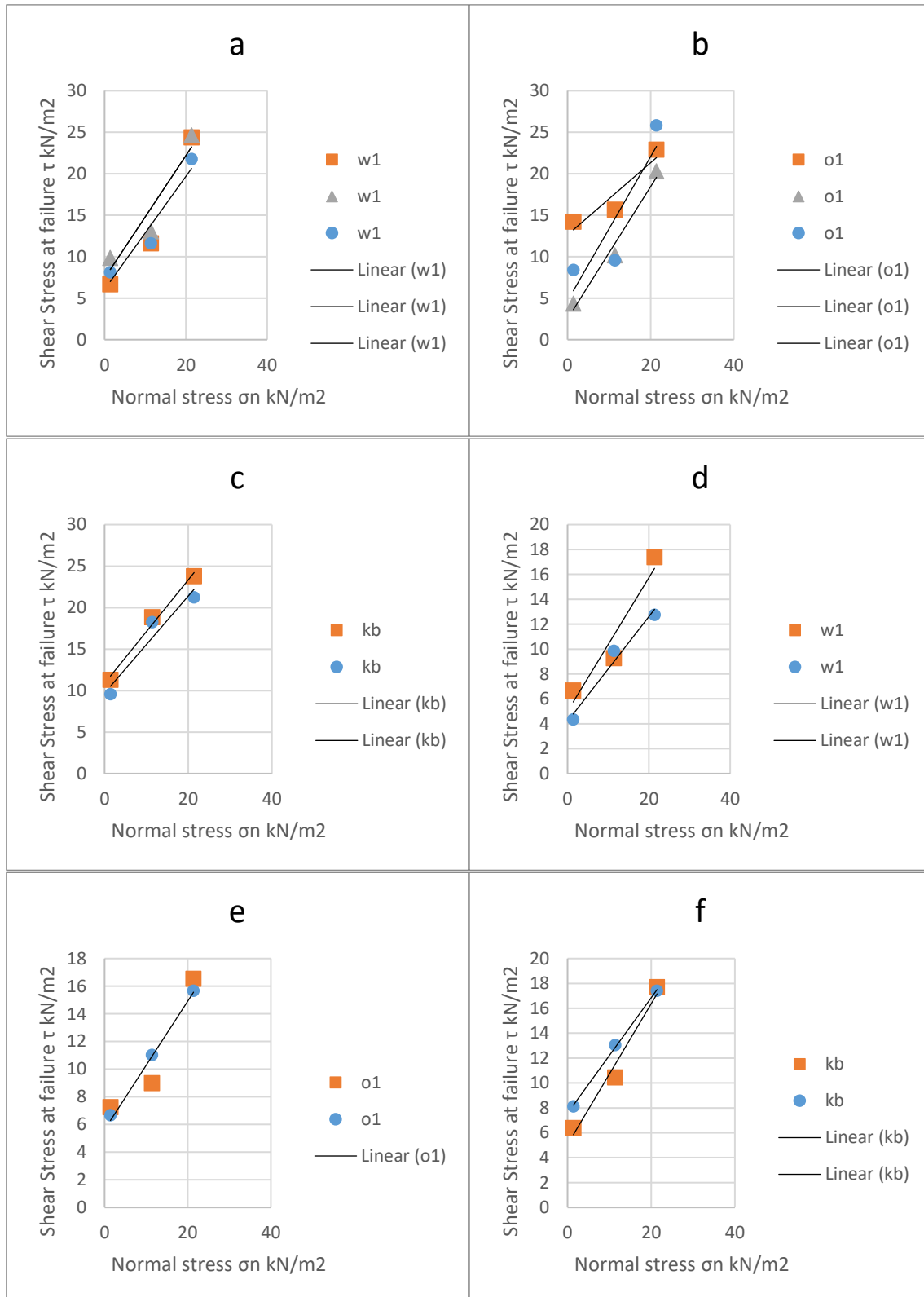
Figure 3.10 Direct shear strength test results from 2017. (a) Wheat (W1), (b) Oilseed (O1), (c) Knockbeg (KB) test at 10% water content. (d) Wheat (W1), (e) Oilseed (O1) and (f) Knockbeg (KB) at 15 % water content.
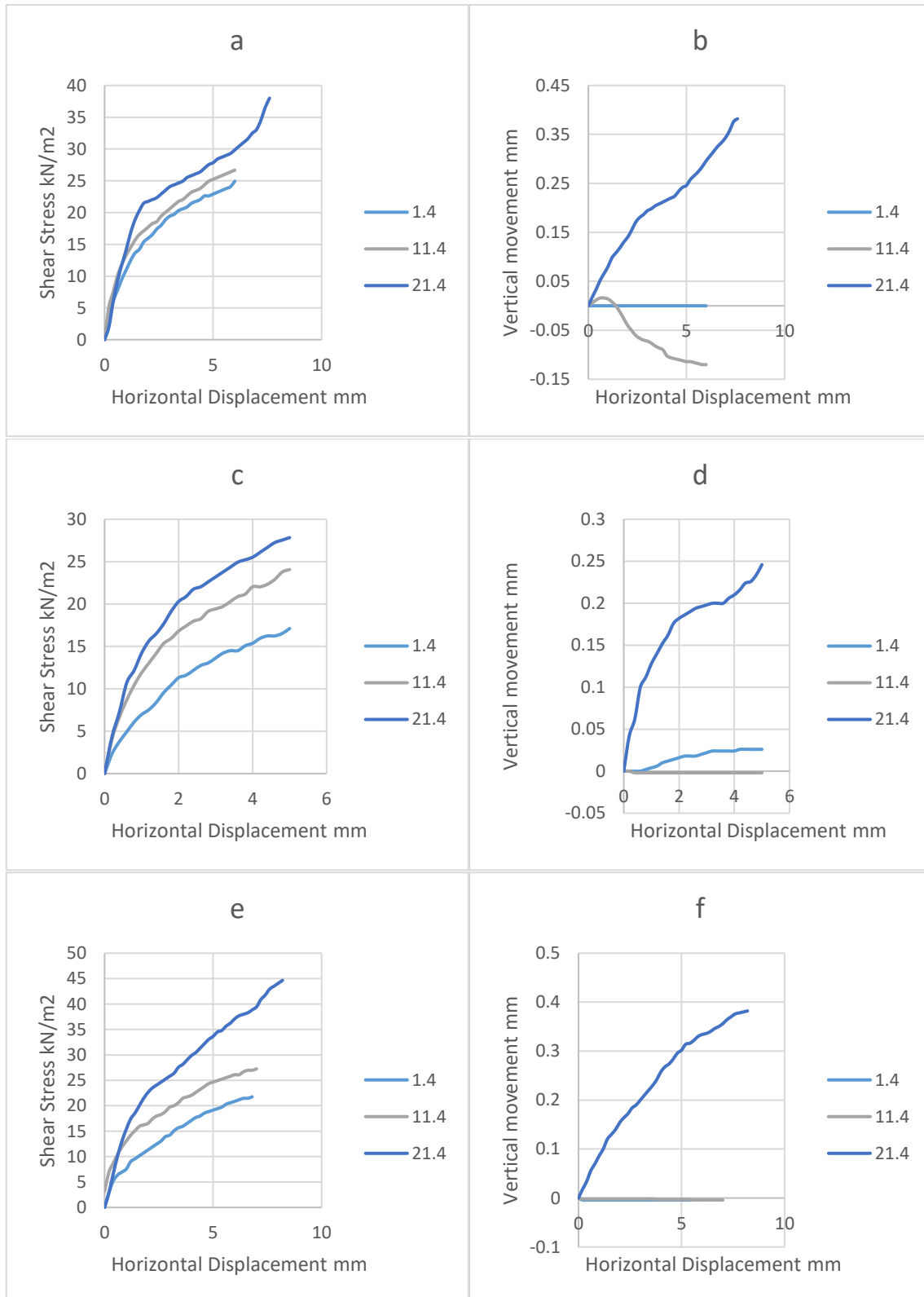
Figure 3.11 Shear box test results for the soils samples related to the (a,b) Wheat , (c,d) Oats and (e,f) Oilseed sites at 15% water content from 2018. The legend shows the stress levels of each test, 1.4, 11.4, 21.4kN/m².
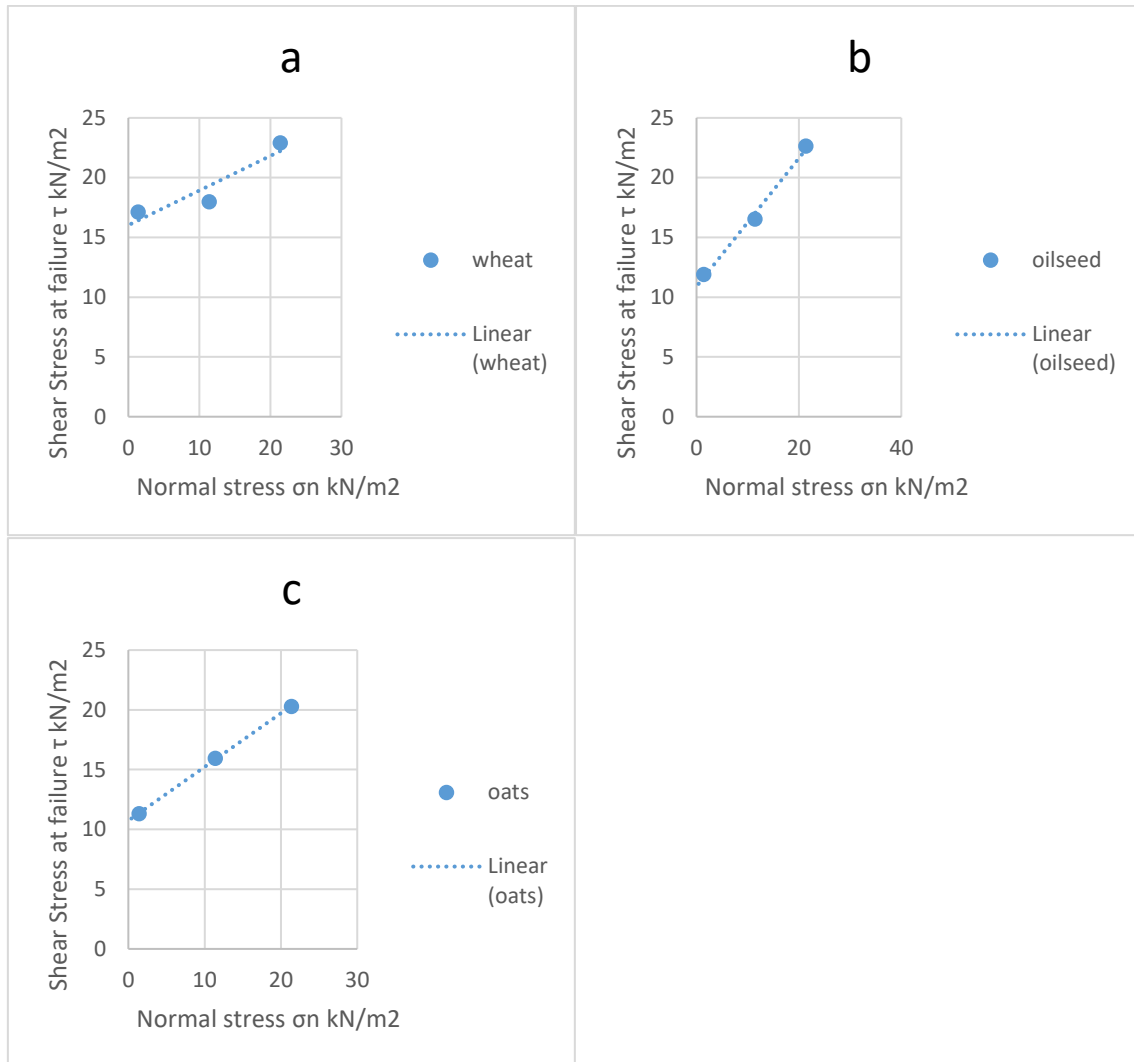
Figure 3.12 Direct shear strength test results from 2018. (a) Wheat, (b) Oilseed, (c) Oats test at 10% water content.

Table 3.8 Summary of Laboratory Work: Soil Characterisation, oilseed (O), wheat (W), Knockbeg (KB) 2017.

Soil Sample (2017)	Particle Size Distribution				Compaction	
	Fine Gravel (%)	Sand (%)	Silt (%)	Clay (%)	Optimum WC (%)	Optimum Dry Density (Mg/m^3)
O 1-1	17.5	40.8	38.4	3.3	24.8	1.47
O 1-2	10.3	43.5	38.1	4.0		
O 2-1	7.4	36.9	48.3	3.3	25.7	1.44
O 2-1	5.2	37.6	46.4	5.4		
W1-1	12.5	40.1	37.4	5.4	21.8	1.51
W1-2	10.0	40.0	36.1	4.8		
W2-1	10.6	40.7	38.7	4.7	21.9	1.53
W2-2	16.7	38.6	33.3	6.0		
KB1	12.9	40.2	32.9	6.7	20.5	1.57
KB2	10.1	41.6	38.3	4.0		

Table 3.9 Summary of Laboratory Work: Soil Characterisation 2017.

Soil Sample (2017)	Soil Water Characteristic Curve		Plasticity Index			Shear strength		Mineralogy
	Field Capacity (%WC)	Wilting Point (WC%)	Liquid Limit (WC%)	Plastic Limit (WC%)	Plasticity Index (WC%)	Effective Angle of internal friction (ϕ')	Cohesion (c)	
O 1-1	23	11	44.1	23.3	20.4	34.37	6.61	Silicate (SiO_4)
O 1-2	22	11	47.5	24.8	22.8			
O 2-1	26	11.5	45.1	25.1	19.9	28.14	7.42	Silicate (SiO_4)
O 2-1	32	11.5	41.4	22.4	20.8			
W1-1	27	11.5	43.6	25.4	18.2	37.40	5.87	Silicate (SiO_4)
W1-2	23	11	43.1	26.4	16.7			
W2-1	23	10.5	41.6	22.2	19.4	31.91	5.37	Silicate (SiO_4)
W2-2	21.5	10	44.3	23.9	20.4			
KB1	22	10	40.5	21.7	18.8	31.12	9.76	Silicate (SiO_4)
KB2	22	10.5	40	22.1	17.9			

3.3.3 Field Anchorage Failure Measurements

3.3.3.1 Field Testing using manual lodging machine

In the 2016, field investigation, anchorage failure was measured using a similar machine to that of Berry et al., (2006) which measures the maximum root failure moment (Nm). The machine consisted of a Mecmesin Smart torque cell (maximum torque 200Nm) with a lodging attachment comprising a curved metal rod (20cm). This was attached to a screwdriver head and inserted into the torque cell. The cell sat within a housing in two bearings that allowed the torque cell to spin freely. A handle was also attached that controlled the rotation of the torque cell. The housing was mounted on a rectangular base. The entire height of the lever arm was (25cm) from the plant base, with the centre of rotation at 12.5cm (Figure 3.13).

Mecmesin Smart torque cell with a lodging attachment, sitting within a cylinder with bearings

Mecmesin Advanced Force and Torque Indicator
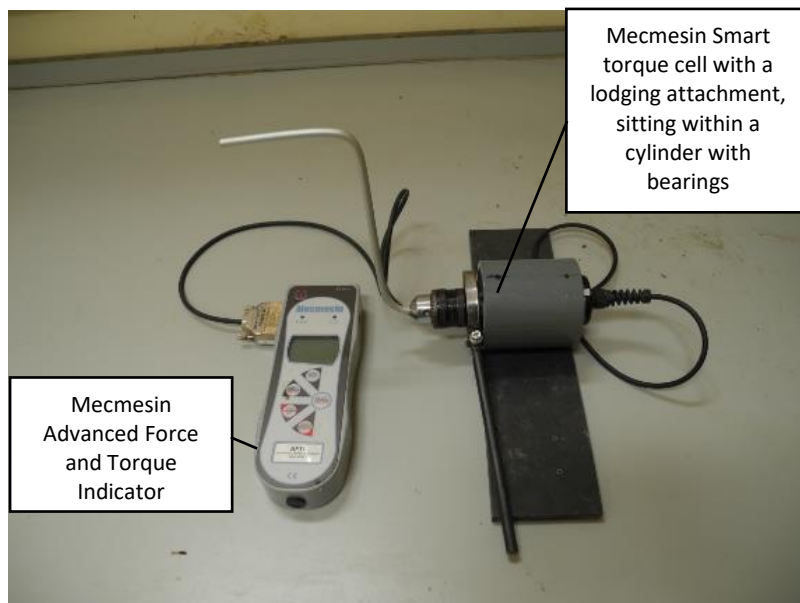
Figure 3.13 Lodging apparatus developed by Berry et al., (2006).

A similar methodology was used as was described by Berry et al., (2006). The plants that were chosen for the experiment were at least three rows into the plot and had adequate space around them to avoid the higher density soils at the edge of the plots. Soil compaction in the

tramline is due to farming vehicles passing. Once, the row within the plot was chosen, three plants of a similar height were tagged for anchorage testing water was added to bring the water content to field capacity. The machine was placed next to the plant, and the maximum torque in Nm to push over the plant was recorded using a Mecmesin Advanced Force and Torque Indicator (AFTI). Each anchorage test took approximately 60 seconds to push the lodging arm from the upright position through 90°. After each test, the soil shear strength (kPa) was measured with the hand-held shear vane, at a depth of 50mm, within 50mm of the test plant (avoiding any interaction with the plant roots). Values were measured with a 19 x 38mm direct reading shear vane (direct reading shear vanes mean that there is no conversion of values after measurement). The values are an estimate of the in-situ undrained shear strength of saturated clays without disturbance. The average of 2 or 3 readings was taken as indicators of the shear strength. Three reading were taken if the first two readings were 5kPa apart. A soil sample was taken from the soil disturbed by the shear vane, to determine the water content according to BSI, (2016). Bulk density samples were taken for every plant sample that was taken. After the soil was sampled the entire plant was removed from the soil, labelled and kept for plant and root measurements.

In 2016, the lodging machine had been modified to include bearings on the inner cylinder to allow for smoother rotation of the torque cell. 94 anchorage measurements were taken on wheat varieties, Cordiale, Stigg and Rockerfeller (Figure 3.14) and were compared with data from Berry et al., (2006) (Figure 3.15). The results from the initial tests showed that the modifications had reduced the readings to 1 order of magnitude below the readings by Berry et al., (2006). Therefore, the machine was restored to the original state and testing completed

in 2017. The data were closer in value to those from the literature. The 2016 data for anchorage testing was not used in future analysis.
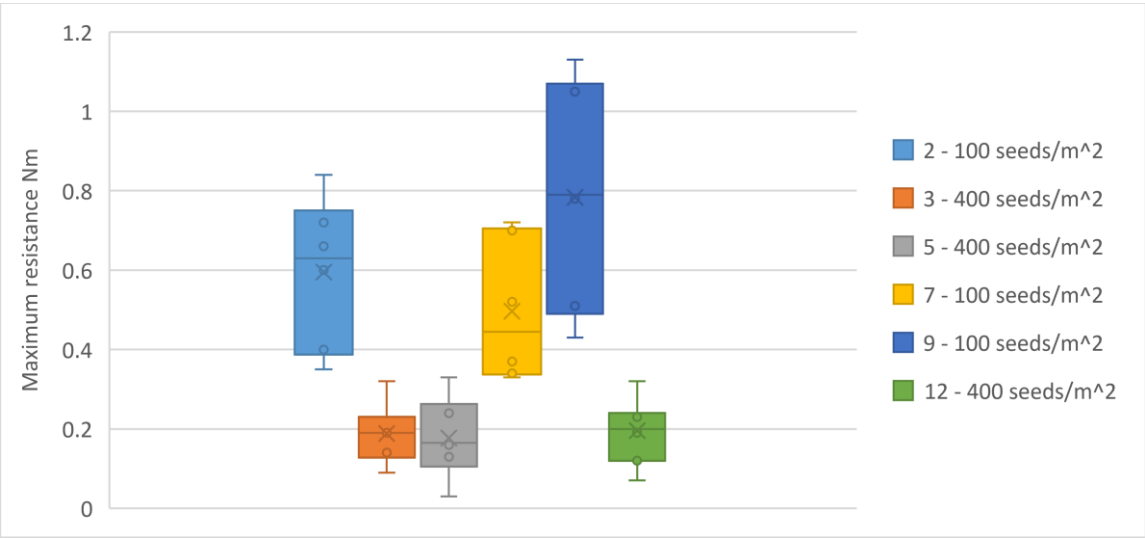
Figure 3.14 Berry et al., (2006) data for wheat plots at 400 and 100 seeding rates.
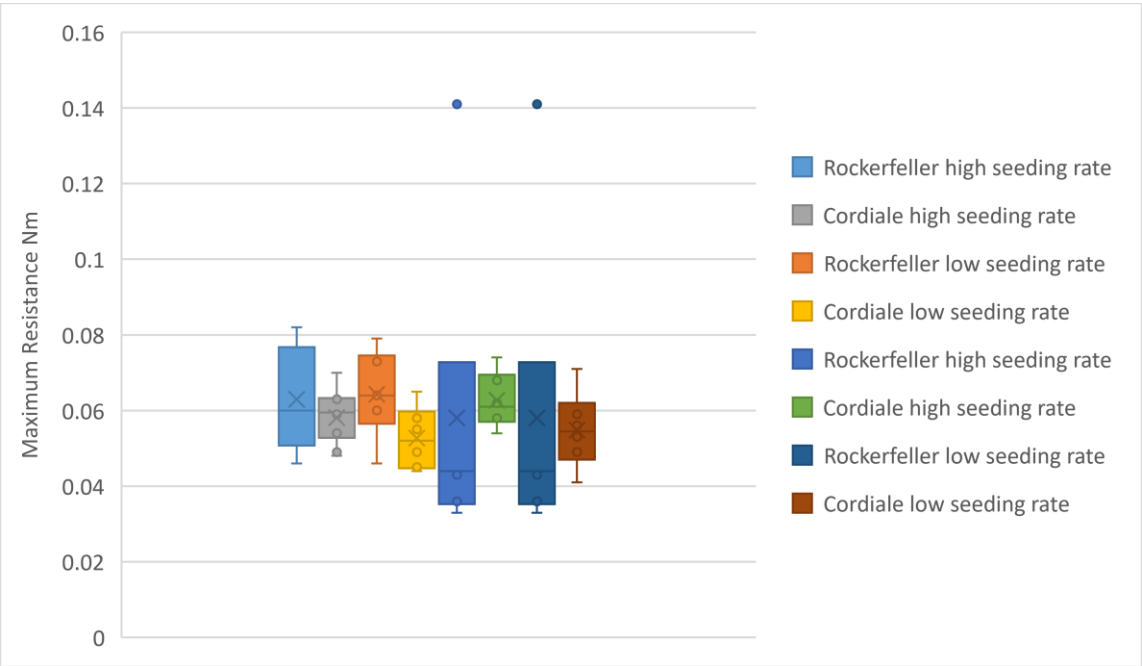
Figure 3.15 2016 data collection for anchorage tests of wheat.

In 2017 the bearings were removed from the cylinder of the lodging instrument, returning the instrument to the original configuration that Berry used in 2006. The values of anchorage

returned to ranges of measured by Berry et al., (2006). However, there was more variation

within the sample in 2017 with values ranging from 0.105-0.669Nm (Figure 3.16), possibly

because of changes to the treatments and the addition of another variety of wheat, JB Diego.

The variation in plant measurements and their impact on anchorage strength will be discussed

further in Section 3.3.3.4

In 2017, anchorage failure was measured on three fields, the wheat (W) oilseed rape (O) and

oats (KB) fields in the plots selected in Section 3.1.1. For the wheat field 24 plots were tested.

Three plants were tested in each plot; therefore 72 lodging measurements were taken in total

for wheat. For oats 21 plots were sampled and 63 measurements were taken. For oilseed rape

2 plots were sampled and 40 measurements were taken. The results of the anchorage testing

will be discussed in section 4.2.1
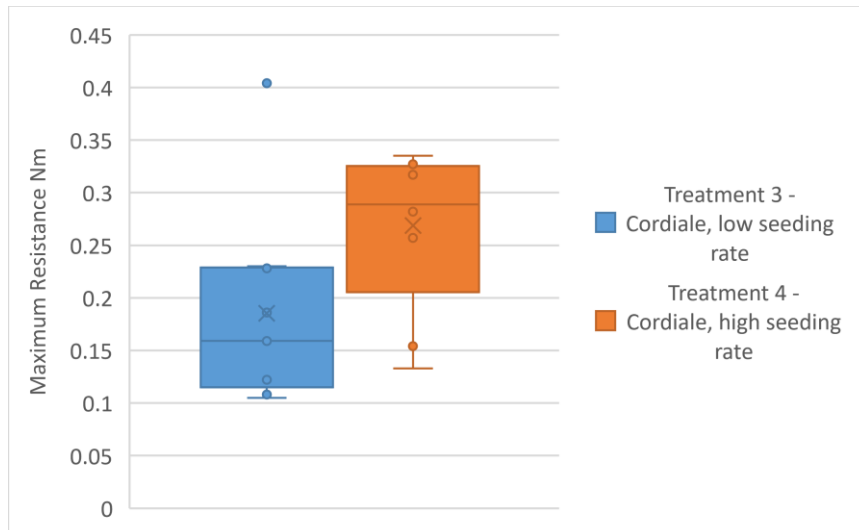
Figure 3.16 2017 data collection for anchorage tests for two treatments of wheat (W).

107

3.3.3.2 Development of a New Lodging Instrument

As highlighted in the literature review, several methods were used to apply a lodging load in root anchorage experiments. A new instrument was created that would address the limitations of past apparatus (Figure 3.17). Limitations of the field anchorage apparatus developed by Berry et al., (2006), included, only allowing one height of pushing, the AFTI only measured maximum values of anchorage resistance and not anchorage resistance and rotational angle, the instrument was operated manually, which could lead to human errors in pushing. Another limitation of the laboratory apparatus was that it was attached to the Instron machine which meant it was not portable.

The new lodging instrument included an automated, mechanically driven arm, which pushed the root model or crop sample measuring the rotational angle and root failure load, which could be converted to a moment. The lodging machine was constructed using an Arduino microcontroller, a servo motor and a load cell. Creating a prototype as shown in Figure 3.17 tested the concept. This machine consists of an arm with a one degree of freedom, which is connected at the joint to a motor to measure the angular displacement. The load cell is mounted at the top of the arm and holes were drilled along the arm to allow for a change in height of the force measurement. This was important in order to allow changes in height of pushing if required. Controlling the arm was done via a computer code written in the Arduino IDE software, which was also used to log the data for further analysis. The load was converted to newtons and then multiplied by the height of pushing to obtain measurements of the root failure moment (Nm) within the code in the Arduino IDE (Appendix C1).

The machine was tested by comparing the results from the manual process and the one using the new instrument for the artificial root lodging experiments (Table 3.10). It was found that the instrument was measuring larger maximum values than the lodging apparatus developed by Berry et al., (2006). As a result, the values were adjusted by the average difference of 0.1Nm to allow values to be compared. The procedure for conducting the lodging test with the artificial roots, the new instrument and the different soil mixes is discussed in the next section.

Table 3.10 Comparison of old lodging instrument and the new instrument for the same experiment.

Old instrument (Nm)	New Instrument (Nm)
0.204	0.289
0.079	0.326
0.253	0.280
0.219	0.292
0.239	0.333
0.205	0.273
0.203	0.319
0.234	0.332
0.212	0.318
0.192	0.285
0.214	0.317
0.258	0.337
0.218	0.321
0.202	0.376
0.208	0.288
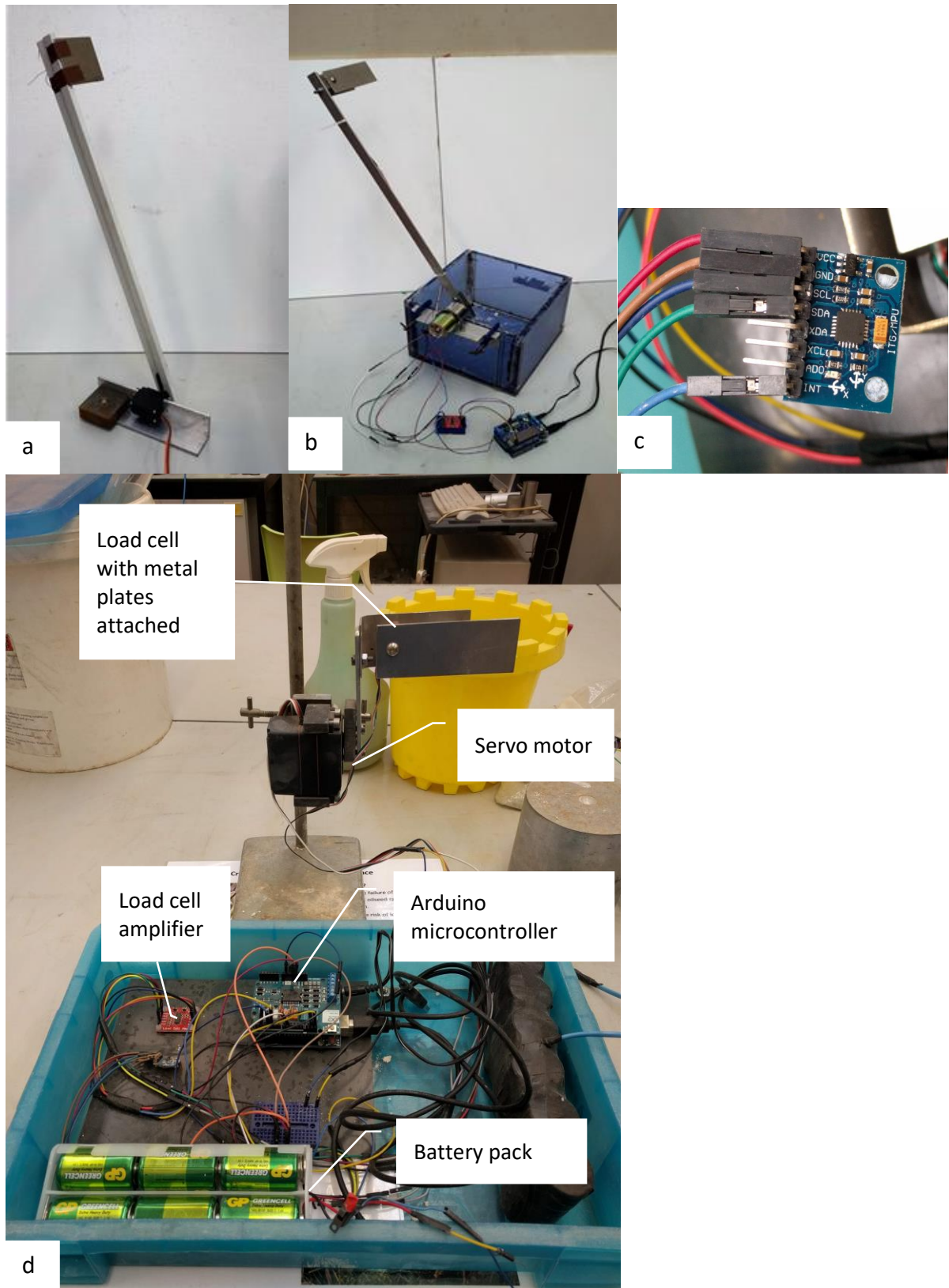
Figure 3.17 (a) Lodging Machine prototype (b) lodging machine with a container attached (c) MPU-6050 sensor (d)) Final lodging machine set up.

3.3.3.3 Field Testing using the new lodging instrument

Field testing was completed in 2018 using the newly developed lodging instrument. Wheat and oats were tested on sites 4 and 6 respectively. Oilseed rape proved to be too strong for the servo motor.

Lodging experiments were completed using a similar methodology as with Berry's manual machine with a few changes. Before any testing began, the plants were watered individually to ensure that the water penetrated to the root system, bringing the water content to field capacity and reducing the shear strength to conditions likely to occur after rainfall. The lodging instrument was set up, and the resistance was measured. The shear strength was also measured three times after the plants were lodged. This was done using the hand shear vane as discussed in Section 3.1.3. Plant samples were taken for characterisation as described in Section 3.3.3. Moreover, the plant roots were washed and pictures were taken for records and later assessment if needed. The water content of the soil was measured using the standard method BSI, (2016) by collecting 3 samples per plant from a depth of 50mm.

After the lodging experiments were completed and the shear strength and bulk density samples were taken. The plant that had been lodged was numbered and removed from the soil with the root system intact. The plants were then taken back to the laboratory at Teagasc to be measured. 2kg soil samples were collected for further soil characterisation tests in the laboratory.

3.3.3.4 Plant Measurements

Methods for plant measurements were completed using a similar methodology as Griffin, (1998) and Berry et al., (2000) who carried out lodging experiments on wheat plant and this will allow comparison between results. After the measurements were completed in the field in 2017 and 2018, the crop and soil samples were moved to the laboratory space at Teagasc cereals building. Figure 3.18a and Figure 3.18b show the structure of the oats and the oilseed rape crops with some of the key parameters which were collected. These key parameters included the crop height, stem diameter, the centre of gravity, natural frequency and shoots per plant.

The crop height was measured by finding the distance from the soil surface to the bottom of the ear. The stem diameter was measured as the outer distance from stem wall to stem wall at the stem base. The centre of gravity was measured as the balance point of the stem when the root was removed. The balance point was found by trial and error. The stem was balanced on a pivot point. The stem was moved along the pivot point until the stem balanced. The natural frequency was measured by identifying the main stem of the plant and separating it from the other stems present. Then, the stem was placed in the clamp of a retort stand, where it was then moved backwards (10cm) from the vertical position and allowed to oscillate freely. Oscillations are counted and the time stopped, but only if the stem moved straight back and forth in the same plane as it was released. The natural frequency was measured as the time for three oscillations and then calculated to find the time for one oscillation. The number of shoots present was recorded as the shoots per plant.
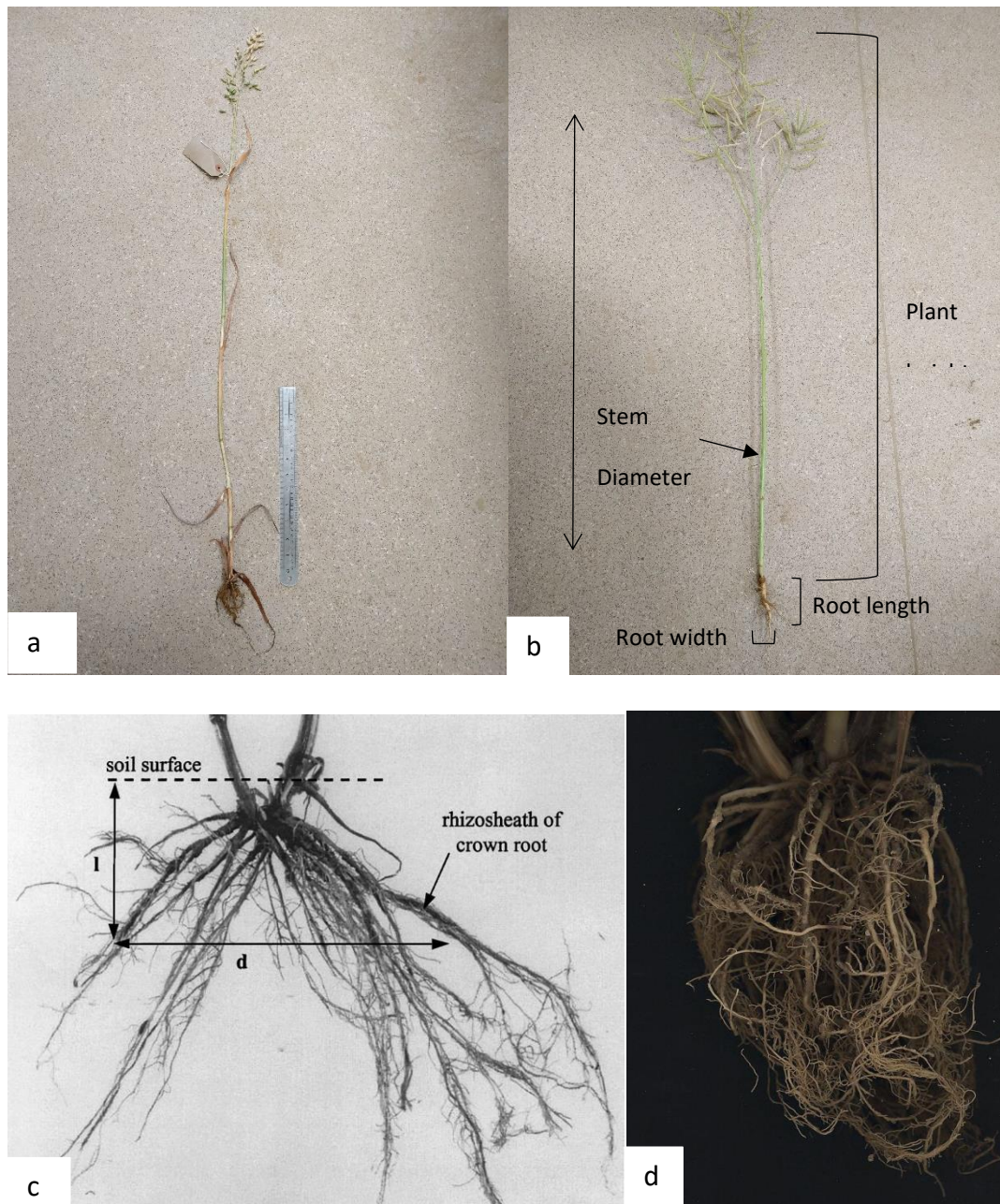
Figure 3.18 (a) An image of the oat plant, (b) An image of the oilseed rape plant showing some of the measurements, (c) image of a plant from Berry et al., (2000) showing a wheat root with measurements for the soil surface and rhizosheath and (d) image captured after the manual root measurements for image analysis.

After completing these initial measurements, the stem was removed, and the following measurements were taken for each plant (72 wheat samples, 63 oat samples and 40 oilseed rape samples): plant weight, root-soil weight, root plate diameter, root depth and internal stem diameter. The plant weight and root-soil weight were both measured using a balance.

Plant weight was measured as the weight of all the stems, and the root-soil weight was the weight of the root system. The inner diameter was the distance from the stem wall to stem wall when the stem had been removed from the root structure. After the second stage of measurements was completed the stems of the crops were discarded.

The root plate diameter was measured as the width of the roots with the soil attached to the structure. This was measured in two directions, the long width, and the short width because the roots tend to grow depending on the direction of wind and will most likely fail along the short direction. The root depth was measured as the length of the longest structural root. The roots were kept in label bags and placed in the refrigerator for further measurements.

Roots were removed from storage, washed and allowed to soak for 24 hours to allow the soil to loosen. The soil was washed from the roots and roots left to dry in the fridge for 24 hours. Roots were placed on the prepared grid for measurement. The following measurements were recorded: root plate diameter, root depth, stem diameter, root diameter, root angle, root number, and root length. All measurements were done using the grid, ruler and calipers.

The coronal roots were defined as roots with lignification or stiffening, otherwise known as the rhizosheath (Figure 3.18c). The plate diameter was measured as the distance between the outer most coronal roots. The root depth was measured as the distance from the first root connection of the stem to the end of the longest root. The stem diameter was measured at the base of the stem. The root diameter was measured for three different coronal roots.

After the root measurements were completed manually, samples were kept in the fridge at 10°C to preserve the roots for future measurements and pictures. Images were captured by

placing the roots on a black background. These images could be used in root image analysis software such as GiaRoot. Images were captured with a Nikon P1000 camera. Two images were taken per root; one presenting the widest cross-section of the root plate diameter and one with the shortest cross section.

Figure 3.19 shows the results of three plant measurements, root plate diameter, stem diameter and root length, completed in 2017. Treatment 4 had the lowest range of values for the three measurements. This could be explained by the high seeding rate for that treatment. Other treatments with high seeding rates had higher values that the low seeding rates. Therefore, for this dataset the treatment did not seem to have the expected effect.

The root plate diameter of the wheat plants ranged from 39.9mm to 165mm with an average of 74.7mm. These results were larger than in past studies, for example, Berry, Sterling and Mooney, (2006) found root cones for wheat plants ranging between 36 to 93mm. The wheat plants had a mean spread of 60mm. Both species averaged four shoots per plant compared with 5 shoots per plant in this study. Baker et al., (1998) found the ranges of plate diameter to be between 10-80mm. Rooting depth ranged between 15-60mm. Berry et al., (2000) found that the root plate spread was between 23.9mm and 54.4mm. The reason for larger values could be differences in varieties of wheat and treatments used in this research compared to treatments in the literature and differences in soil conditions.

a

b
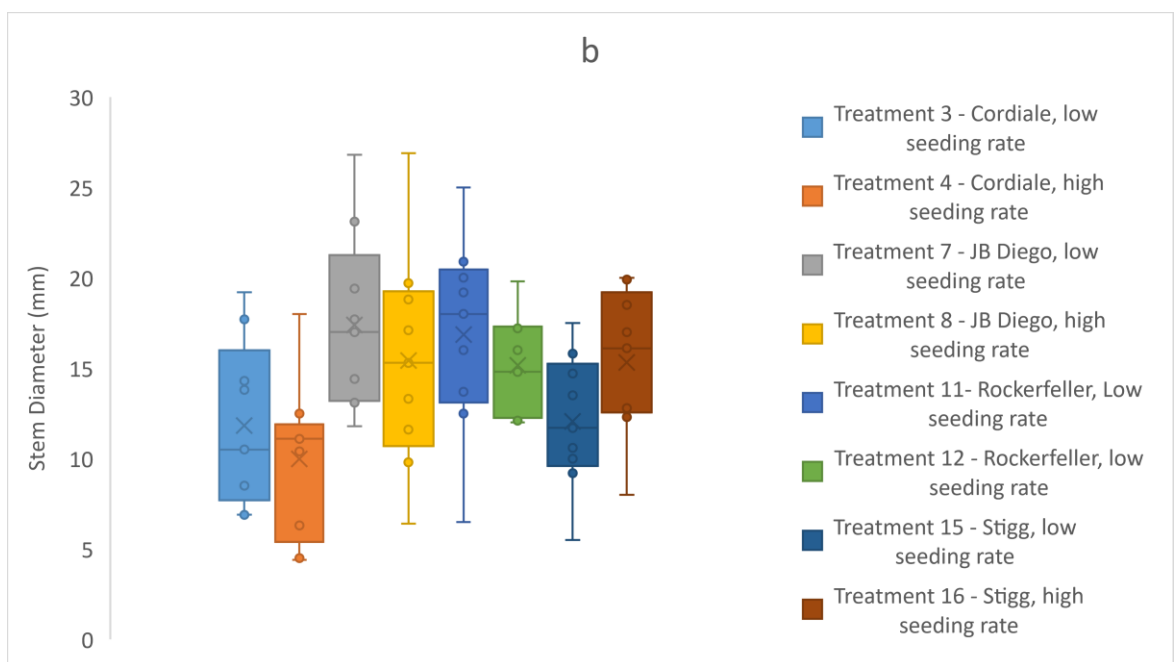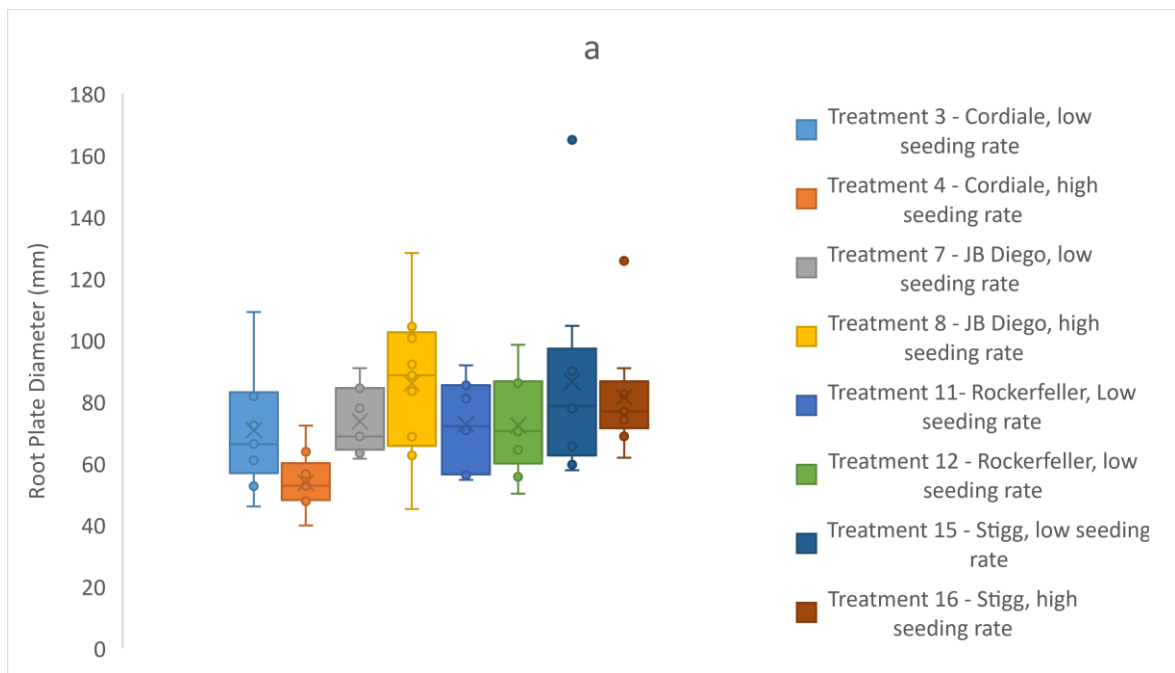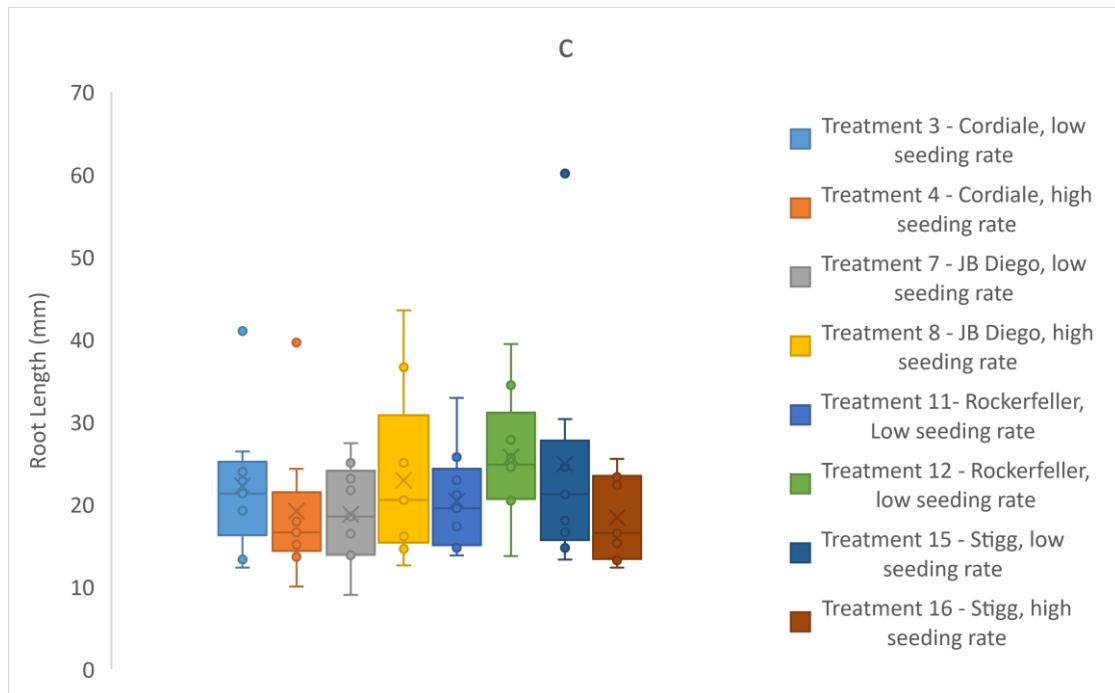
Figure 3.19 Plant measurements of wheat completed in 2017, showing different treatments (a) root plate diameter, (b)stem diameter, (c) root length.

Figure 3.20 shows the corresponding soil measurements collected at each treatment in 2017. These included the average shear strength using the shea vane, water content and bulk density. Treatment 3 had the lowest mean water content compared to the rest of the treatments, while the mean for the average shear strength were around 20kPa, there was some variation in the ranges of values. The bulk density also had a similar range of mean values between 1400 and 1600kN/m^2.

a

b
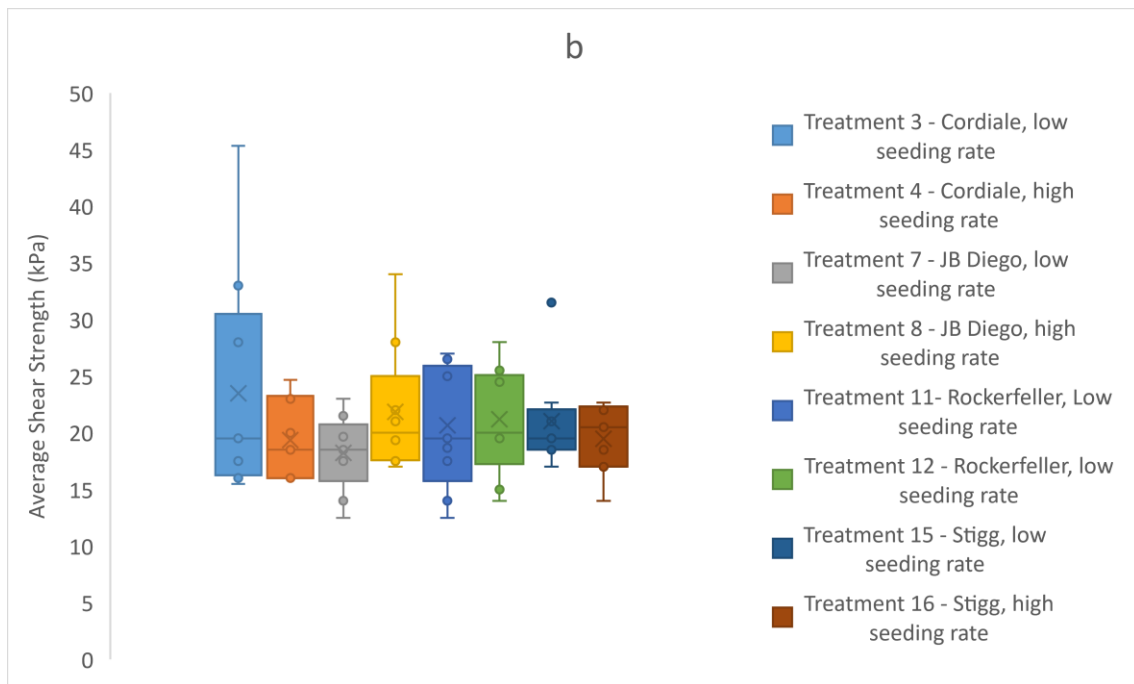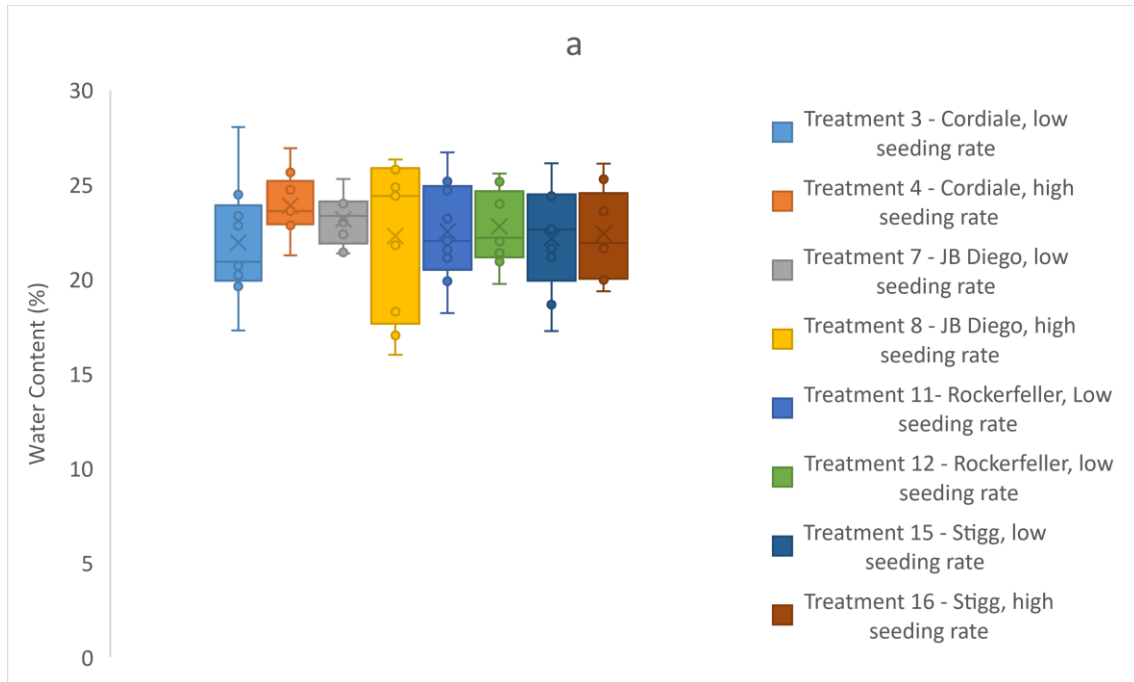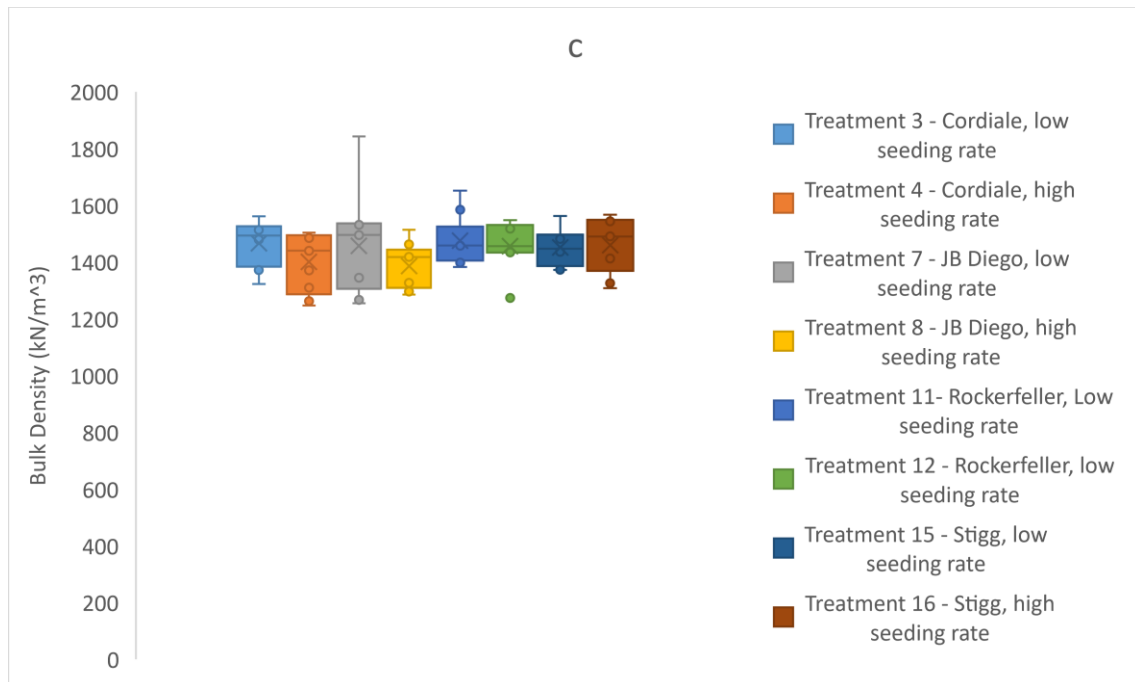
Figure 3.20 Soil measurements taken during the lodging experiments on wheat (W), displayed by treatment (a) water content, (b) average shear strength (c) bulk density.

Figure 3.21 shows the measurements for root plate diameter, root length, root number and average shear strength for the oats in 2017. Treatment 4 had the lowest mean diameter and the highest mean root length. Root number ranged from 5-15 and the average shear strength was highest in Treatment 4 at 43kPa.

a

b
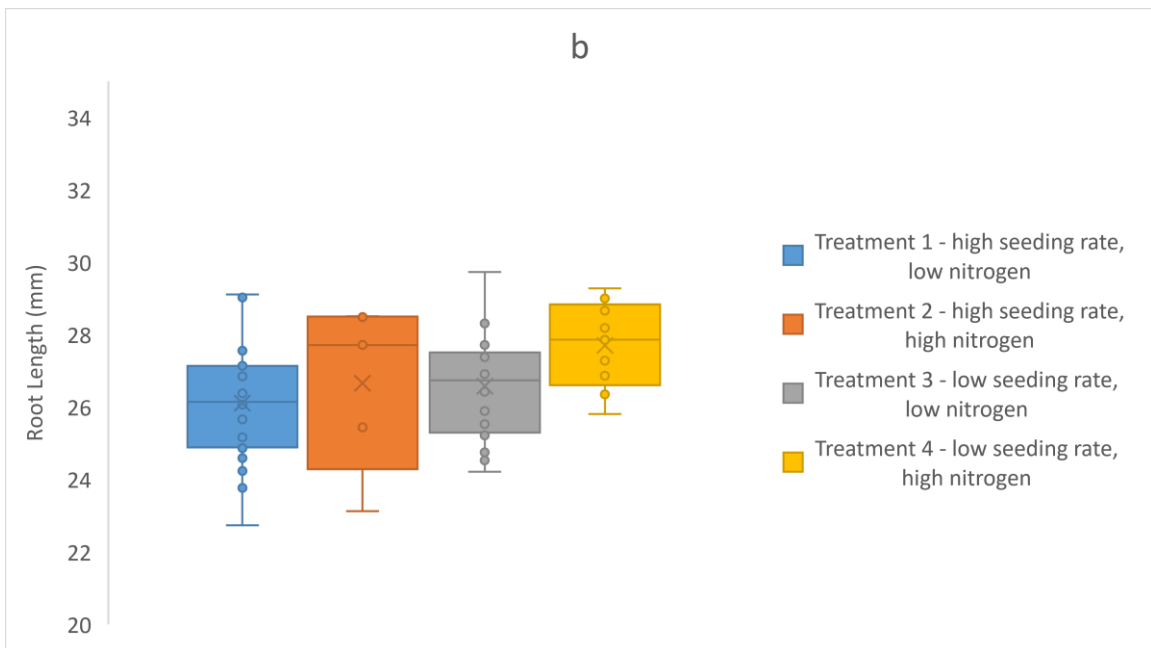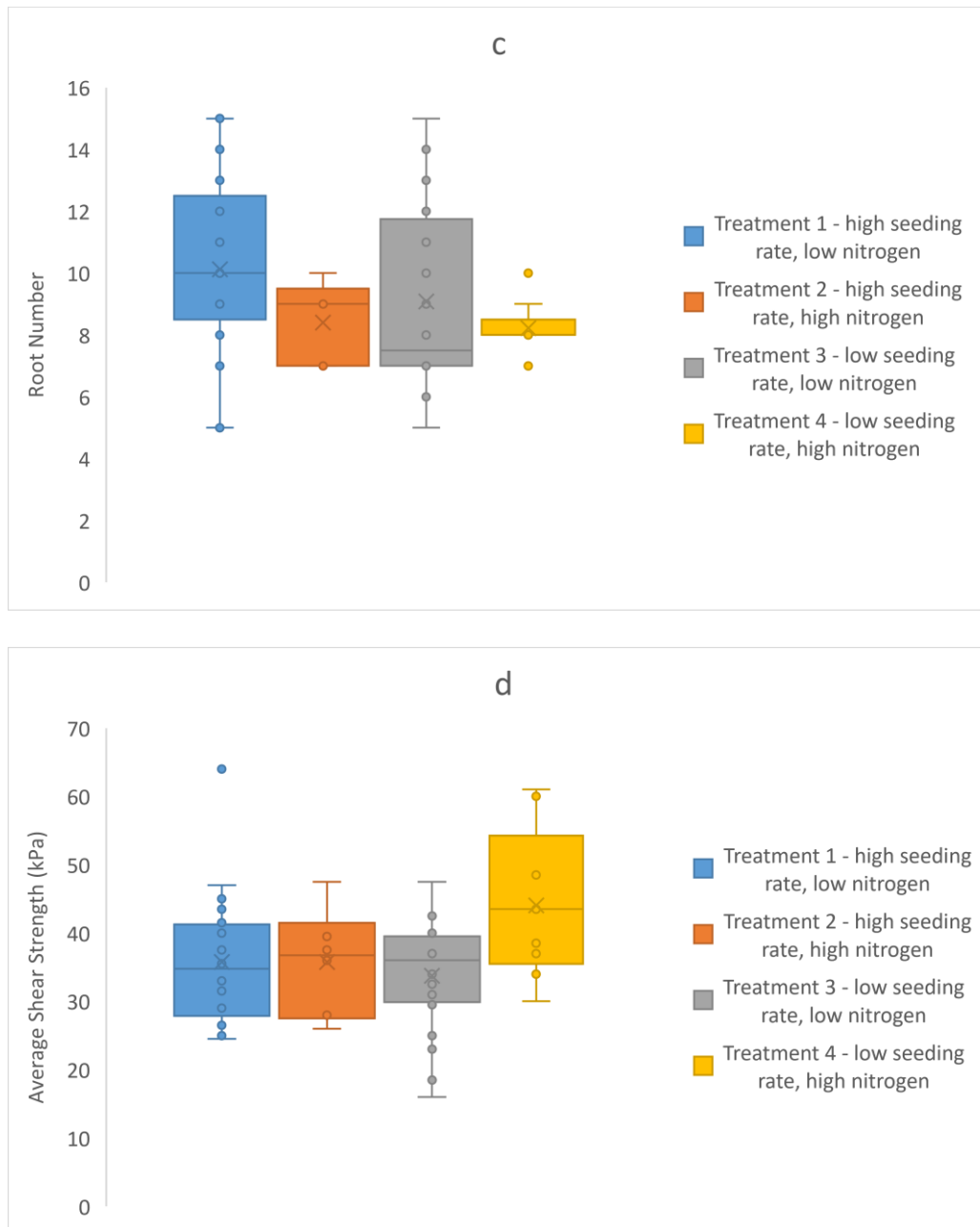
Figure 3.21 Plant and soil measurements of oats (KB) completed in 2017, showing different treatments (a) root plate diameter, (b) root length, (c) root number (d) average shear strength.

Figure 3.22 shows the root length, root diameter and average shear strength for the oilseed rape samples. Sample 2 had a higher mean root length than Sample 1. The root diameters were similar for both samples. The average shear strength was significantly lower for Sample

2 with a mean of 32kPa compared to 42kPa. The average measured tap root diameter was 16.5mm at the top, 14.4mm at 20mm depth and 10.4mm at 40mm depth. The average stem diameter was 14.8mm at the base. Berry et al., (2013) reported tap root thickness and tap root length ranging between 5-20mm and 50-250mm, respectively. They also reported values of 3.72-18.7mm for the root diameter and 64-142mm for root length.
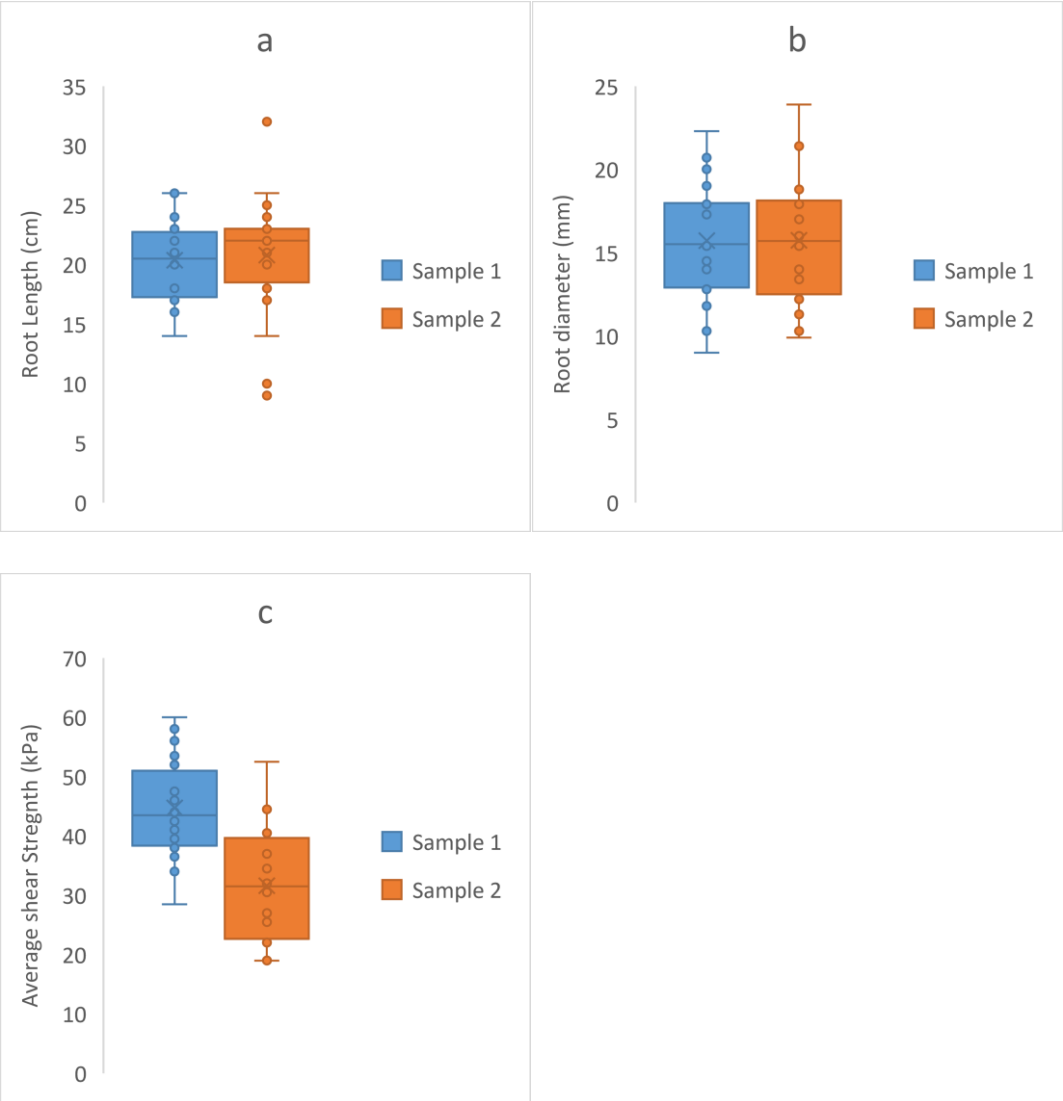
Figure 3.22 Plant and soil measurements of oilseed rape (O) completed in 2017, showing different treatments (a) root length, (b) root diameter, (c) average shear strength.

Figure 3.23 shows an image of oat roots sampled from the same plot. This image illustrates the variability in root dimensions, each plant is different and grows differently. This is why the measurements vary through large ranges of values and the interaction with the soil could cause the measurements of anchorage failure to vary.

Figure 3.23 Oats roots samples from one plot demonstrating the variability of the plants within a plot.

The results for the plant characteristics are summarised in Table 3.11, Table 3.12 and Table 3.13. providing the maximum, minimum, mean and median. 72 plant characteristics were measured for wheat, 63 measured for oats and 40 for oilseed rape in 2017.

Table 3.11 A summary of the data collected in the field for wheat, for 72 plants in 2017.

Measurement	Max	Min	Mean	Median	Variance	Standard Deviation	Coefficient of Variation (%)
Root failure moment (Nm)	0.669	0.105	0.307	0.320	0.0170	0.130	42
Plant Height (cm)	113.8	75.2	91.9	90.7	106.6	10.3	11
Stem Diameter (mm)	5.43	3.04	4.1	4.1	0.3	0.5	13
Height Centre Gravity (cm)	56.4	43.2	49.9	49.9	12.7	3.6	7
Natural Frequency	3.94	1.97	3.0	3.0	0.2	0.5	17
Plant Weight (g)	129.3	11.8	56.3	47.1	783.7	28.0	50
Root Soil Mass (g)	861.6	6.2	260.0	199.0	38372.8	195.9	75
Shoots per plant	13	1	5.6	5.0	7.5	2.7	49
Shoot Internal Diameter (mm)	1.97	0.72	1.3	1.3	0.1	0.3	22
Root Plate Diameter (mm)	165	39.9	74.7	72.2	443.3	21.1	28
Root Depth (mm)	260	16.9	121.0	122.4	1702.0	41.3	34
Stem Diameter (mm)	26.9	4.4	14.3	13.8	25.3	5.0	35
Root Diameter (mm)	3.3	1	1.7	1.6	0.2	0.4	26
Angle (°)	45	0	23.8	25.0	126.3	11.2	47
Root Number	18	5	8.5	8.0	6.9	2.6	31
Root Length (mm)	60.1	9	21.5	20.5	76.9	8.8	41
Water Content (%)	28	16	23	23	7	2.6	11
Shear Strength (kPa)	45	13	21	20	29	5.4	26
Bulk Density (kgm^{-3})	1843	1247	1444	1457	10577	102.8	7
Dry Density (kgm^{-3})	1489	1013	1187	1196	8886	94.3	8
Void Ratio	1.68	0.77	1.29	1.25	0.0318	0.2	14
Porosity	0.63	0.43	0.56	0.56	0.0012	0.0	6
Degree of Saturation	0.75	0.36	0.48	0.47	0.0046	0.1	14
Air Content	0.39	0.11	0.29	0.29	0.0025	0.0	17

Table 3.12 A summary of the data collected in the field for 63 oat plants in 2017.

Measurement	Max	Min	Mean	Median	Variance	Standard Deviation	Coefficient of Variation (%)
Root failure moment (Nm)	0.725	0.066	0.301	0.301	0.0167	0.129	43
Plant Height (cm)	183	133	158.436	158	105.4	10.3	6
Stem Diameter (mm)	8.1	3.8	5.413	5.4	1.0	1.0	18
Plant Weight (g)	176.5	19.3	68.201	60.15	1285.1	35.8	53
Root Soil Mass (g)	818.1	74.7	340.5	325.2	22607.7	150.4	44
Shoots per plant	9	1	3.387	3	2.9	1.7	50
Shoot Internal Diameter (mm)	2.7	0.6	1.461	1.4	0.2	0.4	28
Height to Secondary roots (mm)	34.8	0	9.868	8.8	76.2	8.7	88
Number of Secondary Roots (mm)	8	3	5.96	6	1.4	1.2	20
Root Diameter (mm)	8	6	6	6	0.0002	0.004	6.92
Root Length (mm)	29.51	24.09	25.91	25.96	0.35	0.59	2.28
Plate Diameter (mm)	46.36	10.42	14.50	13.70	21.91	4.68	32.28
Root Number	15	5	9.30	9	7.43	2.73	29.3
Water Content (%)	27.96	11.75	19.90	19.90	6.8	2.6	13
Shear Strength (kPa)	64	16	36.11	36.5	89.4	9.5	26
Bulk Density (kgm^{-3})	1817	1072	1579	1589	18248.1	135.1	9
Dry Density (kgm^{-3})	1528	893	1330	1339	12523.9	111.9	8
Void Ratio	2.07	0.655	1.046	1.02	0.0478	0.2	21
Porosity	0.674	0.396	0.506	0.505	0.0021	0.0	9
Degree of Saturation	0.719	0	0.511	0.530	0.0127	0.1	22
Air Content	0.474	0.124	0.250	0.241	0.0047	0.1	27

Table 3.13 A summary of the data collected in the field for 40 oilseed rape plants in 2017.

Measurement	Max	Min	Mean	Median	Variance	Standard Deviation	Coefficient of Variation %
Root failure moment (Nm)	2.041	0.138	0.792	0.714	0.178	0.422	53
Shear Strength (kPa)	58	15	37	38.5	127.4	11.3	31
Shear Strength (kPa)	66	19	39.325	37	165.9	12.9	33
Plant Height (cm)	38	28	31.1	31	4.5	2.1	7
Stem Diameter (mm)	28.8	10.7	17.7	17.75	14.5	3.8	21
Root Length (mm)	32	9	20.5	21	18.9	4.3	21
Plant Weight (g)	112.6	21	57.2	51.8	565.6	23.8	42
Root Diameter 1 (mm)	23.9	9	15.7	15.6	13.3	3.6	23
Root Diameter 2 (mm)	13.4	3.9	9.01	8.7	5.1	2.3	25
Root Diameter 3 (mm)	2.4	0.6	1.14	0.95	0.2	0.4	37
Root Depth (mm)	74.2	20.3	41.1	41.05	140.7	11.9	29
Number of Lateral Roots	16	2	7.7	8	9	3	39
Water Content (%)	27.80	17.48	22.8	22.67	7.3	2.7	12
Average Shear Strength (kPa)	60	19	38.16	38.75	119.5	10.9	29
Bulk Density (kgm^{-3})	1588	1286	1485	1527	10169	101	7
Dry Density (kgm^{-3})	1299	1066	1222	1240	5392	73	6
Void Ratio	1.55	1.045	1.224	1.18	0.0191	0.1382	11
Porosity	0.61	0.511	0.548	0.542	0.0007	0.0262	5
Degree of Saturation	0.64	0.324	0.508	0.532	0.0077	0.0878	17
Air Content	0.40	0.191	0.272	0.247	0.0037	0.0605	22

In 2018, 30 plants for wheat, 30 plants for oats and 20 plants for oilseed rape were collected. Figure 3.24 shows the data collected in 2018. These datasets were smaller and were used to validate the new models derived in this research. The values were within ranges meaured in 2017 for each crop type except the root plate diameter for oats, which was twice as large. This may be because changes in soil conditions and treatments.
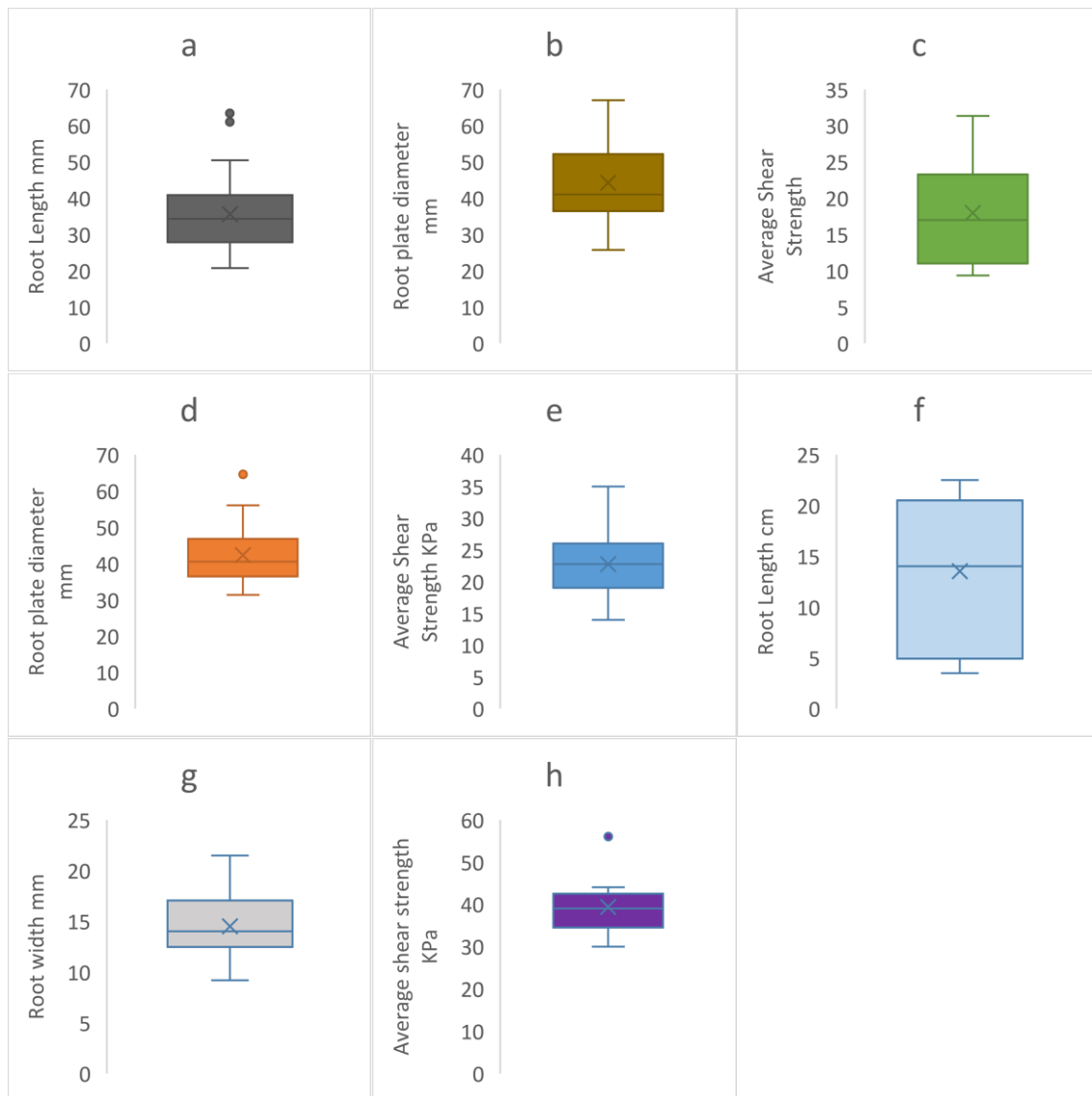
Figure 3.24 Plant and soil measurements for 2018 data collection. (a) root length, (b) root plate diameter (c) average shear strength for wheat. (d) root plate diameter and average shear strength for oats and (f) root length, (g) root diameter and (h) average shear strength for oilseed rape.

In summary, the techniques used to measure soil and plant variables produced a dataset that could be used to test the models. Data derived for the plant characteristics were close to those obtained by Berry et al., (2000) for wheat, and Goodman et al., (2001) for oilseed rape. The variability between plants could impact the predictions and comparisons of the models in Section 4.3.

3.4 Laboratory Experiments on Artificial Roots

During the field work study it was found that the maximum root failure moment had large variations, for wheat 0.105-0.669Nm, for oats 0.066-0.725Nm and oilseed rape 0.138-2.041Nm. The variability in the data may have been due to the differences between varieties of crop, spatail changes in soil strength, plant characteristics and root characteristics. There was a need to test the root failure moment of crops in more controlled testing conditions where the soil water content , soil type and plant charcateristics could be changed.

This section aims to develop suitable small-scale laboratory experiments to test a range of soil types and water contents as well as artificial roots. The main objective was to measure the lateral load-deflection (root failure moment-angle of rotation) curves and observe the root-soil reactions when the lateral force was applied to the artificial root stems. The results of the study would allow a better understanding of root anchorage resistance in different soil types at different water contents and with different artificial roots (none of these parameters have been tested in previous laboratory studies of wheat, oats or oilseed rape).

A series of lodging tests were performed in soil mixtures (coarse-grained and fine-grained) to investigate the load and displacement behaviour of artificial root models. An experiment was

also completed to observe the soil pressure distributions. The first step in developing the methodology was to create soil mixtures and collect soil samples from the field.

3.4.1   Soil Properties

Previous lodging studies using artificial roots have included soil composition and soil shear strength as the main soil parameters. Crook and Ennos, (1993) described their soil as sandy loam, which is a mixture of sand, silt and clay with the highest percentage being sand. The soil shear strength was varied between 4.4, 6.5, 10.2kPa. Goodman et al., (2001) used 66% sand, 14% silt and 20% clay, with a shear strength of 48.4kPa. Neither of these studies varied the soil type or water contents of the soil. In practice, agricultural soils can have soil compositions ranging from 10-66% sand, 18-65% silt and 16-35% clay (Tams et al., 2004). Moreover, soils in the field are subject to rainfall affecting the water content and thus the shear strength of the soil (soil water can reduce the soil strength by 60-80%, (Sterling et al., 2003)). Compaction of the soil can also affect the shear strength; however, too high a level of compaction will restrict the root growth (Merotto and Mundstock, 1999). Therefore, ranges of 1.35-1.45Mg/m^3 of soil density could be used according to Dexter and Birkas, (2004).

Two sources of soils were used for the experiments in this research, laboratory made and field samples. Soils were mixed in the laboratory from individual soil fractions to have similar particle size distributions as those found in the field study in 2017, specifically for fields which had wheat and oats growing in them. These were called Silt Mix 1, 2 and 3. To gain a better understanding of lodging in course grained soil, two soil samples were made with poorly-graded sand and well-graded sand. These were called Sand 1 and Sand 2. These results would be used as a comparison for the silt mixes as the behaviour may be easier to interpret.

The second source of soil samples was collected from ADAS Hereford (in 2017) in the UK. It was found that the soil from the Hereford site had large amounts of fine sand compared to wheat which had smaller amounts of coarse sand (Figure 3.25).

The soil samples were characterised using the same methodology as given in Section 3.3.2: particle size distribution (Table 3.14 and Figure 3.25) using shakers, sedimentation (Figure 3.26), plasticity index (Table 3.15), soil water characteristic curve (Figure 3.27), shear strength (Table 3.16).

Table 3.14 Soil characteristics and water contents used for laboratory testing.

Soil Mix	Fine Gravel Content %	Sand Content %			Silt Content %			Clay Content %	Water content at field capacity %
		Coarse	Medium	Fine	Coarse	Medium	Fine		
Sand 1- (poorly graded)	0.04	97.7	2.0	0.05	0	0	0	0	-
Sand 2- (well graded)	9.2	20.0	65.7	4.6	0	0	0	0	-
Silt Mix 1	15.2	15.9	43.2	19.9	2.3	2.1	0.7	0.1	15.4
Silt Mix 2	18.0	20.5	41.2	15.8	1.7	1.6	0.6	0.1	12.5
Silt Mix 3	18.8	19.4	41.3	14.6	2.4	2.3	0.7	0.1	12.7
Hereford	9.8	16.6	15.1	44.1	7.0	6.0	1.2	0.2	31.3

The water content was varied to determine its effect on root failure moment, which will add to existing research on root failure moments. Sterling et al. (2003) explain that shear strength of wet soil is 60%-80% less than dry soil. The water content in this research study was varied for each soil type. For sand mixes the water content was increased to change the shear strength properties of the sand. Two water contents for sand mixes, 0% and 10%. The water contents were chosen as those at wilting point and field capacity as these water contents are

significant for lodging. Three water contents for the silt mixes were tested, 10%, 12.5% and 15%. For Hereford, the water contents used for testing were 20% and 40%. For all of the soil samples the water contents were chosen to represent partially saturated conditions. This will affect the pore water pressure within the samples. For course-grained soil, such as the sand, the addition of a small percentage of water (10%) will cause an increase in pore pressure, resulting in apparent cohesion between the particles of the sand. This in turn will change the lodging resistance of the sand. In the silt mixes, the pore pressures decrease as the degree of saturation increases in the soil, this will also affect the lodging resistance. When loading in the form of lateral movement during lodging is applied to the soil, there will be changes in pore space distribution and hence, changes in matric suction. However, for this experiment it will be assumed that the pore pressure remains stable during testing as loading is applied for less than 10s, not giving pore pressures the opportunity to change.

Figure 3.25, Figure 3.26 and Table 3.14 summarise the results of the particle size distribution testing. Sand 1 had 97% coarse sand while Sand 2 had 65% medium sand, this difference may cause differences in lodging resistances during the anchorage experiments. The silt mixes were similar to each other in terms of silt and clay contents, with Silt Mix 1 having slightly larger amount of medium sand 43% compared to 41% for Silt Mix 2 and 3 and for fine sand, 19% compared to 15% for Silt Mix 2 and 14% for Silt Mix 3. Therefore, Silt Mix 1 may have different behaviour during the lodging testing. The particle size distributions of the silt mixes were within range of the real soil samples collected from the three fields (see Section 3.2.2.1). The Hereford sample had the largest amount of fine sand, coarse and medium silt, of all of the samples. This affected the soil water characteristic curves and plasticity index testing with the

Hereford sample having higher water contents at field capacity and wilting point (Table 3.14) and at the liquid and plastic limits (Table 3.14). The Hereford sample also had a higher plasticity index which means that the soil will take a larger amount of water before behaviour changes from solid to plastic and plastic to liquid behaviour.
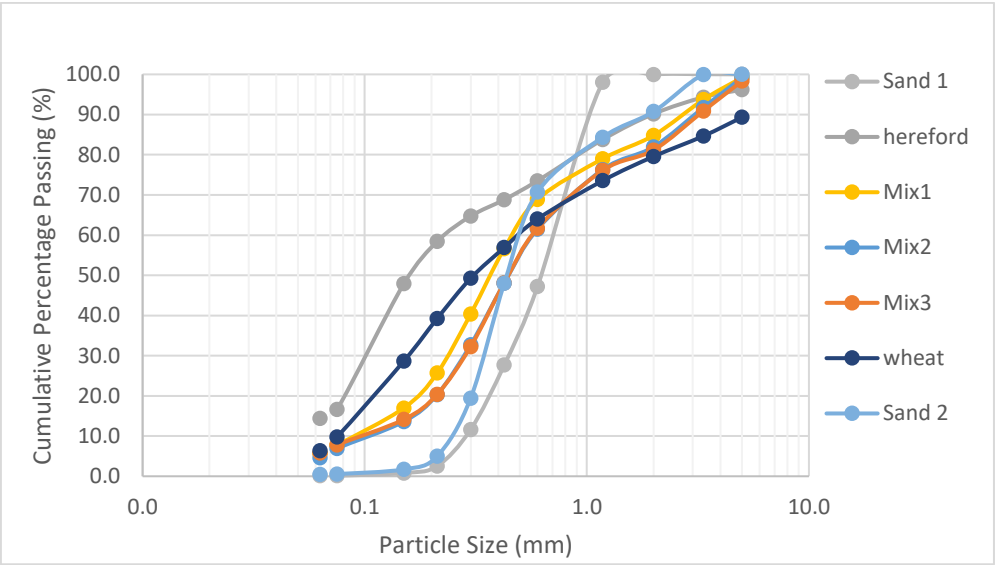
Figure 3.25 Particle size distribution of the five soils mixtures and soils collected in the field.
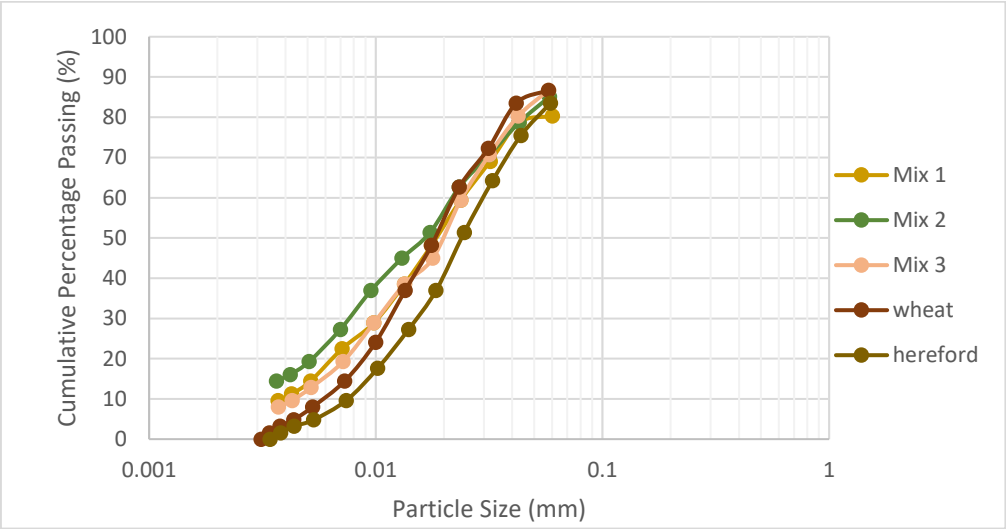
Figure 3.26 Sedimentation test for the soils used in the laboratory tests.
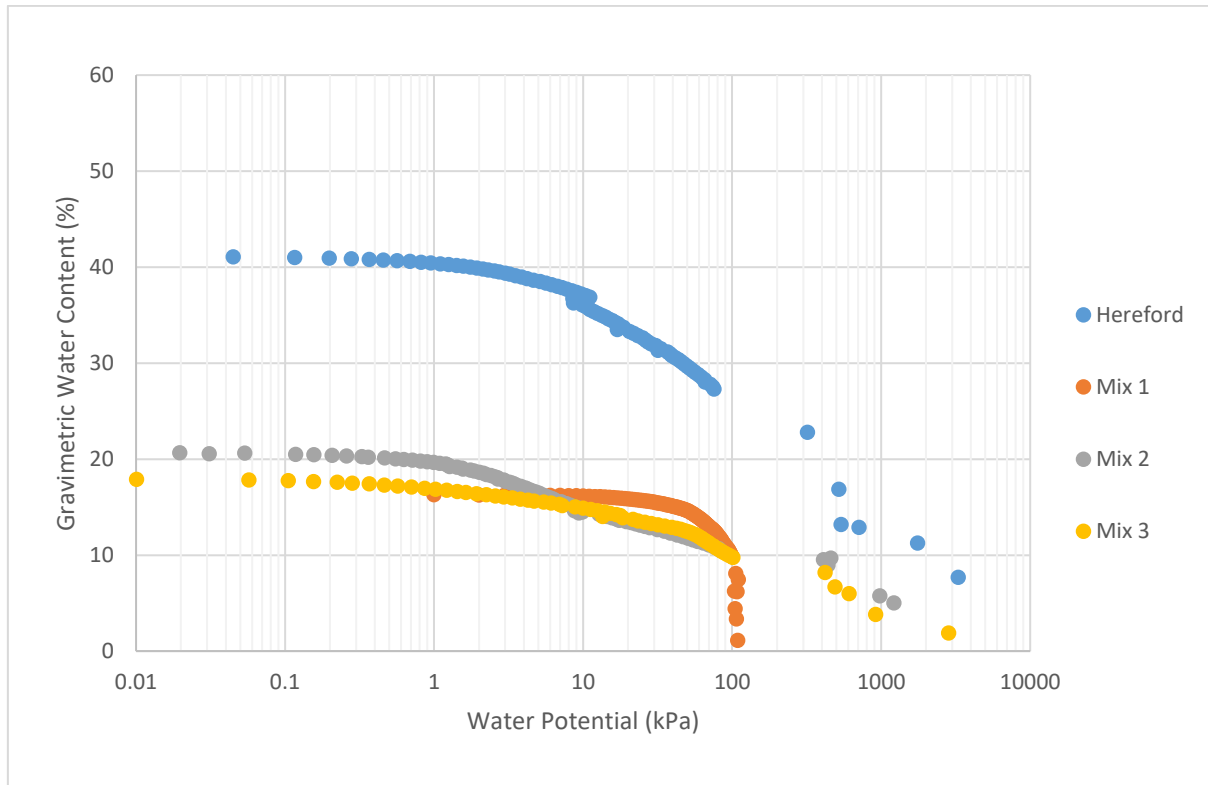
Figure 3.27 Soil water characteristic curve for the silt mixes and Hereford field sample collected.

Table 3.15 Plasticity Index test results for the soils in the laboratory experiment.

Sample Name	Liquid limit (%)	Plastic limit (%)	Plasticity Index
Hereford	39.2	26.3	12.9
Mix1	19.8	15.6	4.1
Mix2	21.6	17.7	3.9
Mix3	20.2	16.0	4.2

Finally, shear box tests were completed on the samples. These were used to understand the relationship of changes in soil strength with water content. The effective internal angle of friction reduced for sand mixes whereas the friction angle increased for silt mixes. Apparent cohesion increased for Sand 1 and decreased for Sand 2 suggesting that matric suction increased for Sand 1 and decreased for Sand 2. Sand 2 had the particle size distribution with more fine sand than Sand 1. The difference in particle size distribution between the sand mixtures affects the soil water characteristics. The difference is due to the capillary water

134

under suction in the soil pores. In Sand 1 (course grained soil), the soil pores are larger, which leads to water being held in the pores for a smaller range of suctions compared to the fine sand. It will also take less water for the matric suction to develop in Sand 1 compared to Sand 2. The apparent cohesion decreased for all of the silt mixes, suggesting that the matric suction also decreased. Ideally, the shear box testing in partially saturated soils should be undertaken using a suction controlled apparatus to understand the soil behaviour as the sample is being sheared. However, this apparatus was not available for this research, so the soil water characteristic curves were used to provide an indication of the matric suction at a given degree of saturation. These results may have different implications for the root anchorage response in different artificial root models. This is discussed further in Section 4.2.

Table 3.16 Results from the shear box testing of the soil samples used in the laboratory experiments. (Appendix D1 for shear box results).

Specimen	Effective Internal Angle of Friction, ϕ' (°)	Apparent Cohesion, c' (kPa)
Sand 1 (poorly graded) - 0% water content	38.6	2.9
Sand 1 (poorly graded) - 10% water content	31.3	4.3
Sand 2 (well graded) - 0% water content	32.5	5.7
Sand 2 (well graded) - 10% water content	31.3	5
Silt mix1 - 10% water content	24.2	17.6
Silt mix1 - 15% water content	31.9	2.6
Silt mix2 - 10% water content	30.7	14.1
Silt mix2 - 15% water content	37.0	0.4
Silt mix3 - 10% water content	22.8	18.8
Silt mix3 - 15% water content	26.2	2.1
Hereford	6.6	21.5

After selecting the most appropriate soil mixtures to test and characterising the key soil parameters, artificial roots had to be created for both wheat and oilseed rape representing the two different root types. This was more appropriate than using real roots, removing the variability of real roots and increase the repeatability of the tests. The development of the artificial root systems is discussed in the next section.

3.4.2 Development of artificial roots

Two methods were used to create 3D CAD designs of the artificial roots, measurements and 3D imaging. Measurements of real plants and measurements completed in Section 3.3.3.4. For wheat roots the root plate diameter ranged from 39.9-165mm, the individual root diameter ranged from 1-3.3mm, the root number ranged from 5-18 and rooting depth ranged from 9-60.1mm. The root models were drawn using CAD software (Autodesk® Fusion 360™) and then created using the CubePro® Duo and ABS (acrylonitrile butadiene styrene) material.(Liang and Knappett, 2013) and Liang et al., (2017) used ABS materials for soil-root interaction testing, in root reinforced shear strength testing. ABS was chosen because of it has tensile strength properties that are within range of real roots. Crook and Ennos (1993) used polyethelene plastic and Goodman et al., (2001) used steel rods.

This resulted in a simplified artificial root as shown in Figure 3.28. Unfortunately, this model had structural problems along the curvatures of the roots, due to a limitation of the CubePro® Duo and creating adequate support for the structure as it was printed. A different 3D printer was used in the Department of Physics. However, only four artificial roots could be printed because of budget restraints. These roots were used in the laboratory work for qualitative study as they were prone to breaking (see Section 4.2.1).

136
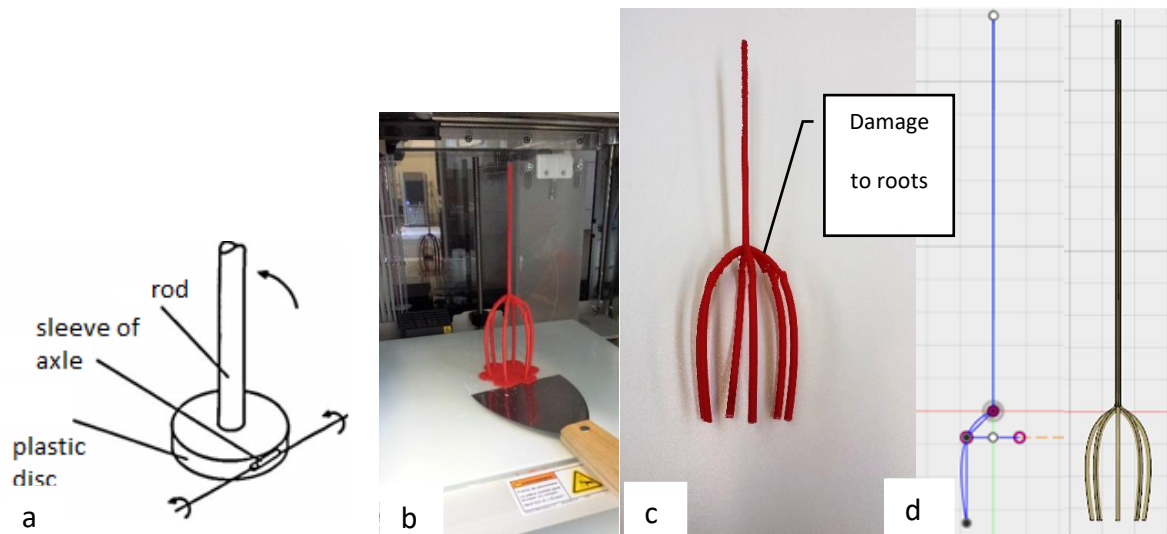
Figure 3.28 (a) Model created by Crook and Ennos, 1993, (b and c) 3D printed models of wheat root with six structural roots, 4mm diameter, 205mm in height (d) the CAD drawing of the root.

In order to create the artificial roots for oilseed rape, roots taken from Hereford in August 2015 and kept in the refrigerator at 5°. The top of the roots were photographed after they had been air dried for several days. The aim was to create a digital model of the root system. Therefore, the root sample was mounted on a stand with a scale and forty overlapping images were taken using a DSLR camera circling the root system twice, as well as taking some images from above. Images were checked for quality and clarity, and any images that were not focussed were discarded and retaken. The collected pictures were then processed using an algorithm developed in the Department of Electrical, Electronics and Systems Engineering, which took the images and virtually stitched them together to create a point file (.ply). This was then processed in MeshLab, a 3D visualisation application, which creates a mesh of the 3D root. The mesh was then uploaded into Autodesk® Fusion 360™, where a model could be built on top of it. Results of the 3D image are shown in Figure 3.29. Although this artificial root system was the most accurate one created, it was too expensive to create duplicates. When

tested in the laboratory the model broke, as the roots were not structurally sound. Therefore, 3D printing was not pursued further.
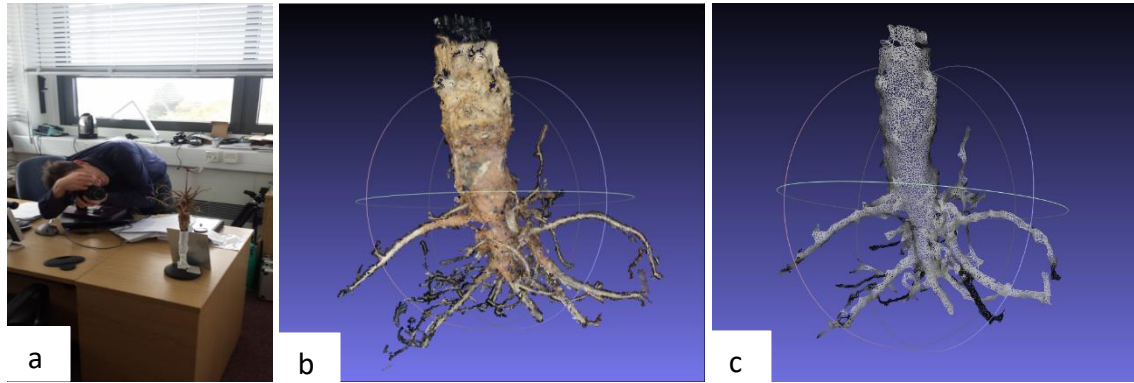
Figure 3.29 (a) Dr Tim Collins (Electrical Engineering) taking the overlapping pictures, (b and c) the results of the algorithm viewed in MeshLab.

After these two techniques were trialled, tests were completed to understand the strength of roots. Tensile strength tests were completed on wheat, oilseed rape and oat roots. For these tests, the first 40 mm of the roots were sliced from the main stem (in the case of oilseed rape the lateral roots were removed from the tap root) and the root diameters were measured at three points along the root to provide an average. They were then inspected for any damage and all intact specimens were placed in a ziplock bag (for an hour at room temperature) in order to retain their water and thus structural characteristics and then taken to the testing machine. Tests took place on an ESH Instron testing machine in the Fatigue and Fracture Laboratory, School of Metallurgy and Materials, University of Birmingham. This machine provides a low constant rate of extension and for these tests it was set to 1mm per minute and it was fitted with a 1kN load cell. The samples were then carefully placed into the grips which were lined with sandpaper as seen in Figure 3.30 in order to increase the friction between the root and the grips so that the root was not slipping out of the grips. Slippage of

the roots had been identified as a problem in initial testing of sunflower roots. The stress and strain were recorded.

Figure 3.30 (a) Wheat root sample set in grips (b) wheat roots being tested in tension.

For oilseed rape root discs, axial compression testing was also completed as these roots were tap roots. Each disc was cut for a single tap root with a length twice the diameter (according to (Keogh et al., 2014) who completed axial compression test on bamboo) from the first 50 mm of the tap root. Samples were tested in compression using again the Instron machine in the Fatigue and Fracture laboratory. These tests were completed to get a general idea of the strength of the roots from Oak Park. The results are shown in Figure 3.32 and Figure 3.31. Oilseed rape tap root crush test were completed on four samples, maximum forces ranged from 20.18-49.59N. The tensile strength of the wheat, oat and oilseed rape lateral roots found slight differences in ranges of values for root tensile strength. Oilseed lateral roots range from 23-82MPa, oats from 33-98MPa and wheat from 10-102MPa.
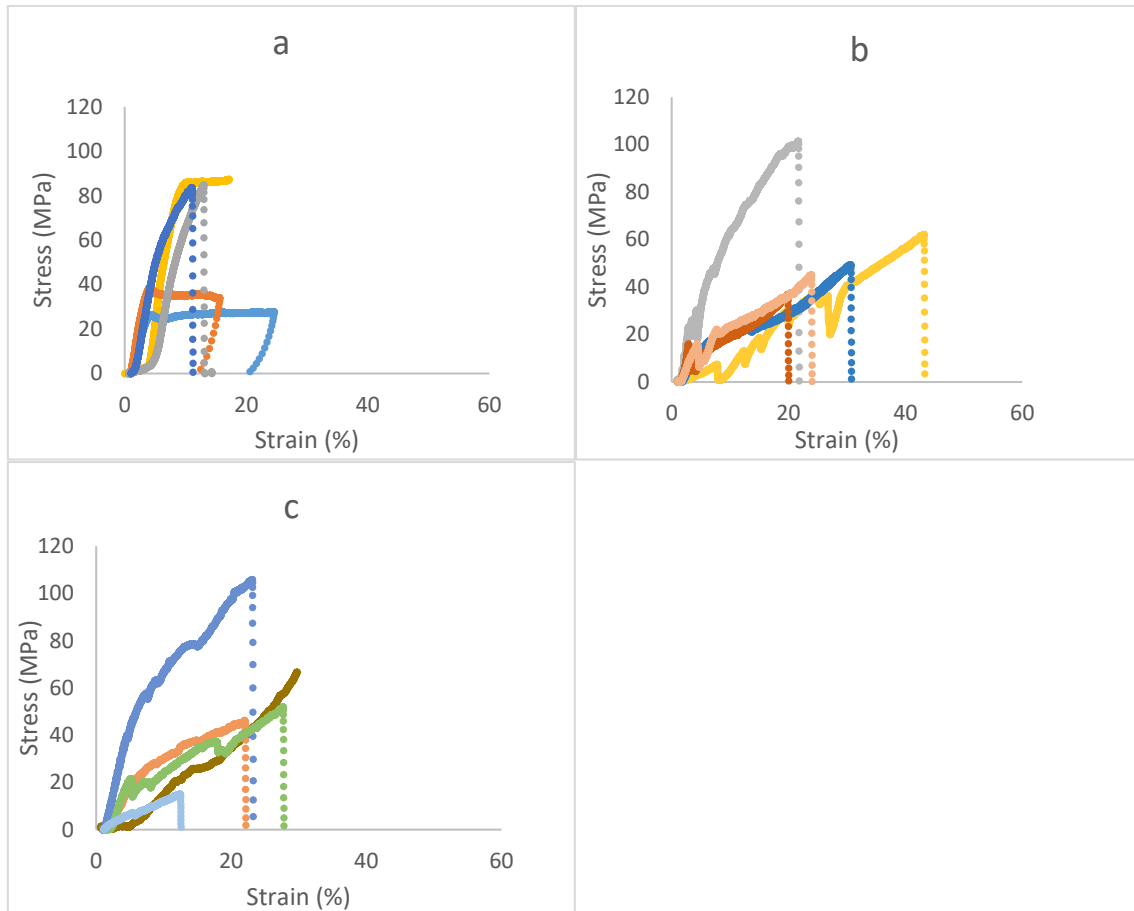
Figure 3.31 Strength testing of oilseed rape, oat and wheat roots. The lateral oilseed rape roots and roots of oats and wheat were tested in tension. (a) Oilseed rape tensile strength test, (b) Oat tensile strength test, (c) Wheat tensile strength test.
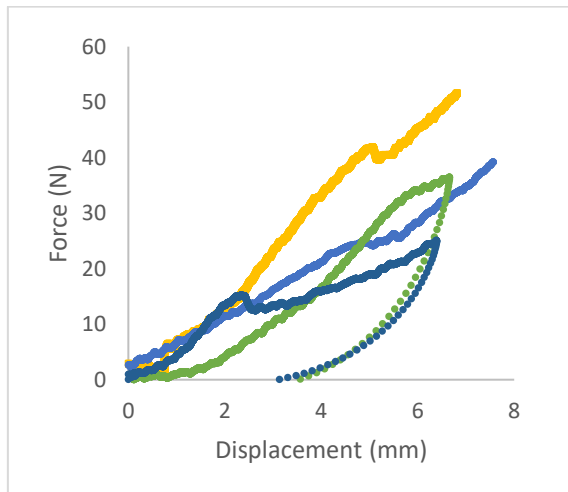
Figure 3.32 Oilseed rape crush tests. Tap roots were tested in compression.

After the initial attempts to created roots and the root strength testing, artificial roots for wheat were created manually by cutting bending and soldering brass and binding wire (Stokes

140

et al., 1996). Binding wire was used for the flexible wheat roots and had a tensile strength between 380-450MPa. Short brass sections were used for the artificial rigid wheat roots. The four different artificial root systems are shown in Figure 3.33 and Table 3.17. The oilseed rape models were simplified to a 16mm nylon rod for the rigid root system and a 6mm nylon rod for the flexible root system. Nylon was used because of the 80MPa strength was closer to real root strengths measured in this research. Crook and Ennos, (1993) and Goodman et al., (2001) used rigid plastic and steel for their models. No root structures were included for wheat model, a disk was used to represent the roots. This research improved the artificial root structures by including root structures and artificial roots with two different flexibilities. This will help in the understanding of the differences between rigid models and real roots by providing results for models with properties closer to reality.

Table 3.17 Summary of the geometry of the models tested in the experiment.

Dimensions	Rigid Wheat/Oats	Flexible Wheat/Oats	Rigid Oilseed	Flexible Oilseed
Root Length	70mm	50mm	50mm	50mm
Root Diameter	3mm	0.6mm	16mm	6mm
Stem Diameter	3mm	3mm	16mm	6mm
Root Cone Diameter	43mm	31.7mm	-	-
Stem Length	27cm	28cm	100cm	100cm
Root Number	6	16	1	1
Weight	51.49g	26.24g	256.58g	37.19g
Material	Brass	Brass and binding wire (380-450MPa)	Nylon 80MPa	Nylon 80MPa
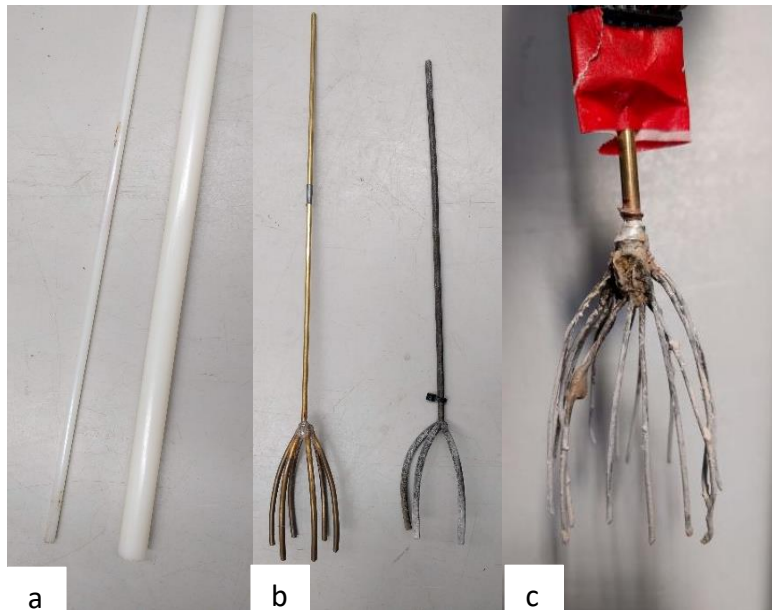
Figure 3.33 Root models used in the laboratory research, (a) the flexible oilseed rape root and the rigid oilseed rape root, (b) the rigid wheat root and the model used in the qualitative tests, (c) the flexible wheat root model.

3.4.3   Anchorage failure measurements on artificial roots

The method for the anchorage failure measurements on artificial roots consisted of preparing the soil in a testing container, planting the artificial root and testing the root with the lodging instrument developed in Section 3.2.3.2. The soil mixture was mixed with the appropriate water content. Gance, (2015), had used a box with dimensions 0.150 x 0.205 x 0.120m which was found to be the appropriate size to allow soil movement without interacting with the side of the box. In these anchorage failure tests, the container had dimensions of 0.201 x 0.201 x 0.13m. In order to evaluate there would be any interaction with the side of the box, the artificial roots were buried to a depth of 70mm, 60mm and 50mm, completely dislodged and the length of the wedge, which had formed at the back of the artificial root model measured. The wedge was approximately 82mm. Eliminating the boundary conditions allows individual responses of the artificial roots to be imposed by the load applied by the machine only.

142

All artificial roots were buried at a depth of 50mm, this was marked onto the model before testing. Compaction around the delicate root structures was difficult and a number of methods for burial of the artificial root systems were investigated involving pushing or rotating the plastic cylinders into the soil (Crook and Ennos, 1993; Goodman et al., 2001), pluviating (pouring) the soil around the root system (Liang and Knappett, 2013; Mickovski et al., 2010) or packing the soil around the model and then saturating the sample as used by (Stokes et al., 1996). Considering the aim of this research was to bury the root structures with as little disturbance of the soil around the roots, pushing the samples into the soil disturbed the soil before testing began and hence this method was not appropriate. Pluviation could not be completed using the silt mixes because of the apparent cohesion of the material. Therefore, the most appropriate method was packing the soil around the roots using fingers and a handheld tamper.

The soil was compacted in two layers to achieve the required density, this is the same procedure as Gance, (2015). Half of the soil mix was placed inside the box. The soil was then compacted with 40 blows from a height of 50mm using a metal cylindrical tamper with a weight of 3.718kg, a diameter of 51mm diameter and a height of 240mm. In the corners of the box a square piece of wood was placed and the tamper applied on top. Then the model was placed into the centre of the box and held with a retort stand. Thereafter, the remaining soil was added around the model and compacted with the handheld tamper around the model. The final depth of the soil was 125mm and 130mm in the container. This resulted in densities ranging between,1546-1687 kg/m^3 which was in range of the soils in all three of the fields tested at the Oak Park field site.

After, the final depth of the artificial root model in the soil was measured. The root model was removed, and the shear strength was measured using the 19mm hand vane shear in the undisturbed areas around the sample ensuring that there was at least a 50 mm gap between the disturbed soil and the side of the box. This was done so there was no interaction between the shear vane and the side of the box. The centre to centre distance between the points of measurement should not be less than 2.3 times the blade width of the shear vane (BS1, 2016) Therefore, 50mm was used as a safe spacing away from the side of the box.

To test the repeatability of the measurement the lodging tests were repeated 8 times and 11 times specifically to understand the output from the lodging instrument. Figure 3.34 and Figure 3.35 show the resistance over time of the lodging of a plastic rod and wooden rod. The maximum resistances vary from 0.07 to 0.13kg for the non-flexible plastic rod and 0.04 to 0.15 for the flexible rod. The depth of the artificial root and the density of the soil were not monitored in these initial experiments which led to the variability of the maximum resistances. However, there were similarities in the shape of the graphs which suggested that the artificial roots were undergoing similar failure mechanisms. The exceptions were two tests on the non-flexible artificial root shown in Figure 3.34. Tests 6 and 8 showed failures associated with the artificial plant toppling over when tested. Therefore, differences in root failure could be identified from the new lodging experiments.

Dry Sand, 6mm
plastic (non-flex)
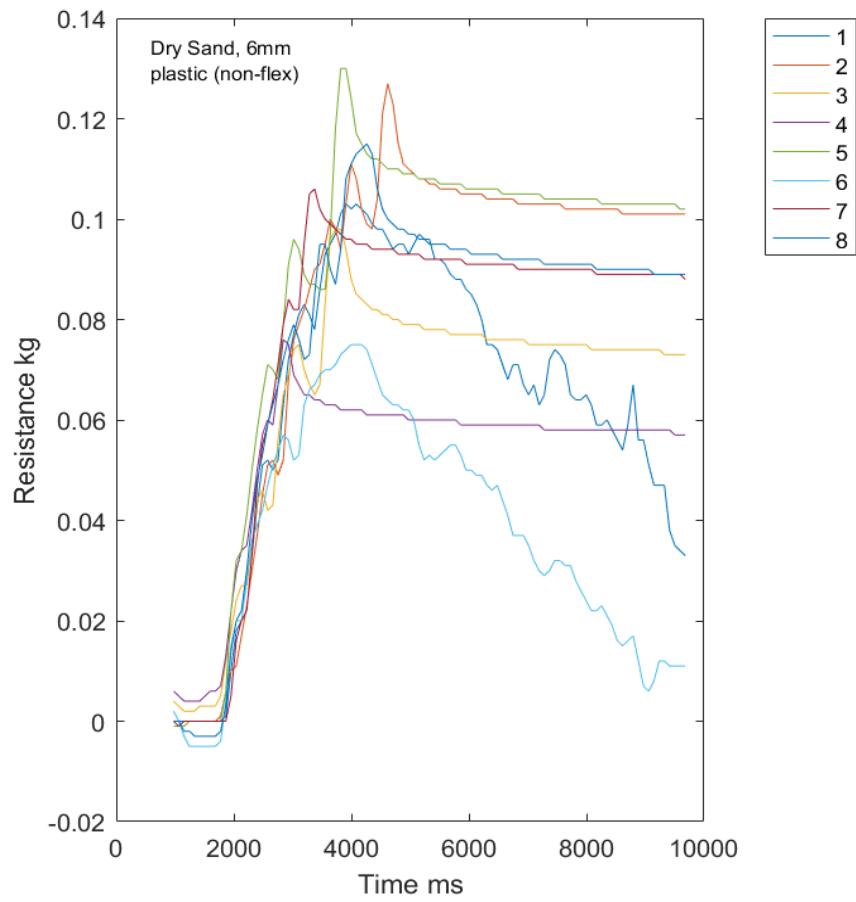
Figure 3.34 Initial test completed using the lodging machine, dry sand and a plastic rod (608 x 16 x 9mm). The test was repeated 8 times.

145
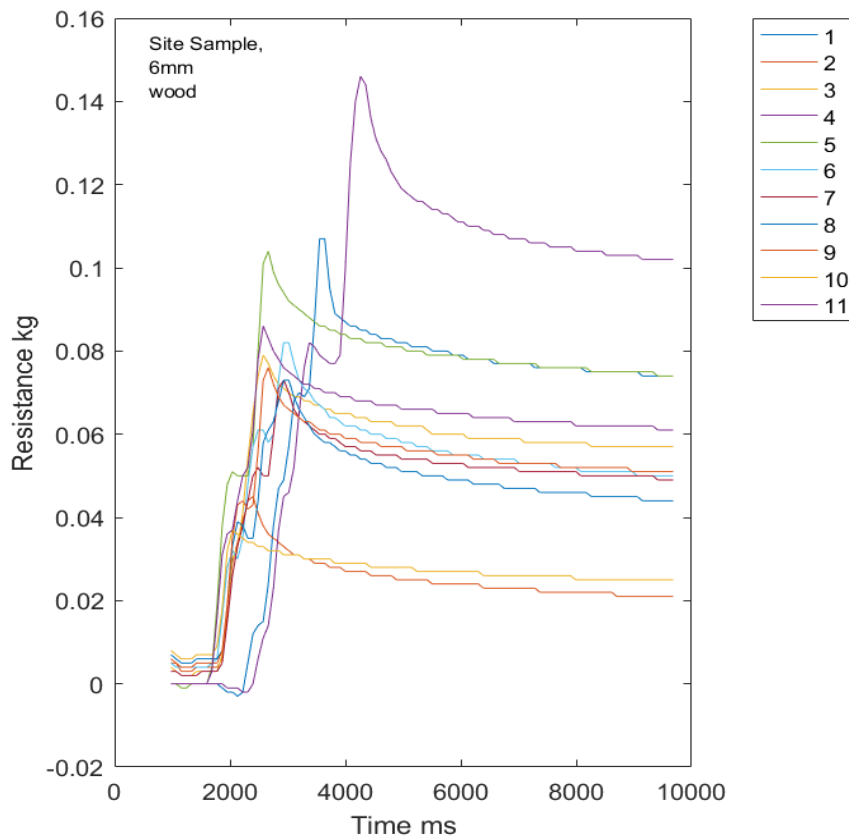
Figure 3.35 Initial tests completed with the site sample and a wooden rod (778 x 9 x 5 mm). The same test was repeated 11 times.

When the testing procedure was used with the density (1450kg/m^3) and planting depth (50mm) monitored carefully, the variability of the results was reduced. This is shown in the results of another preliminary study in Figure 3.36. These tests were repeated three times each. The results were less variable however, Figure 3.36c, there was a result that was considerably lower than the other values and was considered an outlier. From these experiments the lodging tests repeated 2 or 3 times per test as the tests indicate the behaviour is repeatable, the accuracy of the measurements would be variable, and comparison made with caution. These tests also highlighted the differences between flexible and rigid artificial

146

roots. There was a slower possibly more plastic response for the flexible model compared to

the abrupt rise and plateau of root failure moment in the rigid models.
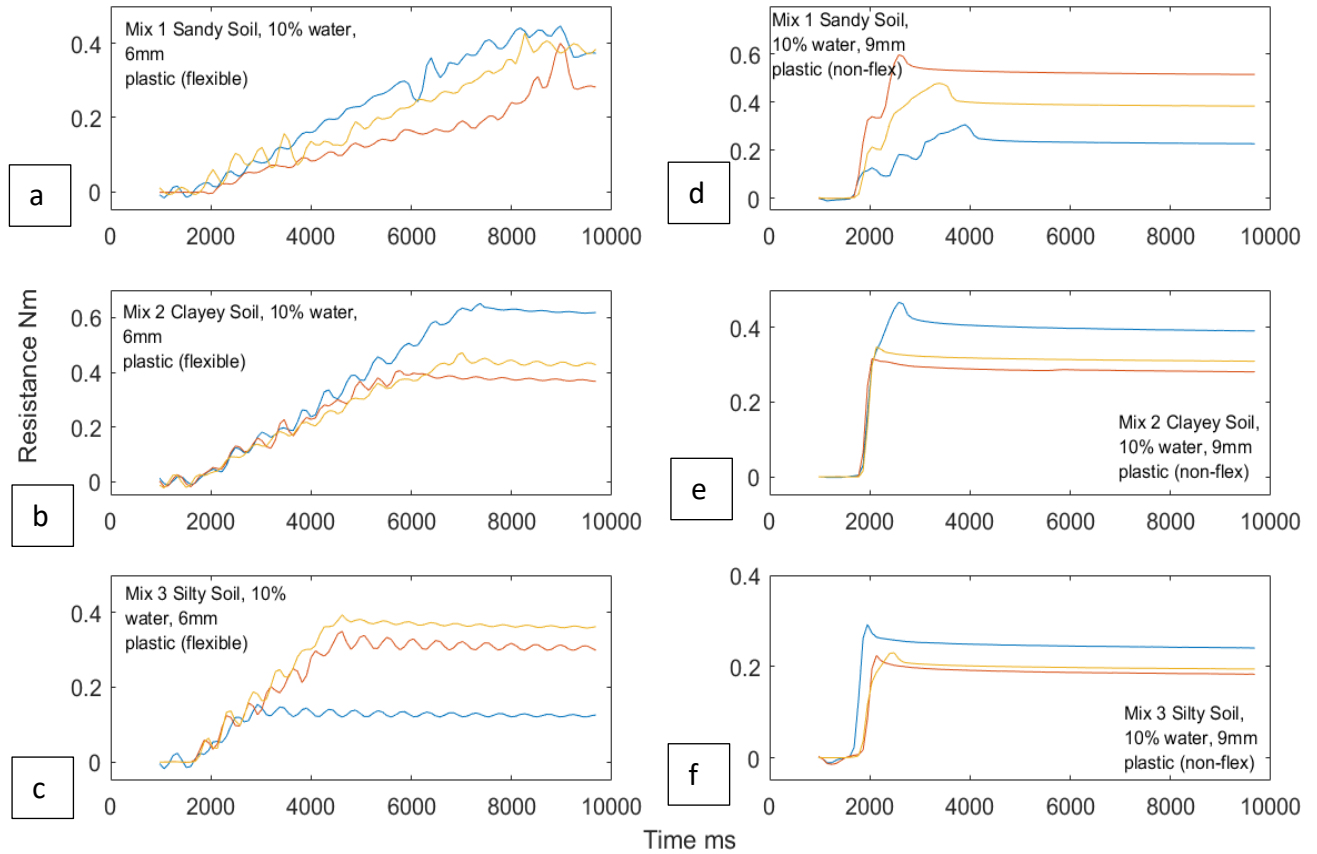
Figure 3.36 Results of tests using 3 soil mixes at 10% water content. The 3 soil mixes were: Mix 1, Mix 2, Mix 3. The mixes were designed to represent soils in the field with variations in clay, silt and sand particle sizes. The model in (a), (b), (c) show an artificial plant (1000 x 6mm dimensions of a wheat stem). In (d), (e), (f), a (608 x 16 x 9mm) plastic rod was used as the non-flexible model.

The measurements from the lodging instrument were converted from kg to Nm (as mentioned

in Section 3.1.3.1), then plotted on graphs of root failure moment against the angle of rotation

as was done in previous research (Figure 3.37). After the lodging tests were completed in the

laboratory, the same lodging device was taken into the field as discussed in Section 3.2.3.3. As

mentioned in Section 3.2.3.3, the root failure moment-angle of rotation data were collected

for real plants in the field. This meant that the results from the test results presented in the

literature, those collected from the field tests and the tests completed in the laboratory could all be compared.
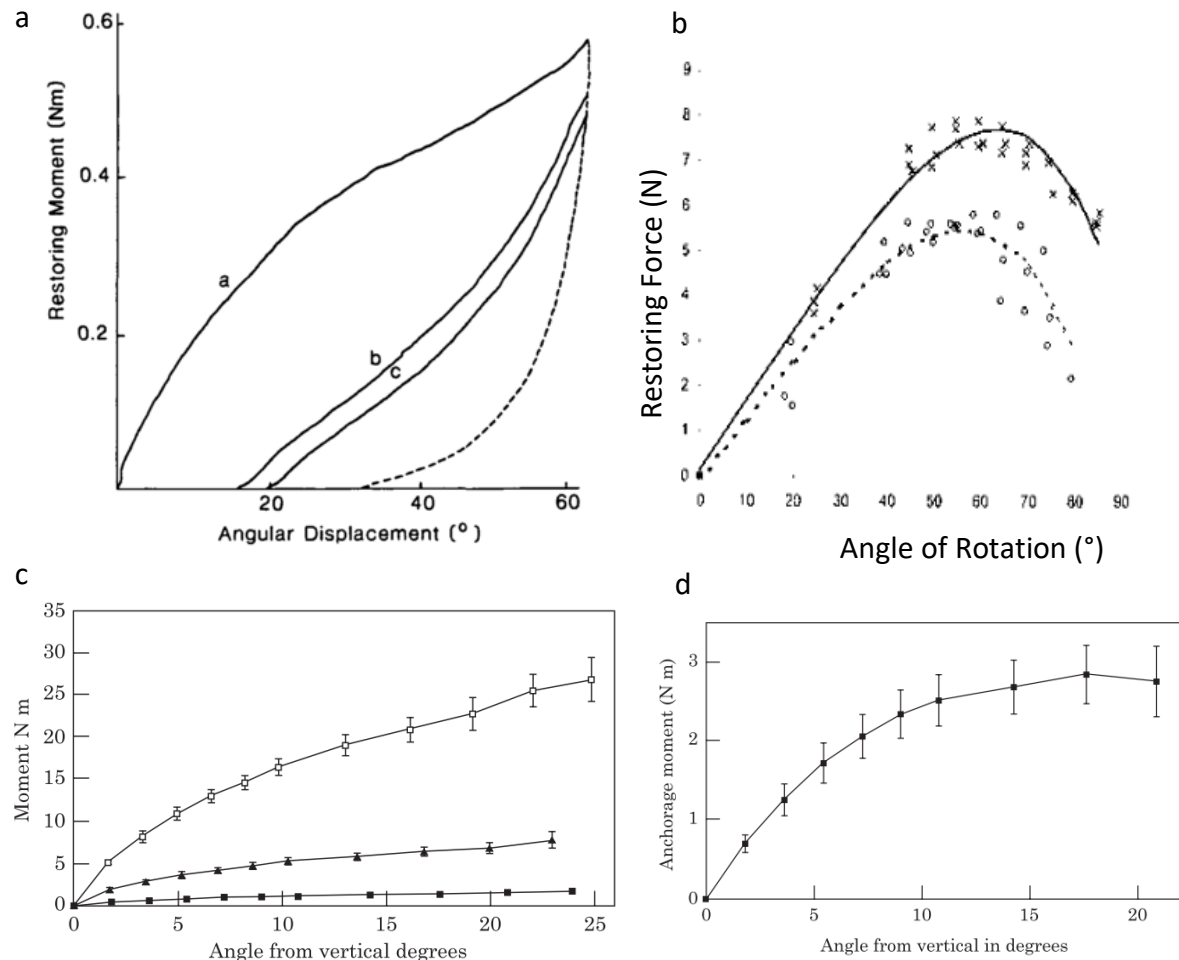
Figure 3.37 (a) The result of one lodging test conducted by Crook and Ennos, (1993), (b) Restoring force-angle of rotation, measured by Berry et al., (2003) (c) The results of 10 model anchorage tests on 15 mm diameter steel tubes at a depth of 30 mm (squares), 60 mm (triangles), 90 mm (empty squares). (d) The results for 13 anchorage tests of winter oilseed rape plants. The resistance reached a maximum at 18 degrees (Goodman et al., 2001).

These graphs can be related to the lateral load-displacement curves for piles, and comparisons can be made about the behaviour of the root models under different conditions. The root failure moment-angle of rotation curves measured in this research are a form of load-displacement or stress-strain curve used to characterise materials. Soils are normally

considered to be elastoplastic materials, meaning that they have a stress-strain relationship as shown in Figure 3.38 (Johnson et al., 2006). When soil is subjected to loading, any deformation contains both recoverable (perfectly plastic) and non-recoverable (perfectly elastic) components. Therefore, a failure criterion is needed in elastic models to define the stress state at which there is non-recoverable plastic deformation. One of the main failure envelopes used in geotechnical engineering is the Mohr-Coulomb surface as shown in Figure 3.38c. The soil will behave elastically if the stress point lies within the failure envelop (below the failure line). If the stress reaches the yield surface, the material will undergo a degree of plastic deformation (Johnson et al., 2006). Like the stress-strain curve, the root failure moment-rotation curves represent the development of the soil resistance response as the angle of rotation increases. This may be directly related to the shearing characteristics of the soil, for example, as the soil water content changes the response would change. Typical root failure curves measured in this research are shown in Figure 3.39.
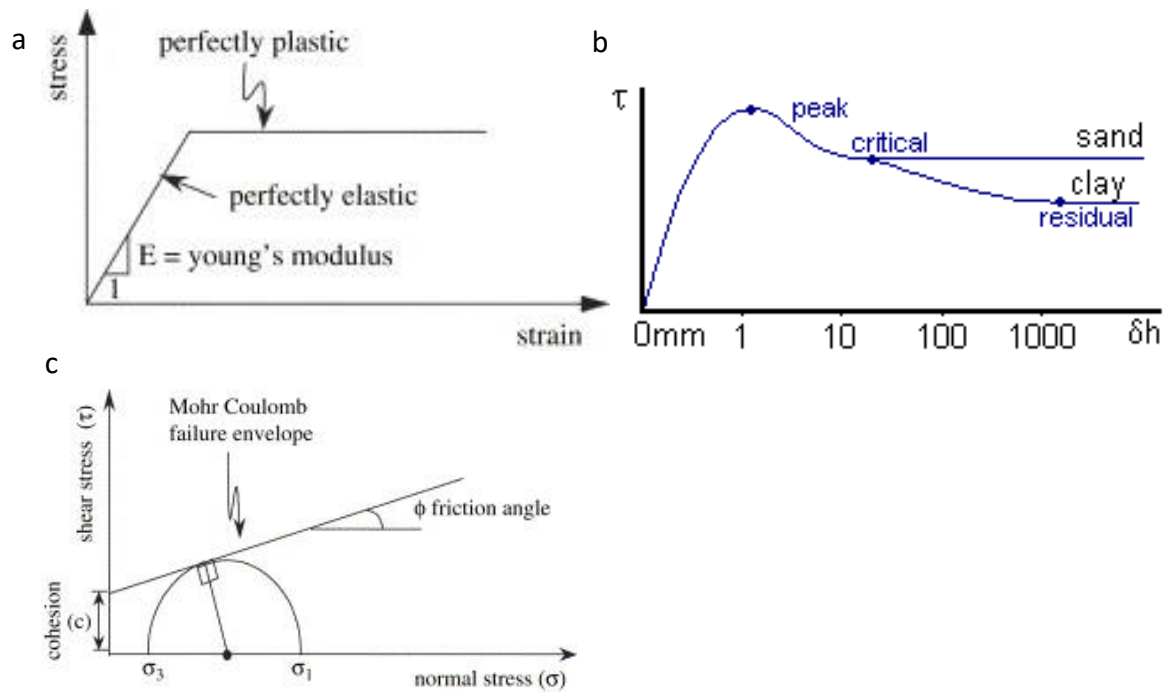
Figure 3.38 (a) Stress-strain relationship for an ideal elastoplastic material (Johnson et al., 2006). (b) The stress-strain relationship for soils (Leslie Davison, 2000). (c) Mohr Coulomb's failure surface (Johnson et al., 2006).
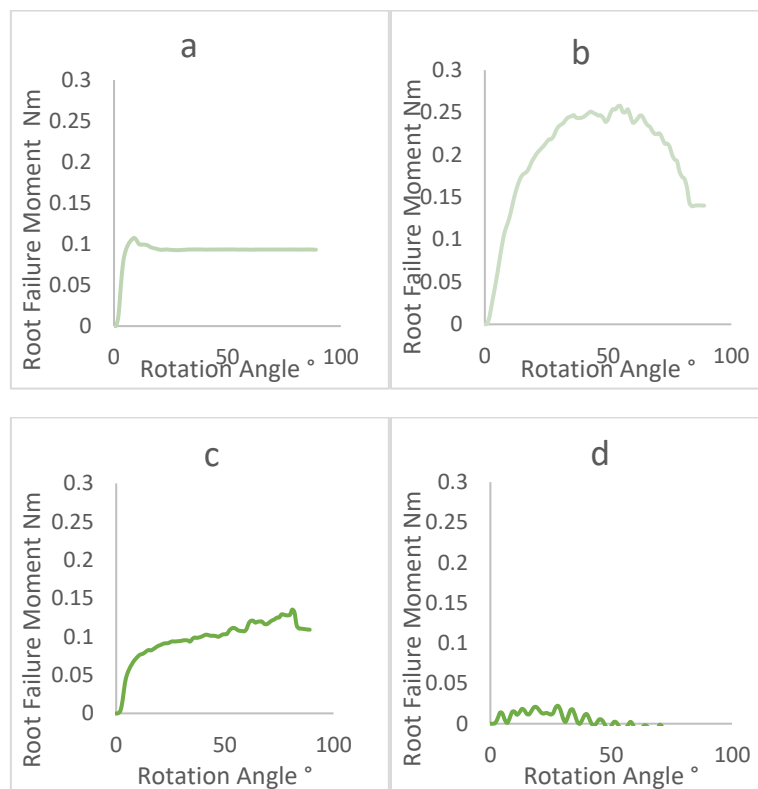
Figure 3.39 Different root failure responses measured in the laboratory research (a) Type A curve, model type W1 Sand 1 0% water content (b) Type B curve, model type W1 Sand 1 0% water content (c) Type C curve W1 Silt Mix 1 10% water content (d) Type D curve 6mm – Sand 1 0% water content.

Figure 3.39a shows a curve where the root failure moment versus rotation angle is behaving similarly to that of shearing a dense sand (see Figure 4.19b), with an initial elastic response followed by a peak resistance and an immediate reduction in resistance (dilation or strain softening) to the residual resistance (plastic equilibrium or critical state). For this research, this behaviour will be called Type A.

Figure 3.39b shows there is an initial elastic response, followed by a further increase in resistance at a lesser gradient, then, after the peak resistance is reached, the resistance decreases as a result of strain hardening because the particles are being compressed together, increasing the resistance. For this research, this behaviour will be called Type B.

Figure 3.39c indicates there is an initial elastic response (with a steep gradient) followed by a transition into a second phase of plastic response (with a shallow gradient, still increasing, still showing compression of soil particles), followed by the peak resistance and a sudden reduction in resistance at the peak strain. For this research, this behaviour will be called Type C. Figure 3.39d shows a reduced response possibly due to soils with lower shear strength, called Type D.

3.4.4 Assessing failure mechanisms through qualitative study

This experiment was designed to observe the mechanism of failure of the simple root models in fine-grained and coarse-grained material in the laboratory. A different box was used for this experiment as the original box shown in Figure 3.17b was not transparent enough. The new box was made of marine plywood with a transparent acrylic sheet placed at the front of the box which allowed the movements of the artificial roots to be recorded by a camera. The artificial roots were buried in the soil and set up to be touching the acrylic. Artificial roots for

oilseed rape of lengths of 6mm and 16mm respectively and half of a simplified wheat root with 4 roots and a cone diameter of 50mm (see Figure 3.33b) utilised in the lodging tests using the same methodology as described in Section 3.13.1. No lodging resistance data were recorded from these experiments as the interaction between the soil and the acrylic sheet would have influenced the results. As mentioned above, these tests were only intended to provide some qualitative results on the behaviour of the soil-root interaction during lodging. Pictures were analysed with ImageJ software and shear planes on both sides of the samples were identified and characterised.

The depth of the embedment of the samples was assessed in order to understand the effect of root depth on resistance. This was done by varying the depth of embedment of the samples using 50mm, 70mm and 100mm for the rigid and flexible oilseed rape roots, which was different to the range of values used by Goodman et al., (2001). They tested anchorage of the metal tubes at depths of 30, 60 and 90mm. Depths were chosen based on the lengths of roots found in the field and the literature which were ranged between 20.3mm and 126mm (Berry et al., 2013).

3.5   Summary

This chapter described the development of the methodologies used for laboratory and field testing focussing on root anchorage and characterisation tests for both the root systems and the soil. These will be used for the comparison of the models in the results section. The chapter provided all the results from the soil characterisation tests, which showed the soils at Oak Park were silty Sands and root measurements were presented which showed variability. The methodology for field anchorage testing was also modified and a new anchorage failure

machine was developed and tested. The development of the laboratory methodology was described. It also detailed how artificial root systems were created using both 3D printing and wires for both the tap root system found in oilseed rape and the plate roots found in wheat. Finally, a method for assessing failure mechanisms was developed and described. This assessment will be used to develop the new model of root anchorage.

4 Results and Discussion: Field investigation, laboratory experiments and development of root anchorage models

4.1 Introduction

This chapter presents the results of the field investigation, laboratory experiments and the development of the anchorage failure models for wheat, oats and oilseed rape. The field anchorage experiments are presented first, with results of field measurements of the root failure moment using both an old lodging instrument and a new lodging instrument presented in Section 4.2. Section 4.3 contains the results for the laboratory experiments on artificial roots, qualitative results of the anchorage failure of artificial roots, experimental root failure moments for sandy soils and experiments of root failure moments for silty soils. Section 4.4 presents results of the comparison of root anchorage models found in the literature and a comparison of the soil strength model by Baker et al., (1998) to measurements of soil strength taken in the field. Section 4.5 contains a description of the under-reamed pile model, followed by the development of the root anchorage for wheat and oats, including a sensitivity analysis and validation of the new model. This is followed by the separate development of the root anchorage model for oilseed rape, including a sensitivity analysis and validation. The final sections include the integration of the models into the lodging risk model by Baker et al., (1998) and a methodology for practitioners to collect data for the new models.

4.2   Field Anchorage Experiments

4.2.1   Field measurements of root failure moment using the old lodging instrument

This section presents the results of the anchorage tests on wheat, oats and oilseed rape. These measurements will be used to compare the predictions of the anchorage models in Section 4.3.1. Figure 4.1 presents boxplots of the results of 72 measurements of wheat root failure measured during the 2017 field trial. As mentioned previously, the boxplot represents a summary of the variability of the data.

Figure 4.1 shows results for the four varieties of wheat, Rockerfeller, JB Diego, Stigg and Cordiale, for the high and low seeding rates. The root failure moment was 0.669Nm for wheat, however, this measurement occurred in the treatment with the most variability, treatment 7, JB Diego with low seeding rate. Cordiale, JB Diego and Rockerfeller had unexpected results, with the mean of the resistances of the low seeding rates being lower than the mean of the high seeding rates. Stigg had the expected outcome, with the low seeding rate having a higher average root anchorage resistance. Reasons for this could be variations between root parameters in varieties.

Berry et al., (2003) found the average root failure moment to be 0.347Nm for wheat, lower than the results for this experiment. This could be because of differences in plant and root structures as well as soil composition and soil strength. The soil composition was loamy sand and the average shear strength was 4kPa. Root plate spread varied from 22-73mm.

155
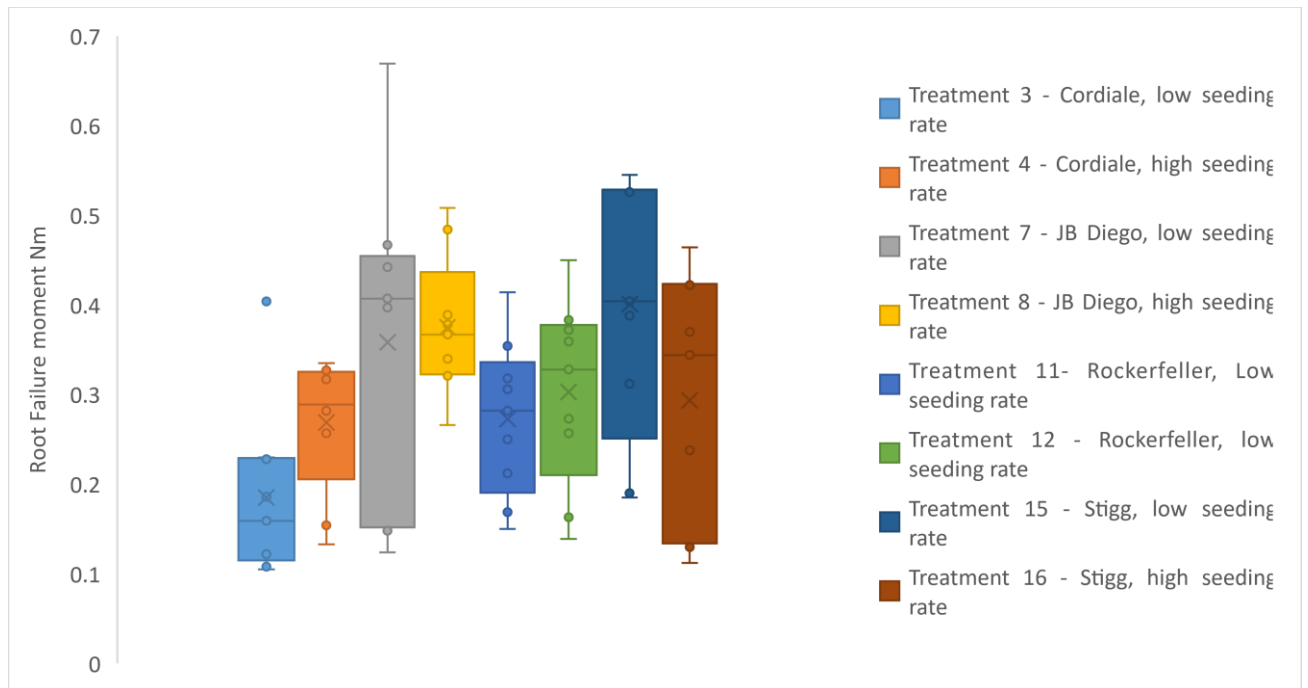
Figure 4.1 Root failure moment readings for eight treatments for wheat. Each boxplot contains 9 measurements.

Figure 4.2 presents the results of the anchorage testing for oats. The variety, Barra was tested.

The resistances range from 0.06 to 0.725Nm for all of the samples. However, the largest value

was outside the 95 percentile and hence was considered an outlier. There was a clear

difference between the treatments with low and high seeding rates compared with the results

from the wheat plants. There values for each treatment had smaller ranges than wheat.
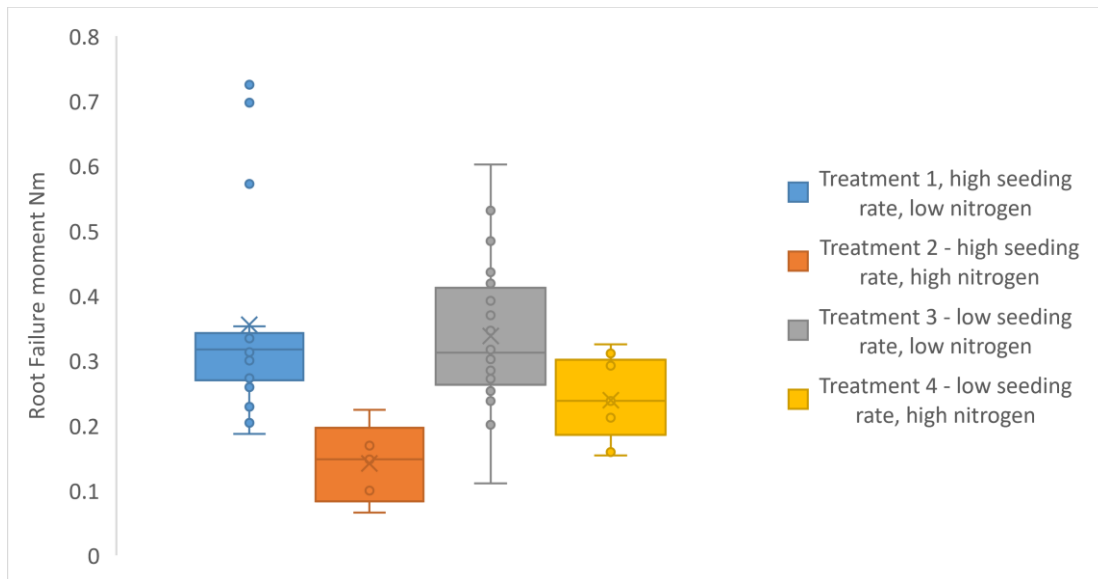
Figure 4.2 Root failure moment readings for two treatments of oats. Each boxplot contains 12 measurements.

Figure 4.3 shows the root failure moment values for oilseed rape. The root failure moment was 2.041Nm for oilseed rape. The range of values for oilseed rape was large between 0.1 to 2.041 for treatment one while the ranges for treatment 2 was smaller. Compared to wheat and oats, oilseed rape had the largest variability for maximum resistance. This variability was reflected in the plant characteristics discussed in Section 3.3.3.4. The mean root failure moment of oilseed rape measured by Goodman et al., (2001) was 2.9Nm, which is similar to the measurements found in this study.

Figure 4.4 shows the results of measuring root failure moments for wheat, oats and oilseed rape in 2018. The values were within ranges collected in 2017 with means of 0.13 for wheat, 0.12 for oats and 0.43 for oilseed rape.
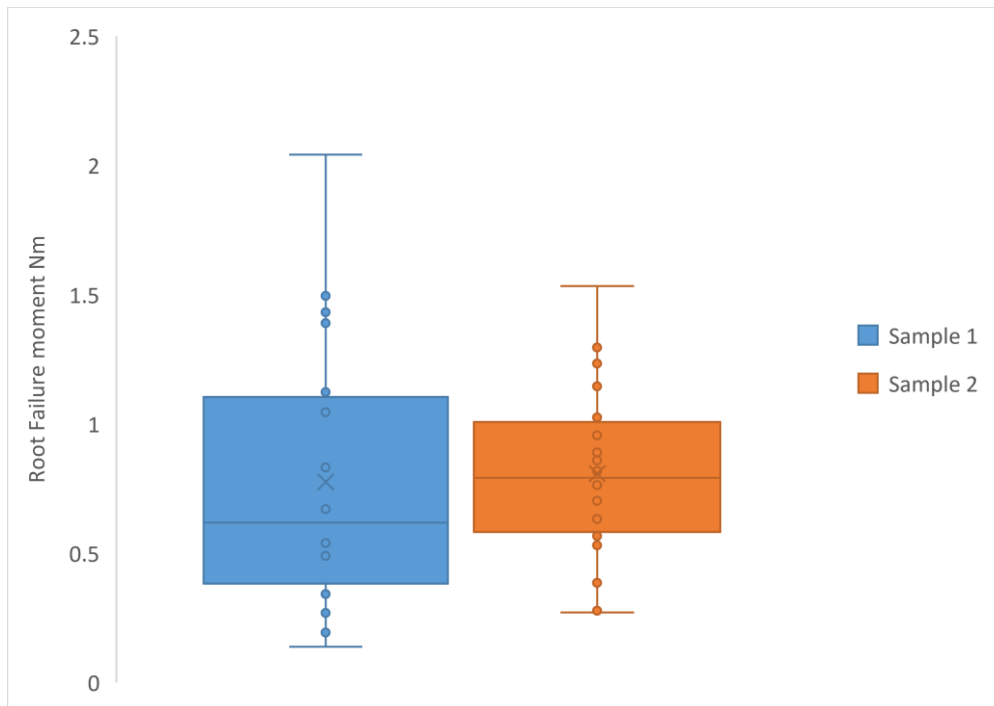
Figure 4.3 Root failure moment readings for two treatments of oilseed rape. Each boxplot contains 20 measurements.
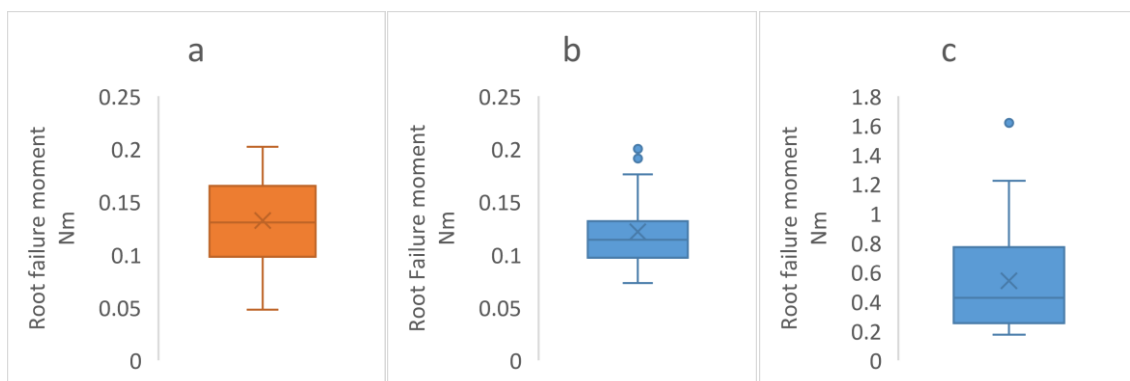
Figure 4.4 Root failure moment measurements taken in 2018. (a) wheat, (b)oats and (c) oilseed rape.

4.2.2   Field measurements of root failure moment using the new lodging instrument

The experiment continued with testing real crops in the field in Ireland in 2018. Figure 4.5a and b, show the root failure moment measurements using the lodging instrument developed in this research project. 24 measurements of wheat and 20 measurements of oats were taken.

The results were very variable with maximum resistances ranging from 0.008 to 0.22Nm for oats. This variability may again have been caused by the variation within plant characteristics. Although, there was a much larger range of values compared to the previous lodging instrument, the new lodging instrument provided more information, data points. Continuous data was able to show the relationship between rotation angle and lodging resistance, which previously was not achieved with the lodging instrument created by Berry et al., (2006).

Based on the curve types described in Figure 3.39c, Type C could be used to describe the root failure moment results in Figure 4.5a and b. There was no indication of an initial elastic response, however, there was a plastic response (with a shallow gradient, still increasing, still showing compression of soil particles), followed by the peak resistance and a sudden reduction in resistance at the peak strain. Artificial root testing could be used to further understand the results because the root and soil parameters would be controllable.
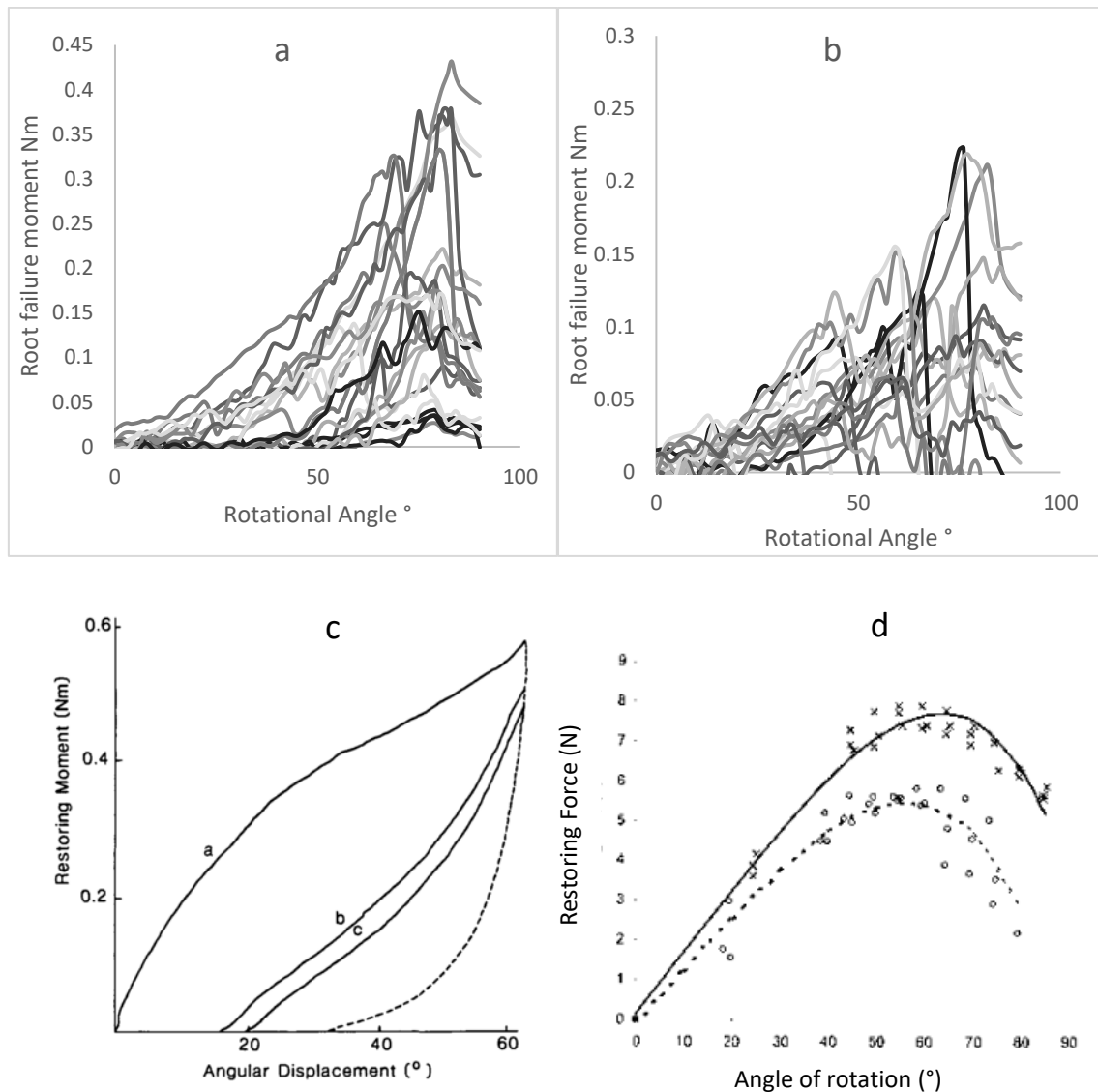
Figure 4.5 The resistance-rotation responses of (a) 20 wheat at a water content of 20%, b) 20 oats at a water content of 25% crops in sandy silts in the field and (c) The typical response for wheat in the tests completed by Crook and Ennos (1993). (d) Exponential equation found by (Berry et al., 2003a) where open circles are Equinox variety of wheat and the x represents values for the Rialto variety.

Crook and Ennos, (1993) completed testing on the resistance of wheat to lodging using 20 plant samples. Samples were collected in soil cores and immersed overnight in water to saturate the soil. The plants were then taken to the laboratory to undergo lodging tests. They found that the resistance increased with increasing deflection before levelling off slightly at angles over 30°.

Crook and Ennos, (1993) extended the experiment to include the removal of loading and retesting of the plant. On removal of the lodging arm, the plants recovered some of the displacement but were still leaning over 20-30°. During reloading, the responses of the plants were different from the initial loading test (see Figure 4.5c, curves labelled b and c). The lodging arm rotated 20-30° before registering any resistance, and the force required to rotate plants by 45° was reduced. When the rotational angle was increased to 60°, the resisting moment rose to a value close to the initial test. On removal of the force, the stems recovered to lean at the same angle as after the first unloading phase. This could be an indication that the soil shear plane developed during lodging was still intact and had not changed. No indication of the water content of the soil at the time of testing was provided by Crook and Ennos (1993).

Similar to the current research, Crook and Ennos, (1993) found that there were also wide variations in resistance both between varieties of wheat but also within the same variety. This is in agreement with the results in this experiment. Crook and Ennos, (1993) connected the variation to inherent differences between individual plants but also suggested there could be differences in the tensile strength of the roots. Upon excavation of their plants after testing, it was revealed that only a few coronal roots snapped along their length and failure was mostly behind the plant in the opposite direction of pushing. This root breakage was not observed during the current research, but it supports the idea that the roots also provide some resistance to lodging forces by mobilising tensile forces (Ennos, 1991).

There was a relationship between the failure moment and the rotational angle which can be described as exponential between the rotational angle and resistance, which is in agreement

with Berry et al., (2003a) (Figure 4.5). Within the current tests on wheat crop samples, there is a threshold root failure moment, which the measurements do not seem to exceed. Oats had a lower root failure moment compared to wheat.

4.2.3   Summary of Field Anchorage Experiments

The anchorage resistance was measured in the 2017 data collection. The anchorage resistances for wheat ranged from 0.105 to 0.669Nm, for oats from 0.06 to 0.725Nm and for oilseed rape from 0.1 to 2.041Nm. Treatments with high seeding rates had lower anchorage resistances, which was also found in the literature.

The new lodging machine was tested on wheat and oats in the field. The tests show that the root failure moment of real plants can be related to the root model testing completed in previous research. However, there was large variability between measurements for 24 plants. This could be due to variations in real plant root parameters, soil types and soil water contents Therefore, more controlled experiments were conducted in the laboratory.

4.3   Laboratory Experiments on Artificial Roots

4.3.1   Qualitative Results of anchorage failure of artificial roots

This section discusses the results of small-scale laboratory experiments to test a range of soil types, including sands and silts, rigid and flexible artificial roots and soil water contents between wilting point and field capacity. During the qualitative study described in Section 3.3.4 the artificial roots were pushed over by the lodging instrument and the movement of the artificial root were observed. Figure 4.6 and Figure 4.7 show images of these tests. Figure 4.7 shows the movements of the rigid and flexible oilseed rape models. The entire sequence of images shows the failure mechanism of the four different artificial root models simulating

oilseed rape. The failure mechanism was similar to the failure of piles under lateral loading in terms of observed soil pressure distribution. As the displacement of the stem increased there were four sections of reaction within the soil, which can be divided into the left side and right side of the artificial root above and below the rotation point as shown in Figure 4.6. On the left side (leeward) the artificial root is being pushed into the soil. On the right-hand side (windward) the artificial root moved away from the soil. Below the rotation point, there was the opposite response. The artificial roots exhibited movements similar to those relating to the theories of lateral earth pressure (Barnes, 2010). Lateral earth pressure was discussed and connected to the theory of laterally loaded piles in the literature review, Section 2.3.2.
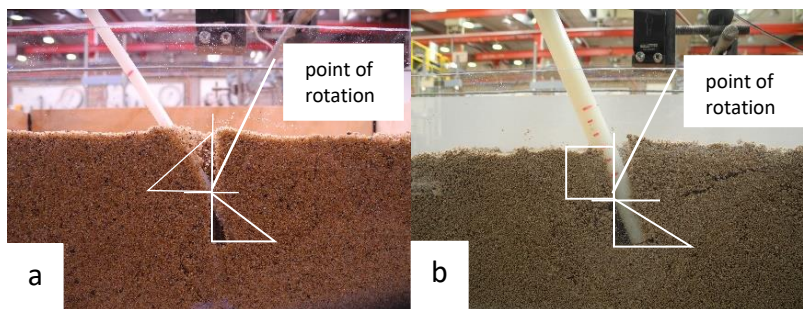
Figure 4.6 Variation of the soil resistance along the artificial roots (a) for a flexible model in coarse-grained soil, (b) for a rigid model in fine-grained soil (Silt Mix 3).

Fleming et al., (2009) describe the changes in the soil as a pile is pushed over. According to their descriptions, normal stresses in the soil increase *in front* of the pile, with soil is moving radially *away* from the pile. Normal stresses decrease *behind* the pile, with the soil is moving radially *towards* the pile. As the loading angle increases, a gap opens behind the pile at the ground surface. In front of the pile, the soil is pushed upwards, failing as a wedge type mechanism.

163

Figure 4.7 (a) Results for flexible oilseed rape root models in sand at a depth of 5cm (b) Results for flexible oilseed rape root models in Silt Mix 3 (see section 3.2.3) at 5cm depth (c) Results for the rigid oilseed rape models in sand at 5cm depth, (d) Results for the rigid oilseed rape model in Silt mix 3 at 5cm depth. As the model is pushed in the soil the active and passive earth pressures are being developed. Above the point of rotation (black dot), on the left-hand side of the sample, the model is being pushed into the soil. This mobilises the passive earth pressure. On the right-hand side of the sample, the model is moving away from the soil, which activates the active earth pressure.

Interestingly, past studies on root lodging noted similar mechanisms, with the soil on the leeward side of the plant subsiding slightly, but not moving appreciably on the windward side. Crook and Ennos, (1993) and (Pinthus, 1974) observed cracks parallel to the planting rows on the windward side of the root in lodged plants. (Easson et al., 1992b) reported clear evidence of "plants pulling away from the soil" during root lodging.

Fleming et al., (2009) also describe that the soil further down the pile shaft fails by flowing around the pile with no gap. The flow of soil could not be observed in the current experiments from the images taken for artificial roots buried at a depth of 50mm. However, there was a gap at the bottom of all of the artificial roots in Figure 4.7. This was because below the point of rotation the base of the artificial roots was pushed into the soil behind the roots. The reason for the difference between the artificial roots and the processes observed for piles could be the depth of burial below the ground surface. Figure 4.8 and Figure 4.9 show flexible artificial roots embedded at depths of 70mm and 100mm respectively. As the depth of embedment increased, the resistance to rotation was increased (Figure 4.10). Measurements taken from the pictures using ImageJ to calculate the size of the wedges, which had formed in front and behind the artificial roots (Figure 4.11). Table 4.1 and Table 4.2 summarise the results of the image measurements. As the burial depth increased, the size of the wedges increased, which explains the increased root failure moment observed in the experiments for both the rigid and flexible artificial roots (more images are in Appendix E1).

.

Figure 4.8 Depth of the model increased to 7cm, flexible oilseed rape models in coarse sand.

Figure 4.9 Depth of the model increase to 10cm, flexible oilseed rape models in coarse sand.
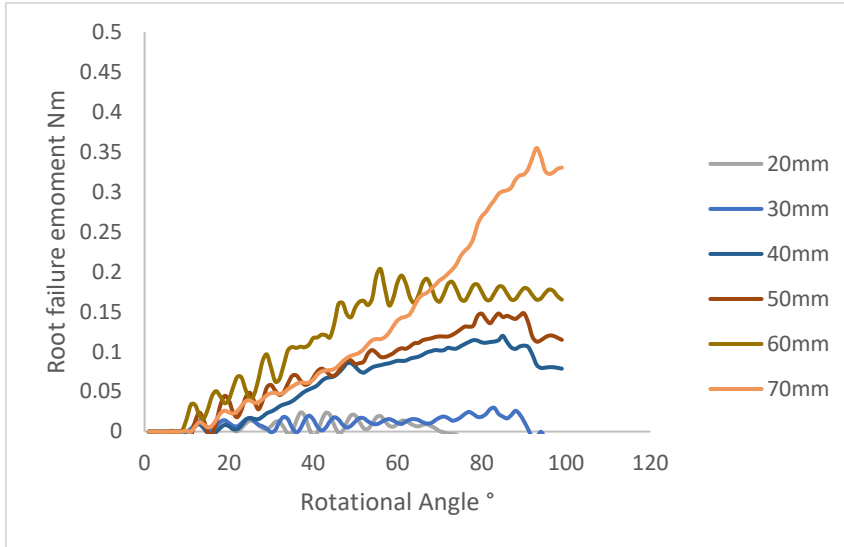
Figure 4.10 Root failure moments when the depth was increased for the 6mm flexible oilseed rape model in sand.
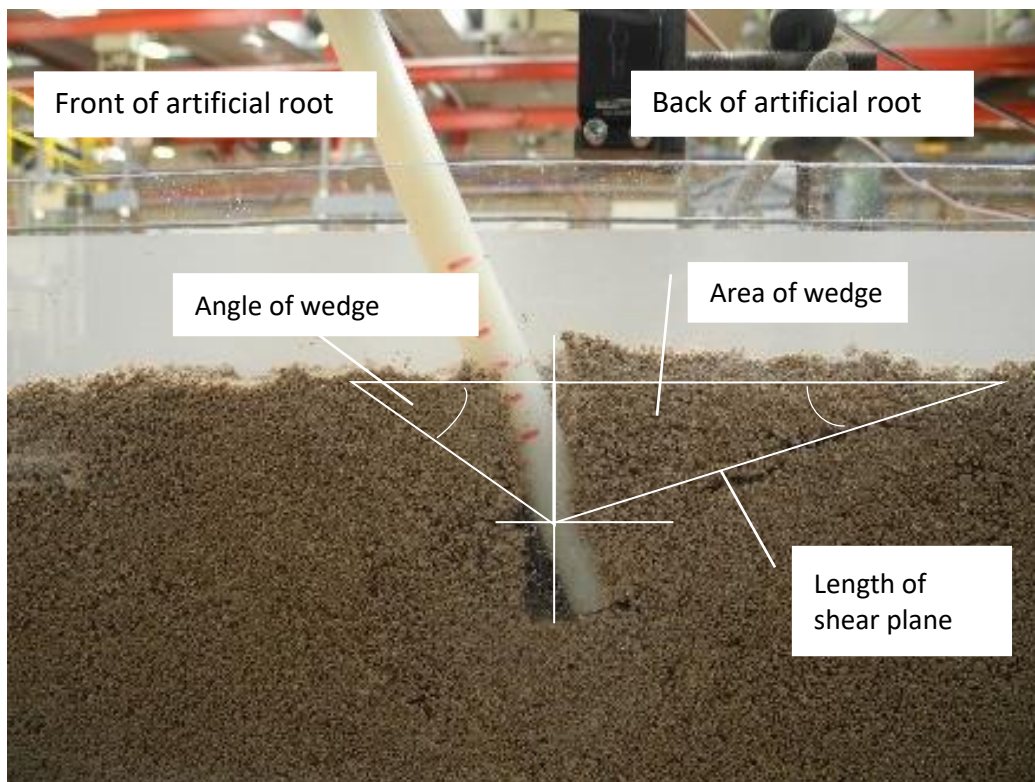
Figure 4.11 Measurements of the images taken in ImageJ software.

Table 4.1 Results for the analysis of the pictures in the qualitative study of root failure mechanisms.

Depth	Model Diameter	Mix	Rotation point (mm)	Area of the wedge at the back (mm²)	Area of the wedge at the front (mm²)	Length of shear plane at the back (mm)	Length of shear plane at the front (mm)	Angle of the wedge at the back (°)	Angle of the wedge at the front
5	6mm	Sand	28.6	2745.3	317.4	107.7	41.4	62.5	28.1
5	6mm	Mix3	23.0	1353.8	154.6	63.3	26.1	51.1	29.4
7	6mm	Sand	29.7	3059.3	352.8	105.7	50.1	51.7	21.1
7	6mm	Mix3	33.9	2161.3	407.5	88.4	51.3	44.9	20.4
10	6mm	Sand	41.7	4179.1	413.0	127.7	58.3	39.8	15.2

Table 4.2 Results for the analysis of Figure 4.7, Figure 4.8, Figure 4.9 in the qualitative study.

Depth	Model	Mix	Rotation point (mm)	Area of the wedge at the back (mm²)	Area of the wedge at the front (mm²)	Length of shear plane at the back (mm)	Length of shear plane at the front (mm)	Angle of the wedge at the back	Angle of the wedge at the front
5	16mm	Sand	34.4	1893.3	320.0	82.9	37.7	50.2	38.0
5	16mm	Mix3	21.8	1409.0	125.4	66.1	29.0	52.5	22.2
7	16mm	Sand	44.9	2456.7	506.5	94.8	45.7	39.6	31.3
7	16mm	Mix3	40.5	3950.5	284.4	115.0	34.6	61.1	32.1
10	16mm	Sand	40.8	3995.5	731.7	124.5	67.6	38.6	27.9
10	16mm	Mix3	5.1		2.92				13.3

Another reason for the opening of the gap behind the artificial root could be because the artificial stem of the artificial roots increased the rotation and caused an increased moment due to the self-weight of the root. The rigid 16mm artificial root had the largest self-weight of the artificial roots adding to the lateral loading, which caused a second wedge to form at the back of the model, ultimately causing the root to topple over. At greater depths, the second wedge did not form (see Figure 4.8 and Figure 4.9).

Figure 4.12 shows the reactions for the wheat root model in sand and in Silt mix 3 (see Table 3.14 for the soil characteristics). The movements for the wheat roots had some similarities and some differences compared to the experiments using the oilseed rape roots. The key difference was the formation of three wedges, one at the base of the root-soil cone, another behind the root and the final one in front of the root. This failure was similar to results from (Dupuy et al., 2005, 2007)) who completed numerical simulations on tree root systems in different soil types. They found that the forces from the loading were transmitted by the roots into the soil thereby inducing a deformation of the entire root-soil plate (Figure 4.13 and Figure 4.14). The soil in front of the tree model, which was under compression, tended to move downwards. Roots at the back of the model moved upwards. After a critical displacement (not given in the research) the failure yield criterion was reached in certain regions of the soil. These failure areas are highlighted by the field equivalent plastic strain areas in Figure 4.13.
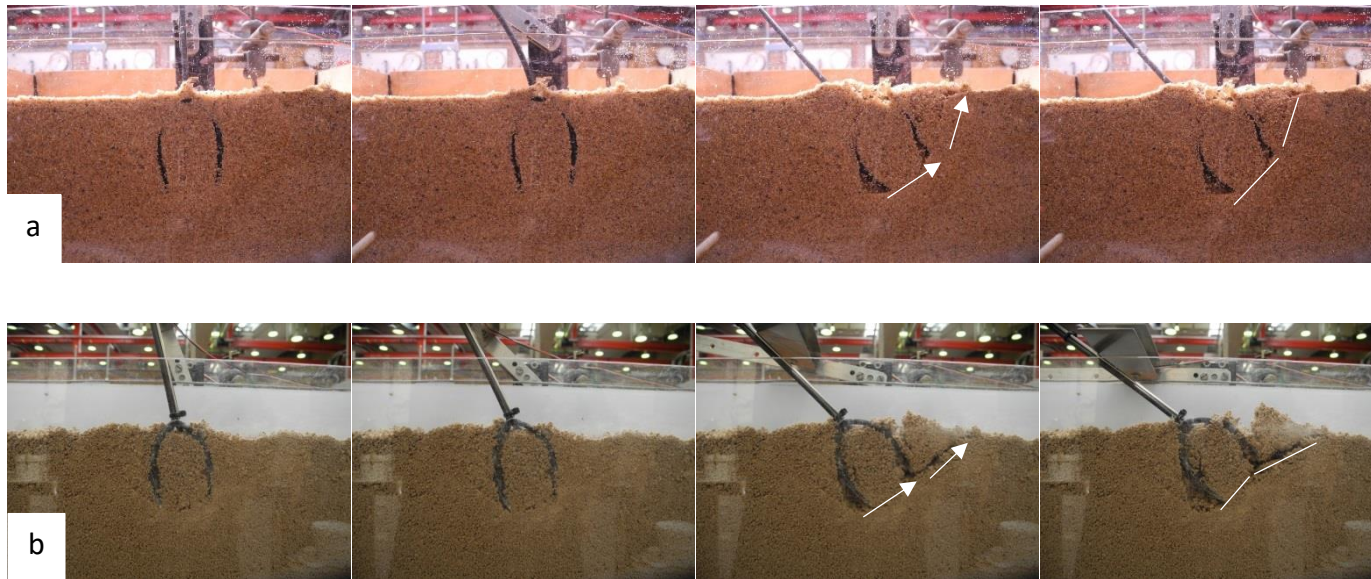
Figure 4.12 (a) Movement of wheat root model in sand and (b) Silt Mix 3. Arrows indicate the development of two wedges, one within the root-soil cone and one behind the models.

Interestingly, Crook and Ennos, (1993) also observed similar movements of the real wheat plant roots in agricultural soil. For small loading angles (displacements), plants rotated about the stem base with roots bending at the base. Where Crook and Ennos, (1993) differ though is at larger displacements, where the cone of the soil that is surrounded by the coronal roots rotated further down into the ground which may suggest that the soil under the root is also collapsing. This would suggest that the soil was also being compressed when anchorage failure is occurring which could suggest that the soil density and soil strength was lower than the density in the current research during their observational study.

a   b
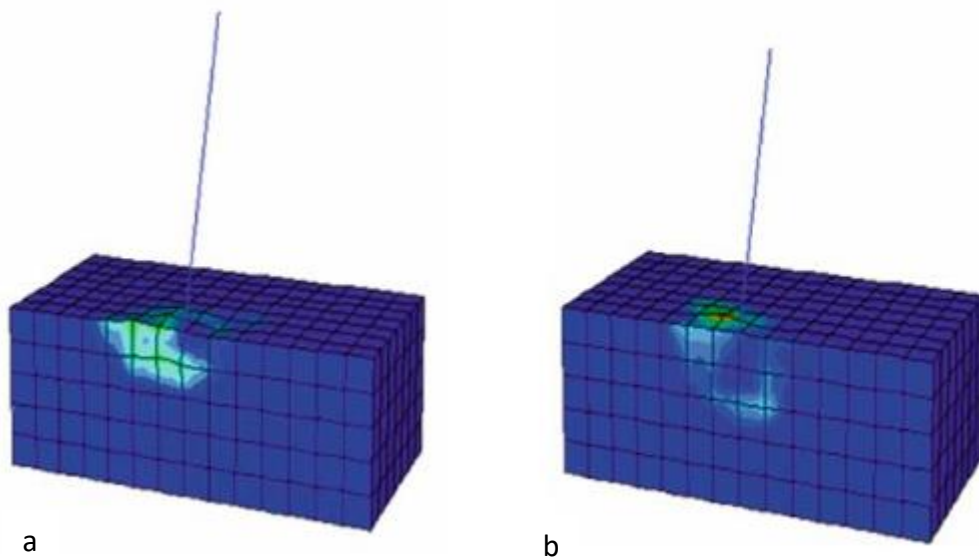
Figure 4.13 (a) Plastic strain for plate root system and (b) plastic strain for tap root system in clay (Young's modulus-20MPa, Poisson's ratio-0.49, cohesion-50kPa, friction angle-0°, volumetric weight 20kN/m³) (Dupuy et al., 2005).
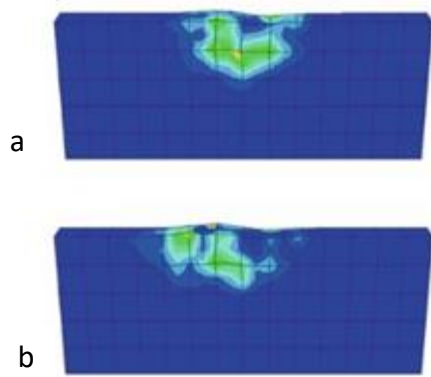
Figure 4.14 (a) Plastic strain in hard clay (Young's modulus-20MPa, Poisson's ratio-0.49, cohesion-50kPa, friction angle-0°, volumetric weight 20kN/m³) and (b) plastic strain in dry sand (Young's modulus-20MPa, Poisson's ratio-0.30, cohesion-2kPa, friction angle-30°, volumetric weight 20kN/m³) for the plate root system (Dupuy et al., 2005).

Numerical simulations allow for the visualisation of strains that may not be observed in physical laboratory testing. Dupuy et al., (2005) developed a numerical model and conducted simulations for both tap root and plate root systems for different soils using the Mohr-Coulomb elasto-plastic model (Figure 4.14). They found that in sand permanent strains expanded further away on the windward side, compared to the leeward side. In the clay, the wedge was larger than that observed for the sands and roughly symmetrical and circular. Although numerical simulations can provide additional insight into the failure mechanisms and were considered as part of the current research, it was regarded as outside the scope as the focus of the current work is on assessing how well existing models performed when predicting root anchorage failure and if new models needed to be developed.

4.3.2   Experimental root failure moments for sandy soils

Figure 4.15a shows the response of the artificial thin flexible oilseed root (6mm) in Sand 1 (poorly graded, see Table 3.15 for details). The root failure moment was small at 0.025Nm. As the root was pushed over with the lodging instrument, oscillations of the stem were observed. These oscillations are represented in Figure 4.15a by the sharp increase and decrease of

resistance, as the rotational angle is increased. Approximately, five oscillations occurred for each test.
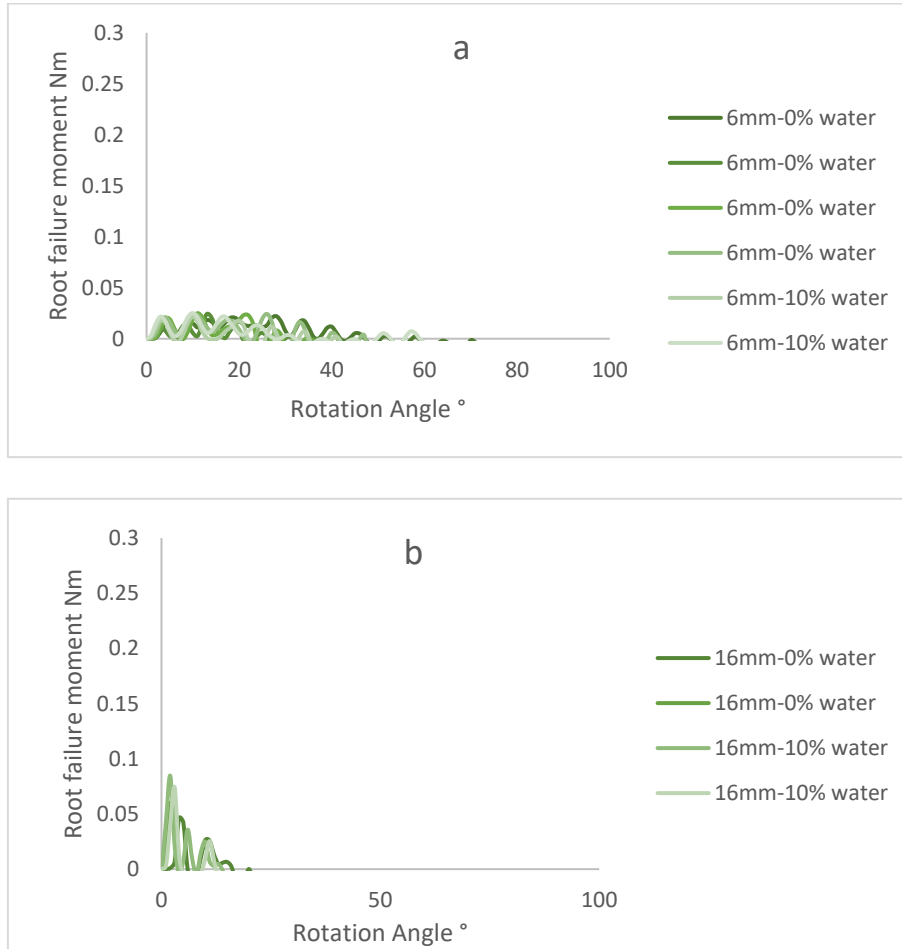
Figure 4.15 Results for Sand 1 (poorly graded) at water 0% and 10% water content for (a) flexible oilseed model and (b) rigid oilseed model.

Figure 4.15b shows the rigid oilseed synthetic root (16mm) in Sand 1. The difference between Figure 4.15a and b were due to the difference in diameter of the artificial root resulting in an increased stiffness. This resulted in an increased root failure moment of 0.085Nm. The impact of the increased stiffness of the 16mm root can also be observed in the smaller number of oscillations and the sudden failure of the models at rotational angles less than 20 degrees. Only two oscillations were observed for some of the tests.

As the roots moves within the sand, the force placed on the stem is transferred down the stem into the soil. The soil reacts with the soil resistance. According to earth pressure theory, the magnitude of the reaction is due to the soil shear strength (Barnes, 2016). Sand 1 (poorly graded) had a very small range of particle sizes (coarse 2mm-fine sand 0.06mm) and represented a coarse-grained, poorly graded soil. Coarse-grained soils derive shear strength from intergranular contact and friction developed between particles. During shear strength tests, Sand 1 showed that under low normal stresses, there was little volume change and the shearing resistance was low at 1.4kN/m^2 (see Figure 4.16). This is similar to the behaviour of a loose sand in shear strength tests as reported in Barnes, (2016). The low shearing resistance would have impacted the development of the soil resistance as the root moved. Also, during shearing at low normal stresses, the sand showed elastic behaviour and plastic behaviour. Therefore, in the root failure moment tests, it takes a small amount of movement for plastic deformation to be initiated. This is reflected in the tests shown in Figure 4.15a and b. The yield criterion is reached within a few degrees of movement and soils fail by either collapsing in front of the model or being pushed upwards behind the model (See Figure 4.7c).
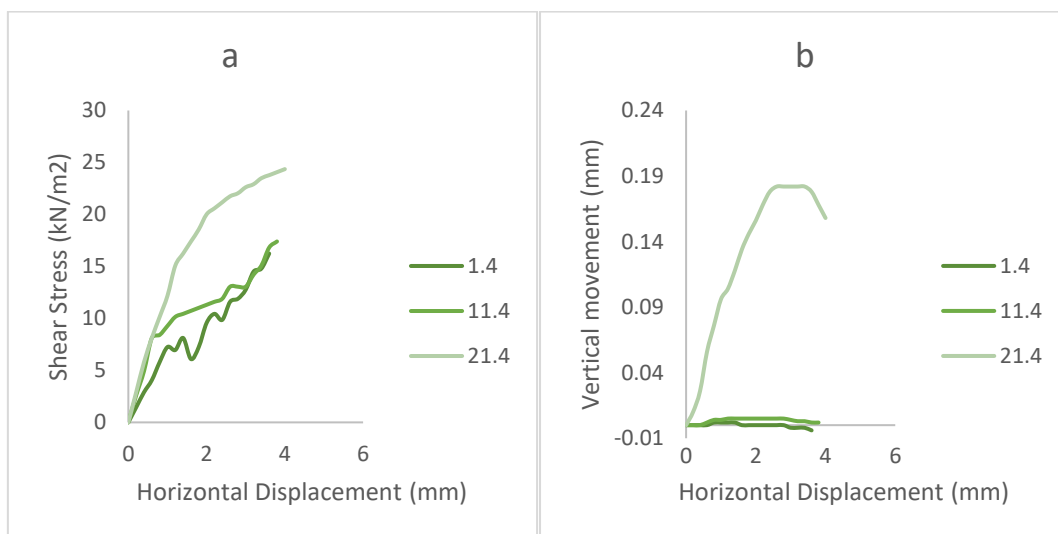
Figure 4.16 Shear box results for Sand 1 (poorly graded sand) at 0% water content (a) shear stress results and (b) vertical and horizontal movements. The legend shows the stress levels of each test, 1.4, 11.4, 21.4kN/m^2.
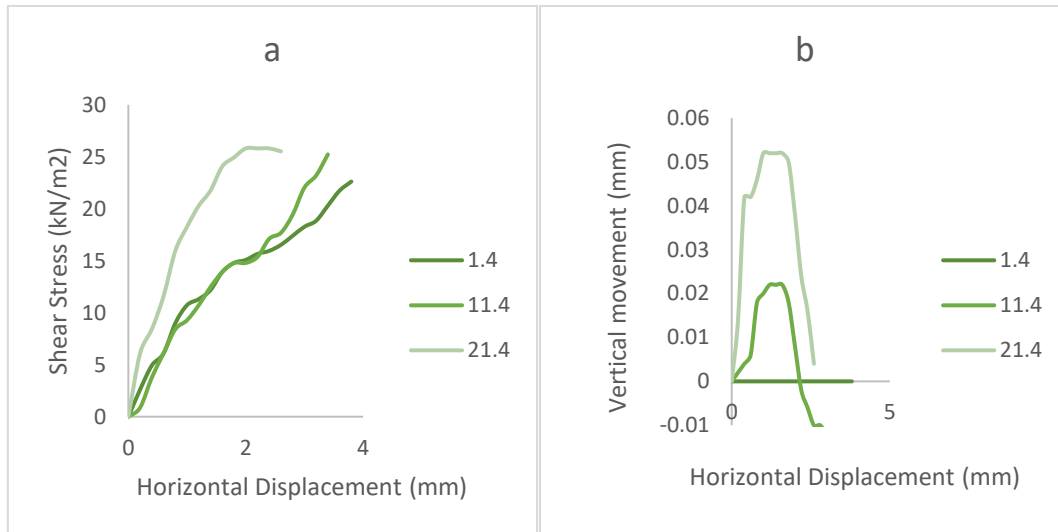
Figure 4.17 Shear box results for Sand 1 (poorly graded sand) at 10% water content (a) shear stress results and (b) vertical and horizontal movements. The legend shows the stress levels of each test, 1.4, 11.4, 21.4kN/m².

Figure 4.15b shows the impact of the water content on the resistance for the 6mm and 16mm oilseed rape roots in Sand 1. Figure 4.15b indicates that there was a slight increase in the resistance when the water content was increased, while the shear strength tests indicated no increase in strength with increasing water content (Figure 4.17). However, the apparent cohesion increased from 2.9kPa (0% water content) to 4.3kPa (10% water content). The root failure moment may have increased because of the increased pore water pressures (increased matric suction) within the soil fabric.

This is demonstrated further by Figure 4.18a and b which show the root failure moment curves for the artificial wheat roots in Sand 1 at two different water contents. The rigid wheat roots in Figure 4.18a shows a change from a more brittle behaviour in the 0% water content tests compared to more plastic behaviour in the 10% water content models. There was also an increase in resistance from 0.12Nm (0% water content) to 0.25Nm (10% water content). This difference could be a result of changes in matric suction (apparent cohesion increasing from 2.9-4.3kPa). As the water content is increased in sands, the degree of saturation and the effective stress also increase in the soil matrix through matric suction (Fern et al., 2014). When

a certain amount of water is added to the soil, a suction pressure is exerted on the particles acting to increase the apparent cohesion between particles due to the capillary effect. This is in agreement with the findings from Dupuy et al., (2007), who did numerical modelling of tree root models and who showed that cohesion was the most influential parameter about uprooting. The internal friction angle and modulus of rigidity of the root (MOR) also influenced the uprooting resistance. However, it was less sensitive to these parameters. A similar result was found in Rahardjo et al., (2009) who also did numerical modelling of tree roots and who showed that the cohesion increased the resistance of shorter roots (1m) compared to longer roots (3m).

Figure 4.18a and b show the root failure moment for both rigid and flexible artificial wheat roots tested in Sand 1 at two different water contents. Figure 4.18a shows three different patterns of root failure moment curves for different water contents. When the soil is dry (0% water content), Type A (brittle behaviour) responses occur (see Figure 3.39 for response types). Within the initial 4 degrees of movement, there is elastic behaviour. After another 4 degrees of rotation, there is plastic behaviour. In the sand, the particles interlock and try to move past each other, causing particles to rotate at the slip surface. As the strain increases, the particles eventually slip past each other. As the water content increases, the response transitions into Type B (elastic-plastic) behaviour. The peak root failure moment increases from 0.108Nm and 0.126Nm to 0.215Nm and 0.246Nm respectively (Figure 4.18a). The increase is due to an increase in soil strength and the development of a secondary slip surface.

The artificial wheat root structures increased the reinforcement of the soil against shear failure. When looking closely at Figure 4.12, there are three zones or wedges of failure for the

artificial wheat root, which could increase the root failure moment in sands compared to the artificial oilseed rape tap root.

Figure 4.18b shows the resistance versus rotation angle for the flexible root model for wheat. The flexible root model has a similar response as was seen for Type C. In this case, the reduced response was due to the flexibility of the roots. When the root was moving, the soil pressures were building. Then the root yielded, resulting in a smaller failure moment. After the maximum elastic response, the resistance decreases with increasing rotation until a rotation of approximately 80-85° when the peak resistance is reached. The root failure moment increases with increasing water content in rigid wheat roots, possibly due to the increased matric suction mentioned before. Root flexibility may reduce the soil reaction (pressure) and hence reduce the resistance to lodging, which is in agreement with the findings by Ennos, (1991), who suggested that the root strength impacts the resistance and the weaker roots will bend more easily as a result of the stem movement and root displacement.
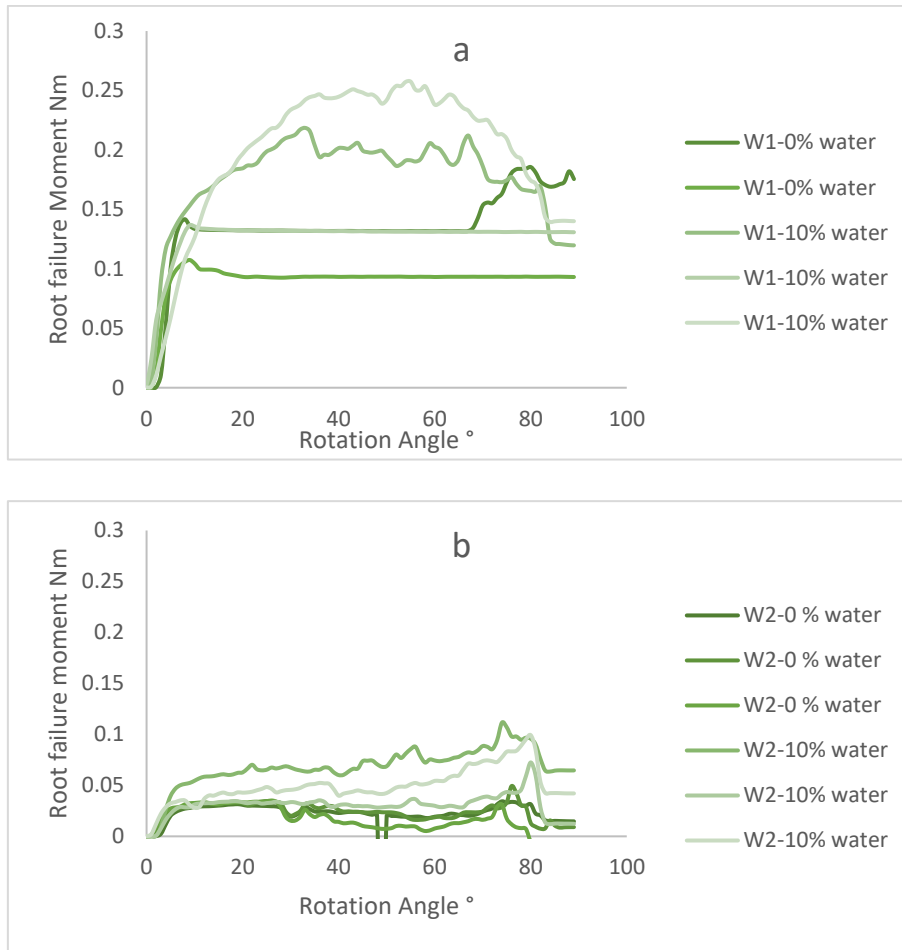
Figure 4.18 Results for Sand 1 (poorly graded) for (a) rigid wheat model (W1) and (b) flexible wheat model (W2).

Figure 4.19a and b show the root failure moments for the artificial wheat roots in Sand 2 (well-graded sand) at two different water contents for both the rigid and flexible wheat root system. At 0% water content, the root failure moment is small following the Type A response with a peak value of 0.0953 Nm. Some samples are reaching the root peak failure moment, then gradually decreasing with increasing rotational angle. This is similar to the results presented in Figure 4.18 suggesting that the grading of the soil is less important. No change in behaviour was observed between Sand 1 and Sand 2 for the oilseed rape model (6mm and 16mm). Results for Sand 2 can be seen in Appendix F1.

This change in root failure moment compared with the response for Sand 1, could be because with the well-graded sand, the small particles fill the voids around larger particles, increasing the inter-particle contacts and, hence increasing friction. However, this increase in friction was not observed in the shear box tests presented in Table 3.16.
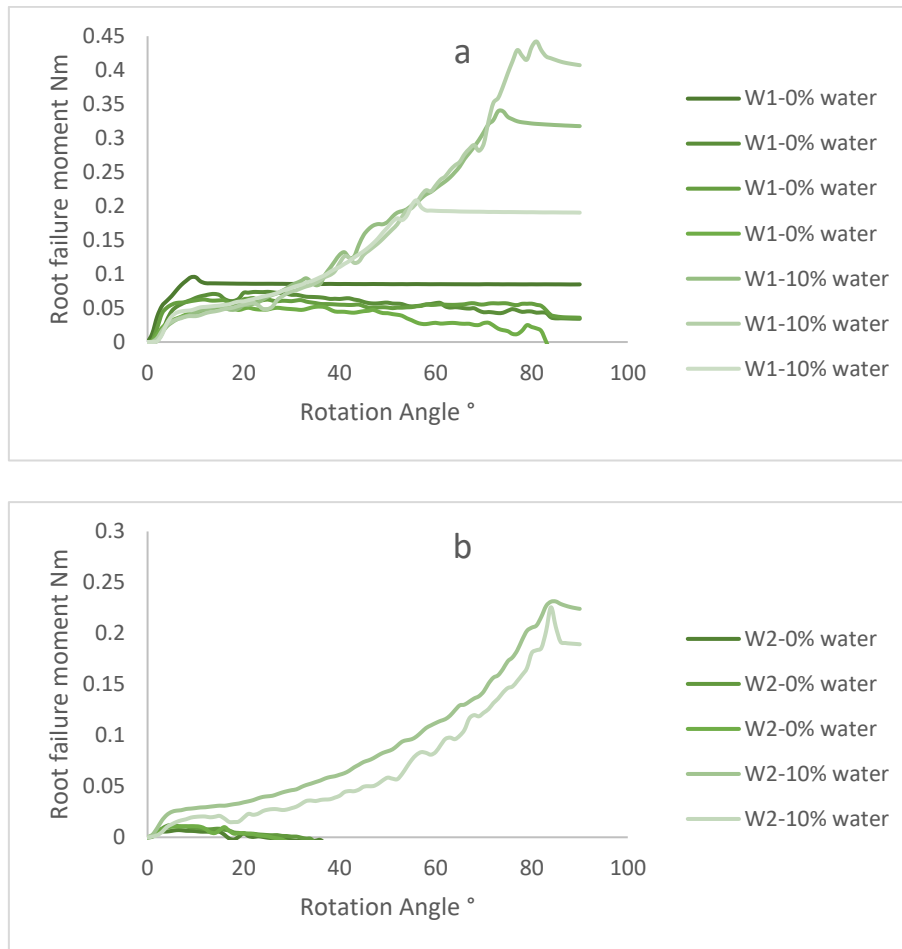
Figure 4.19 Results for Sand 2 (well graded) for (a) rigid wheat models (W1) and (b) flexible wheat models (W2).

There was a change in the behaviour of the failure moment when the water content was increased, which increased the resistance exponentially to a peak failure moment of 0.434Nm which is higher than achieved in previous tests. The mechanism for this change could be the matric suction in Sand 2 (well graded) causing the soil shear strength to increase. This would increase the resistance to forming the failure plane. In the case of the flexible wheat model

(Figure 4.19b), the increase in water content increased the resistance through a similar mechanism, but not to the same degree as for the rigid wheat root model.

In summary, for coarse-grained soil samples at low water contents, the resistance was below 0.02Nm for all of the models except the rigid wheat model (W1) in both sand mixes. When the water content was increased, the degree of saturation increased, causing the matric suction to increase and the effective stress to increase, hence, the root failure moment increased. There was an improved root failure moment when the roots were rigid. Rigid root models had higher root failure moments than flexible models. The presence of root systems increases the volume of soil being mobilised during lateral movement. The weight of the plant increases the propensity for lodging. Bending due to stem flexibility affected the load transferred into the soil by creating oscillations.

4.3.3 Experimental root failure moments for silty soils

For comparison to the sand mixes, fine-grained silt mixes were tested. Fine-grained soil samples consisted of three silt mixes and a sample taken from the Agricultural Development Advisory Service (ADAS) at Hereford (Table 3.16). Figure 4.20a shows the results for the flexible oilseed rape models. The root failure moment ranged from 0.08 to 0.277Nm, changes in water content did not seem to have an effect on the peak resistance. Figure 4.19b presents the results for the rigid oilseed rape where the root failure moment ranged from 0.05 to 0.34Nm, indicating that increasing the water content reduced the resistance by 7 times.
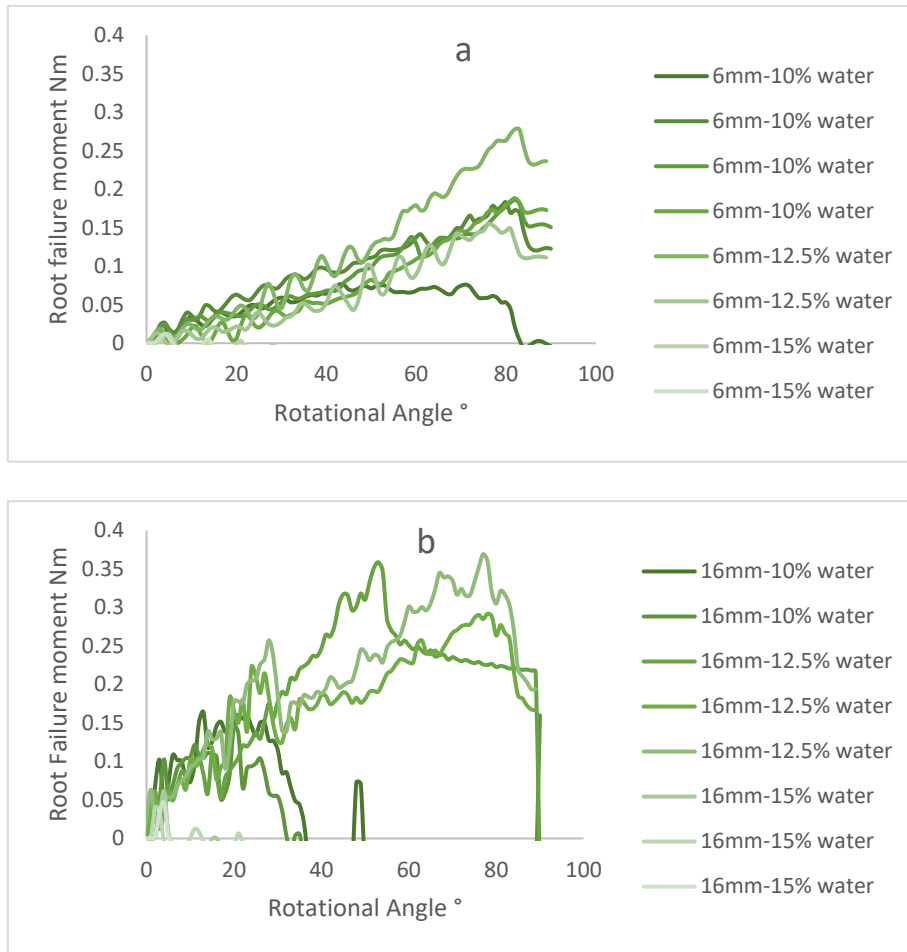
Figure 4.20 Results for Silt mix 1 for (a) flexible oilseed root model (6mm) and (b) rigid oilseed root model (16mm). The oscillations of the stem were still present in this test.

Using silt mixes changed the root failure moment compared to the coarse-grained soil. The internal friction angle was similar to that for the sand mixes (Table 3.16). The cohesion was three times higher (Table 3.16). The increase in cohesion, which in turn increased the root failure moment, was due to the inclusion of silt and clay fractions in the soils (Nik et al., 2016). The particles filled the voids between the sand particles preventing sliding and rolling (shear failure). A second effect was the higher matric suction pressures due to partial saturation of the soil at a 10% water content (Fern et al., 2014). These two additional stresses, which formed in the silt mixes, increased the root failure moment compared to the sands tested in this research. The resistance increased by 90% as shown in the response of the flexible oilseed

rape root model, in Figure 4.20a (for Silt mix 1), compared to the resistance in Sand 1. The root failure moment curves in Figure 4.20a display a Type C behaviour for all tests. In Figure 4.20a, the response does not have an elastic section but starts in the plastic phase (slightly exponential) increasing to the peak root failure moment. In terms of soil resistance, the larger wedge behind the root model would seem to be mobilised because failure occurs after a rotation of 80° as shown in Figure 4.7c. At a water content of 12.5%, there was no apparent change in the resistance of the models.

At 15% water content, the root failure moment was reduced considerably. The response of the flexible oilseed root model in Silt mix 1 was similar to the response of the same root structure in Sand 1 at 0% water content. In both of these cases, the soils were in a weaker state with Sand 1 (poorly graded) being non compacted, loose sand and Silt mix 1 had a water content of 15% which is just below the plastic limit (Table 3.15). This results in a significant loss of shear strength (at $21.4kN/m^2$- shear stress reduced from 28.13 to $16.53kN/m^2$ when the soil water was changed from 10% to 12.5% in shear box tests) and hence a reduction in root failure moment.

Figure 4.20b shows three different responses for the rigid oilseed rape root model (16mm diameter) in Silt mix 1, with water contents of 10%, 12.5% and 15% respectively. The rigid oilseed rape model showed a plastic response at a water content of 10%. However, there was an abrupt decrease of root failure moment to zero at rotation angles of approximately 25° to 30°, because the root models were completely dislodged from the soil. When the water content was increased to 12.5%, the resistance increased, possibly because of an increase in matric suction. The behaviour was closer to the Type C response. However, the root failure

moment fell to zero after rotations beyond 90°, when the root model was dislodged from the soil. The larger model was more susceptible to toppling over in these experiments because of the additional self-weight of the artificial root acting to increase the loading. When the water content was increased to 15%, the reduction in matric suctions and effective stress and then the corresponding reduction in soil strength caused the models to fail within the first 10° of rotation.

The rigid wheat root model (W1) showed Type A and Type C responses for the failure moment and rotation angle as shown in Silt mix 1 (Figure 4.21a). In the rigid wheat root (W1), the resistance was identical or higher than the resistance in soils with lower water contents. One result was 43% higher than the other results and was treated as an outlier. The increase in resistance of the rigid wheat root (W1) in Silt mix 1 was not expected and may be due to the change in artificial root type. The movement of the artificial root in the soil was different (as shown in Figure 4.7 and Figure 4.12). A larger slip surface formed when W1 was moved through the soil, which increased the root failure moment or a smaller slip surface crossing the roots, which would increase the resistance (Schwarz et al., 2011). Although this was not observed in the qualitative results presented in Section 4.3.1.

For the flexible wheat root model (W2) in Silt mix 1 at water contents of 10% and 12.5%, there was a completely plastic response (Type C) shown in Figure 4.21b. When exceeding a rotational angle of greater than 80°, the soil reached the peak root failure moment and thereafter the failure moment reduced to a lower value as a result of strain softening to the critical state or residual strength. A major change was observed when the water content was increased to 15% (Figure 4.21b), with the root failure moment reducing from 0.252 to

0.073Nm. The resistance decreased significantly for artificial root W2, these artificial roots followed the trend of decreasing root failure moments with increased water contents. There is a reduction in root failure, to 1/5 of the resistance compared with the results from Silt mix 1. This could be due to the flexible roots, soil flowing around the roots and reduced soil reaction mentioned earlier.
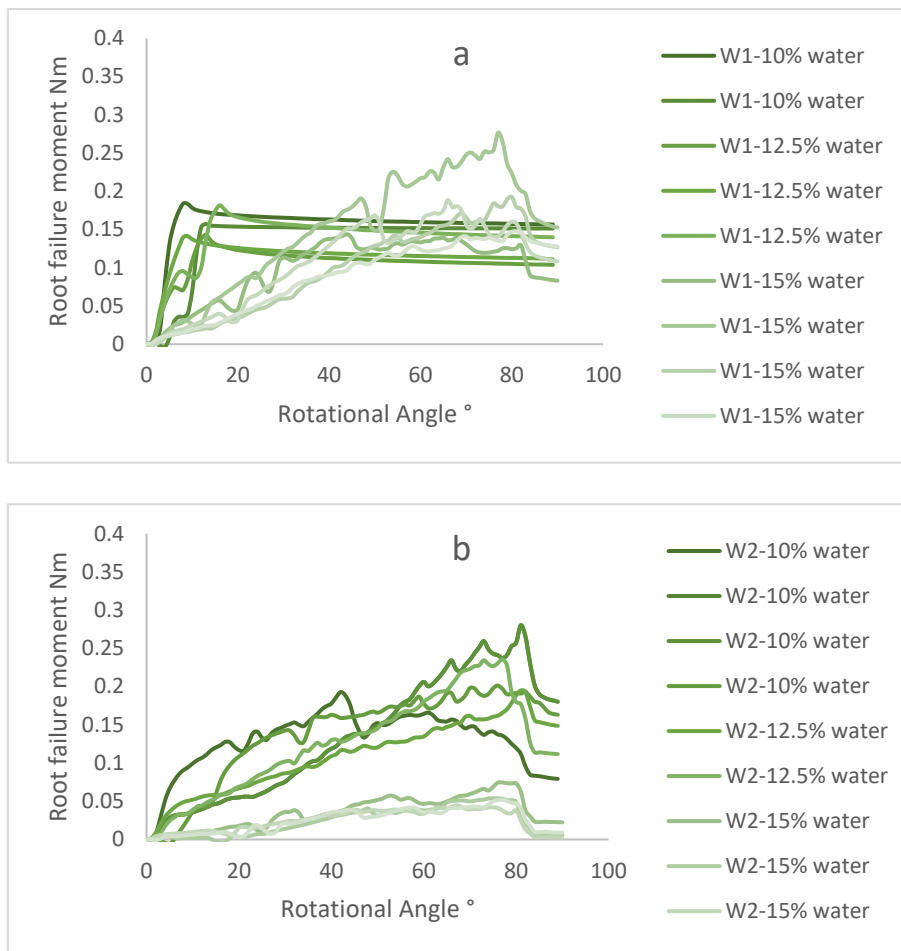
Figure 4.21 Results for Silt mix 1 for (a) rigid wheat models (W1) and (b) flexible wheat model (W2).

Silt mix 2 was used as a repetition of Silt mix 1, to test the repeatability of the testing and showed similar responses to Silt mix 1 (Appendix G1 and H1). Silt mix 2 was similar to Silt mix 1 in particle size distribution (Table 3.14).

Silt mix 3, shown in Figure 4.22 and Figure 4.23, demonstrated similar trends to Silt mix 1 and Silt mix 2 in all water contents for all of the root models except the rigid wheat root model W1. The response to the increase in water content from 10% to 12.5% was even greater. The root failure moment increased by 100% compared to Silt mix 1 as shown in Figure 4.23b. These results suggest that small variations in particle size distribution affected the soil through matric suction, which changed the behaviour of the artificial roots.
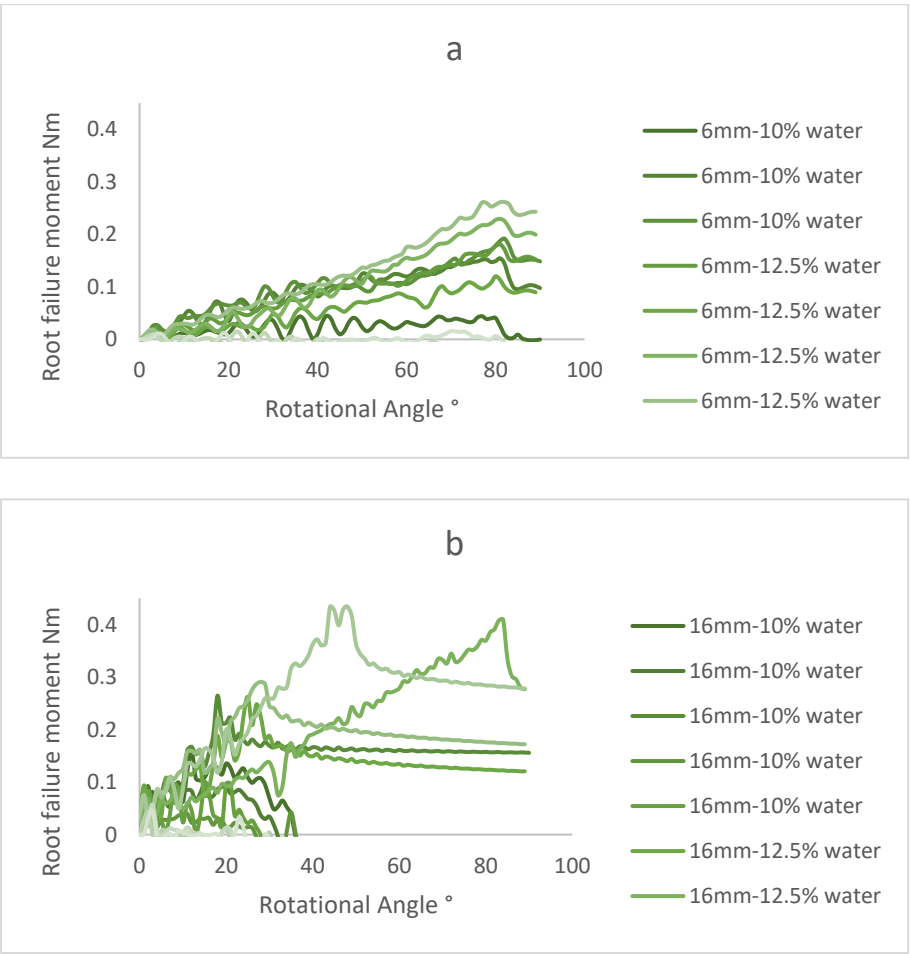
Figure 4.22 Results for Silt mix 3 for (a) flexible oilseed root model (6mm) and (b) rigid oilseed root model (16mm)
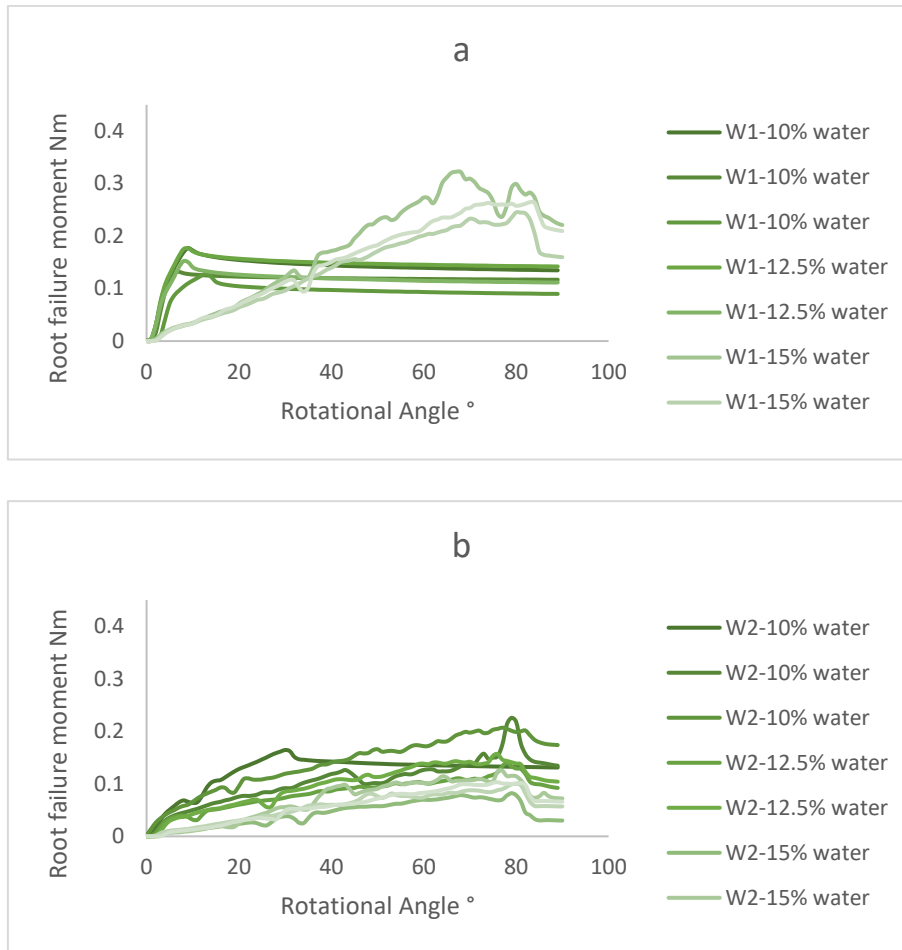
Figure 4.23 Results for Silt mix 3 for (a) rigid wheat models (W1) and (b) flexible wheat model (W2).

The final soil tested was the one collected from the Hereford site, which had a higher

proportion of fine sand, 44.1%, coarse silt, 7% and medium silt, 6% (Table 3.14). Hereford was

tested at water contents of 20% and 40%, which were close to the plastic and liquid limits of

the soil respectively. In terms of soil mechanics, the degree of saturation of the sample is

increasing, the effective stresses will be larger at the plastic limit as the matric suction will be

higher, and at the liquid limit the effective stress will decrease because the matric suction

decreases. As can be seen in Figure 4.24, the results for Hereford were very similar to those

for the silt mixes in terms of the shape of the responses being close to a Type A. The root

failure moment, however, was higher with a maximum of approximately 0.4-0.45Nm

compared to 0.3-0.35Nm for the flexible oilseed rape root model tested in Silt mix 1 and 2 at

a water content closer to the plastic limit. When the water content was increased close to the

liquid limit, there would have been a decrease in effective stresses and a corresponding

decrease in soil strength, meaning that the root failure decreased. The behaviour changed to

a Type C response (Figure 4.25) suggesting that increases in water content changed the failure

mechanism of the artificial roots, hence, reducing the root failure moment.
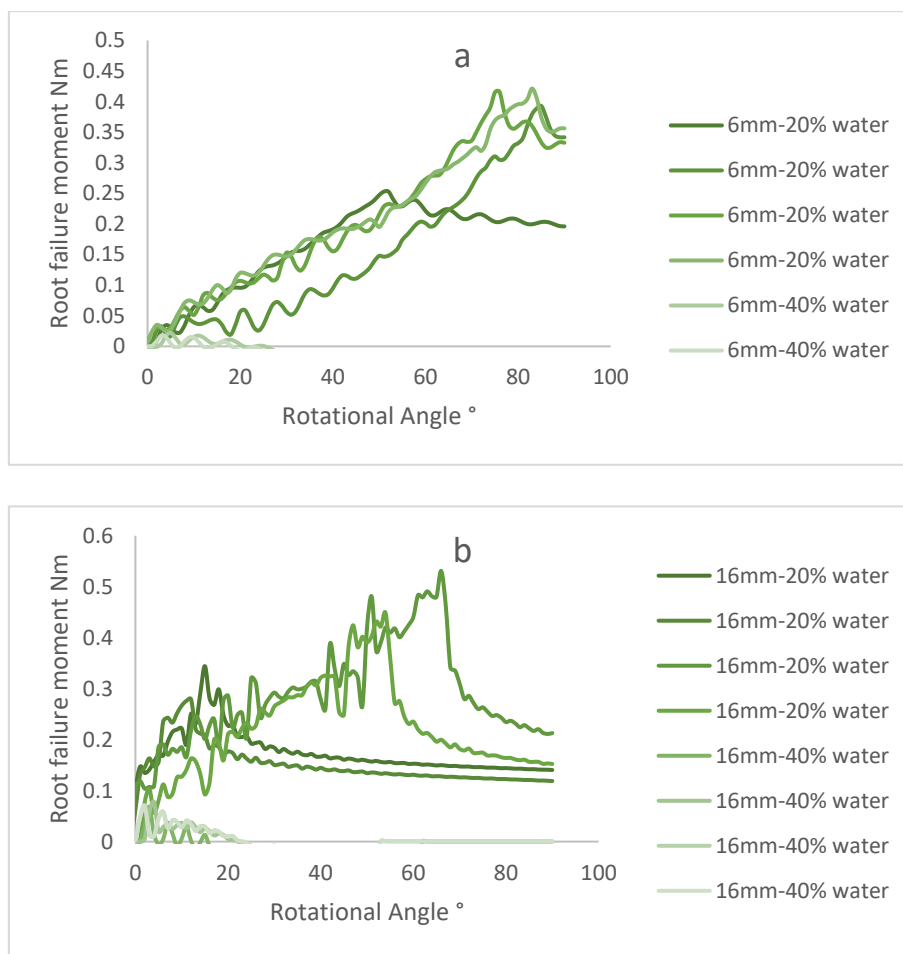
Figure 4.24 Results for Hereford for (a) flexible oilseed root model (6mm) and (b) rigid oilseed root model (16mm).
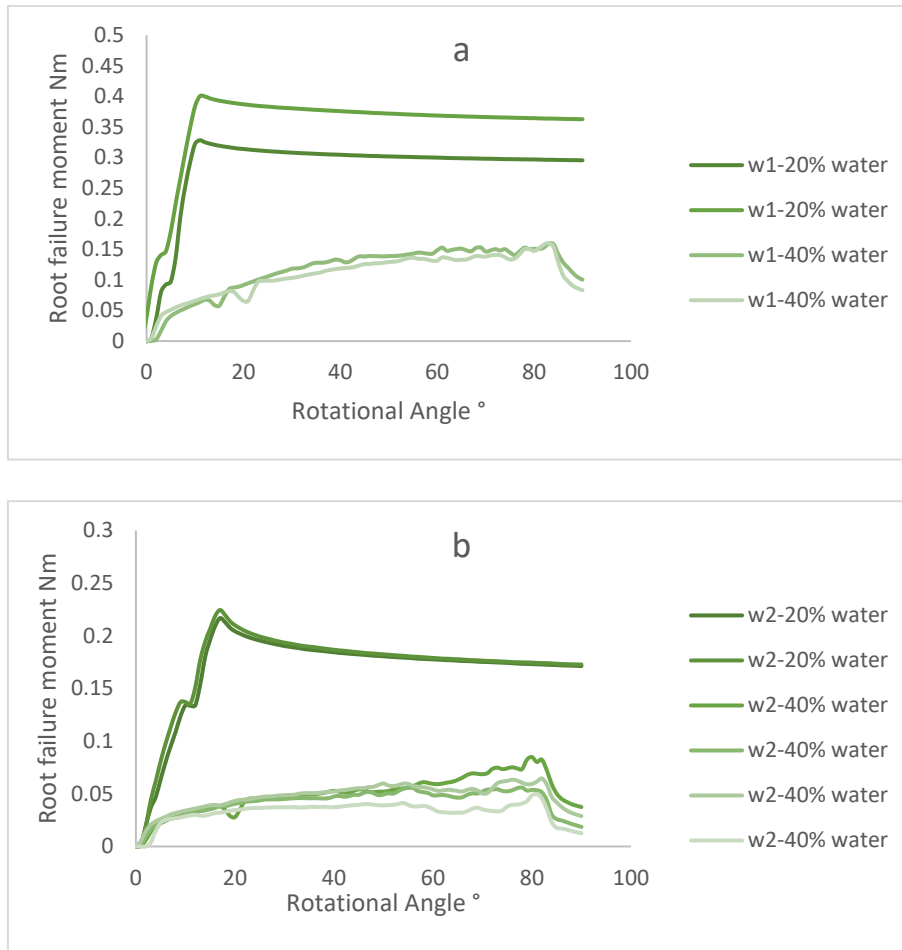
Figure 4.25 Results for Hereford for (a) rigid wheat models (W1) and (b) flexible wheat model (W2).

As mentioned in section 4.2.2 the real root testing completed in the field had high variability, with maximum values of the root failure moment ranging between 0.008 and 0.22Nm. The maximum root failure moment values for the flexible oilseed rape model and the flexible wheat model in the silt mixes ranged from 0.01 to 0.3Nm. This suggests that the laboratory methods could be compared to field methods. Also, the failure Type C was similar for field and laboratory testing, meaning that a link could be made between the behaviour observed in the qualitative study and the root failure moment experiments.

In summary, artificial roots tested in silt mixes showed increased root failure moments by 4-5 times compared to roots in Sand mixes (which was closer to values measured in the field).

There was a decrease in the root failure moment with increasing water content in silt mixes in all of the models except W1, the rigid wheat model. Fine-grained material increases the anchorage root failure moment at low water contents; however, at higher water content the root failure moment is reduced. As there was variability in all of the testing, more tests need to be completed to improve the understanding of the root failure moment rotation relationship for artificial and real root structures.

4.3.4   Summary of Laboratory Experiments

The responses to root lodging of the artificial root models varied considerably depending on the root model type, soil particle size distribution and soil water content. The failure of the root models can be related to the lateral resistance of pile foundations. Lodging resistance decreased with increasing degree of saturation (effective stresses decreasing) and increased root flexibility in silt mixes. In sand, the lodging resistance increased with increasing water content (because in coarse-grained materials the increase in water content increased the matric suction, giving particles apparent cohesion) and decreased with root flexibility.

The results of the artificial root experiments were compared with the field testing of the new lodging instrument. The artificial root tests show that the root failure moment of real plants can be related to the root model testing completed in this research suggesting that the failure mechanisms identified for the root models can be applied and changes due to particle size distribution and water content could be similar in real wheat and oat crops.

4.4 Comparison of root anchorage models with field measurement of root anchorage

Models of root anchorage were compared using datasets collected in the field study in 2017 for wheat and oat root structures. The 2016 dataset was disregarded and the 2018 data was kept to validate the new model developed in this research study. The 2017 datasets for wheat, oats and oilseed rape were not split into treatments for this analysis. Therefore, the models were tested on 72 data points for wheat, 63 data points for oats and 40 data points for oilseed rape. The anchorage models were compared with each other and measurements of maximum root failure moment from the lodging instrument in 2017. This section also includes the comparison of the predictions of the soil strength model by Baker et al., (1998) to the soil parameters collected in the field in 2017.

Root anchorage models were compared using the normalised root mean squared error, the root mean squared error and the gradient of the linear regressions. Normalised root mean squared error (NRMSE) is a statistical formula that evaluates the standard deviation of the residuals (prediction errors). The NRMSE measures how concentrated the predictions are to the measured value. The smaller the value of NRMSE the more accurate the model (Dong, et al., 2015).

Predicted root failure moment and measured root failure moment have been compared using the graph shown in Figure 4.26, which is the method used by Berry et al., (2003). Figure 4.26 shows the relationship between the lodging resistance, B_r and sd^3. Using Figure 4.26, the gradient of the best fit line, k, can be determined, which shows what the relationship is between B_r and sd^3, i.e. what the gradient is if you assume that $B_r = ksd^3$. The closer the value

of k to 1 the closer to a 1:1 relationship. Boxplots were used for a simple visual comparison of the models, which is a method used by Yan et al., (2016).
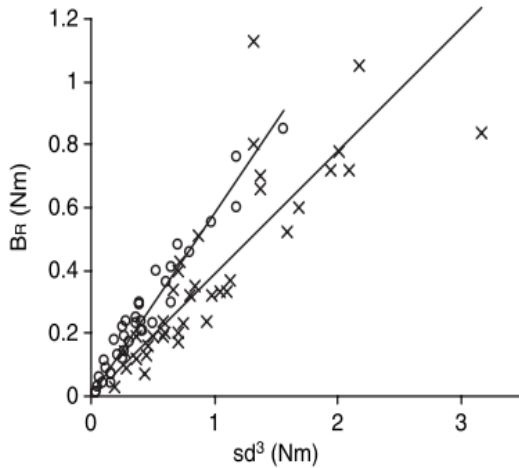
Figure 4.26 Scatter plot created by Berry et al., (2006), to compare the model, sd³ (x-axis) against the measured lodging resistance, B_R (y-axis), open circles represent winter barley and x represent winter wheat.

4.4.1   Comparison of root anchorage models

Wheat anchorage was the first comparison completed. The first anchorage models compared were Crook and Ennos, (1993) (developed for wheat), Goodman, et al., (2001) (developed for oilseed rape) and Niklas (1992) models (developed for tobacco). Figure 4.27a shows the measured resistance is extremely low compared to the predictions of the three models. This is because the Crook and Ennos, (1993) and Goodman et al., (2001) models were not factored using the k value as previously mentioned. This resulted in higher value for the predictions of wheat root anchorage . Crook and Ennos, (1993) showed especially high values, 100 times the measured values. There were two ouliers due to high values of root plate diameter.

This could be because of the assumption of a relationship between soil strength and root cone diameter cubed. This was not the intention of the original model created by Broms, (1964). Broms, (1964) intended the cross-sectional area of the pile foundation and the depth of the

pile to be used in the equation. The models by Goodman et al., (2001) and Niklas, (1992), use these dimensions and the results were closer to the measured values.
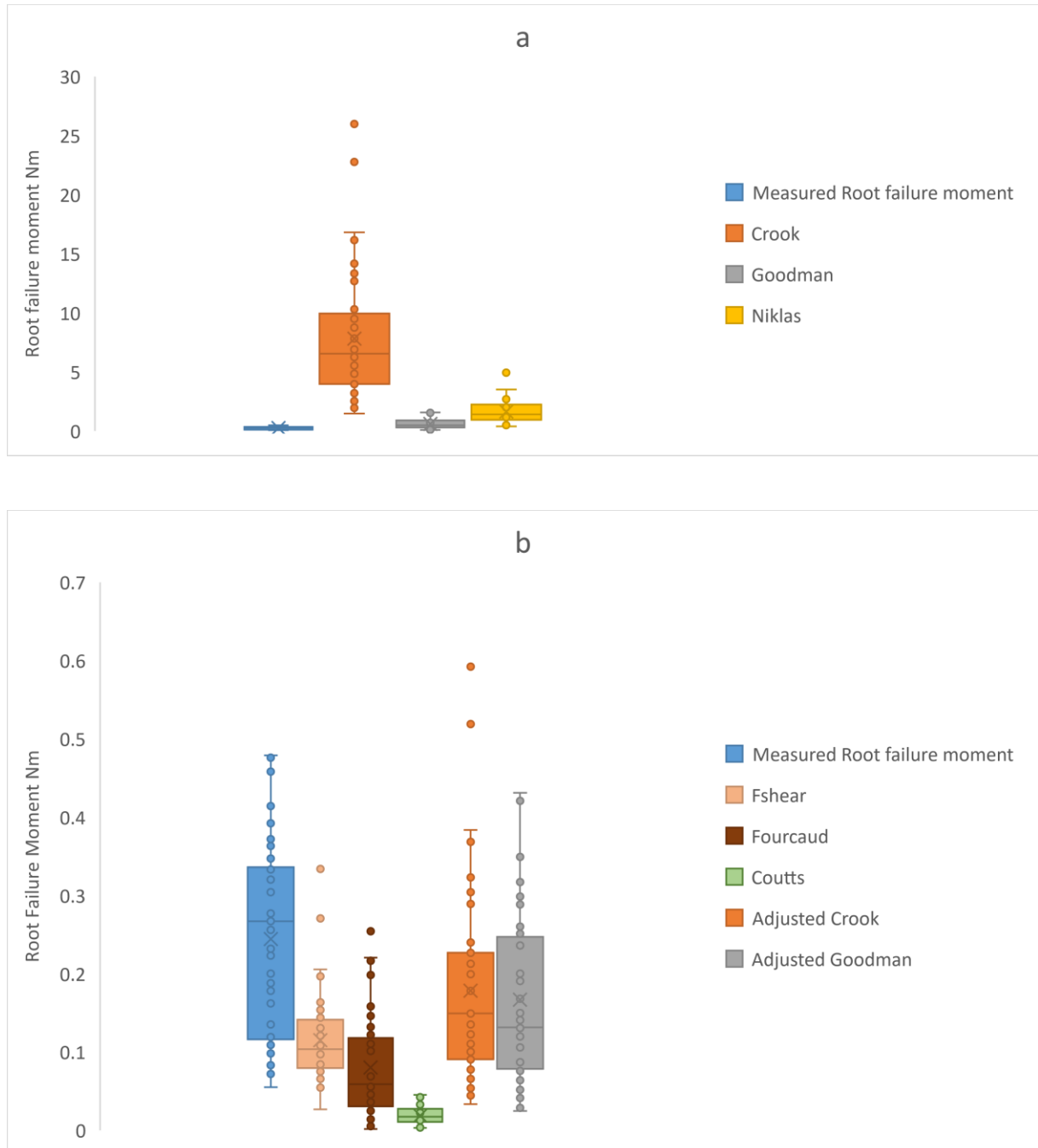
Figure 4.27 Model Comparisons for wheat, showing the predictions of different models from the literature compared with maximum root failure moment. (a) Boxplots of the model comparison for models by Crook and Ennos, (1993), Goodman et al., (2001) and Niklas, (1992). (b) The boxplots of the model calculations for Rahardjo et al., (2009) (Fshear), Fourcaud et al., (2008), Coutts et al., (1999) and finally, the Crook and Ennos, (1993) and Goodman et al., (2001) models with the k used to fit the model to the data (adjusted).

The models for the wheat comparison were compared using the RMSE, NRMSE, and gradient/slope recorded in Table 4.3. The models with the lowest NRMSE values were added to the boxplot (Figure 4.27b) for easy comparison. Crook and Ennos, (1993) and Goodman et al., (2001) were adjusted by using the k value. The Rahardjo et al., (2009) model was split into Fshear, Ftensile, Fslip (Equation 2.26-2.29).

The Fshear model from Rahardjo et al., (2009) and the Fourcaud et al., (2008), Coutts et al., (1999) presented results that were closer to the measured resistance, however, were lower than the measured values of root failure moment. Rahardjo et al., (2009) Fshear model used Equation 2.26. It assumes a relationship between the number of roots, the surface area of each root, the shear strength of the root and root failure moment. However, the Fshear model still underestimated root failure moment suggesting that this combination of variables does not represent root failure in wheat and oats for this dataset.

The Fourcaud et al., (2008) model uses the root-soil mass and the root cone diameter. The Coutts et al., (1999) model use the plant weight and plate diameter. These root measurements were correlated with the root failure moment. However, the models underestimated lodging suggesting that the correlation does not explain the relationship between these variables and root failure moment completely.

Table 4.3 Summarising the results of the model comparisons analyses using the RMSE and slope for wheat.

				Rahardjo				
Statistics	Crook	Goodman	Niklas	Fshear	Fslip	Ftensile	Coutts	Fourcaud
RSME	9.103	0.583	1.701	0.151	0.222	0.219	0.209	0.171
NRMSE	21.470	1.375	4.013	0.356	0.524	0.516	0.494	0.402
Slope	0.023	0.277	0.114	1.761	19.901	32.892	11.147	1.979

A similar pattern occurred for the oats model comparison results. Again, the Crook and Ennos, (1993), Goodman et al., (2001) and Niklas, (1992) models were overpredicting root failure moment. However, in this case, the Goodman et al., (2001) predictions were higher than the other models, possibly because of reduction in root plate diameter and root length of oats compared to wheat shown in Table 3.11 and Table 3.12. The Goodman et al., (2001) model also put more emphasis on the root length (using root length squared in their equation). Therefore, increases in root length would exaggerate the results of this model.
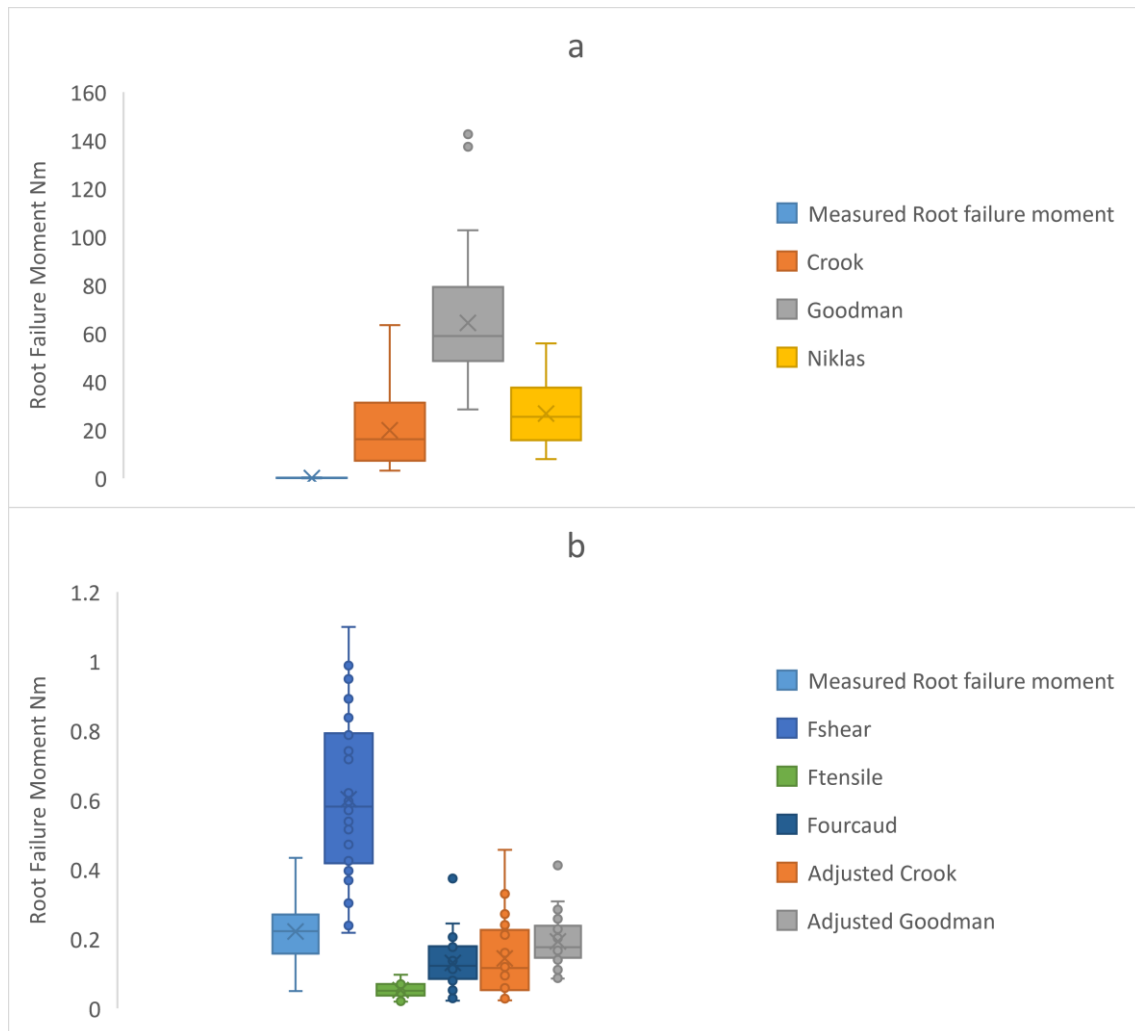
Figure 4.28 Model Comparisons for oats, showing the different models from the literature. None of these models were developed for oats, specifically (a) Boxplots of the model comparison for models by Crook and Ennos, (1993), Goodman et al., (2001) and Niklas, (1992). (b) The boxplots of the model calculations for Rahardjo et al., (2009) (Fshear and Ftensile), Fourcaud et al., (2008) and the adjusted Crook and Ennos, (1993) and Goodman et al., (2001) models.

For oats, Rahardjo et al., (2009) (Ftensile and Fshear) and the Fourcaud et al., (2008) were models closer to the measured resistances. The boxplots are shown in Figure 4.28b, and the statistics are shown in Table 4.4. The Rahardjo et al., (2009) model for tensile strength was one of the lowest NRMSE scores. This model used the sum of the product of the area of the roots in the system and the tensile strength of an individual root. This suggest the root failure moment of oats may be influenced by the tensile strength of the roots. The Fshear model by Rahardjo et al., (2009) also had a low NRMSE. However, the root failure moment was overestimated. The Fourcaud et al., (2008) model was also suggested to make adequate predictions again highlighting the root-soil cone as a factor that may affect root failure moment.

Table 4.4 Summarising the results of the model comparisons analyses using the RMSE and slope for oats.

					Rahardjo			
Statistics	Crook	Goodman	Niklas	Fshear	Fslip	Ftensile	Coutts	Fourcaud
RMSE	24.444	68.882	29.519	0.493	0.162	0.147	0.169	0.108
NRMSE	63.656	179.381	76.873	1.285	0.421	0.383	0.439	0.280
Slope	0.0072	0.003	0.0066	0.3204	5.6067	3.6225	7.3117	1.3805

Figure 4.29 and Figure 4.30 show the models that were closer to the measured values, with the k values on the graphs. Each of the models could be modified to improve the predictions of resistance, bringing the k values closer to 1. There is scatter in these graphs that could be explained by the variability of measuring real plants and soils. Each plant is different, and soil can vary, even in small areas.

Using the models by Crook and Ennos, (1993) and Goodman et al., (2001) require continuous

updating of the fitting parameter, k. Therefore, if any conditions change, for example, the soil

type (shear strength or the variety of wheat or oats) the value will change.
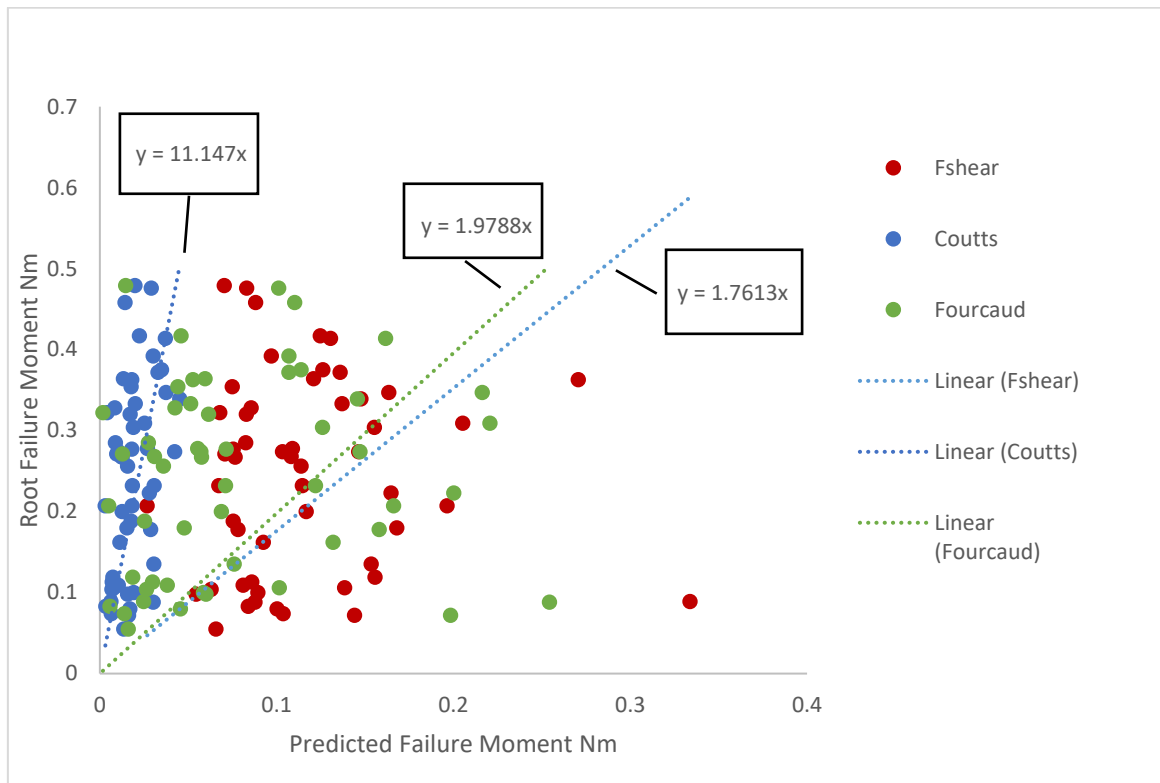
Figure 4.29 Model comparisons for wheat and linear regressions with intercept set to zero.
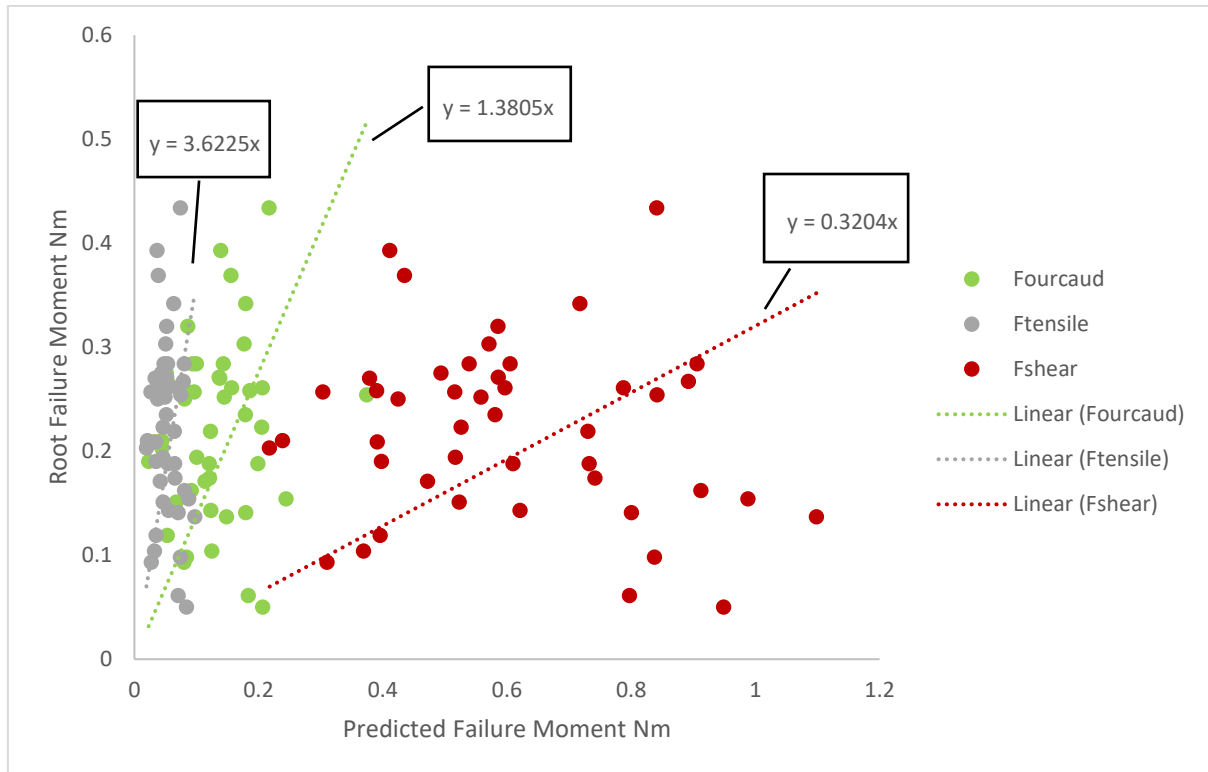
Figure 4.30 Model comparisons for oats and linear regressions with intercept set to zero.

Figure 4.31a and Figure 4.31b show the model comparison results for oilseed rape. Table 4.5

shows the underlying data. In this comparison, root failure moment was estimated by the

Niklas, (1992) model because of the underlying assumptions of using soil resistance and the

dimensions of the tap rooted system. Figure 4.31a shows that the Crook and Ennos, (1993)

model underpredicted the root failure moment, because the model uses the relationship

between root cone diameter and soil shear strength as the basis for the prediction. Again,

oilseed rape consists of a tap root system, and the root length is longer than the root diameter,

which may impact the root failure moment.
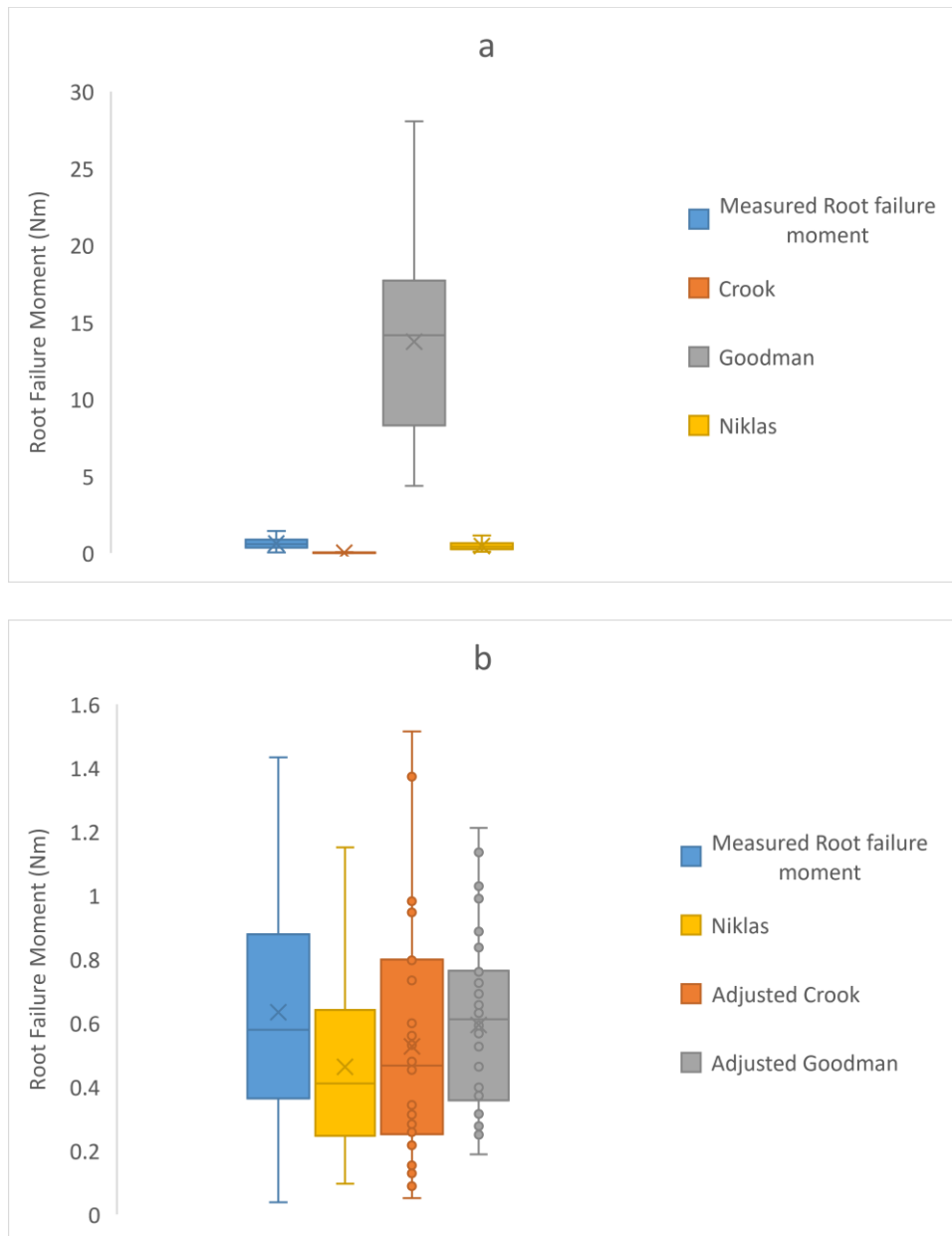
Figure 4.31 Model Comparisons for oilseed rape, showing the different models from the literature. (a) Boxplots of the model comparison for models by Crook and Ennos, (1993), Goodman et al., (2001) and Niklas, (1992). (b) The boxplots of the model calculations for Niklas, (1992) and the adjusted Crook and Ennos, (1990) and Goodman et al., (2001) models.

Table 4.5 Results of the model comparisons analyses using the RMSE and slope for oilseed rape.

Statistics	Crook	Goodman	Niklas
RMSE	0.712	14.406	0.368
NRMSE	0.510	10.327	0.264
Slope	19.8	0.043	1.235

The Goodman et al., (2001) model overestimated the root failure moment. The underlying assumption was that root failure moment was related to DL^2, however, in this dataset the relationship did not provide accurate predictions of anchorage unless the parameter k was used to adjust the relationship. Figure 4.32 shows the Niklas, (1992) model, which appears to be the most accurate of all the models evaluated for oilseed rape. This is likely to be as a result of the assumptions made within the model and the parameters used as the soil pressure is calculated using the area of the tap root (length multiplied by width) and not simply the diameter DL^2 of the root as proposed by Goodman et al., (2001). These results suggest that the anchorage failure of the tap root system of oilseed rape can be accurately predicted using the root diameter, root length and soil strength. Existing models work well within the parameter ranges found in the field experiments. However, theres is still variability within the dataset that measn there is still some uncertainty in these results.
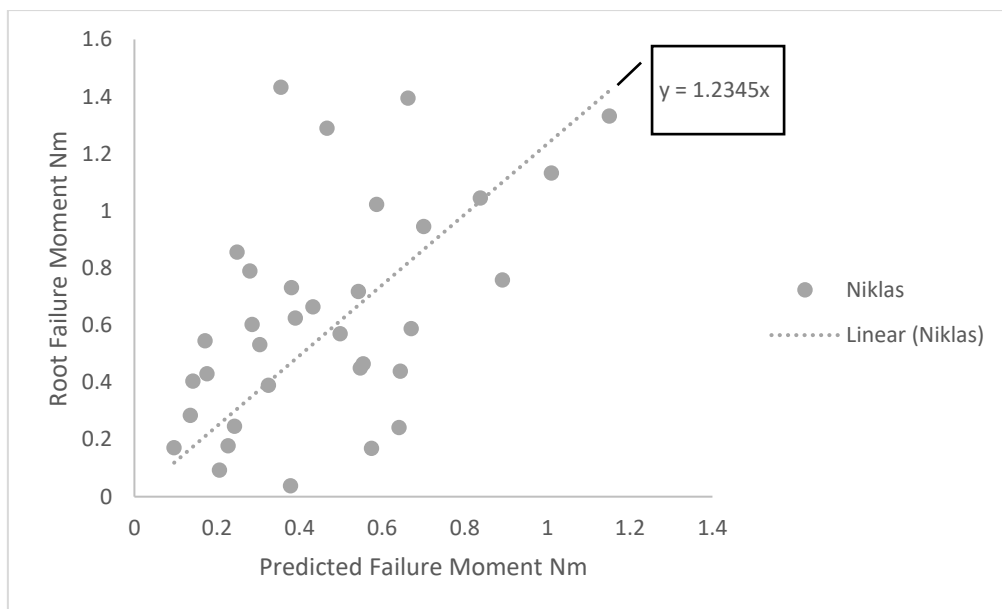
Figure 4.32 Model comparisons for oilseed rape and linear regressions with intercept set to zero.

After considering and testing root anchorage models found in the literature in Section 2.4, it was found that the current model proposed by Crook and Ennos, (1993) predicts root failure moments accurately once the k value is calibrated for each specific dataset. When k = 1, the model overpredicts the root failure moment. Fourcaud et al., (2008) and Rahardjo et al., (2009) models for root anchorage were also over or under predicting lodging or required data that was difficult to acquire. The model for oilseed rape by Goodman et al., (2001) also had a fitting parameter, k. The model proposed by Niklas, (1992) was found to be the most accurate for oilseed rape. Soil strength can also be predicted using the model proposed by Baker et al., (1998). The next section compares a dataset of soil characteristics and measured shear strength values with the predictions of the model.

4.4.2   Comparison of soil strength model with field measurements of soil strength

This section discusses the comparison of measured values of soil strength and the prediction of the soil strength using the model proposed by Baker et al., (1998). This is the only model reviewed in the literature, which predicted soil strength based on basic soil parameters such as clay content, visual score and water content at field capacity and wilting point. Figure 4.33a, b and c show the results of vane shear tests from the field data collection for wheat, oats and oilseed rape respectively. The differences between years relates to the different crops cultivated on the different fields due to crop rotation. In 2016, the shear strength was lower for wheat and oilseed rape than 2018, and the opposite was true for oats. In 2017, the oats were located in the Knockbeg field, which had a slightly higher amount of fine silt and clay than other sites (Table 4.6).
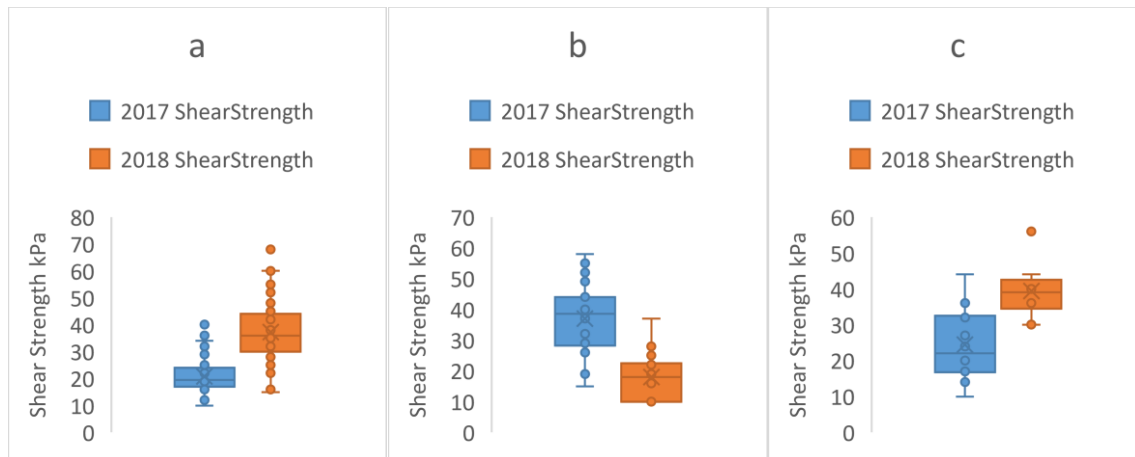
Figure 4.33 Box plots showing the measured values of the shear strength in the fields of (a) wheat, (b) oats and (c) oilseed rape from 2017 (blue, left) and 2018 (orange, right).

Table 4.6 Values used to predict the shear strength of soil using the model by Baker et al., (1998). All of the values were collected in 2017. Coarse, medium and fine silt fractions were combined to give the silt content %.

Model Variables	Measured Values in field- W1, W2, O1, O2, KB	Range of Values (Baker et al., 1998)
Water content at wilting point (%)	11, 11.5, 11.5, 10.5, 10	10-20
Water content at field capacity (%)	23, 26, 27, 23, 22	20-35
Clay content (%)	3.3, 5.5, 5.3, 6.2, 8.3	20-40
Silt content (%)	26.8, 38.5, 38.1, 32.1, 38.4	Not included
Visual Score	2	2-8
Rooting depth	135mm	15-60mm
Mean Daily Rainfall	1mm	1-3mm
Density of Soil	1750kg/m^3	Not included
Density of water	1000kg/m^3	1000kg/m^3

Figure 4.34 and Figure 4.35 compare the results obtained from applying the soil model by Baker et al., (1998). Figure 4.34 shows the predictions determined by applying Equations 2.6-2.8 from Baker et al. (1998) using the clay fraction from the soil collected in the field work completed in 2017 (Table 4.6). The predictions are extremely low, compared to the values measured in the field (summarised in Figure 4.33). This is because the clay content is very low for the fields measured in Oak Park, which are outside the ranges of values for the UK and the equations suggested by Baker et al., (1998) were developed using a semi-empirical approach

201

of curve fitting on data they collected. Thus, it is not surprising that the equations do not accurately predict the measured soil strength and indicates that the equations proposed by Baker et al., (1998) are not applicable to all soils.
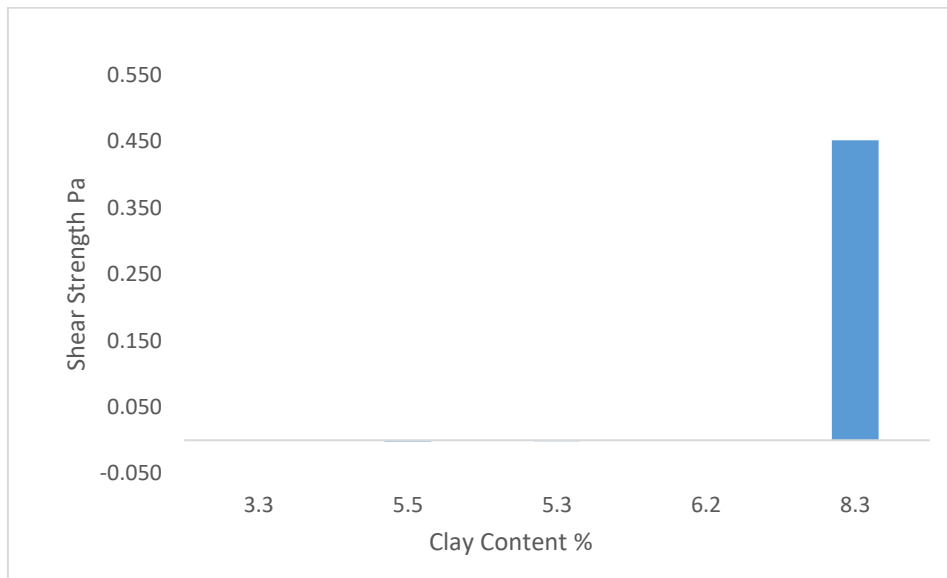
Figure 4.34 Model calculation for field soil strength. Clay contents (3.3, 5.5, 5.3, 6.2, 8.3%) from fields, W1, W2, O1, O2 and KB.

Figure 4.35 shows the predictions if the clay content is combined with the silt content to produce larger fractions. This newly combined fraction gave a much closer prediction of the soil strength, which might suggest that, for future datasets, the clay and silt fractions should be combined to get more accurate predictions of the soil strength using the equations proposed by Baker et al., (1998). Another option would be to try and fit the model to site specific data as found in this research.
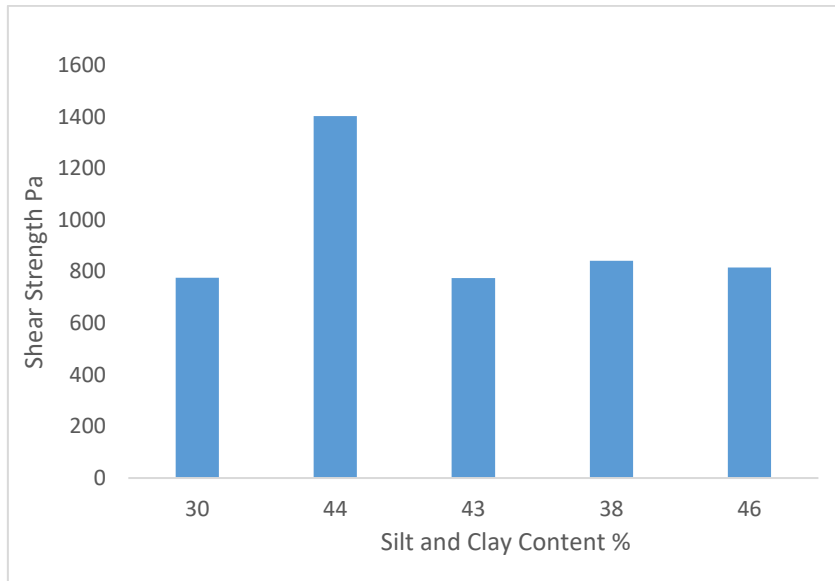
Figure 4.35 Model results when clay and silt were combined from fields, W1, W2, O1, O2 and KB.

A sensitivity analysis was completed using the ranges of values given for the soils at O1 in Table 4.6 to understand the sensitivity of the model to uncertainty and changes in the input parameters. When the values were outside the range given in by Baker et al., (1998), the model predictions for the shear strength were not close to those measured in the field. The exponential relationship between the water content, particle size distribution and soil strength are the most important of all the relationships. The entire prediction is influenced by the exponential relationships. As noted by Baker et al., (1998), the relationships for soil strength are empirical and rely on correlations. Equations 2.6-2.8 were developed for specific ranges of water contents and clay contents.

This indicates the limitations of the existing model. Therefore, for a useful, unifiable model predicting the shear strength should be able to predict the shear strength for larger variations in soil particle size distributions. This could be achieved by using models and relationships found in soil mechanics, related to the shear strength and the soil water characteristic curve rather than relying on empirical fit equations which are very specific to the soil parameters

they are based on. There are also other methods of estimating shear strength, utilising limited soil strength variables such as degree of saturation and suction pressure. One of the methods found in the literature was by Han and Vanipalli, (2016), who used the relationship between the degree of saturation, shear strength and suction pressure, present in unsaturated soils. This method is applicable here, as the field bulk density discussed in Section 3.3.1 indicates that the soil at Teagasc is considered unsaturated or partially saturated.
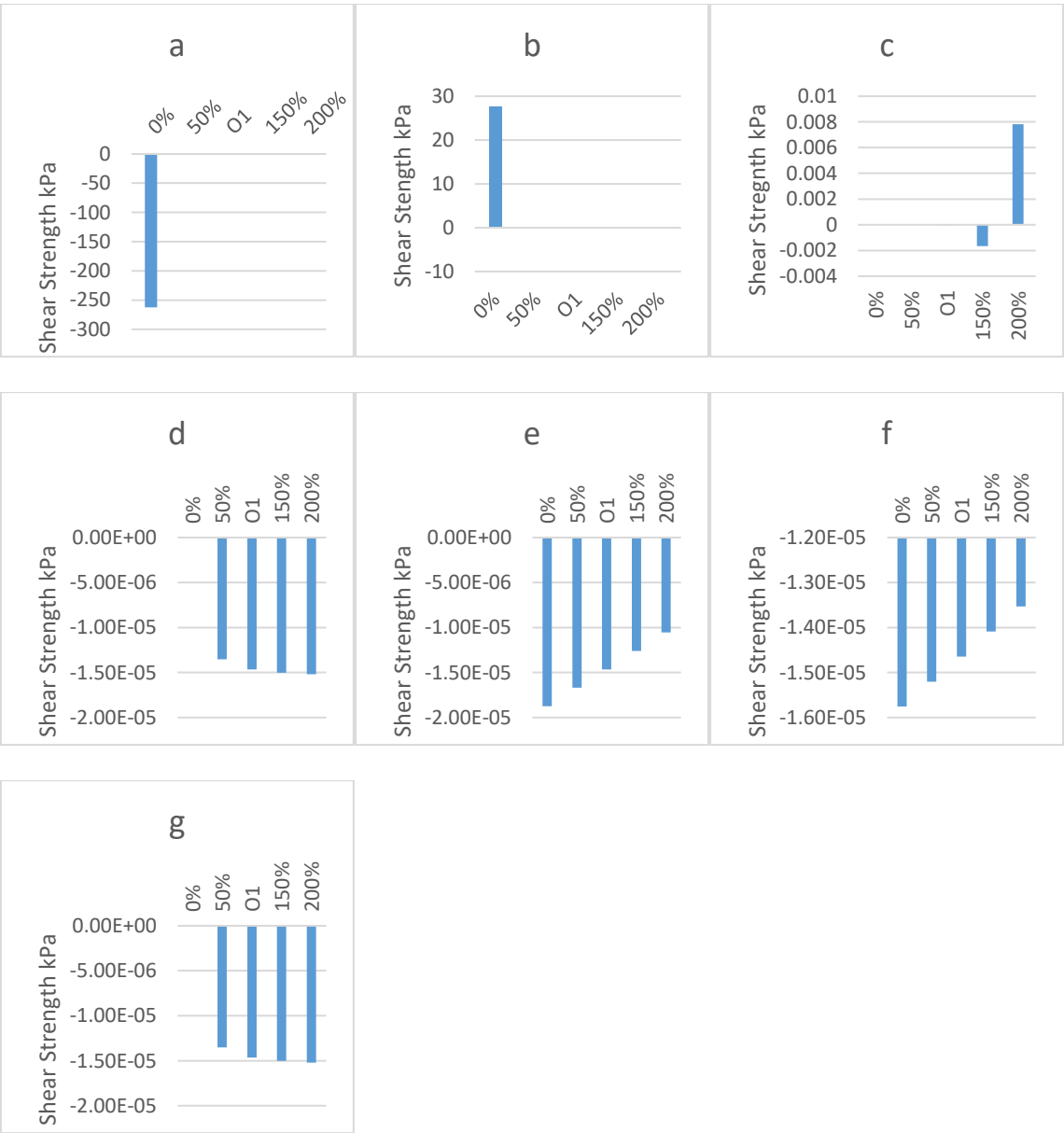
Figure 4.36 Parametric analysis for the model by Baker et al., (1998).(a) wilting point (b) field capacity(c) clay content(d) root depth(e) visual score (f) rainfall (g) density of soil

After applying the soil model by Baker et al., (1998) to predict shear strength, the study continued by using the predictions of shear strength in the model by Crook and Ennos, (1993) model to predict root anchorage. As is used in Baker et al., (2014). Equation 2.8 was used as τ (shear strength (kPa)) in Equation 2.24. It was found that the root failure moment was significantly underpredicted while using the shear strength model as shown in Figure 4.37a and Figure 4.37b. This was because the clay content was lower than the model was originally designed to accommodate. Equation 2.24 calculated negative values for root failure moment as a result. Clay and silt combinations resulted in values closer to the measured root failure moment values as shown in Figure 4.37b. The model using the clay content only would have had to be adjusted by a factor of -5×10^7 to get values close to the accuracy of the clay silt combination based on the data collected in 2017. This suggests that the model proposed by Baker et al., (1998) may work better when the clay and silt fractions of the soil are combined as an input parameter.
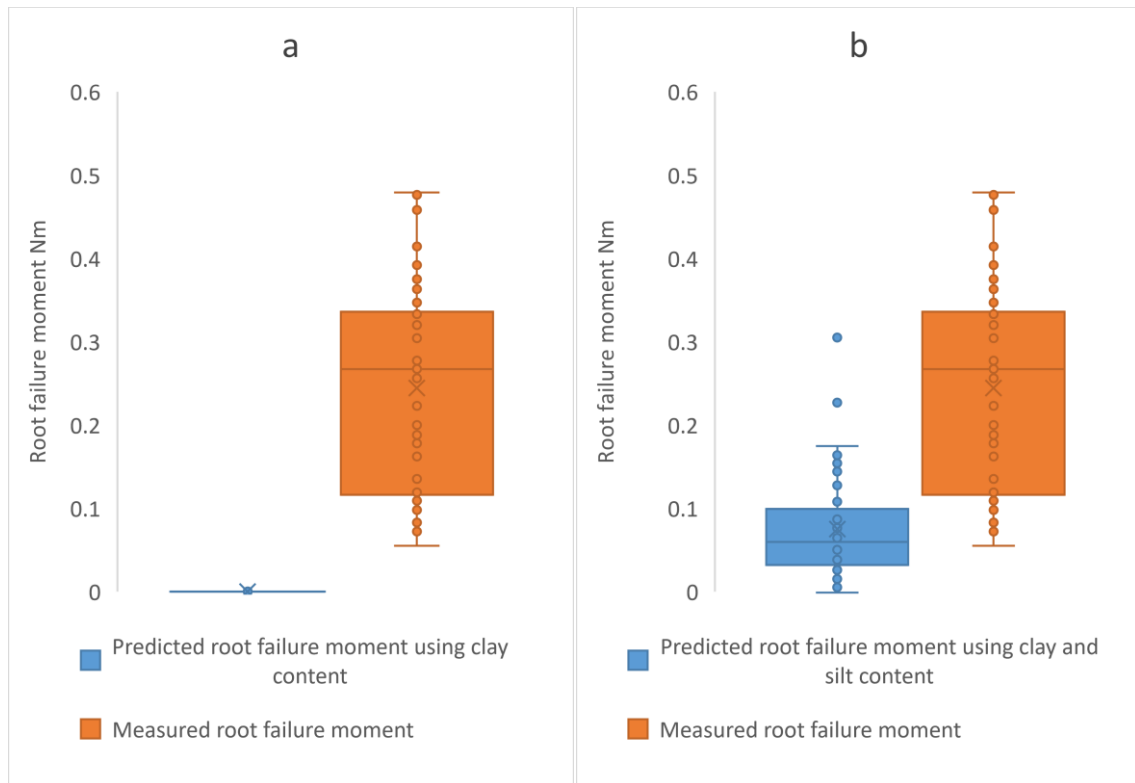
Figure 4.37 Boxplots comparing the prediction root failure moments using the Crook and Ennos (1993) model including the Baker et al., (1998) equations for soil shear strength with (a) clay fraction only, (b) clay and silt fractions.

4.4.3   Summary of Model Comparisons

The models by Crook and Ennos, (1993) and Goodman et al., (2001) are not universally applicable to all soils and are based on empirical relationships. Therefore, soil strength needs to be adjusted to fit the soil specific data. The Crook and Ennos, (1993) model was two orders of magnitude larger than the resistances measured in the field in this study.

For wheat, the existing model that was closest to measured values was the Fshear model by Rahardjo et al., (2009) with an NRMSE of 0.356. This was because of the assumed relationship between root number and root strength. For oats, the existing model that was closest to measured values was the Fourcaud et al., (2008) with an NRMSE of 0.280. This was because of the assumption of a relationship between root cone diameter and root-soil mass. The model that was most accurate for oilseed rape was by Niklas, (1992) (NRMSE of 0.264)

because of the assumed relationship between root length, root diameter and soil strength. However, these models provided predictions that either under or overestimated root failure moment because the relationships suggested may not completely explain the root failure moments measured for wheat oat and oilseed rape. The models were created for specific wheat varieties grown in specific soils. Therefore, an alternative model could be investigated that is based on geotechnical principles. This is investigated in Section 4.4.

The predictions of soil strength using the equations developed by Baker et al., (1998) were found to be significantly lower than the measured values if only the clay content was used for the fine material. However, when combined with the silt fraction to give an overall value for the percentage of fines, the predicted values were significantly closer to the measured values.

4.5   Development of a new model for root anchorage

Recognising the drawbacks in the empirical models using fitting parameters, this chapter adapts a variation of the pile theory proposed by Broms, (1964a and b), normally used for under-reamed piles to predict root anchorage of wheat, oats and oilseed rape root systems. Under-reamed piles are bored and cast-in-situ concrete piles having one or more bulbs formed by enlarging the pile stem using a suitable cutting tool (Barnes, 2016). The under-reamed pile model for lateral loads uses the net passive pressure and additional resistance of the bulb (Figure 4.38).
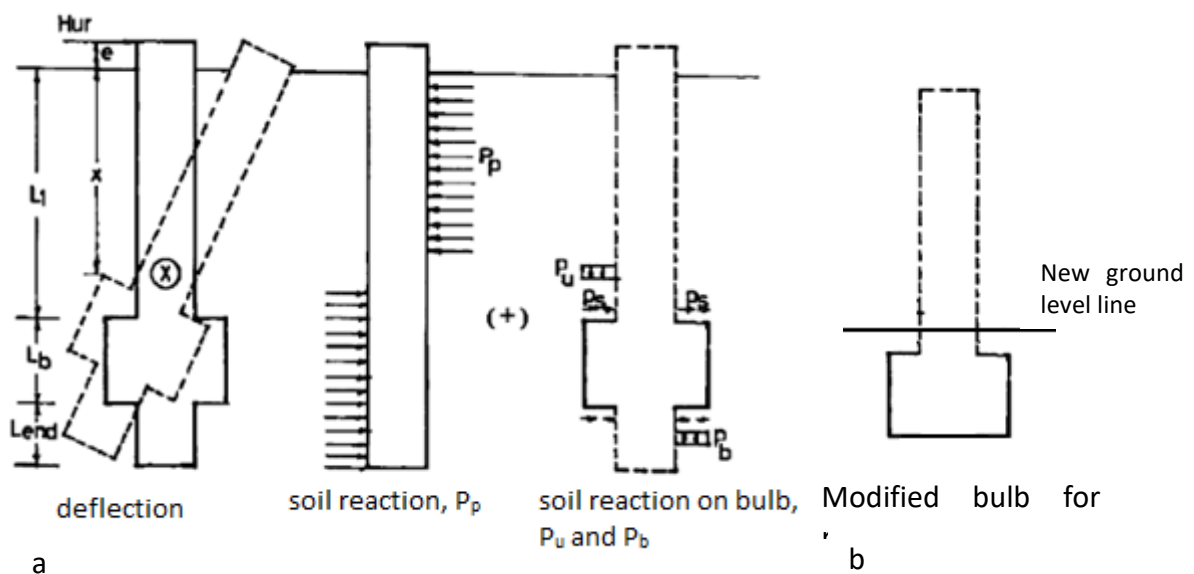
Figure 4.38 (a) Kinematics and pressure distribution on the single under-reamed pile (Prakash and Ramakrishna, 2004) where, H_{ur}–ultimate lateral resistance of the under-reamed pile, e-eccentricity, L-length, X-point of rotation, x- depth to the point of rotation, L_b-length of bulb, Lend-length to the end of the bulb, P_p passive resistance on the shaft of the pile, P_u-uplift resistance on the top of bulb, P_s-additional resistance on the surface of bulbs, P_b bearing resistance on the bottom of bulb. (b) Modified under-reamed pile model for wheat and oats.

Root anchorage mechanisms are affected by similar parameters as the stability of foundations. Parameters such as the root plate diameter, the root depth, soil particle distribution and root-soil interface properties can be related to the pile diameter, pile length and interface parameters such as the adhesion factor for piles. However, the interactions

between soil parameters and root structures are different to foundations because of the scale (metres for foundations compared to centimetres for roots), material properties (concrete or steel compared to lignin and cellulose in plants) and soil-structure interface (adhesion factor and wall frictions for foundations compared to rhizosheath which is the interface between the root and the soil). The effect of adapting a foundation model to root failure needs to be investigated.

This section of the research investigates whether the under-reamed model can be used to predict root anchorage failure for wheat, oats and oilseed rape, focusing on whether modifications to the model (Figure 4.38b) can be made to improve the predictions, for example including or excluding additional parameters and whether this leads to an improvement in predictions of measured values, over existing root anchorage models proposed in the literature.

At this stage, the results of the model comparison and the small-scale laboratory experiments would be considered together. Based on the results of the previous sections, a new model was found to describe root anchorage failure. It was determined that the evidence from the literature review, model comparisons and small-scale laboratory studies indicated that a different approach to modelling wheat and oats was required. Specifically, evidence from the laboratory tests showed that the lateral movement was modified by the root plate. However, there were some reservations around the artificial roots used and the link to real plants (whether the model's movement was the same as real plants in the field). This led to a method being suggested to predict root anchorage failure for wheat and oats, adapting a pile theory for under-reamed piles. It was determined that for oilseed rape the Niklas, (1992) model had

the lowest NRMSE and hence was more accurate than other models. However, the under-reamed pile model was also adapted to oilseed rape to see the effect on accuracy of predictions of measured values.

Matlock and Reese, (1960) and Brinch and Hansen, (1961) developed approaches for analysing piles under lateral loading in coarse-grained soils and Broms, (1964a) developed a model for fine-grained soils. Matlock and Reese, (1960) and Brinch and Hansen, (1961) used lateral earth pressure theory (described in Section 2.3.2) to derive the passive resistance of uniform pile shafts (see Figure 4.39). Broms, (1964a) approach simplified the passive resistance model proposed by Brinch and Hansen, (1961) by limiting the pressure distribution only to the passive pressure (as shown in Figure 4.39). Broms, (1964a) also suggested that the model may overestimate the lateral resistance of the pile.
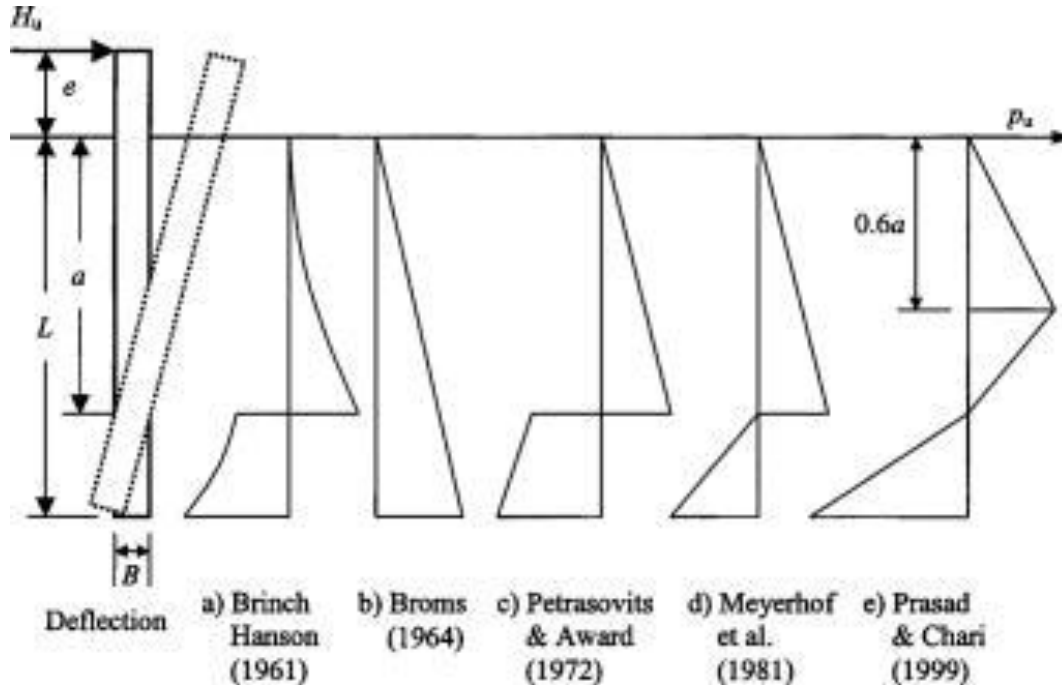
Figure 4.39 Different passive resistance assumptions from different research for a piles in sands under horizontal loading (Zhang et al., 2005), Hu is the lateral force on the pile, e is the eccentricity of the force, L is the length of the pile and a is the depth to the point of rotation.

Prakash and Ramakrishna, (2004) modelled an isolated free-headed under-reamed pile subjected to pure lateral load alone. Their analysis follows similar lines as the approach proposed by Broms, (1964a and b) for laterally loaded straight-shafted piles but in their work (Prakash and Ramakrishna, (2004)), they added the resistance of the bulb. The analysis has options for different scenarios: rigid under-reamed pile, flexible under-reamed pile, in fine-grained soil (c-soils) and coarse-grained soils (φ-soils). The under-reamed pile is treated as rigid, which means that the pile rotates in the soil under lateral loads. The ultimate lateral resistance (resistance to lodging) is governed by the passive pressure distribution of the soil and the point of rotation. Then the resistance of the bulb is calculated and added to the resistance of the pile. This approach may be suitable for lodging models for wheat and oats.

4.5.1   The under-reamed pile model

The equations proposed by Prakash and Ramakrishna, (2004) shown in Equation 4.1 for c-soils and Equation 4.5 for φ-soils. The entire derivation of the model can be found in Appendix L1. The c-soil under-reamed pile model is calculated using Equations 4.1-4.4. The equations in Equation 4.1 are solved simultaneously to find a value for x, the point of rotation about ground level. X is then used in Equation 4.2. The final moment of the under-reamed pile is calculated using Equation 4.4.

$$x^2 + x(2e) - C = 0 \qquad\qquad 4.1$$

$$C = C_1 + C_2 + C_3$$

$$C_1 = Le + 0.5L^2$$

$$C_2 = 0.22\frac{A_a}{D}\alpha_h L_1$$

$$C_3 = 0.22A_2\frac{N_c}{D}$$

$$A_3 = 9c_uD(x^2 - 0.5L^2) \ (c \ soils) \tag{4.2}$$

$$R_s = 2A_a(\alpha_h \ c_u) \quad (c \ soils) \tag{4.3}$$

$$Hur = A_3 + R_sL \tag{4.4}$$

Where, H_{ur} the moment of the under-reamed pile (Nm), A_3 is the moment of the net passive resistance or the ultimate lateral resistance of a straight shafted pile about ground level (kN), R_s is the additional resistance of the bulb, c_u is the undrained shear strength (for fine-grained soils) (kPa), D is the diameter of the pile (m), x is the location of the point of rotation (m), L is the length of the pile (m), α_h is the adhesion factor in the horizontal direction in the case of c-soils, N_c is a bearing capacity factors and are functions of ϕ (values can be found in Barnes, 2016), A_a = projected area of the bulb = $\frac{\pi}{4}(D_u^2 - D^2)$, A_2 is the coefficient representing the lever arm between the centre of gravities of these forces and the pile shaft = $\left[(\frac{D_u^3}{12} - \frac{D^3}{12})\right]$.

The model for ϕ-soils is given by Equation 4.5-4.8 and is solved in similar manner as the c-soils equation.

$$x^3 + x^2(1.5e) - C = 0 \tag{4.5}$$

$$C = C_1 + C_2 + C_3$$

$$C_1 = 0.75L^2e + 0.5L^3$$

$$C_2 = \frac{A_a tan\varphi}{DK_p} \sum_{i=1}^{n} L_i \left(e + \sum_{i=1}^{n} L_i\right)$$

$$C_3 = \frac{N_q}{DK_p} A_2 \sum_{i=1}^{n} L_i + nA_2 \frac{N_y}{K_p}$$

$$A_3 = 3K_p \gamma D(2x^3 - L^3) \quad (\varphi \; soils) \qquad\qquad 4.6$$

$$R_s = A_a(\gamma \; tan\delta)(2L_i + L_b) \quad (\varphi \; soils) \qquad\qquad 4.7$$

$$Hur = A_3 + R_s L \qquad\qquad 4.8$$

Where, A_3 is the moment of the net passive resistance or the ultimate lateral resistance of a straight shafted pile about ground level (kN), D is the diameter of the pile (m), x is the location of the point of rotation (m), L is the length of the pile (m), K_p is the coefficient of passive earth pressure = $tan^2(45 + \frac{\varphi}{2})$ and γ is the unit weight of sand (for coarse-grained soils) (kN/m^3). A_a = projected area of the bulb = $\frac{\pi}{4}(D_u^2 - D^2)$, γ is the unit weight of sand and δ is the angle of wall friction in the case of ϕ-soils, L_i = location of the bulb below the ground surface, L_b is the length of the bulb. N_q, N_c, N_y are bearing capacity factors and are functions of ϕ (values can be found in Barnes,2006), M_{bu} is the moment of the bearing and uplift resistances, A_2 is the coefficient representing the lever arm between the centre of gravities of these forces and the pile shaft = $\left[\left(\frac{D_u^3}{12} - \frac{D^3}{12}\right) \right]$. A_2 changes to $\frac{1}{D_u - D}\left[\left(\frac{D_u^4}{16} - \frac{D^4}{16}\right) - \left(\frac{DD_u^3}{12} - \frac{D^4}{12}\right) \right]$ when the inclined surface of the bulb is considered.

In both under-reamed pile models the effect of water content on the shear strength parameters of the soil need to be considered. Since the soil parameters obtained from the shear box and the shear vane testing (Section 3.3.2.5) were measured with soils with water contents at field capacity and wilting point, undrained shear strength (c_u) and effective

internal friction (ϕ') values were obtained. These values will be used in the development of the under-reamed pile model for root anchorage.

The under-reamed pile can also be treated as flexible which means that if the pile has exceeded a limiting length, the material strength of the pile governs the ultimate lateral resistance. There was no addition of the bulb resistance in this case. This approach may be more applicable to the tap-rooted system of oilseed rape plants. This approach also has options for fine-grained soils and coarse-grained soils. Which will be referred to as c-soils (fine-grained) and ϕ-soils (coarse-grained) and is derived in Appendix L1.

4.5.2 Development of the root anchorage model for wheat and oats

The under-reamed pile model was developed using datasets collected in the field study in 2017 for wheat and oat root structures. The 2016 dataset was incomplete and the 2018 data was kept to validate the model after development. The 2017 datasets for wheat, oats and oilseed rape were not split into treatments for this analysis. Therefore, the model was tested on 72 points of the wheat dataset, 63 point dataset for oats and 40 point dataset for oilseed rape. This was done in order to understand the performance of the under-reamed pile model.

The analysis was completed in stages to investigate different scenarios for applying the under-reamed model to root anchorage. Each scenario was coded using Matlab; examples of the code can be found in Appendix M1. The results were compared to the data obtained from the field experiments in 2017 and the model proposed by Crook and Ennos, (1993). The modified model was then validated using datasets collected in 2018. To judge the accuracy of the model predictions the RMSE, NRMSE and the gradient were used as the comparison statistics. The model with the lowest NRMSE was the most accurate.

Figure 4.40 shows boxplots of the under-reamed pile model was applied using the equations for c-soils and φ-soils. The model for φ-soils had the highest accuracy with a NRMSE of 0.464 compared to 21.470 for the Crook and Ennos, (1993) model for wheat root failure. The statistics are given for wheat and oats in Table 4.7 and Table 4.8 for comparison. Both models were tested because the soil characterisation found that the soils on the three sites could be classified as sandy silts, which means that the soil could exhibit both frictional and cohesive characteristics.

The models for the φ-soils were also more accurate for the oat root failure (NMRSE of 0.430 compared to 63.550 for Crook and Ennos, (1993)). These NRMSE values were similar to the ones reported in Fourcaud et al., (2008) (NRMSE of 0.403) and Coutts, Nielsen and Nicoll, (1999) (NRMSE of 0.494) in the section 4.4. However, the Prakash and Ramakrishna, (2004) model incorporates fundamental geotechnical engineering principles, which make the model more general and able to handle different conditions than the original measured datasets, which were used in the empirical derivation of these other models. This result also suggests that in the context of the under-reamed pile model, the soil collected from the field in Ireland may be considered a φ-soil, with more frictional characteristics.
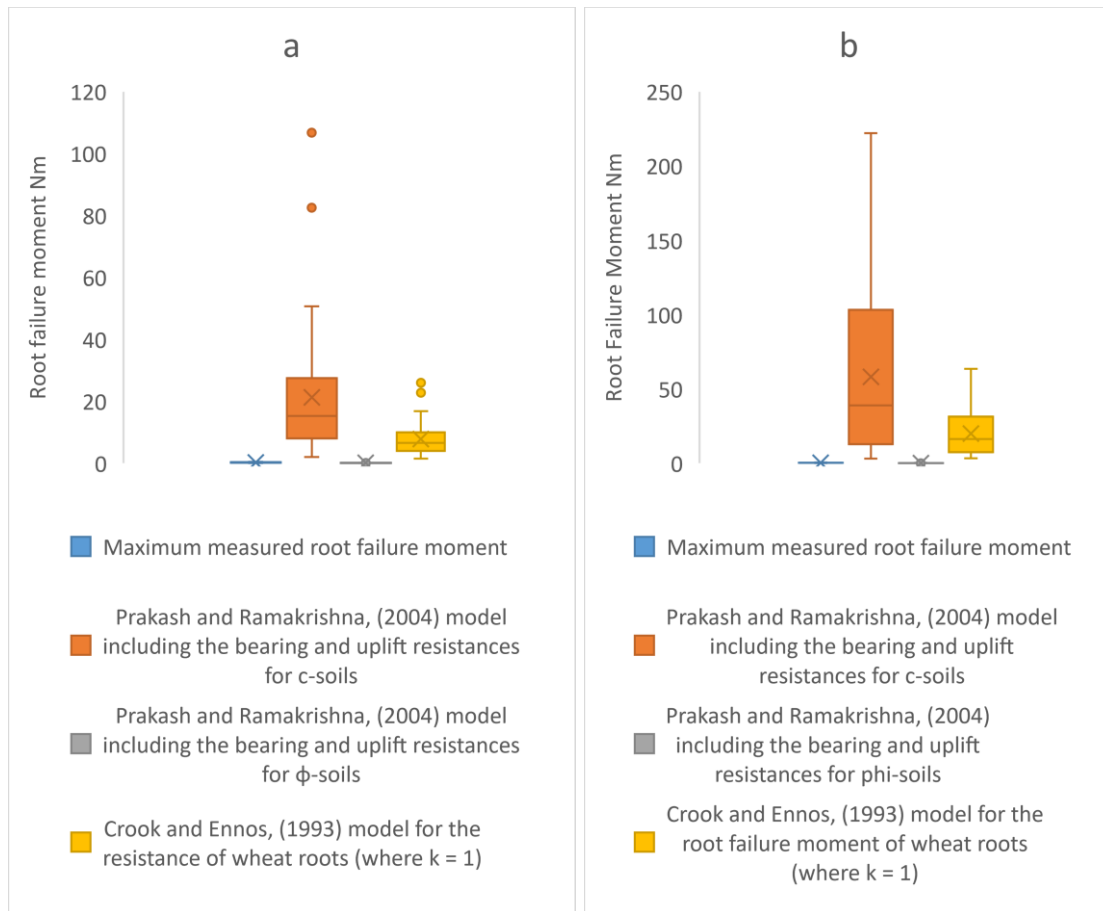
Figure 4.40 (a)Wheat and (b) oat root failure moment values predicted by the Prakash and Ramakrishna, (2004) model for under-reamed piles compared with the Root failure moment and the root failure moment predicted by Crook and Ennos, (1993).

Table 4.7 Statistics for the performance of the Crook and Ennos, (1993) model to the Prakash and Ramakrishna models for c-soils and ϕ-soils for wheat root failure moments.

Statistics	Crook and Ennos, (1993) model for the root failure moment of wheat roots (where k = 1)	Prakash and Ramakrishna, (2004) model including the bearing and uplift resistances for c-soils	Prakash and Ramakrishna, (2004) model including the bearing and uplift resistances ϕ-soils
RMSE	9.103	28.652	0.197
NRMSE	21.470	67.577	0.464
Slope	0.023	0.006	2.344

Table 4.8 Statistics for the performance of Crook and Ennos, (1993) model to the Prakash and Ramakrishna models for c-soils and ɸ-soils for oat root failure moments.

Statistics	Crook and Ennos, (1993) model for the root failure moment of wheat roots (where k = 1)	Prakash and Ramakrishna, (2004) model including the bearing and uplift resistances for c-soils	Prakash and Ramakrishna, (2004) model including the bearing and uplift resistances φ -soils
RMSE	24.403	79.472	0.165
NRMSE	63.550	206.957	0.430
Slope	0.007	0.002	1.713

Figure 4.40 shows that the model for c-soils over predicts the failure moment with a NRMSE value of 67.577 (206.957 for oats) compared with a value of 21.470 (63.550 for oats) for the Crook and Ennos, (1993) model. This over-prediction may be because the model assumes the plant is under similar pressures as an under-reamed pile foundation. The plants would not mobilise the same soil pressures as a foundation. The model could be calibrated to either reduce the pressures exerted or to reduce inputs that affect the model significantly. The next stage was to investigate different aspects of the model that could be changed based on the differences between the model assumptions and the real wheat and oat root systems observed in the laboratory experiments (Section 4.2.1). Prakash and Ramakrishna, (2004) found that when their model was compared to field measurements, the model overestimated the lateral capacity of the under-reamed piles. Interestingly, the ɸ-model provided good predictions with the bearing and uplift pressures included, which again suggests that the soils collected in the field in Ireland could be considered ɸ-soils.

Figure 4.41 shows the effect of including and excluding the bearing and uplift pressures. Removing the uplift pressure reduced the root failure moment determined by the model by almost 50% and removing both bearing and uplift reduced the modelled data to values that

were closer to the measured root failure moments. The NRMSE reduced from 67.6 to 27.0 when the uplift was removed. When the terms for bearing and uplift were both removed from the Equation 4.1 and 4.5 the NRMSE value reduced again to 1.83. The lower the NRMSE, the better the accuracy of the predictions. This suggests that the bearing and uplift pressures may not be part of the failure mechanism of the wheat and oat root systems. Bearing and uplift had a similar effect on oats. The changes in the NRMSE are shown in Table 4.9.
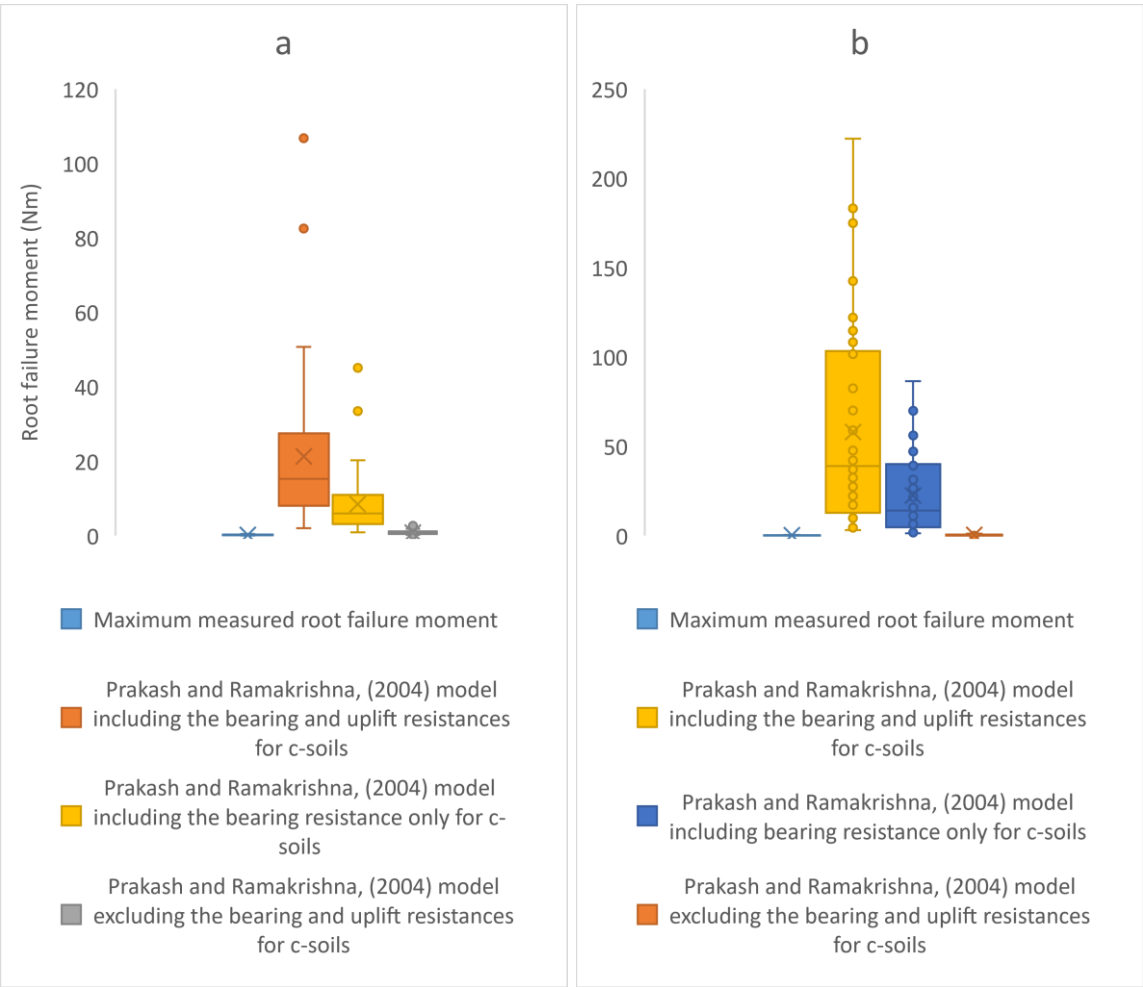
Figure 4.41 Predictions by the Prakash and Ramakrishna (2004) model for removing the uplift pressure and removing both the uplift and bearing pressures for (a) wheat (b) oats.

Table 4.9 Statistics for the performance of Crook and Ennos, (1993) model to the Prakash and Ramakrishna models for c-soils for wheat root failure moments.

Statistics	Crook and Ennos, (1993) model for the resistance of wheat roots (where k = 1)	Prakash and Ramakrishna, (2004) model including the bearing and uplift resistances for c-soils	Prakash and Ramakrishna, (2004) model including the bearing resistance only for c-soils	Prakash and Ramakrishna, (2004) model excluding the bearing and uplift resistances for c-soils
RMSE	9.103	28.652	11.467	0.774
NRMSE	21.470	67.577	27.044	1.827
Gradient	0.023	0.006	0.015	0.219

Figure 4.42 shows the failure mechanism for bearing and uplift. These shear planes were not observed in the root model experiments. Bearing resistance is related to the normal pressure in the ground, which is a function of depth. Considering the observations of movement of the root models observed in the laboratory experiments, it can be suggested that the bearing and uplift pressures may not have been present.

a

b
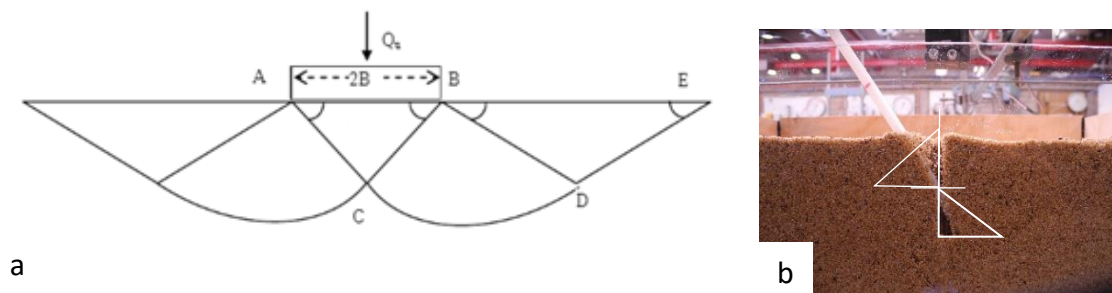
Figure 4.42 (a) Failure mechanism for bearing capacity (Dewaikar et al., (2005)) where Q- bearing pressure, 2B is the width of the foundation, (a,b,c,d,e) are wedges of soil (b) failure mechanism observed in the laboratory (section4.3.1).

The differences in the material and scale between the under-reamed pile foundation and the wheat or oat root system, explains some of the differences in the bearing and uplift resistances. Also, if there was an effect from the rotational movement of the root systems pushing downwards into the soil, there might possibly be bearing pressure initiated. There would be less uplift pressure because of the depth of the root systems in the soil. The root structures in this study are near to the surface. Therefore, the uplift pressures may not develop because there is only a small layer of soil covering the roots. In other words, pressures from the soil layer above would be very low or zero. This led to the variations of the model where the uplift was removed, and the bearing and uplift were removed from the equilibrium equations.

Figure 4.43, Figure 4.44 and Figure 4.45 show the results of changing the limiting soil pressure (or the soil reaction to the deflection of the plant) $9c_u$ and reducing it to $2c_u$ and changing the adhesion factor to predict root failure moment in wheat and oats. These were changed for each of the three scenarios, including bearing and uplift resistance, including bearing resistance only and excluding both bearing and uplift resistances. The boxplots also include the Crook and Ennos, (1993) model for easy comparison. Figure 4.45 shows that with bearing and uplift resistances included predictions were very high with maximum values of nearly 80Nm for wheat and 330Nm for oats. These values were for predictions including where the limiting pressure was changed and will be discussed further. Figure 4.44 and Figure 4.45 show the decrease in predictions of root failure moments as only bearing resistance was included and then when both bearing and uplift were excluded. Figure 4.45 shows that the predictions of the Prakash and Ramakrishna, (2004) model are now closer to the measure root failure moments than the Crook and Ennos, (1993) model.
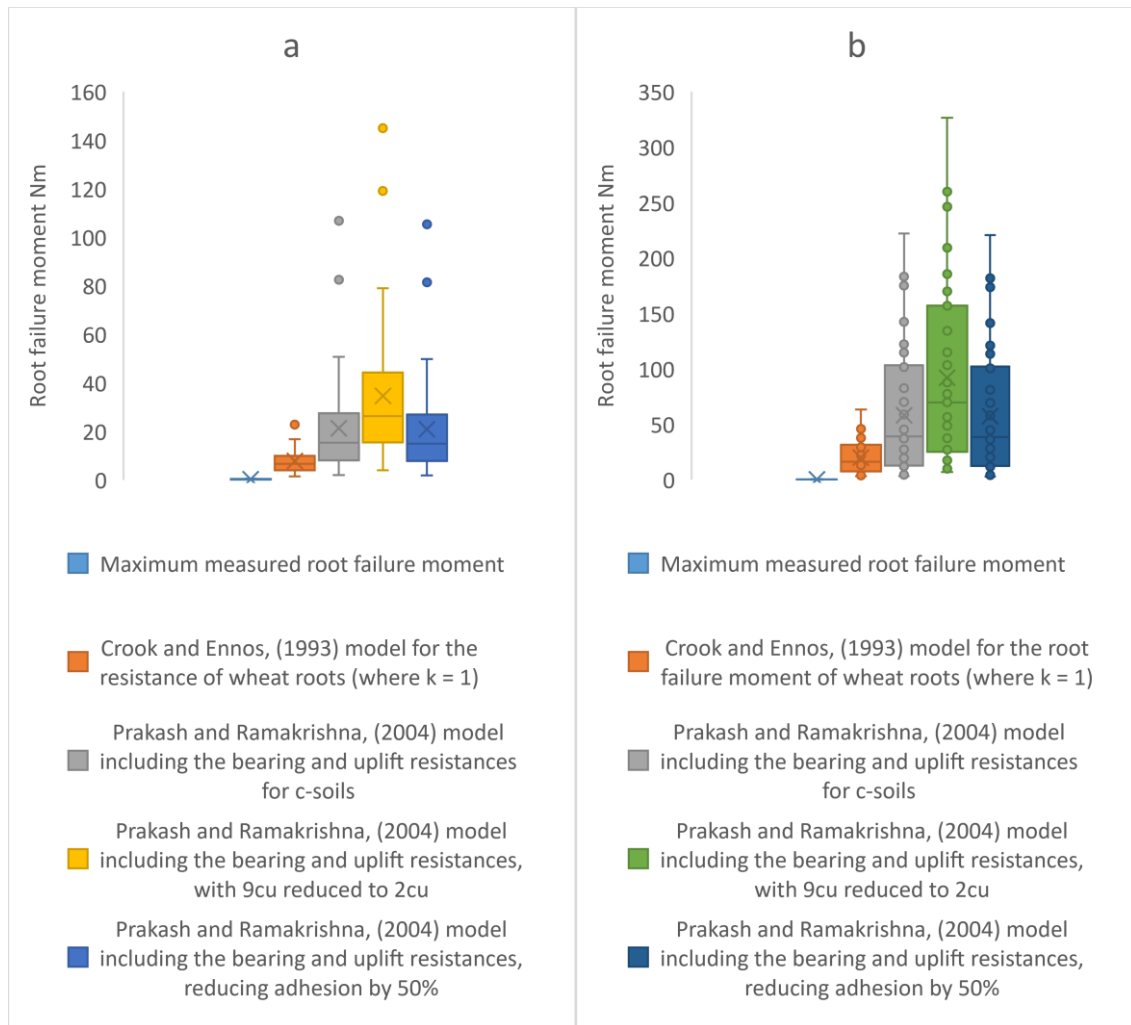
Figure 4.43 Model predictions for the Prakash and Ramakrishna, (2004) model with (a) bearing and uplift included (a) wheat (b) oats.

a

Root failure moment Nm

- ■ Maximum measured root failure moment

- ■ Crook and Ennos, (1993) model for the resistance of wheat roots (where k = 1)

- ■ Prakash and Ramakrishna, (2004) model including the bearing resistance only for c-soils

- ■ Prakash and Ramakrishna, (2004) model including the bearing resistance only, with 9cu reduced to 2cu

- ■ Prakash and Ramakrishna, (2004) model including the bearing resistance only, reducing adhesion by 50%

b

Root failure moment Nm

- ■ Maximum measured root failure moment

- ■ Crook and Ennos, (1993) model for the root failure moment of wheat roots (where k = 1)

- ■ Prakash and Ramakrishna, (2004) model including bearing resistance only for c-soils

- ■ Prakash and Ramakrishna, (2004) model including the bearing resistance only, with 9cu reduced to 2cu

- ■ Prakash and Ramakrishna, (2004) model including the bearing resistance only, reducing adhesion by 50%

Figure 4.44 Model predictions for the Prakash and Ramakrishna, (2004) model with only the bearing resistance included (a) wheat, (b) oats.
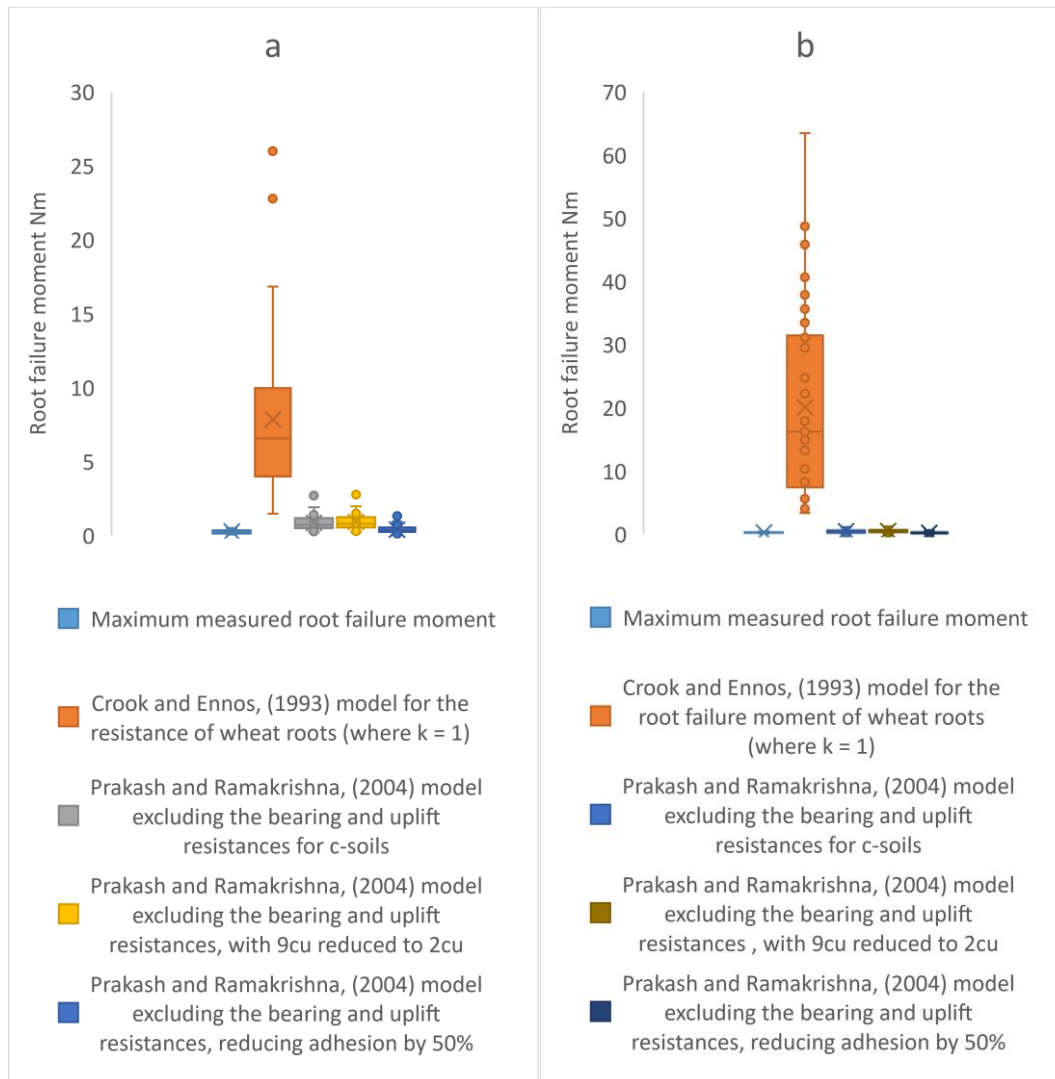
Figure 4.45 Model predictions for the Prakash and Ramakrishna, (2004) model with both the bearing and uplift resistances removed (a) wheat (b) oats.

Figure 4.43, Figure 4.44 and Figure 4.45 show the results of changing the assumptions of $9c_u$ to $2c_u$, (where c_u is the undrained shear strength of clay) for the limiting soil pressure or soil reaction to deflection, which increased the predicted root failure moment. This was the opposite response to what was expected as it was anticipated that reducing $9c_u$ to $2c_u$ would reduce the root failure moment. When the lateral pile theory was developed by Broms, (1964a), the limiting pressure of $9c_u$ was chosen based on empirical data measured for concrete piles. Fleming et al., (2009) and Reese, (1958) (cited by Broms, (1964a) proposed a

224

value of $2c_u$, suggesting less soil pressure developed during their experiments of deflecting concrete piles. Therefore, with the soil pressure ranging from $9c_u$ to $2c_u$, the latter was chosen for this research, assuming that the roots would also have a less soil pressure development compared to a pile foundation (based on the scale difference between a foundation and wheat and oat roots). However, the model reacted by increasing the root failure moment. This was because of the structure of the simultaneous equations, reducing the limiting pressure increases the value of the point of rotation from 0.1075 (mean) to 0.3509 (mean). Thus, increasing the root failure moment, not reducing it as was needed to bring the predicted values closer to the measured values.

Figure 4.45, Figure 4.44 and Figure 4.45 also show the results of changing the additional resistance of the bulb, specifically the adhesion factor. The additional resistance of the bulb is based on the interaction between the surface area of the bulb and the soil (skin friction or interface properties). In foundation engineering, an adhesion factor is applied to incorporate the additional friction between the pile and the soil. The piles can be constructed out of concrete or steel. The adhesion between the soil and pile surface differs for these two materials and will be different for plant roots. The adhesion factor is normally considered to be in the vertical direction as the pile would be driven into the soil vertically. However, in the case of the bulb in under-reamed piles the adhesion factor must be applied to the horizontal surfaces of the bulb.

Therefore, in c-soils, the horizontal adhesion factor, alpha, was taken as 40% of the adhesion factor in the vertical direction for piles in c-soils according to Smith, (1987). Smith, (1987) suggested different methods for converting the vertical subgrade modulus factors (factors

affecting the drag of piles in soils) into horizontal factors. These values were derived for pile foundations (made of concrete in the case of Prakash and Ramakrishna, (2004)) interacting with the soil. Therefore, these adhesion factors could be too large for smaller root structures like those in wheat or oats with different surface properties to concrete. The rhizosheath is a secretion around the roots that facilitates the uptake of nutrients from the soil. In this research, this secretion is assumed to create a smaller value of friction than the interaction between a concrete surface and the soil. The Crook and Ennos, (1993) model does not incorporate the resistance of the root-soil cone. Changing the adhesion factor was difficult because of the uncertainty and lack of data around the root-soil adhesion or slippage strength (see Section 2.1 discussing approaches to root anchorage modelling). Despite the lack of information, the adhesion factor was manipulated in the calibration of the c-soils model. Figure 4.45 shows the results when the adhesion factor is reduced from 0.28 to 0.14 for wheat.

After each of the factors was investigated separately, they were all combined to assess the effect of the modifications on the predictions of the root failure moment. This is shown in Figure 4.46. Each change to the model decreased the NRMSE (Table 4.10 for wheat and Table 4.11 for oats). It was found that the combination of the reduction of the bearing resistance, $9c_u$ to $2c_u$ and the adhesion factor produced the closest predictions to the measured values.
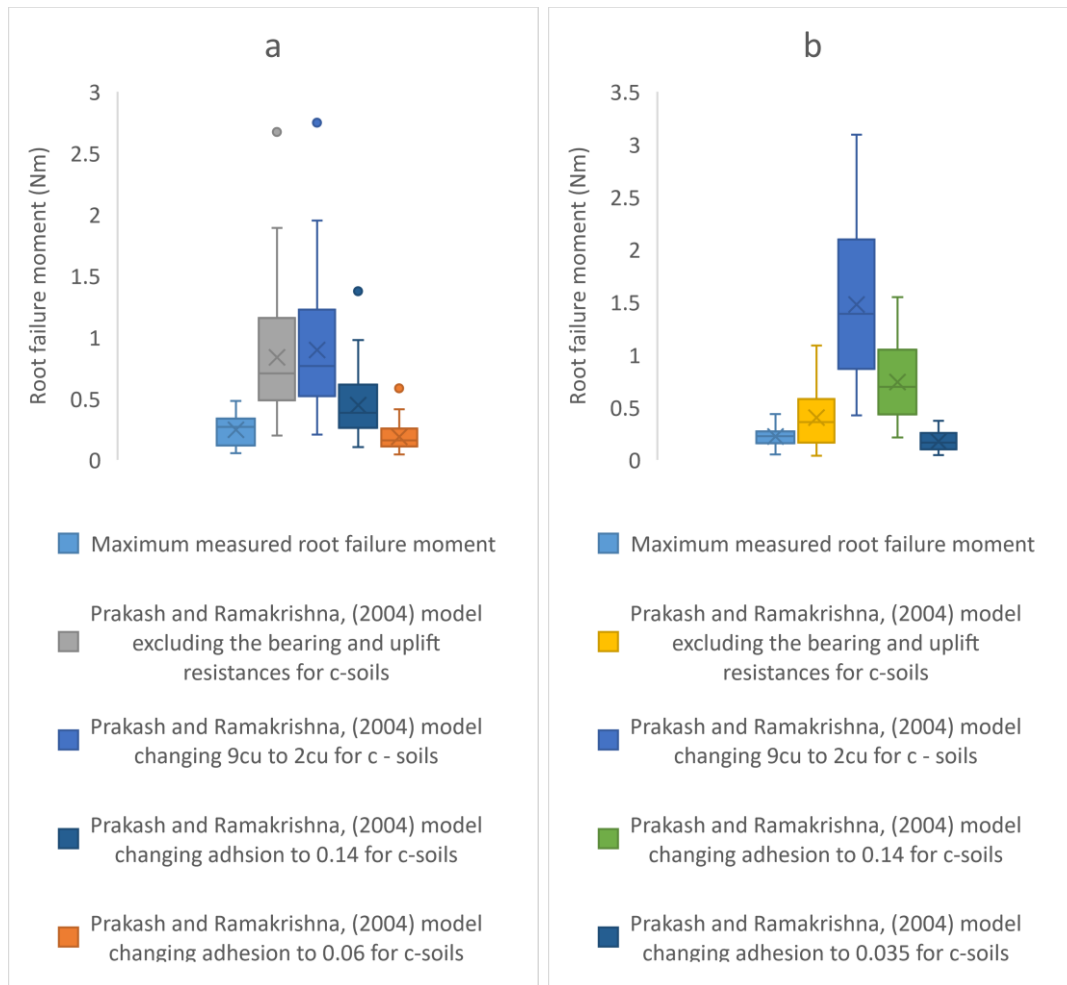
Figure 4.46 Model comparisons combining adaptations included for (a) wheat and (b) oats

Table 4.10 Statistics for the performance of changes to the different assumptions in the under-reamed pile model for wheat root failure moments.

Statistics	Crook and Ennos, (1993) model for the resistance of wheat roots (where k = 1)	Prakash and Ramakrishna, (2004) model including the bearing and uplift resistances for φ-soils	Prakash and Ramakrishna, (2004) model including the bearing and uplift resistances for c-soils	Prakash and Ramakrishna, (2004) model excluding the bearing and uplift resistances for c-soils	Prakash and Ramakrishna, (2004) model changing 9cu to 2cu for c-soils	Prakash and Ramakrishna, (2004) model changing adhesion to 0.14 for c-soils	Prakash and Ramakrishna, (2004) model changing adhesion to 0.06 for c-soils
RMSE	9.103	0.197	28.652	0.774	0.832	0.345	0.169
NRMSE	21.470	0.464	67.577	1.827	1.961	0.814	0.399
Slope	0.023	2.344	0.006	0.219	0.207	0.413	0.985

Table 4.11 Statistics for the performance of changes to the different assumptions in the under-reamed pile model for oats root failure moments.

Statistics	Crook and Ennos, (1993) model, oats roots (where k = 1)	Prakash and Ramakrishna, (2004) including the bearing and uplift resistances for φ -soils	Prakash and Ramakrishna, (2004) model including the bearing and uplift resistances for c-soils	Prakash and Ramakrishna, (2004) model excluding the bearing and uplift resistances for c-soils	Prakash and Ramakrishna, (2004) model changing 9cu to 2cu for c-soils	Prakash and Ramakrishna, (2004) model changing adhesion to 0.14 for c-soils	Prakash and Ramakrishna, (2004) model changing adhesion to 0.035 for c-soils
RMSE	24.403	0.165	79.472	0.324	1.451	0.639	0.136
NRMSE	63.550	0.430	206.957	0.844	3.779	1.664	0.354
Slope	0.007	1.713	0.002	0.391	0.119	0.238	0.980

An additional consideration was the shape of the bulb that is being considered during modelling. Prakash and Ramakrishna, (2004) idealised the shape of the bulb to a cylinder, and this was used in the main calculation of their models. However, they also included considerations of a bulb with inclined surfaces (see Appendix L1: Equations 4.9-4.14). In wheat and oats, the shape of the bulb can be described as a cone. A cylinder with the same diameter as a cone would have a larger surface area and hence would have a higher resistance. Also, with respect of the cylindrical option, two other options were analysed to mimic the root-soil cone (shown in Figure 4.47), the surface area of a cone and the surface area of the top of the cone.

Figure 4.47 Model comparisons for wheat, where the additional resistance of the pile was reduced.

229

Results for the comparison between the calculations found that assuming a cylinder shape produced larger values than assuming cone shapes; however, the cone surface area including the bottom surface still had high values compared to the cone alone. When the cone surface area was used alone, the values dropped towards negative values of root failure moment; the equations also predicted negative values if the angle of the inclined surfaces was larger than 90°. Therefore, this modification to the original equations was not used in the final model. Table 4.12 and

Table 4.13 show the statistics for the new models for root failure moment in wheat and oats, Equations 4.9-4.12 for c-soils and Equations 4.13- for ɸ-soils.

$$x^2 + x(2e) - C = 0 \qquad\qquad 4.9$$

$$C = C_1 + C_2 + C_3$$

$$C_1 = Le + 0.5L^2$$

$$C_2 = \frac{A_a}{D}\alpha_h L$$

$$A_1 = 2c_u D(x^2 - 0.5L^2) \ (c\ soils) \qquad\qquad 4.10$$

$$A_2 = 2A_a(\alpha_h\ c_u)\ L \quad (c\ soils) \qquad\qquad 4.11$$

$$Rfm = A_1 + A_2 \qquad\qquad 4.12$$

Where, R_{fm} is the root failure moment for c-soils, A_1 is the net passive resistance the root (N), A_2 is the additional resistance of the bulb, c_u is the shear strength (for fine-grained soils) (kPa), D is the diameter of the pile (m), x is the location of the point of rotation (m), L is the length

of the pile (m), e is the eccentricity (m), A_a = projected area of the bulb $= \frac{\pi}{4}(D_u^2 - D^2)$, D_u is

the root plate diameter and α_h is the adhesion factor = 0.06 for wheat and 0.035 for oats.

$$x^3 + x^2(1.5e) - C = 0 \qquad\qquad 4.13$$

$$C = C_1 + C_2 + C_3$$

$$C_1 = 0.75L^2e + 0.5L^3$$

$$C_2 = \frac{A_a tan\varphi}{DK_p} L_i(e + L_i)$$

$$C_3 = \frac{N_q}{DK_p} A_2 (L_i + A_2 \frac{N_y}{K_p})$$

$$B_1 = 3K_p\gamma D(2x^3 - L^3) \ (\varphi \ soils) \qquad\qquad 4.14$$

$$B_2 = A_a(\gamma \ tan\delta)(2L_i + L_b) L_b \ \ (\varphi \ soils) \qquad\qquad 4.15$$

$$Rfm = B_1 + B_2 \qquad\qquad 4.16$$

Where, R_{fm} is the root failure moment for c-soils, B_1 is the net passive resistance the root (N),

B_2 is the additional resistance of the bulb, D is the diameter of the stem (m), x is the location

of the point of rotation (m), L is the length of the root (m), K_p is the coefficient of passive earth

pressure $= tan^2(45+\frac{\varphi}{2})$ and γ is the unit weight of sand (for coarse-grained soils) (kN/m³). A_a =

projected area of the bulb $= \frac{\pi}{4}(D_u^2 - D^2)$, D_u is the diameter of the root plate, δ is the angle

of wall friction in the case of ɸ-soils, L_i = location of the bulb below the ground surface, L_b is

the length of the bulb (m). N_q, N_y are bearing capacity factors and are functions of ɸ, A_2 is the

coefficient $= \left[(\frac{D_u^3}{12} - \frac{D^3}{12})\right]$.

Table 4.12 Final under-reamed pile model prediction statistics for wheat.

Statistics	Prakash and Ramakrishna, (2004) model including the bearing and uplift resistances for φ-soils	Adapted Prakash and Ramakrishna, (2004) model changing adhesion to 0.06 for c-soils
RMSE	0.197	0.169
NRMSE	0.464	0.399
Slope	2.344	0.985

Table 4.13 Final under-reamed pile model prediction statistics for oats.

Statistics	Crook and Ennos, (1993) model, oats roots (where k = 1)	Prakash and Ramakrishna, (2004) including the bearing and uplift resistances for φ-soils	Adapted Prakash and Ramakrishna, (2004) model changing adhesion to 0.035 for c-soils
RMSE	24.403	0.165	0.136
NRMSE	63.550	0.430	0.354
Slope	0.007	1.713	0.980

4.5.2.1 Parametric Study for wheat and oats

A parametric analysis was completed on all of the model parameters to give an idea of the parameters that most affect the new models for oats and wheat. The values used in the parametric study are shown in Table 4.14. The range of values varied for different parameters but was kept within the ranges of values found in the field (Table 3.11 and Table 3.12). The plant root measurements were varied between 50% and 150% of the mean value based on data collected from the field. The soil parameters were varied according to the ranges of each parameter in the field collected during this research. The results are shown in Figure 4.48.

Table 4.14 Values used for the parametric study for the new under-reamed pile models for c-soils and ϕ-soils for wheat and oats.

Parameters	Range of values
Eccentricity of the load, e_m	0.17, 0.33, 0.5
Diameter of the root-soil bulb, D_{um}	50%, 75%, Dum, 125%, 150%
Length of the structural roots, L_m	50%, 75%, Lm, 125%, 150%
Stem diameter below the ground, D_m	50%, 75%, Dm, 125%, 150%
Undrained shear strength of the soil, c_u (only for c-soils)	80%, 90%, cu, 110%, 120%
Unit weight of the soil, gamma (only for ϕ-soils)	80%, 90%, gamma, 110%, 120%
Depth of the bulb below ground level, L_{mi}	110%, 120%, Lmi, 130%, 140%
Adhesion factor, $alpha_h$ (only for c-soils)	0.04, 0.05, 0.06, 0.07, 0.08
Angle of internal friction, ϕ (only for ϕ-soils)	60%, 70%, 80%, 90%, phi
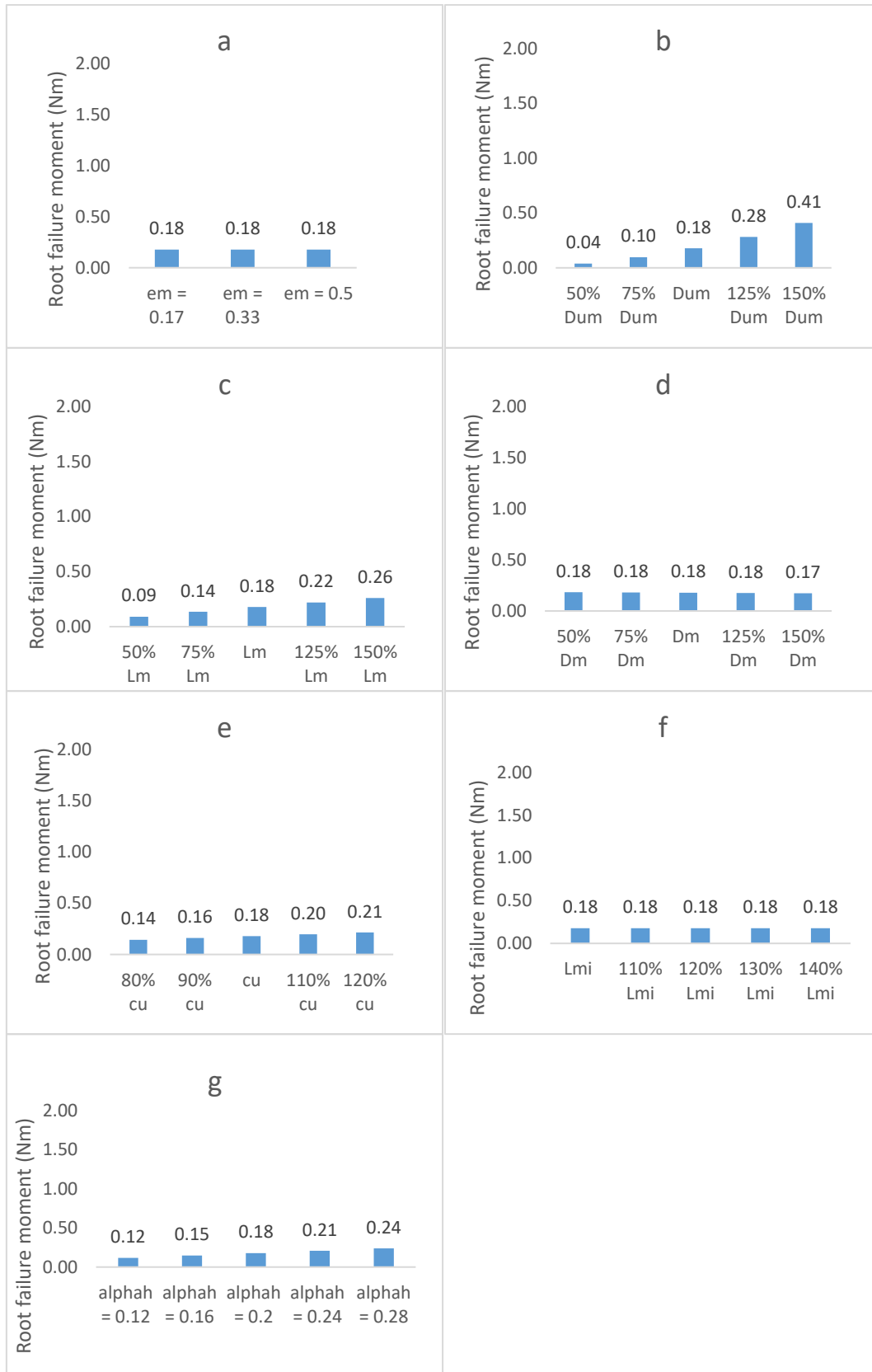
Figure 4.48 Parametric study for wheat for c-soils (a) eccentricity (m), (b) root plate diameter (m) (c) root length (m) (d) stem diameter (m), (e) soil shear strength (kPa) (f) depth to the root plate (m), (g) root plate angle (°).
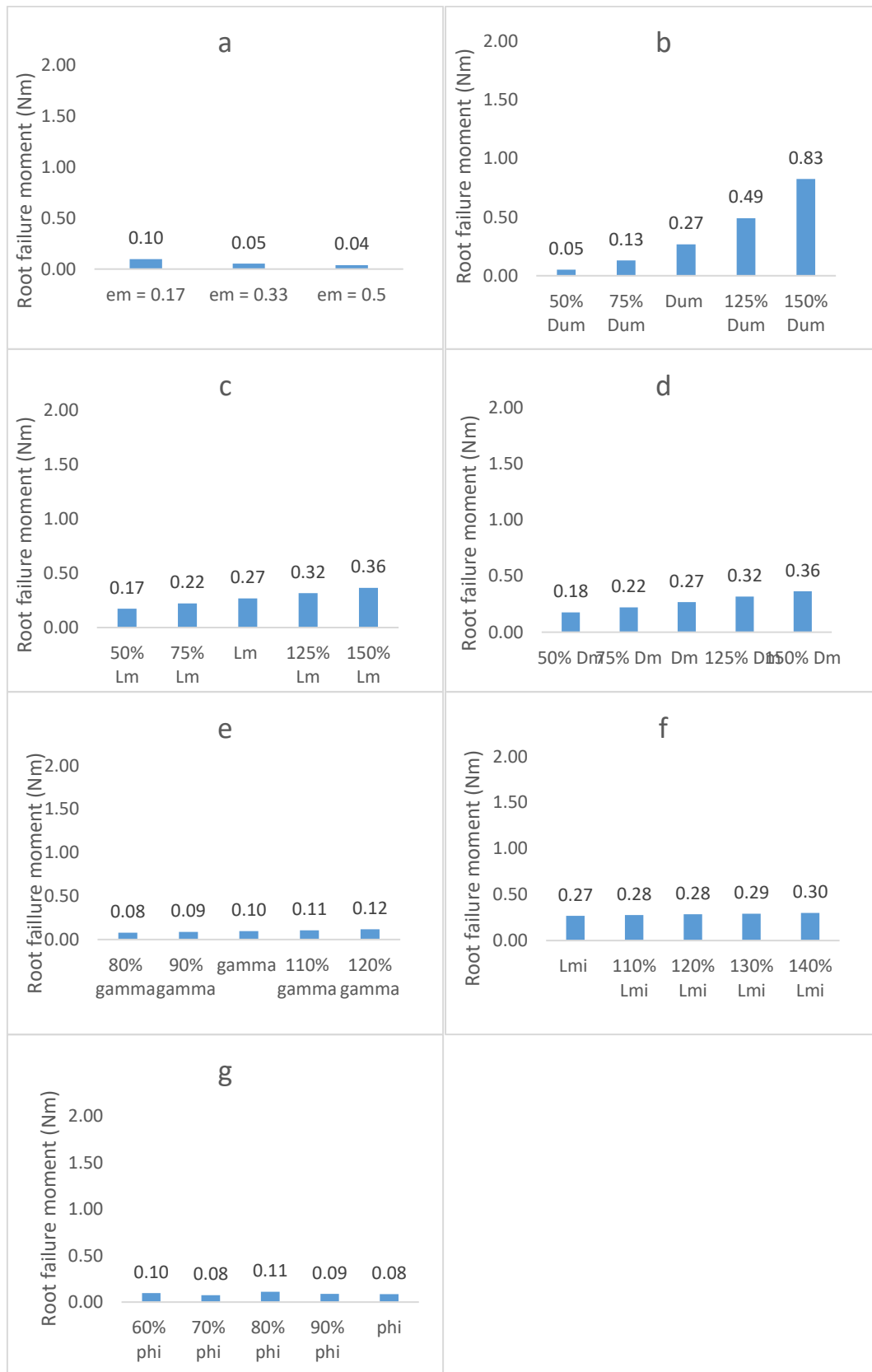
Figure 4.49 Parametric study for wheat for φ-soils (a) eccentricity (m), (b) root plate diameter (m) (c) root length (m) (d) stem diameter (m), (e) unit weight of sand (kN/m³) (f) depth to the root plate (m), (g) φ-angle (°).
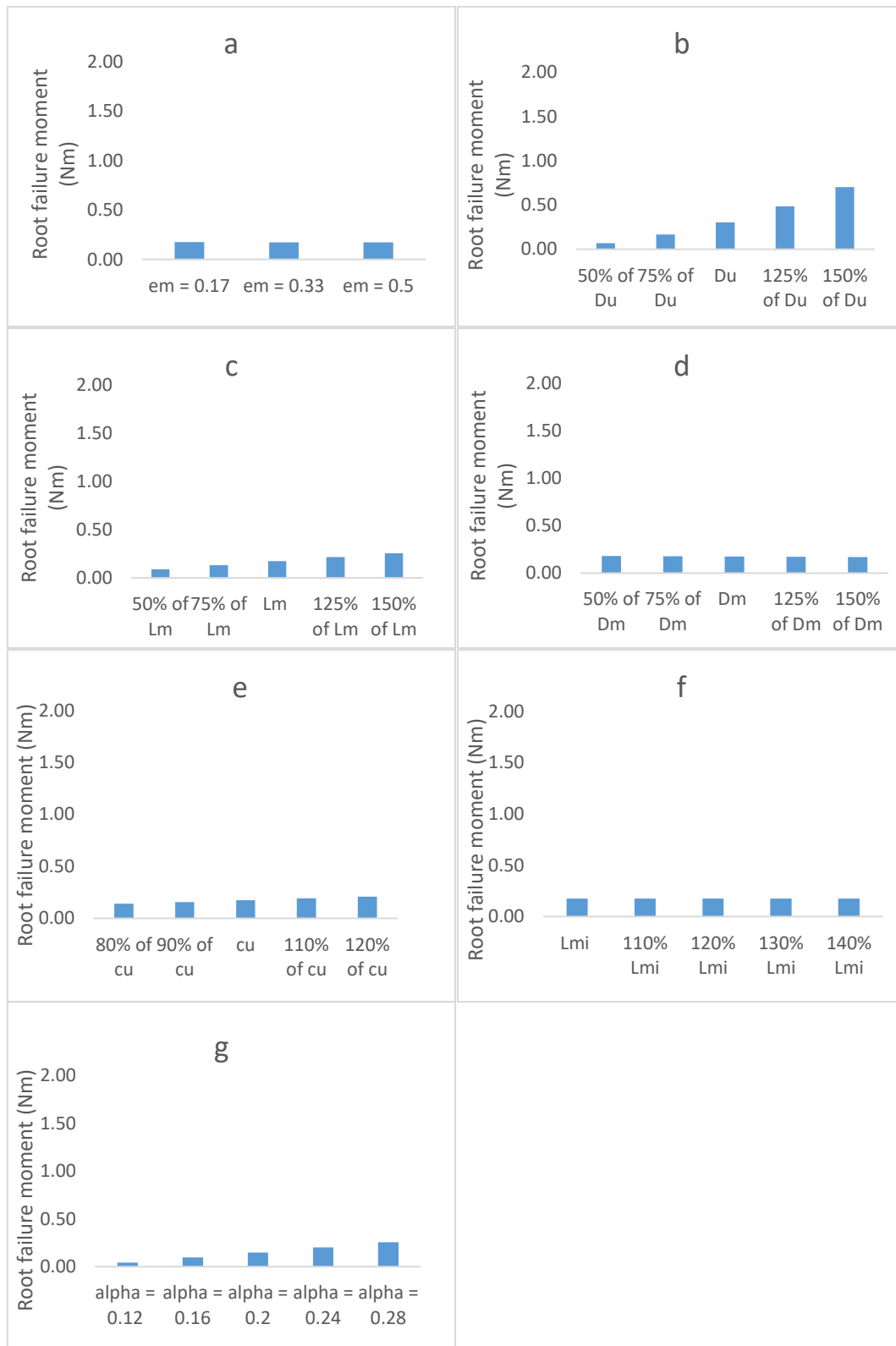
Figure 4.50 Parametric study for oats for c-soils (a) eccentricity (m), (b) root plate diameter (m) (c) root length (m) (d) stem diameter (m), (e) soil shear strength (kPa) (f) depth to the root plate (m), (g) root plate angle (°).
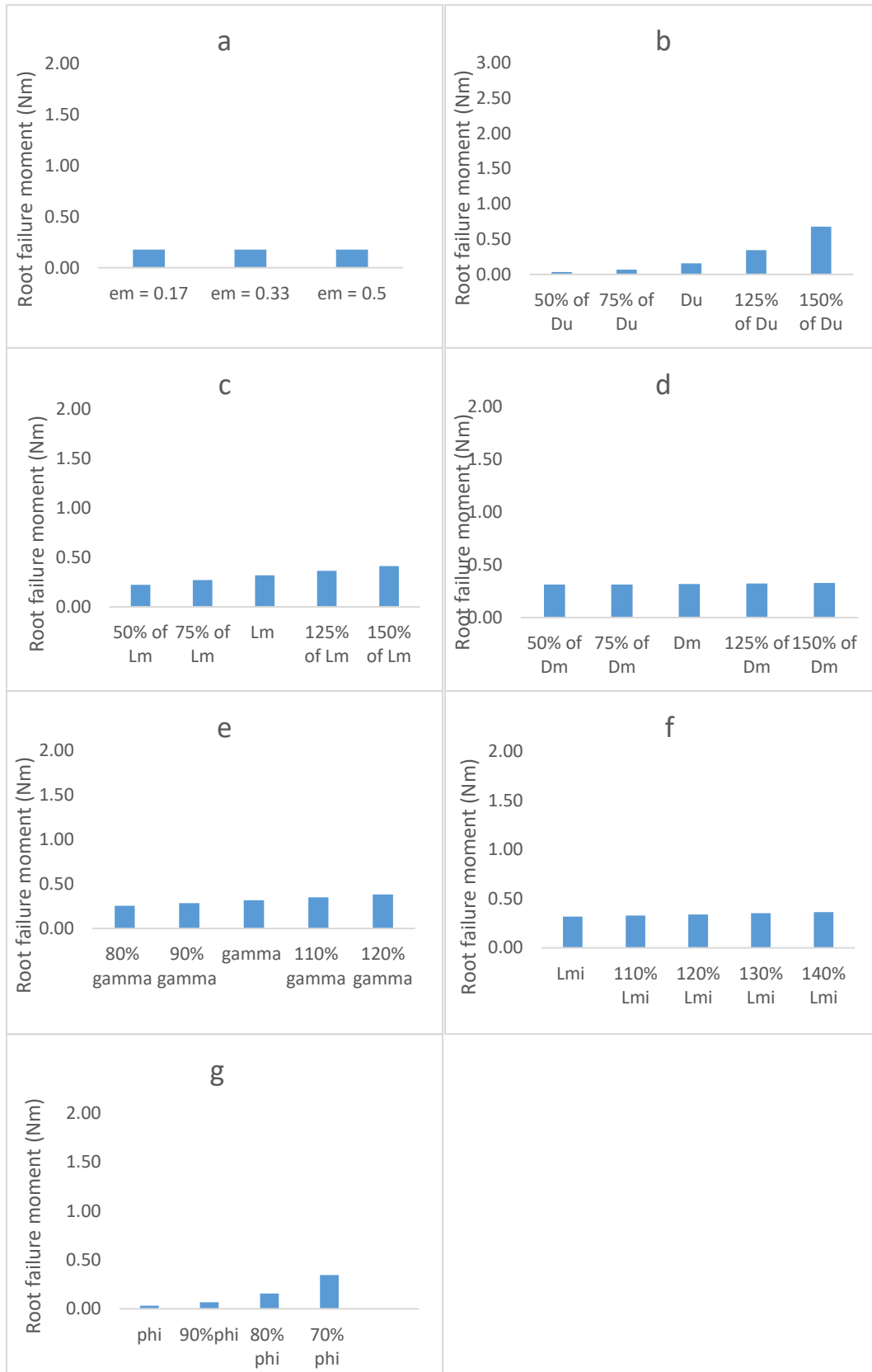
Figure 4.51 Parametric study for oats for φ-soils(a) eccentricity (m), (b) root plate diameter (m) (c) root length (m) (d) stem diameter (m), (e) unit weight of sand (kN/m³) (f) depth to the root plate (m), (g) φ-angle (°).

The parametric analysis found that the under-reamed pile model for wheat responded to root cone diameter and root length in c-soils (Figure 4.48). In φ-soils, the model was affected by the root cone diameter, root length and stem diameter (Figure 4.49). Therefore, variations in these measurements will cause greater changes in the predicted values from the modified model. The parametric study using oat measurements had similar outcomes to wheat with the exception of the φ value, which had a significant impact (Figure 4.50 and Figure 4.51). A study of resistance of model root systems to uprooting in sand (0.05-2mm particle size distribution) by Stokes et al., (1996) found that the dominant factors influencing the pull-out resistance (resistance to vertical pulling or uprooting) were also depth and length of the roots in the soil. They also found that the most efficient type of root architecture (branching pattern) was one with an increased number of roots deep in the soil. This is supported by Fourcaud et al., (2008), who completed numerical studies of overturning mechanisms in fine and coarse-grained soils. They found that the longest roots influenced the size of the root-soil plate formed in fine-grained soils. In coarse-grained soils, modifying the shape and size of the root-soil cone altered the point of rotation and hence, the anchorage resistance.

4.5.2.2 Validation of the calibrated model for wheat and oats

The new models for wheat were applied to a dataset collected in the field using the manual lodging machine (Dataset1) and a dataset collected in the field using the new lodging machine (Dataset2) to validate the generic application to predict of root failure moments compared with measured values using data which was not used for the development of the models. Both datasets were collected in 2018.

The results are shown in Figure 4.52a and b. Figure 4.52a shows a bar chart of the values of the new model and the measured root failure moments. Figure 4.52b shows a scatterplot of the predictions with the gradients of 2.27 for ϕ-soils and 0.746 for c-soils, indicating that the c-soils model was more accurate. The NRMSE values are given in Table 4.15. Figure 4.53a and b show the same charts but for Dataset2. Figure 4.52b shows the predictions with the gradients of 7.8 for ϕ-soils and 0.90 for c-soils, indicating that the predictions from the c-soils model were closer to the measured values. The NRMSE values are given in Table 4.16. Both the ϕ-soils and c-soils under-reamed pile models had lower NRMSE values than Crook and Ennos, (1993).
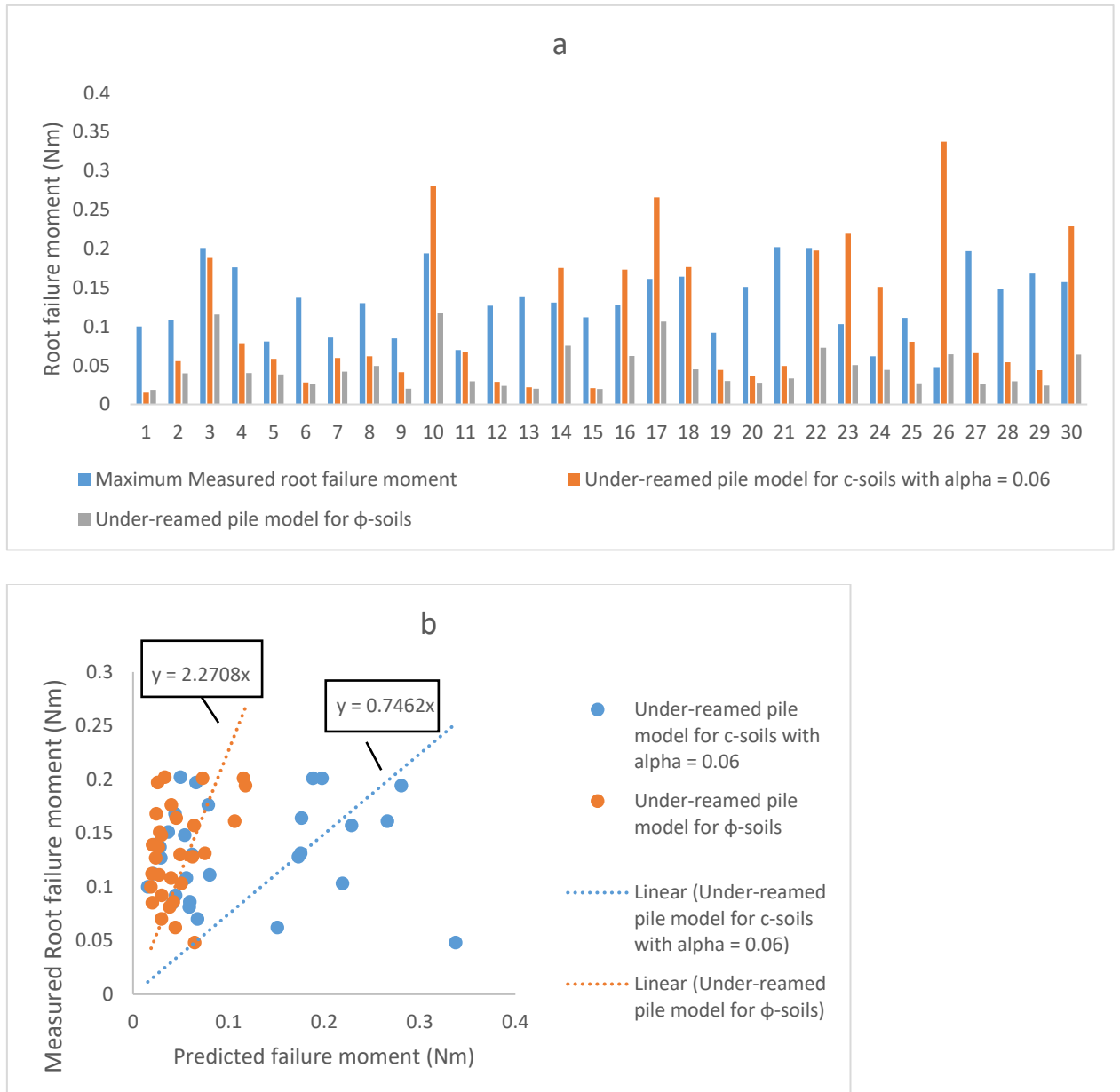
Figure 4.52 Results using the new model to predict measured values collected using the new apparatus developed in this research. (a) Bar chart comparing the measured values with the predicted values predicted by the c-soil model and the φ-soils. (b) Scatterplot of the predictions with the gradients of 2.27 for φ-soils and 0.746 for c-soils, indicating that the c-soils model was more accurate.

Table 4.15 Statistics for the new models for wheat based on the Dataset 1.

Statistics	Crook and Ennos, (1993) model, oats roots (where k = 1)	Under-reamed pile model for c-soils with alpha = 0.06	Under-reamed pile model for φ-soils
RMSE	2.577	0.097	0.096
NRMSE	16.733	0.633	0.622
Slope	0.035	0.746	2.271
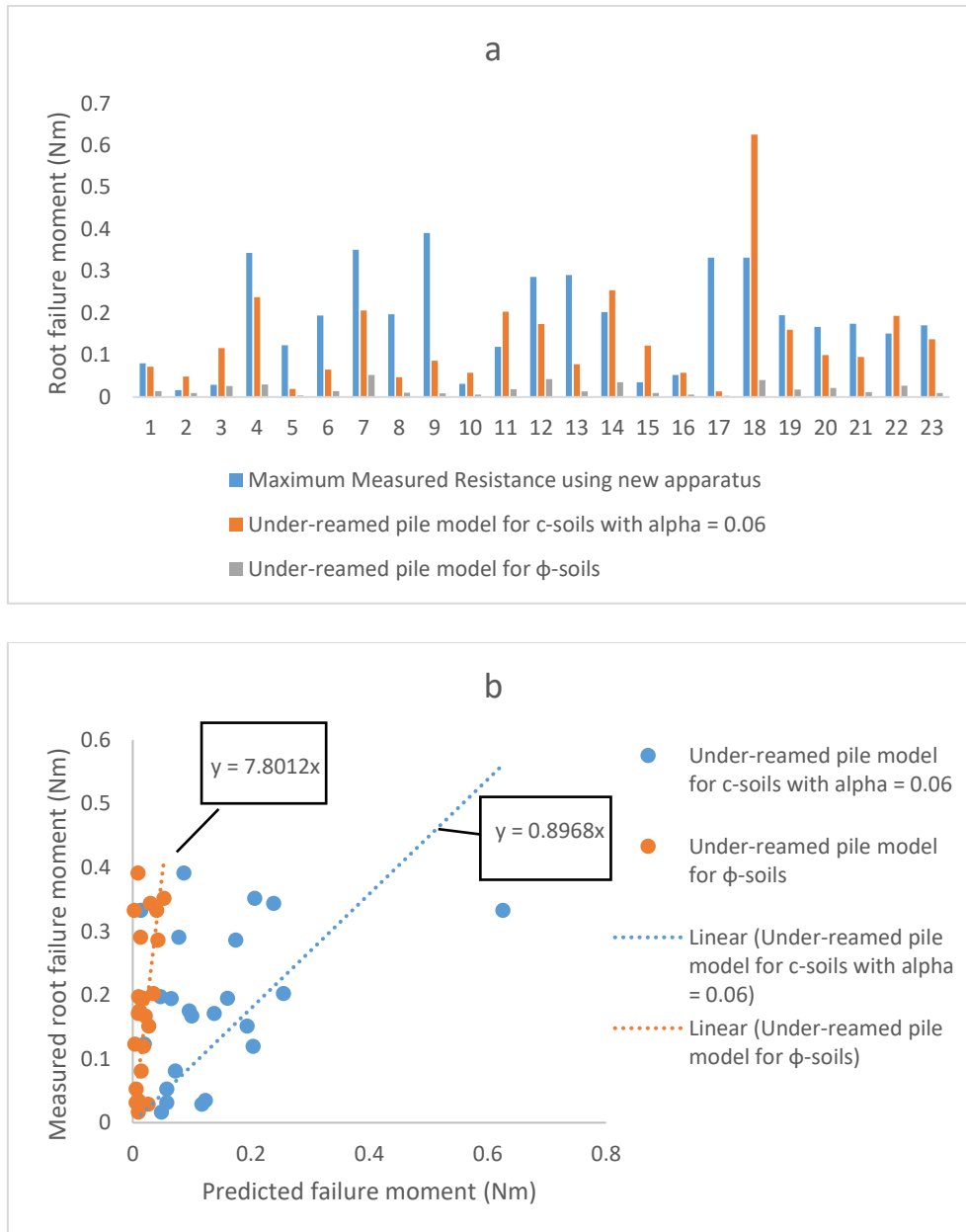
Figure 4.53 Results using the new model to predict measured values collected using the new apparatus developed in this research. (a) Bar chart comparing the measured values with the predicted values predicted by the c-soil model and the φ-soils. (b) Scatterplot of the predictions with the gradients of 7.8 for φ-soils and 0.90 for c-soils, indicating that the c-soils model was more accurate.

Table 4.16 Statistics for new models for wheat based on the dataset collected using Dataset2.

Maximum Measured Resistance using new apparatus	Crook and Ennos, (1993) model, oats roots (where k = 1)	Under-reamed pile model for c-soils with alpha = 0.06	Under-reamed pile model for φ-soils
RMSE	1.315	0.162	0.199
NRMSE	3.511	0.433	0.532
Slope	0.111	0.897	7.801

The new models for oats were applied to a dataset collected in the field using the manual lodging machine in 2018. The results are shown in Figure 4.54. Figure 4.54a shows a bar chart of the values of the new model and the measured root failure moments. Figure 4.54b shows a scatterplot of the predictions with the gradients of 2.8 for ϕ-soils and 1.4 for c-soils, indicating that the c-soils model was more accurate. The NRMSE values were 0.526 for ϕ-soils and 0.470 for c-soils (with the adjusted adhesion factor). Both the ϕ-soil and c-soil under-reamed pile models had lower NRMSE values than Crook and Ennos, (1993).

Even though the predicted values using the new model are closer to the measured values in most cases, there are some over and under-predictions. This is because there is variability between the crops discussed in section. Also, there could be influences from the strength of the roots, or number of roots for each plant altering the root failure moment. These aspects of root anchorage are not captured in this new model but could be included in future research.
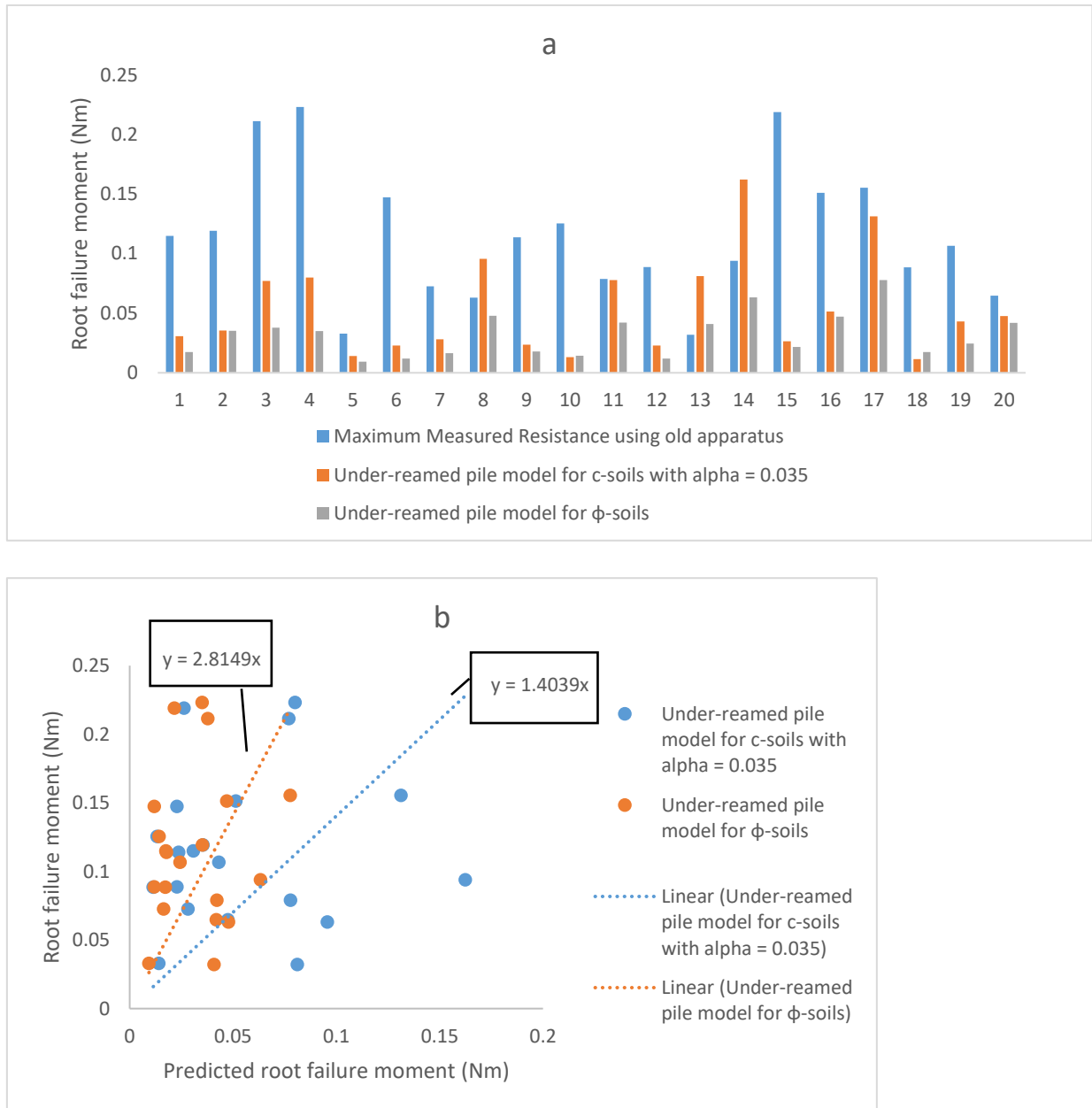
Figure 4.54 Results using the new models for oats to predict measured values collecting using the older apparatus created by Berry et al., (2004) (a) a bar chart comparing the measured values with the predicted values predicted by the c-soil model and the φ-soils. (b) Scatterplot of the predictions with the gradients of 2.8 for φ-soils and 1.4 for c-soils, indicating that the c-soils model was more accurate.

Table 4.17 Validation statistics for new models for oats based on the dataset collected in 2018.

Statistics	Crook and Ennos, (1993) model, oats roots (where k = 1)	Under-reamed pile model for c-soils with alpha = 0.035	Under-reamed pile model for φ-soils
RMSE	2.244	0.090	0.101
NRMSE	11.738	0.470	0.526
Slope	0.044	1.404	2.815

After the validation stage, it was found that using Dataset 2 for wheat, the c-soil model, after several adjustments, had the lowest value of NRMSE, 0.433 compared to 0.532 for the ɸ-soil model. In contrast, Dataset 1 for wheat, showed that the ɸ-soils had the lowest NRMSE of 0.622 compared to 0.633 for c-soils. While both models could be utilised to predict root failure moments, the soils on the site were classified in Section 3.3.2 as silty Sands making them ɸ-soils. Also, the fact that the ɸ-soils model was able to predict root anchorage without any modifications can be taken as a further indication that the soils at Oak Park are showing frictional behaviour. Therefore, the under-reamed pile model for ɸ-soils is recommended to predict the root failure moment of wheat and oats.

4.5.3 Development of the root anchorage failure in oilseed rape

Prediction of root failure moments for oilseed rape was different to wheat and oats. The nature of the oilseed rape tap root meant that only the equations representing the straight-shafted model were included (the bulb was removed). The predictions from the Prakash and Ramakrishna, (2004) model were compared with the model by Goodman et al., (2001) created for oilseed rape roots, the Niklas, (1992) model and the cantilever sheet pile model (Section 2.4). The results of the comparisons are shown in Figure 4.55 and Table 4.18.The under-reamed pile model for c-soils and ɸ-soils over-predicted the root failure moment for oilseed rape. A similar result as was found when applying the model to wheat and oats; the c-soil model over predicted. The under-reamed pile model for c-soils was modified similarly to wheat and oats models, discussed in Section 4.5.1, where the bearing, uplift resistances and the soil resistance value $9c_u$ were manipulated. However, Figure 4.55, shows that even with the modifications the Prakash and Ramakrishna, (2004) model overestimated root failure

moment. For ɸ-soils, the bearing and uplift resistances were removed. However, these adjustments did not reduce the predictions close to the measured values.

The overestimation for the Prakash and Ramakrishna, (2004) model may have been due to the assumptions around the shape of the tap root and the soil resistance. The tap root was assumed to be the same as a cylindrical pile, however, when tap roots taper along the length to a point, they may curl or curve in different directions. The idealisation to a cylinder would increase the area of the soil that would be resisting rotation and hence, increase the predictions for root failure moment.
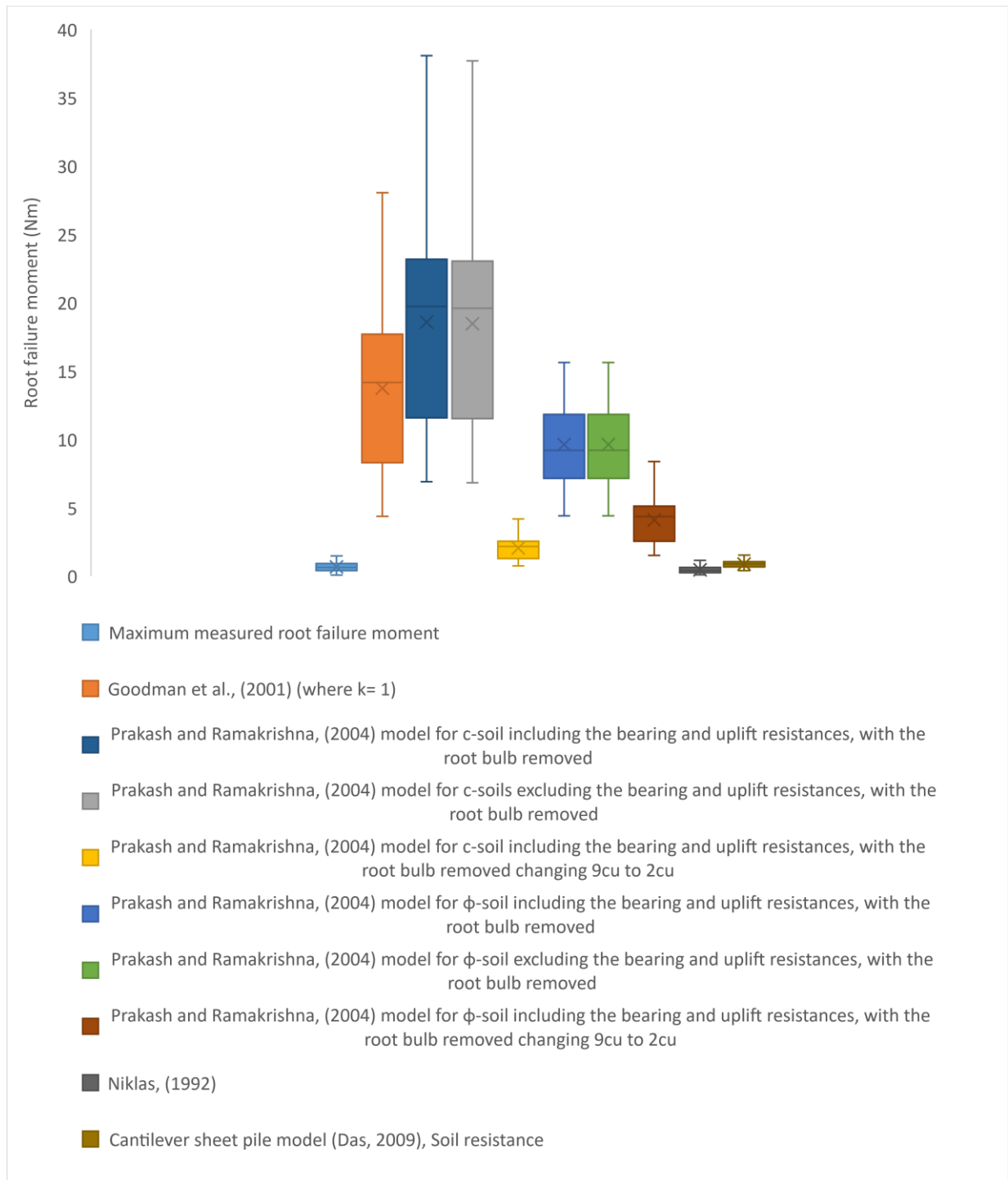
Figure 4.55 Oilseed rape root failure moment values predicted by the Prakash and Ramakrishna, (2004) model for under-reamed piles.

Table 4.18 Statistics for different assumptions in the under-reamed pile model for oilseed root failure moments.

Statistics	Goodman et al., (2001) (where k= 1)	Prakash and Ramakrishna, (2004)					
		Model for c-soil including the bearing and uplift resistances, with the root bulb removed	Model for c-soils excluding the bearing and uplift resistances, with the root bulb removed	Model for c-soil including the bearing and uplift resistances, with the root bulb removed changing 9cu to 2cu	Model for ϕ-soil including the bearing and uplift resistances, with the root bulb removed	Model for ϕ-soil excluding the bearing and uplift resistances, with the root bulb removed	Model for ϕ-soil including the bearing and uplift resistances, with the root bulb removed changing 9cu to 2cu
RMSE	14.360	19.503	19.371	1.572	9.398	9.399	3.778
NRMSE	10.294	13.980	13.886	1.127	6.737	6.737	2.708
Slope	0.046	0.035	0.035	0.313	0.070	0.070	0.157

An alternative model provided by Prakash and Ramakrishna, (2004) was that of the flexible under-reamed pile. This model was applied using the oilseed rape dataset and values found in Goodman et al., (2001). The model first checks whether the pile or root can be considered as flexible.

There are criteria the dimensions of the tap root have to meet for both c-soils and ϕ-soils, to be considered flexible. For c-soils, if βL (see Appendix L1) was greater than 2.5, then the root would be considered flexible. The oilseed rape tap roots were not considered flexible in the case of c-soils; they did not meet the criteria. Therefore, the calculation was not continued.

The oilseed rape tap roots did meet the criteria for flexible piles in ϕ-soils. Z_{max} (see Appendix L1) ranged from 5.82-16.9, which met the criteria for flexible piles in ϕ-soils. The next stage was to calculate the lateral resistance using the model for flexible piles which incorporates the strength of the pile.

When the lateral resistance for flexible under-reamed piles was calculated using the values for oilseed rape, the predictions were found to be comparable to the measured values of root failure moment, with NRMSE values of 0.283 compared to 10.29 for the Goodman et al., (2001) model (Figure 4.56 and Table 4.19). This model incorporates the root strength into the analysis which was found to be a factor in the root failure moments of the artificial roots in Section 4.3.2 and 4.3.3. The rigid oilseed rape model had higher root failure moment values than the flexible model. However, there was some uncertainty in the values for permissible yield stress, modulus of elasticity and modulus of subgrade reaction as there were measurements of these values for plant roots. More testing would need to be completed

before using this model for root failure moments. Therefore, the flexible pile was not used for the final model at this stage.

Therefore, other models were chosen to compare predictions, the modified Niklas, (1992) model and the soil resistance equation for the cantilever sheet pile model (Das, 2011). Both of these models gave more accurate results with NRMSE values were 0.282 and 0.249 respectively (Figure 4.56 and Table 4.19). Both models were used in the parametric study in the following section.
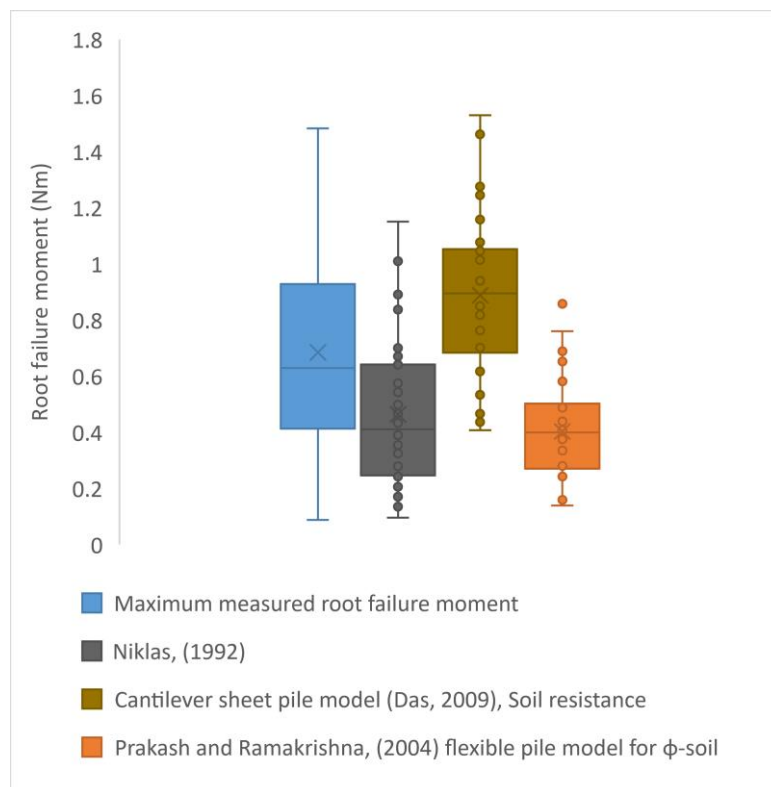
Figure 4.56 Model comparisons for oilseed rape.

Table 4.19 Statistics for the models with the lowest NRMSE values for oilseed rape root failure moment.

Statistics	Niklas, (1992)	Cantilever sheet pile model (Das, 2009)	Prakash and Ramakrishna, (2004) flexible pile model for φ-soil
RMSE	0.394	0.348	0.395
NRMSE	0.282	0.249	0.283
Slope	1.317	0.784	1.672

4.5.3.1   Parametric Study for oilseed rape

A parametric analysis was completed on both the Niklas, (1992) model and the cantilever sheet pile model (Das, 2011). The models were varied using the values found in Table 4.20. The results are shown in Figure 4.57 and Figure 4.58. The root diameter and the root length affected the Niklas, (1992) model more than the soil shear strength. The root diameter had the highest impact increasing the values of root failure moment by more than 100% when the diameter was increased by 50%. This is because the amount of soil mobilised is increased hence increasing the soil resistance and the root failure moment. The cantilever sheet pile model was most affected by plant height, stem diameter and wind speed. With wind speed having the greatest effect. The cantilever sheet pile model was not used in the final validation because the model calculates the soil resistance by using the plant characteristics and not the root characteristics.

After the parametric analysis was completed, the Niklas, (1992) model is recommended for the prediction of oilseed rape root anchorage because it had the lowest NRMSE values. The anchorage model is represented by Equation 4.17.

$$R_{fm} = \frac{c_u \pi D^2 L}{2} \qquad \qquad 4.17$$

Where, c_u is the shear strength of the soil (kPa), D is the diameter of the root (m) and L is the length of the root (m).

Table 4.20 Values used for the parametric study the Niklas, (1992) and cantilever Das, (2011) for oilseed rape.

Parameters	Range of values
Diameter of the root, D_m	50%, 75%, Dm, 125%, 150%
Length of the structural roots, L_m	50%, 75%, Lm, 125%, 150%
Undrained shear strength of the soil, cu (only for c-soils)	80%, 90%, cu, 110%, 120%
Unit weight of the soil, gamma (only for ϕ-soils)	80%, 90%, gamma, 110%, 120%
Angle of internal friction, ϕ (only for ϕ-soils)	60%, 70%, 80%, 90%, phi
Wind Speed, v	50%, 75%, v, 125%, 150%
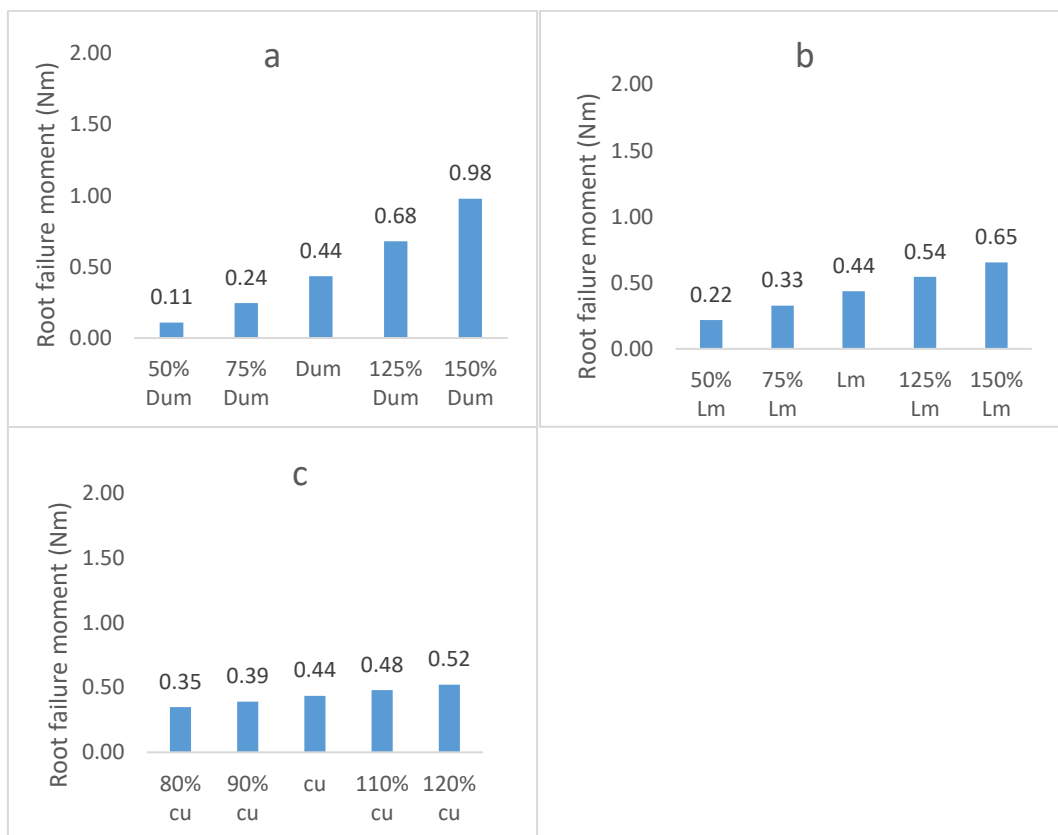
Figure 4.57 Parametric analysis of the root failure moment using the Niklas, (1992) model (a) root diameter (m) (b) root length (m) (c) shear strength (kPa).
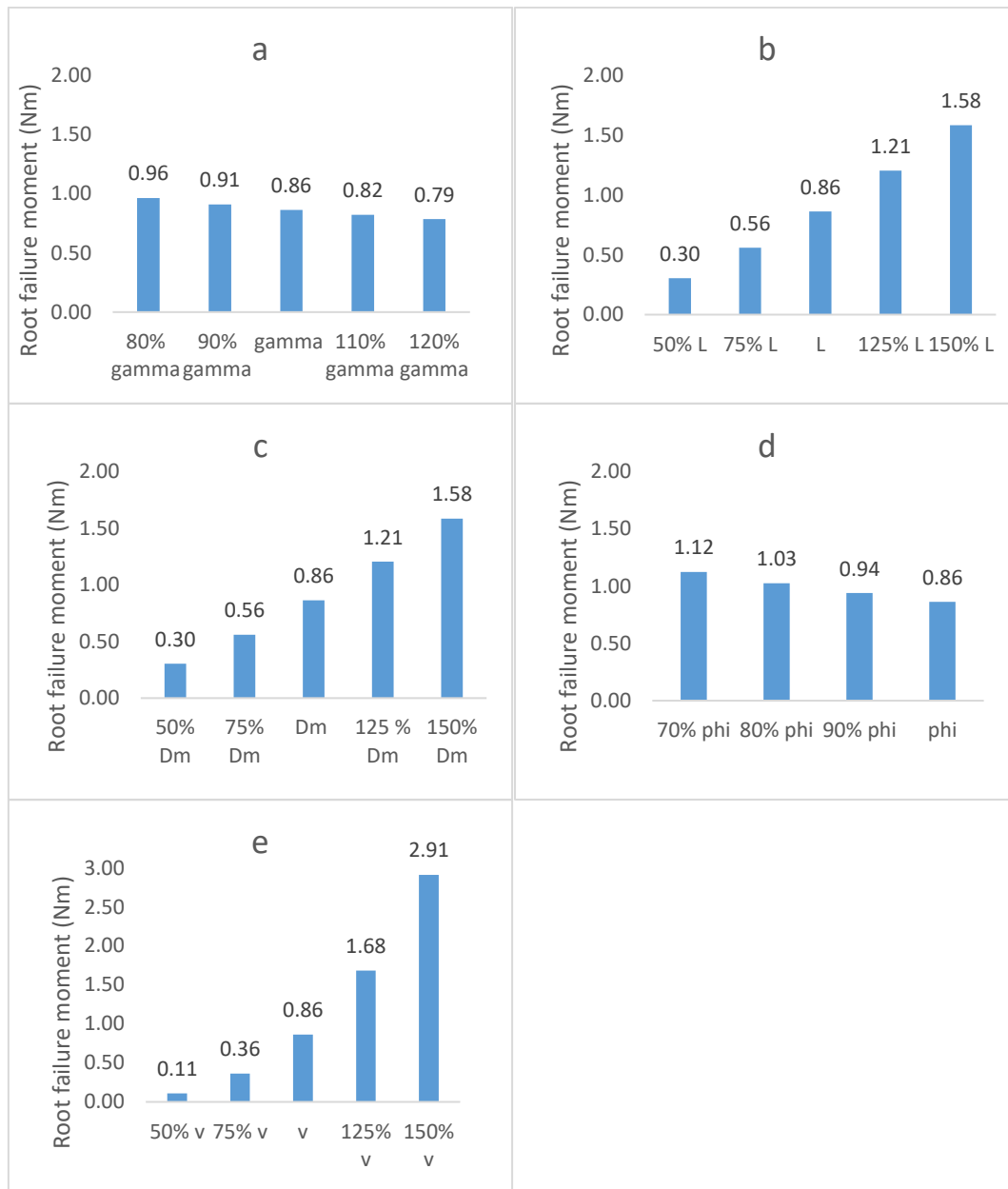
Figure 4.58 Parametric analysis using the cantilever sheet pile model (Das, 2009) (a) unit weight of sand (kN/m³) (b) root length (m) (c) root diameter(m) (d) ϕ angle (e) wind speed (m/s).

4.5.3.2   Validation of the model for Oilseed rape model

Figure 4.59 and Table 4.21 show the results of the validation of oilseed rape root failure moment, using the dataset collected in the field in 2018 using the manual lodging machine.

Using the validation dataset, the Niklas, (1992) model was not as accurate as when the model

was calibrated. However, in comparison to the Goodman et al., (2001), the original Niklas, (1992) model was more accurate. In these validation tests, Niklas, (1992) also showed significant variations between measured values and predicted. This is because of the variability between each plant discussed in section 3.3.3.4. The root strength is a factor not incorporated into the model. This is where the flexible pile model could be used to increase accuracy. Oilseed rape tap roots also have lateral roots, which influence the root failure moment, depending on their strength, size and orientation. Finally, comparing the failure mechanisms observed in Section 4.3.1, there may be more soil movement around the roots as they lodge. These factors require more investigation.
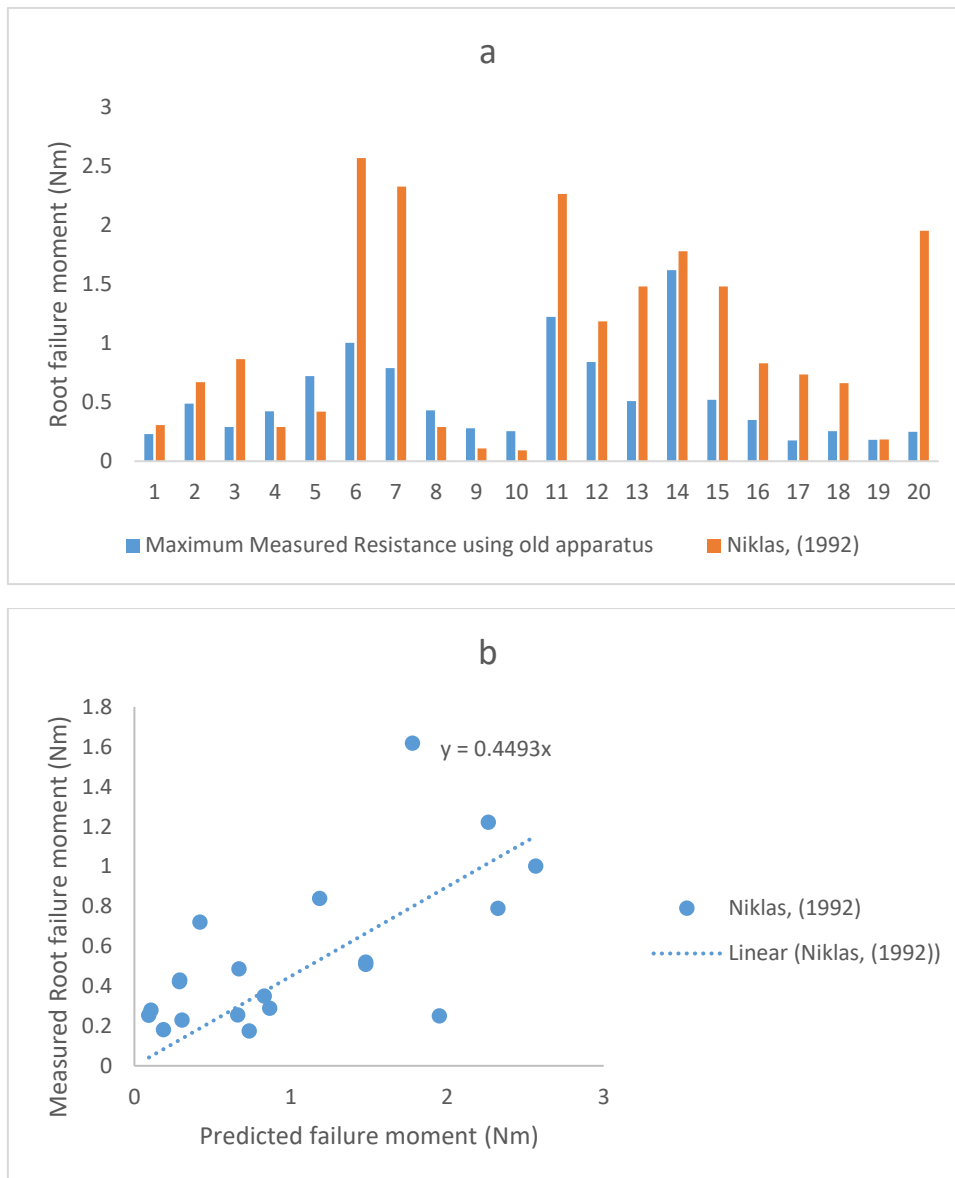
Figure 4.59 Results of the validation of the most accurate model for oilseed rape model. The model (a) bar chart showing the differences between the measured and predicted values, (b) Scatterplot of the predictions by Niklas, (1992) model.

Table 4.21 Final statistics of model predictions using the new model and the previous model (Goodman et al., (2001)), based on the validation datasets.

Statistics	Niklas, (1992)	Goodman, et al., (2001) (where k= 1)
RMSE	0.776	18.858
NRMSE	0.538	13.073
Slope	0.449	0.062

4.5.4   Methodology for Practitioners

The final section of the research focussed on proposing a methodology for applying the findings of this research in the field, to provide predictions of root failure moment to farmers. The method requires the practitioner to collect the parameters required for each model provided in Table 4.22, shear vane measurements, the wind and rain conditions and the current size of the root systems of their crops, to give an idea of the strength of the root and soil.

Table 4.22 Parameters needed for the new model of root anchorage in wheat, oats and oilseed rape.

Wheat and Oats:	Advantages of the new model	Disadvantages of the new model
ϕ' effective internal angle of friction D is the diameter of the pile (m) L is the length of the pile (m) e is the height of plant (m) D_u is the root plate diameter (m) γ' effective unit weight of soil	Improved accuracy of model compared to Crook and Ennos, (1993). Easy to measure plant and root parameters Model uses parameters from soil mechanics and geotechnical engineering. Model incorporates water content of soil within the measurement of soil strength.	Eventually will require the measurement of the effective stress parameters under suction control; this is time consuming and requires specialist equipment
Oilseed rape:	**Advantages of the new model**	**Disadvantages of the new model**
c_u is the shear strength of the soil (kPa) D is the diameter of the root (m) L is the length of the root (m)	Improved accuracy compared to Goodman et al., (2001) Easy to measure plant and root parameters Model incorporates water content in the measurement of the soil strength	Requires the undrained shear strength of the soil to be measured

A flowchart showing the proposed method is given in Figure 4.60. The initial measurements by the farmer or practitioner are shown in the blue boxes. From these measurements the soil water content, shear strength and the relevant strength parameters can be obtained. These

are used as inputs to the model proposed in this research for the root failure moment. The lodging risk model by Baker et al., (2014) could then be used to evaluate the stem base bending moment and the two moment could be compared. If the stem base bending moment exceeds the root failure moment, then the crops will fail. If the root failure moment is larger than the stem base bending moment, then the crops will be ok.

During this research project, it was found that the root failure moments change depending on the relationship between soil particle size distribution and soil water content. Therefore, a practitioner could find or measure the soil particle size distribution or soil texture of their fields to understand the strength of the soil. The British Geological Society, BGS and the Irish Soils Information Service websites provide soil maps with descriptions and texture analysis that could be used to get a general idea of the particle size distribution of the soil. There is also a method to identify soils in the field using the British Standard, 2016, BS5930 chart. The farmer or practitioner could also collect soil strength measurements using the vane shear.

Next, the water content of the soil needs to be measured. One possibility could be to monitor the water content using water probes or use the simple soil water content test described in this research. Once the soil particle size distribution and water content are known, they can be related to a range of soil strength parameters using Table 4.23.

The next step is to measure several root samples over the growing season from areas where lodging occurs in order to track the size of the root parameters. Once these parameters are collected, the root failure moment can be calculated using the model.

Finally, wind speed data needs to be collected. The wind speed is required for the calculation of the stem base bending moment using the model by Baker et al., (2014) or to estimate the

stem bending moments. The stem bending moment can be compared to the root failure model. If the root failure moment is smaller than the stem bending moment than the crops will lodge. Table 4.23 and Table 4.24 give ranges of values from this research, which could be used as part of the methodology.

The new model for wheat and oats can be integrated in the generalized model by Baker et al., (2015). The new model would replace both the shear strength calculation and the root failure moment calculation completely, because it predicts the root failure moment at field capacity, as it uses the effective angle of friction. There are a series of steps to derive the equations (given in Appendix L1). To use the equations, the practitioner would need the variables listed in Table 4.22 as well as a calculation of A_a (Equation 4.18), the projected area of the root plate, the coefficient, A_2 (Equation 4.19), N_q, N_c and N_y (Equation 4.20, 4.21 and 4.22), and K_p, the coefficient of passive earth pressure (Equation 4.23). Then the values for C (Equation 4.25) can be calculated. From this a value for x is found from Equation 2.4 and then x can be used in Equation 4.26. R_{fm} is found by Equation 4.28.

$$A_a = \frac{\pi}{4}(D_u^2 - D^2)$$ 4.18

$$A_2 = \left[\left(\frac{D_u^3}{12} - \frac{D^3}{12}\right)\right]$$ 4.19

$$N_q = e^{\pi tan\varphi} tan^2\left(45 + \frac{\varphi'}{2}\right)$$ 4.20

$$N_c = (N_q - 1)cot\varphi'$$ 4.21

$$N_y = 2.0(N_q - 1)tan\varphi'$$ 4.22

$$k_p = tan^2\left(45 + \frac{\varphi}{2}\right)$$ 4.23

$$x^3 + x^2(1.5e) - C = 0 \qquad\qquad 4.24$$

$$C = C_1 + C_2 + C_3 \qquad\qquad 4.25$$

$$C_1 = 0.75L^2e + 0.5L^3 \qquad\qquad 4.25a$$

$$C_2 = \frac{A_a \tan\varphi}{DK_p} \sum_{i=1}^{n} L_i \left(e + \sum_{i=1}^{n} L_i \right) \qquad\qquad 4.25b$$

$$C_3 = \frac{N_q}{DK_p} A_2 \sum_{i=1}^{n} L_i + nA_2 \frac{N_y}{K_p} \qquad\qquad 4.25c$$

$$B_1 = 3K_p\gamma D(2x^3 - L^3) \ (\varphi \ soils) \qquad\qquad 4.26$$

$$B_2 = A_a(\gamma \tan\delta)(2L_i + L_b) L_b \ (\varphi \ soils) \qquad\qquad 4.27$$

$$R_{fm} = B_1 + B_2 \qquad\qquad 4.28$$

Where R_{fm} is the root failure moment, B_1 is the net passive resistance the root (N), B_2 is the additional resistance of the bulb, D is the diameter of the stem (m), x is the location of the point of rotation (m), L is the length of the root (m), and γ' is the unit weight of sand (for coarse-grained soils) (kN/m³). D_u is the diameter of the root plate, δ is the angle of wall friction in the case of ɸ-soils, L_i = location of the bulb below the ground surface, L_b is the length of the bulb (m). N_q, N_y are bearing capacity factors and are functions of ɸ.

For oilseed rape, the shear strength at field capacity would be measured by a shear vane. The model would replace the soil strength calculation as the water content is considered within the shear strength and the root anchorage model for oilseed rape (Equation 4.29).

$$R_{fm} = \frac{c_u \pi D^2 L}{2} \qquad\qquad 4.29$$

Where, c_u is the shear strength of the soil (kPa), D is the diameter of the root (m) and L is the length of the root (m). This model is recommended for the prediction of root failure moments in oilseed rape plants.
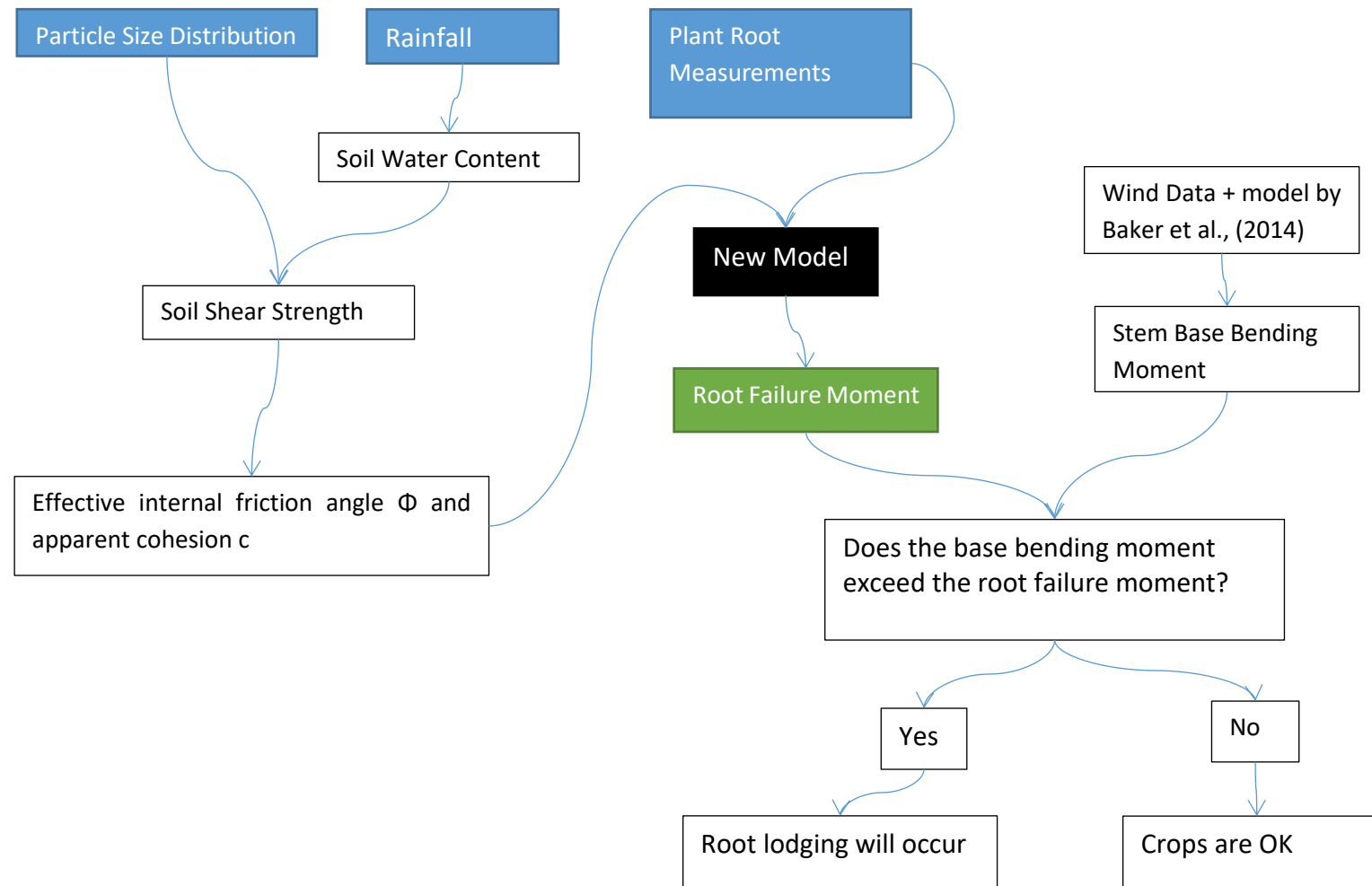
Figure 4.60 Flow chart for the methodology for farmers to understanding the risk of root lodging.

Table 4.23 Showing the ranges of values for each soil type, with corresponding root measurements, root failure measurements and root failure predictions.

Soil Sample	Particle Size Distribution				Shear strength Parameters		Shear Strength at field capacity (kPa)		Root Cone diameter or Root diameter (mm)		Root length (mm)		Plant height (cm)		Root failure moment (Nm)	
	Fine Gravel (%)	Sand (%)	Silt (%)	Clay (%)	Angle of internal friction (ϕ)	Apparent cohesion (c)	Max	Min	Max	Min	Max	Min	Max	Min	Max	Min
Oilseed Site 1	18	41	38	3	34.37	6.61	60	19	24	9	32	9	38	28	2.041	0.138
Wheat Site 1	13	40	37	5	37.40	5.87	45	13	165	40	60	9	113	75	0.669	0.105
KnockBeg Site	13	40	33	7	31.12	9.76	64	16	46	10	30	24	183	133	0.725	0.066

Table 4.24 Soil Data table part 2, giving the threshold for water contents above which the soil strength decreases rapidly.

Soil Sample	Field Capacity (Water Content %)	Plastic Limit (Water Content %)
Oilseed Site 1	23	23.3
Wheat Site 1	27	25.4
KnockBeg Site	22	21.7

4.5.5 Summary of model development

A model calculating the capacity for under-reamed pile foundations was adapted for root systems of wheat, oats and oilseed rape. The models had options for both fine-grained and coarse-grained soils. It was found that for wheat, the coarse-grained model and an adjusted fine-grained model had the highest accuracy. The coarse-grained model had a normalised root mean squared error (NRMSE) of 0.464 and the fine-grained model had an NRMSE of 0.399 compared to 21.5 for the past model by Crook and Ennos, (1993). For oats, the same models as wheat had the highest accuracy with the coarse-grained model and fine-grained models having an NRMSE of 0.430 and 0.354 respectively, compared to 63.5 for the model by Crook and Ennos, (1993). However, the course grained (ɸ-soils) model was recommended to predict root failure moment in wheat and oats. For oilseed rape, it was found that the Niklas, (1992) model was the most accurate model having an NRMSE of 0.282 compared to 10.3 for the past model by Goodman et al., (2001). A sensitivity analysis found that the models for wheat and oats were sensitive to the adhesion factor; the root length and diameter were important factors. For oilseed rape root length was still the most important factor. Finally, there was a discussion about how the model would be integrated into the model by Baker, (1998) and an outline of how practitioners may be able to collect data for the model and apply the model were presented.

5   Conclusions and Recommendations for Further Research

This research aimed to improve the calculated accuracy of root-soil interaction models for predicting the measured root failure moment for wheat, oats and oilseed rape. A key contribution of this research has been the development of more accurate models that are able to predict the root failure moment by utilising simple to measure parameters.

The first objective of the study was achieved by completing a literature review which demonstrated that there was very little research on the root anchorage mechanisms of oats. There was more research conducted on the anchorage of wheat and oilseed rape, with the root failure being related to the behaviour of short rigid piles by Crook and Ennos, (1993) and Goodman et al., (2001) using semi-empirical equations. Both models had limited validation. These models were subsequently used by Baker et al., (2014) in a model for lodging risk. Several alternative models were reviewed in this research to understand other theories and aspects that influence root anchorage. Field and laboratory data were used to evaluate the different models. This demonstrated that there was uncertainty around the accuracy of the predictions from the models and a number of elements associated with the failure mechanisms, e.g. the root failure moment-rotation curves. The models for predicting root anchorage had not been previously compared to understand their relative accuracy and there was no dataset in the literature that could provide the parameters needed to compare the models.

5.1   Conclusions

The work presented in this thesis resulted in a number of key conclusions:

- The literature showed that a limited number of well characterised data on wheat, oat and oilseed rape existed upon which existing models could be evaluated. This meant that a suitable methodology to carry out lodging experiments was developed to obtain a dataset of soil and plant parameters, achieving the second objective of the study. A new lodging machine was developed and used in the field for collecting root anchorage data combined with corresponding plant, root, soil parameters and images, for 72 wheat plants, 63 oat plants and 40 oilseed rape in three sites in the field in 2017.

- The field experiments showed that the root failure moments were variable and challenging to control due to the varying nature of both the soil and the plant parameters. The anchorage resistances for wheat ranged from 0.105 to 0.669Nm, for oats from 0.06 to 0.725Nm and for oilseed rape from 0.1 to 2.041Nm.

- In order to control the parameters, laboratory experiments were conducted, but as there was no existing lodging machine for small scale testing, a new methodology was developed for testing of flexible and rigid artificial wheat and oilseed rape roots in coarse and fine-grained soils, at different water contents, achieving the third objective of the study. The key findings were:

  - In coarse-grained soil, the root failure moment increased with increasing degree of saturation and decreasing effective stress.

  - In fine-grained soils, the root failure moment was 4-5 times larger than for coarse-grained soils and closer to values measured in the field, which was expected. When the water content was increased to the plastic limit in these fine-grained soils (causing the effective stress and the shear strength to decrease), the root failure moment decreased rapidly. It was also found that the

weight of the artificial oilseed root model contributed a self-weight moment, and the flexibility of the artificial wheat stem affected the load transferred into the soil. There was an improved root failure moment when the roots were rigid.

- The failure mechanism of the artificial oilseed rape root models could be related to the lateral resistance akin to that of a pile foundation with a point of rotation established within the tap root in the case of oilseed rape. The failure mechanism for wheat and oats involved the root-soil plate and the root depth and was more akin to that of a shallow under-reamed pile.

- When applying the datasets from the field and the laboratory to models developed by Crook and Ennos, (1993) (NRMSE 21.470 for wheat, 63.656 for oats) and Goodman et al., (2001) (NRMSE 1.375 for wheat, 179.381 for oats), they over-predicted root anchorage compared to the measured root failure moments. These models incorporated soil shear strength, root plate diameter, root diameter and root length. Models originally developed for trees, for example, Fourcaud et al., (2008) (NRMSE 0.494 for wheat, 0.280 for oats) were more accurate for the datasets collected for wheat and oats. In oilseed rape, the results showed a model suggested by Niklas, (1992) (NRMSE of 0.264) was the most accurate.

- Overall, all the models identified from the literature struggled to predict the root failure moment accurately, because they relied on empirical or semi-empirical relationships, therefore, a new model was adapted to the root failure moment in wheat, oats and oilseed rape using geotechnical principles addressing the fourth objective.

- A new model for the wheat, oat and oilseed root systems was developed based on an analytical model for calculating the capacity of under-reamed pile foundations by Prakash and Ramakrishna, (2004), with an adjustment to the soil resistance (from $9c_u$ to $2c_u$, where c_u is the undrained shear strength of clay) removing bearing and uplift pressures and reducing the adhesion factor. This new model allowed both fine-grained and coarse-grained soils to be assessed by incorporating the diameter of the root-soil cone and the friction (shear stresses mobilised) between the interface of the soil and roots. It was found that for wheat and oats, the coarse-grained model had the lowest NRMSE and hence was closest the measured values (most accurate).

  - When the new model was used, the coarse-grained model had a normalised root mean squared error (NRMSE) of 0.464, and the fine-grained model had a NRMSE of 0.399. This compared very favourably to an NRMSE of 21.500 seen with the past model by Crook and Ennos, (1993). The course-grained model was chosen as the new model for wheat root anchorage because the model represented the soil behaviour in the field without being changed to fit the measured data.

  - For oats, the highest accuracy of prediction was achieved for fine-grained soils having a NRMSE of 0.430 and 0.354 respectively, and again this compared very favourable with other models, e.g. NRMSE of 63.500 for the model by Crook and Ennos, (1993). The course-grained model was chosen as the new model for oat root anchorage for the same reasons as the wheat model.

  - For oilseed rape, the new model had a NRMSE of 0.283 meaning the values were close the measured values. More data are required to test the model, but initial results proved encouraging. However, it was found that the model developed by

Niklas, (1992) was still slightly more accurate having a NRMSE of 0.282. While this difference is not significant. The Niklas, (1992) model was easier to use based on the model inputs and thus is recommended for future use.

- The sensitivity analysis showed that the models for wheat and oats were most sensitive to the root length and root plate diameter, demonstrating the importance of these parameters. For oilseed rape, the root length was the most important factor. Field and laboratory data collected in 2018 were used to validate the proposed models, and it was found that the new models could predict the newly measured root anchorage for all plant crops tested addressing the fifth objective.

- The new model proposed in this research can be integrated into the lodging risk model by Baker et al. (2015) to improve the accuracy of the root anchorage predictions. A method to enable farmers to use existing information to populate the new model has been proposed.

5.2   Contributions to the field of root anchorage studies

The main contributions to the field of root anchorage in cereal crops from this research are:

- The accuracy of root anchorage modelling techniques in the literature have been collated, synthesised and tested.
- A methodology has been developed for collecting the data required to compare root failure moment models.
- A lodging machine has been development and constructed to record the load and deflection curves, instead of providing only root failure moment values. This allows anchorage resistance and rotation angle to now be measured in the laboratory and in the field.

- An improved understanding has been obtained of the effect of soil composition, root model flexibility and water content on root failure within models to enable better prediction of actual root failure to be made.

- A successful connection has been made between geotechnical failure mechanisms associated with laterally loaded piles, including under-reamed piles, and root lodging. From which better predictions of root anchorage failure were achieved for wheat and oats.

- Adapting the under-reamed pile model for coarse-grained and fine-grained soil to predict the root failure moment in wheat and oats showed that this was the model that could predict measured root anchorage based on the data collected as part of this research.

- It was demonstrated that the Niklas, (1992) model was the most accurate model for predicting measured values of oilseed rape root failure moment and it was also easy to use. More data are needed to fully demonstrate the model.

- It was demonstrated that the flexible under-reamed pile model for coarse-grained soils provides an alternative model to predict the root failure moment in oilseed rape.

5.3   Recommendations for Further Research

Although significant progress has been made as part of this research to better understand the root-soil interaction experienced during lodging of cereal crops, and a new model has been proposed which can substitute the existing model in the risk assessment of lodging, further work is still needed to validate some of the findings and extend these to additional data. These include:

- Collecting a more extensive dataset of soil characteristics and root measurements possibly using rapid phenotyping and characterisation of soils and roots on site. This can incorporate:
    - Monitoring root and soil changes over time and changes with field area, plant species and husbandry.

- o Completing matric suction-controlled shear box testing on agricultural soils
- o Incorporating soil water content changes and soil suction in areas with and without roots.
- o X-ray tomography and MRI scanning of root-soil cores that have and have not lodged.
- o Improving the root measurement methodology by measuring roots in situ.
- Testing and further developing the method for farmers suggested in Section 4.5.4 in order to evaluate the impact of using more generic data in the new root anchorage model rather than using site and plant specific information at a small scale.
- Further developing the laboratory experiment to include:
  - o Measuring the modulus of subgrade reaction for roots for use in the flexible pile model.
  - o Understanding the influence of lateral roots in root failure moments for oilseed rape and how this could be related to root strength.
  - o Carefully instrumenting the ground directly around roots attaching sensors to roots.

References

Abed, A. and Vermeer, P. (2006) 'Foundation analyses with unsaturated soil model for different suction profiles', [Online]. DOI: 10.1201/9781439833766.ch79.

Achim, A. and Nicoll, B. C. (2009) 'Modelling the anchorage of shallow-rooted trees', *Forestry*, vol. 82, no. 3, pp. 273–284 [Online]. DOI: 10.1093/forestry/cpp004.

AHDB (2015) 'AHDB Recommended Lists 2015 / 16 for cereals and oilseeds Using the AHDB Recommended Lists'.

Baker, C. J., Berry, P., Spink, J., Sylvester-Bradley, R., Griffin, J., Scott, R. and Clare, R. (1998) 'A method for the assessment of the risk of wheat lodging', *Journal of theoretical biology*, vol. 194, no. 4, pp. 587–603 [Online]. DOI: 10.1006/jtbi.1998.0778.

Baker, C. J. (1995) 'The development of a theoretical model for the windthrow of plants', *Journal of Theoretical Biology*, vol. 175, no. 3, pp. 355–372 [Online]. DOI: 10.1006/jtbi.1995.0147.

Baker, C. J., Sterling, M. and Berry, P. (2014) 'A generalised model of crop lodging', *Journal of Theoretical Biology*, vol. 363, pp. 1–12 [Online]. DOI: 10.1016/j.jtbi.2014.07.032.

Barboza, R., Souza, M. D., Junior, D., Iori, P., Alcivânia, F. and Silva, D. M. (2015) 'Prediction of soil shear strength in agricultural and natural environments of the Brazilian Cerrado', no. 1, pp. 82–91 [Online]. DOI: 10.1590/S0100-204X2015000100009.

Barnes, G. and Graham E. (2010) *Soil mechanics: principles and practice*, 4th Edition., Basingstoke, Palgrave Macmillan.

Berry, P. M., Kendall, S., Rutterford, Z., Orford, S. and Griffiths, S. (2015) 'Historical analysis of the effects of breeding on the height of winter wheat (Triticum aestivum) and consequences for lodging', *Euphytica* [Online]. Available at http://link.springer.com/article/10.1007/s10681-014-1286-y.

Berry, P. M., Griffin, J. M., Sylvester-Bradley, R., Scott, R. K., Spink, J. H., Baker, C. J. and Clare, R. W. (2000) 'Controlling plant form through husbandry to minimise lodging in wheat', *Field Crops Research*, vol. 67, no. 1, pp. 59–81 [Online]. DOI: 10.1016/S0378-4290(00)00084-8.

Berry, P. M., Spink, J. H., Gay, A. P. and Craigon, J. (2003a) 'A comparison of root and stem lodging risks among winter wheat cultivars', *The Journal of Agricultural Science*, vol. 141, no. 2, pp. 191–202 [Online]. DOI: 10.1017/S002185960300354X.

Berry, P. M., Spink, J., Sterling, M. and Pickett, A. A. (2003b) 'Methods for rapidly measuring the lodging resistance of wheat cultivars', *Journal of Agronomy and Crop Science*, vol. 189, pp. 390–401 [Online]. DOI: 10.1046/j.0931-2250.2003.00062.x.

Berry, P. M., Sterling, M., Baker, C. J., Spink, J. H. and Sparkes, D. L. (2003c) 'A calibrated model of wheat lodging compared with field measurements', *Agricultural and Forest Meteorology*, vol. 119, no. 3–4, pp. 167–180 [Online]. DOI: 10.1016/S0168-1923(03)00139-4.

Berry, P. M., Sterling, M. and Mooney, S. J. (2006) 'Modelling / Site Specific Analysis / Biometrics / Technologies Development of a Model of Lodging for Barley', vol. 158, pp. 151–158.

Berry, P. M., Sterling, M. and Mooney, S. J. (2006) 'Development of a Model of Lodging for Barley', *Journal of Agronomy and Crop Science*, vol. 192, no. 2, pp. 151–158 [Online]. DOI: 10.1111/j.1439-037X.2006.00194.x.

Berry, P. M., Sterling, M., Spink, J. H., Baker, C. J., Sylvester-Bradley, R., Mooney, S. J., Tams, A. R. and Ennos, A. R. (2004) 'Understanding and Reducing Lodging in Cereals', *Advances in Agronomy*, vol. 84, pp. 217–221 [Online]. DOI: 10.1016/S0065-2113(04)84005-7.

Berry, P. M., White, C., Sterling, M. and Baker, C. J. (2013) 'Develop a model of lodging risk in oilseed rape to enable integrated lodging control to reduce PGR use', CRD Project PS2146.

Berry, P. M. (1998) 'Predicting lodging in winter wheat', PhD Thesis, University of Nottingham.

Blackwell, P. G., Rennolls, K. and Coutts, M. P. (1990) 'A Root Anchorage Model for Shallowly Rooted Sitka Spruce', *Forestry*, vol. 63, no. 1 [Online]. DOI: 10.1093/forestry/63.1.73.

Brinch-Hansen J. (1961) 'The Ultimate Resistance of Rigid Piles against Transversal Forces', *Geoteknisk Instit., Bull.* [Online]. Available at https://ci.nii.ac.jp/naid/10016214495/.

British Standards Institute (2016) 'Methods of Testing for Soils for Engineering Purposes', in *BS 1377*, British Standards Institute.

Broms, B. (1964a) 'Lateral resistance of piles in cohesive soils', Journal of the Soil Mechanics and Foundation Division, vol. 90(2), pp. 27–64.

Broms, B. (1964b) 'Lateral resistance of piles in cohesionless soils', Journal of Soil Mechanics and Foundations Division, vol. 90(3), pp. 123–158.

Casada, J. H., Walton, L. R. and Swetnam, L. D. (1980) 'Wind Resistance of Burley Tobacco as Influenced by Depth of Plants in Soil', *Transactions of the ASAE*, vol. 23, no. 4, pp. 1009–1011 [Online]. DOI: 10.13031/2013.34706.

Coder, K. (2010) *Root Strength and Tree Anchorage*, vol. 7912.

Cohen, D., Schwarz, M. and Or, D. (2011) 'An analytical fiber bundle model for pullout mechanics of root bundles', *Journal of Geophysical Research: Earth Surface*, vol. 116, no. 3, pp. 1–20 [Online]. DOI: 10.1029/2010JF001886.

Coutts, M. P. (1986) 'Components of tree stability in sitka spruce on peaty gley soil', *Forestry*, vol. 59, no. 2, pp. 173–197 [Online]. DOI: 10.1093/forestry/59.2.173.

Coutts, M. P., Nielsen, C. C. N. and Nicoll, B. C. (1999) 'The development of symmetry, rigidity and anchorage in the structural root system of conifers', *Plant and soil*, vol. 217, no. 1–2, pp. 1–15 [Online]. DOI: 10.1023/A:1004578032481.

Crook, M. J. and Ennos, A. R. (1993) 'The Mechanics of Root Lodging in Winter-Wheat, Triticum-Aestivum L', *Journal of Experimental Botany*, vol. 44, no. 264, pp. 1219–1224.

Crook, M. J. and Ennos, A. R. (1994) 'Stem and root characteristics associated with lodging resistance in four winter wheat cultivars', *The Journal of Agricultural Science*, vol. 123, no. 02, p. 167 [Online]. DOI: 10.1017/S0021859600068428.

Crook, M. J. and Ennos, A. R. (1996) 'The anchorage mechanics of deep rooted larch, Larix europea × L. japonica', *Journal of Experimental Botany*, vol. 47, no. 10, pp. 1509–1517 [Online]. DOI: 10.1093/jxb/47.10.1509.

Das, B. M. (2011) *Principles of foundation engineering*, Cengage Learning.

Dexter, A. R. and Birkas, M. (2004) 'Prediction of the soil structures produced by tillage', *Soil and Tillage Research*, vol. 79, no. 2, pp. 233–238 [Online]. DOI: 10.1016/J.STILL.2004.07.011.

Dong, Y., McCartney, J. S. and Lu, N. (2015) 'Critical Review of Thermal Conductivity Models for Unsaturated Soils', *Geotechnical and Geological Engineering*, vol. 33, no. 2, pp. 207–221 [Online]. DOI: 10.1007/s10706-015-9843-2.

Dupuy, L., Fourcaud, T., Lac, P. and Stokes, A. (2007) 'A Generic 3D Finite Element Model of Tree Anchorage Integrating Soil Mechanics and Real Root System Architecture', vol. 94, no. 9, pp. 1506–1514.

Dupuy, L., Fourcaud, T. and Stokes, A. (2005) 'A numerical investigation into factors affecting the anchorage of roots in tension', *European Journal of Soil Science*, vol. 56, no. 3, pp. 319–327 [Online]. DOI: 10.1111/j.1365-2389.2004.00666.x.

Dupuy, L., Fourcaud, T. and Stokes, A. (2005) 'A numerical investigation into the influence of soil type and root architecture on tree anchorage', *Plant and Soil*, vol. 278, no. 1–2, pp. 119–134 [Online]. DOI: 10.1007/s11104-005-7577-2.

Easson, D. L., White, E. M. and Pickles, S. J. (1992) *Project Report No. 52: A Study of Lodging in Cereals*, HGCA.

Ennos, A. R. (1990) 'The Anchorage of Leek Seedlings: The Effect of Root Length and Soil Strength', *Annals of Botany*, vol. 65, no. 4, pp. 409 –416.

Ennos, A. R. (1991) 'The mechanics of anchorage in wheat Triticum aestivum L.: II. Anchorage of mature wheat against lodging', *Journal of Experimental Botany*, vol. 42, no. 12, pp. 1607–1613 [Online]. DOI: 10.1093/jxb/42.12.1607.

Ennos, A. R., Crook, M. J and Grimshaw, C. (1993a) 'A Comparative Study of the Anchorage Systems of Himalayan Balsam Impatiens glandulifera and Mature Sunflower Helianthus annuus', *Journal of experimental botany*, vol. 44, no. 1, pp. 133–146 [Online]. DOI: 10.1093/jxb/44.1.133.

Ennos, A. R., Crook, M. J. and Grimshaw, C. (1993b) 'The Anchorage Mechanics of Maize, Zea mays', *Journal of Experimental Botany*, vol. 44, no. 1, pp. 147–153 [Online]. DOI: 10.1093/jxb/44.1.147.

Environmental Protection Agency (2014) *Irish Soil Information System*, [Online]. Available at http://gis.teagasc.ie/soils/ (Accessed 27 June 2016).

European Union (1991) *Official Journal of the European Communities*, European Union [Online]. Available at https://eur-lex.europa.eu/legal-content/EN/TXT/PDF/?uri=CELEX:31991L0414&from=EN.

Farquhar, T. and Meyer-Phillips, H. (2001) 'Relative safety factors against global buckling, anchorage rotation, and tissue rupture in wheat.', *Journal of theoretical biology*, vol. 211, no. 1, pp. 55–65 [Online]. DOI: 10.1006/jtbi.2001.2330.

Fern, J., Soga, K. and Robert, D. (2014) 'Shear strength and dilatancy of partially saturated sand in direct shear tests', in *Geomechanics from Micro to Macro*, CRC Press, pp. 1391–1396 [Online]. DOI: 10.1201/b17395-252.

Fleming, W. G. K. (2009) *Piling engineering*, Taylor & Francis.

Fourcaud, T., Ji, J.-N. N., Zhang, Z.-Q. Q. and Stokes, A. (2008) 'Understanding the impact of root morphology on overturning mechanisms: a modelling approach', *Annals of botany*, vol. 101, no. 8, pp. 1267–1280 [Online]. DOI: 10.1093/aob/mcm245.

Fraser, A. I. (1962) 'The Soil and Roots as Factors in Tree Stability', *Forestry*, vol. 34, no. 2, pp. 117–127 [Online]. DOI: 10.1093/forestry/34.2.117.

Fraser, A. I. (1964) 'Wind tunnel and other related studies on coniferous trees and tree crops', *Scottish Forestry*, vol. 22, pp. 23–30.

Fraser, A. I. (1965) 'The uncertainties of wind-damage in forest management', *Irish Forestry*, vol. 22, pp. 23–30.

Fraser, A. I. and Gardiner, J. (1967) 'Rooting and stability in Sitka spruce', *Forest Comm. Bull.*, vol. 40, p. 28.

Fredlund, D. G. and Xing, A. (1994) 'Equations for the soil-water characteristic curve', *Canadian Geotechnical Journal*, vol. 31, no. 3, pp. 521–532.

Gance, D. (2015) 'Development of a root-soil interaction model, analysing root lodging of agricultural crops', Master's Dissertation, University of Birmingham.

Garthwaite, D. (1995) *Pesticide usage survey report 127: arable farm crops in Great Britain 1994.*, London, M.A.F.F.

Goodman, A. M., Crook, M. J. and Ennos, A. R. (2001) 'Anchorage Mechanics of the Tap Root System of Winter-sown Oilseed Rape (Brassica napus L.)', *Annals of Botany*, vol. 87, no. 3, pp. 397–404 [Online]. DOI: 10.1006/anbo.2000.1347.

Gorelick, N., Hancher, M., Dixon, M., (2017) 'Google Earth Engine: Planetary-scale geospatial analysis for everyone', *Elsevier* [Online]. Available at https://www.sciencedirect.com/science/article/pii/S0034425717302900.

Graham, J.A., (1983). Crop lodging in British wheats and barleys, PhD Thesis, The University of Reading.

Griffin, J. M. (1998) 'Understanding and Assessing Lodging', PhD Thesis, The University of Nottingham.

Guerif J. (1990) 'Factors influencing compaction induced increases in soil strength.', *Soil Tillage Research*, vol. 16, pp. 167–178.

Guerif, J., Soane, B. D. and Van Ouwerkerk, C. (1995) 'Effects of compaction on soil strength parameters', *International Journal of Rock Mechanics and Mining Sciences and Geomechanics Abstracts*, vol. 5, no. 32, p. 214A.

Han, Z. and Vanapalli, S. K. (2016) 'Stiffness and shear strength of unsaturated soils in relation to soil-water characteristic curve', *Géotechnique*, vol. 66, no. 8, pp. 627–647 [Online]. DOI: 10.1680/jgeot.15.P.104.

Johnson, K., Lemcke, P., Karunasena, W. and Sivakugan, N. (2006) 'Modelling the load–deformation response of deep foundations under oblique loading', *Environmental Modelling & Software*, vol. 21, no. 9, pp. 1375–1380 [Online]. DOI: 10.1016/J.ENVSOFT.2005.04.015.

Keogh, L., Hanlon, P. O., Reilly, P. O. and Taylor, D. (2015) 'Fatigue in bamboo', *International Journal of Fatigue*, vol. 75, pp. 51–56 [Online]. DOI: 10.1016/j.ijfatigue.2015.02.003.

Knappett, Jonathan. and Craig, R. F. (2012) *Craig's soil mechanics*, Spon Press.

Laman, M. (2011) *Lateral Resistance of A Short Rigid Pile In A Two-Layer Cohesionless Soil*, [Online]. Available at http://www.fg.uni-mb.si/journal-ags/pdfs/AGS_2011-2_article_2.pdf.

Liang, T. and Knappett, J. (2013) 'Scale modelling of plant root systems using 3-D printing', *Proceedings of the 6th International Conference on Physical Modelling in Geotechnics-Physical Modelling in Geotechnics-6th ICPMG'06*, vol. 1, pp. 361–366.

Liang, T., Knappett, J. A., Bengough, A. G. and Ke, Y. X. (2017) 'Small-scale modelling of plant root systems using 3D printing, with applications to investigate the role of vegetation on earthquake-induced landslides', *Landslides*, vol. 14, no. 5, pp. 1747–1765 [Online]. DOI: 10.1007/s10346-017-0802-2.

Lu, N. and Likos, W. (2004) *Unsaturated Soil Mechanics*, John Wiley & Sons [Online]. Available at https://www.wiley.com/en-us/Unsaturated+Soil+Mechanics-p-9780471447313.

Lynch, J. (1995) *Root Architecture and Plant Productivity'*, [Online]. Available at https://www.ncbi.nlm.nih.gov/pmc/articles/PMC157559/pdf/1090007.pdf.

MAFF (1982) 'Visual assessment of soil structure', in *Reference Book 441*, London, HMSO.

Martinez-Vazquez, P. and Sterling, M. (2011) 'Predicting wheat lodging at large scales', *Biosystems Engineering*, vol. 109, no. 4, pp. 326–337 [Online]. DOI: 10.1016/j.biosystemseng.2011.04.012.

Matlock, H. and Reese, L.C., (1962). 'Generalized solutions for laterally loaded piles'. *Transactions of the American Society of Civil Engineers*, 127(1), pp.1220-1247.

Mayhead (1973) 'Some drag coefficients for British forest trees derived from wind tunnel studies', *Agricultural Meterology*, vol. 12, pp. 123–130.

Mayhead, G., Gardiner, J. and Durant, D. (1975) 'A report on the physical properties of conifers in relation to plantation stability', *For. Comm. Res. Dev.Div*, p. 38.

Merotto, a and Mundstock, C. (1999) 'Wheat root growth as affected by soil strength', *Revista Brasileira de Ciência do Solo*, no. 1, pp. 197–202.

Mickovski, S. B. (2002) 'Anchorage mechanics of different types of root systems', *Architecture*.

Mickovski, S. B., Bransby, M. F., Bengough, a. G., Davies, M. C. R. and Hallett, P. D. (2010) 'Resistance of simple plant root systems to uplift loads', *Canadian Geotechnical Journal*, vol. 47, no. 1, pp. 78–95 [Online]. DOI: 10.1139/T09-076.

Moore, J. R. (2000) 'Differences in maximum resistive bending moments of Pinus radiata trees grown on a range of soil types', *Forest Ecology and Management*, vol. 135, no. 1–3, pp. 63–71 [Online]. DOI: 10.1016/S0378-1127(00)00298-X.

Nik N. D., Ru Hui, K. and Azmi Juliana, A. G. (2016) 'The Effect of Soil Particle Arrangement on Shear Strength Behavior of Silty Sand', Abd Rahman, N., Mohd Jaini, Z., Yunus, R., and Rahmat, S. N. (eds), *MATEC Web of Conferences*, vol. 47, p. 03022 [Online]. DOI: 10.1051/matecconf/20164703022.

Niklas, K. J. (1992) *Plant Biomechanics: An Engineering Approach to Plant Form and Function*, University of Chicago Press.

Norfolk Agricultural Station (1976) *68th Annual Report*, pp. 14-17.

Oladokun, M. A. O. and Ennos, A. R. (2006) 'Structural development and stability of rice Oryza sativa L. var. Nerica 1', *Journal of Experimental Botany* [Online]. DOI: 10.1093/jxb/erl074.

Oram, B. (2014) *A Brief Explanation on Well Water Quality Groundwater Flow Systems* [Online]. Available at https://water-research.net/index.php/water-testing/groundwater-testing/groundwater-hydrogeology (Accessed 5 September 2019).

Peltola, H. and Kellomäki, S. (1993) 'A mechanistic model for calculating windthrow and stem breakage of Scots pines at stand age.', [Online]. Available at https://helda.helsinki.fi/bitstream/handle/10138/15665/27-No 2_Peltola1.pdf?sequence=1.

Pinthus, M. J. (1967) 'Spread of the Root System as Indicator for Evaluating Lodging Resistance of Wheat1', *Crop Science*, vol. 7, no. 2, p. 107 [Online]. DOI: 10.2135/cropsci1967.0011183X000700020005x.

Pinthus, M. J. (1974) 'Lodging in Wheat, Barley, and Oats: The Phenomenon, its Causes, and Preventive Measures', *Advances in Agronomy*, vol. 25, pp. 209–263 [Online]. DOI: 10.1016/S0065-2113(08)60782-8.

Prakash and Ramakrishna (2004) 'Lateral Load Capacity of Under-reamed piles - An analytical Approach', *Soils and Foundations*, vol. 44, no. 5, pp. 51–65.

Prasad, Y. and Chari, T. (1999) 'Lateral capacity of model rigid piles in cohesionless soils', *jstage.jst.go.jp*, vol. 39, no. 2, pp. 21–29.

Hackett, R. (2018) 'A comparison of husked and naked oats under Irish conditions', *Irish Journal of Agricultural and Food Research*, vol. 58, pp. 1–8 [Online]. DOI: 10.1515/ijafr-2018-0001.

Rahardjo, H., Harnas, F. R., Leong, E. C., Tan, P. Y., Fong, Y. K. and Sim, E. K. (2009) 'Tree stability in an improved soil to withstand wind loading', *Urban Forestry & Urban Greening*, vol. 8, pp. 237–247 [Online]. DOI: 10.1016/j.ufug.2009.07.001.

Rosemaund, A., Wynne, P. and Hr, H. (2003) 'A comparison of root and stem lodging risks among winter wheat cultivars', pp. 191–202 [Online]. DOI: 10.1017/S002185960300354X.

Schutten, J., Dainty, J. and Davy, A. J. (2005) 'Root anchorage and its significance for submerged plants in shallow lakes', *Journal of Ecology*, vol. 93, no. 3, pp. 556–571 [Online]. DOI: 10.1111/j.1365-2745.2005.00980.x.

Sposaro, M. M., Berry, P. M., Sterling, M., Hall, A. J. and Chimenti, C. A. (2010) 'Modelling root and stem lodging in sunflower', *Field Crops Research* [Online]. DOI: 10.1016/j.fcr.2010.06.021.

Sterling, M., Baker, C. J., Berry, P. M. and Wade, A. (2003) 'An experimental investigation of the lodging of wheat', *Agricultural and Forest Meteorology* [Online]. DOI: 10.1016/S0168-1923(03)00140-0.

Stokes, A. (2002) 'Biomechanics of Tree Root Anchorage', in *Plant Roots*, CRC Press, pp. 175–186 [Online]. DOI: 10.1201/9780203909423.ch10.

Stokes, A. and Mattheck, C. (2007) 'Variation of wood strength in tree roots', *Journal of Experimental Botany*, vol. 47, no. 5, pp. 693–699 [Online]. DOI: 10.1093/jxb/47.5.693.

Tams, A. R., Mooney, S. J. and Berry, P. M. (2004) 'The effect of lodging in cereals on morphological properties of the Root-Soil Complex', *Super soil 2004 3rd Aust. New*.

Tanaka, N., Samarakoon, M. B. and Yagisawa, J. (2012) 'Effects of root architecture, physical tree characteristics, and soil shear strength on maximum resistive bending moment for

overturning Salix babylonica and Juglans ailanthifolia', *Landscape and Ecological Engineering*, vol. 8, no. 1, pp. 69–79 [Online]. DOI: 10.1007/s11355-011-0151-6.

Twarakavi, N. K. C., Sakai, M. and Šimůnek, J. (2009) 'An objective analysis of the dynamic nature of field capacity', *Water Resources Research*, vol. 45, no. 10, pp. 1–9 [Online]. DOI: 10.1029/2009WR007944.

UMS GmbH (2015) *Operation Manual HYPROP*, [Online]. Available at http://www.ums-muc.de/static/Manual_HYPROP-FIT.pdf.

Yan, W. M., Zhang, L., Leung, F. T. Y. and Yuen, K. V. (2016) 'Prediction of the root anchorage of native young plants using Bayesian inference', *Urban Forestry and Urban Greening*, vol. 19, pp. 237–252 [Online]. DOI: 10.1016/j.ufug.2016.06.027.

YARA International ASA (2019) *Wheat growth and development | Yara UK*, [Online]. Available at https://www.yara.co.uk/crop-nutrition/wheat/wheat-growth-and-development/ (Accessed 6 April 2019).

Zhang, L., Silva, F. and Grismala, R. (2005) 'Ultimate Lateral Resistance to Piles in Cohesionless Soils', *Journal of Geotechnical and Geoenvironmental Engineering*, vol. 131, no. 1, pp. 78–83 [Online]. DOI: 10.1061/(ASCE)1090-0241(2005)131:1(78).

Zhang, N. and Wang, Z. (2017) 'Review of soil thermal conductivity and predictive models', *International Journal of Thermal Sciences*, vol. 117, pp. 172–183 [Online]. DOI: 10.1016/j.ijthermalsci.2017.03.013.

Appendices

A.1 Preliminary shear box testing

y = 0.7685x - 2.4099
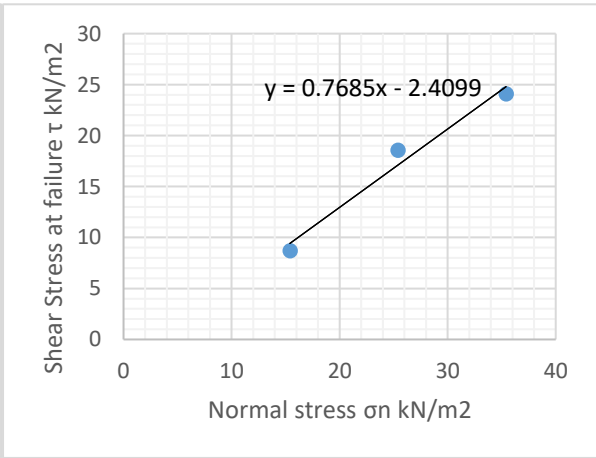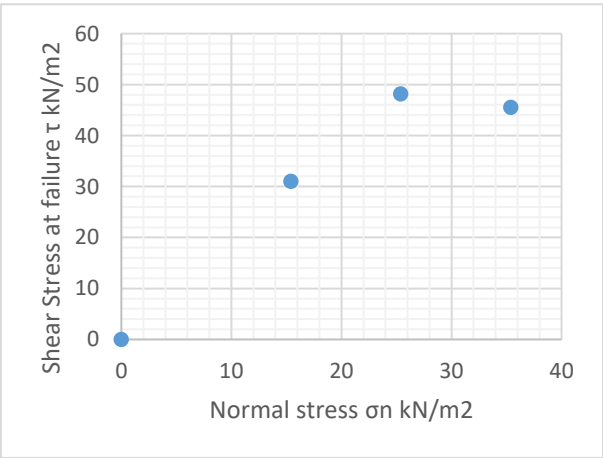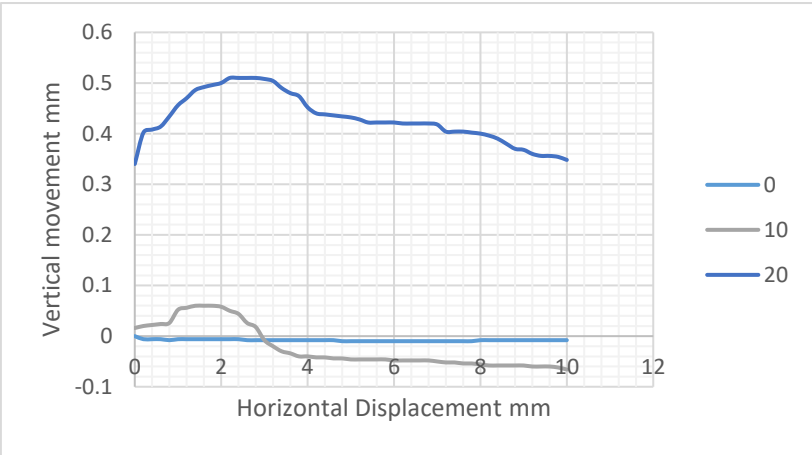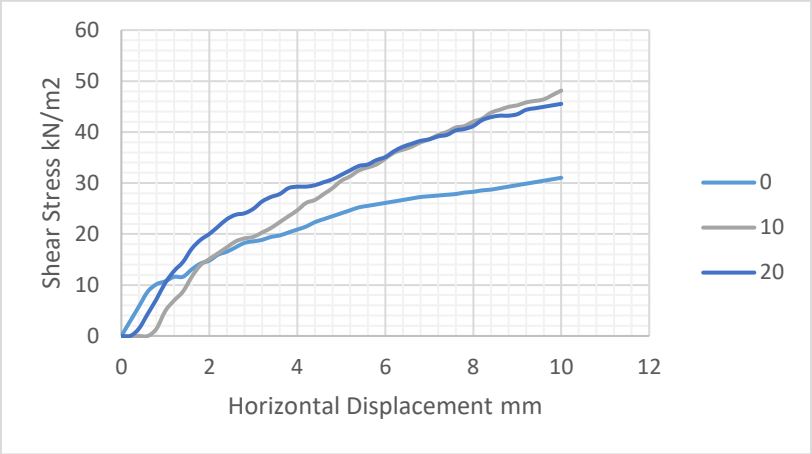
W1, water content, 17.3%, rate of testing = 1mm/min

y = 1.4442x - 1.3259

y = 1.653x - 32.619
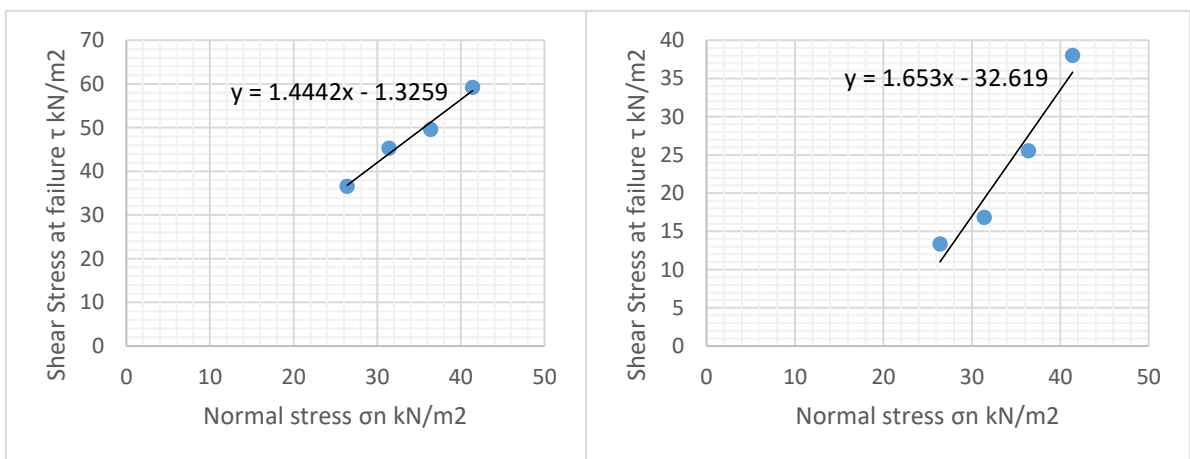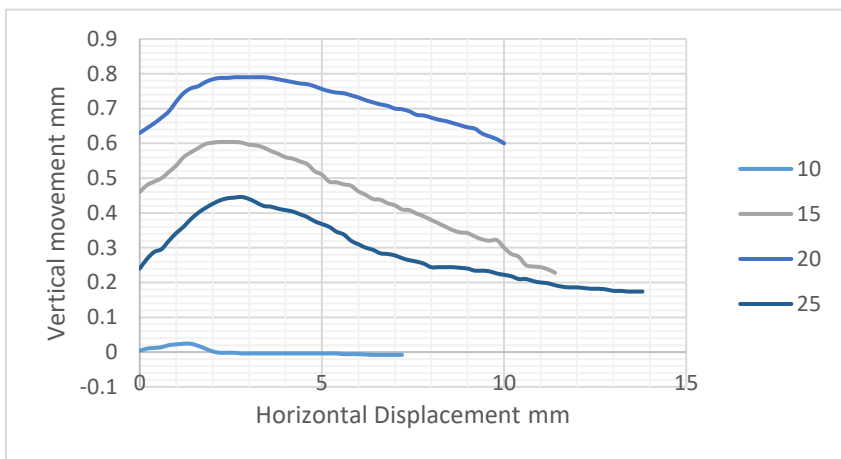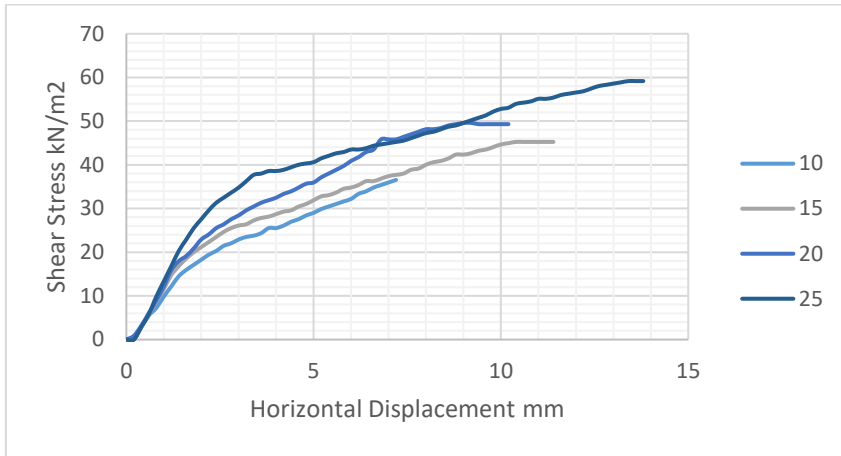
W1, water content, 17.3%, rate of testing = 0.5mm/min

284
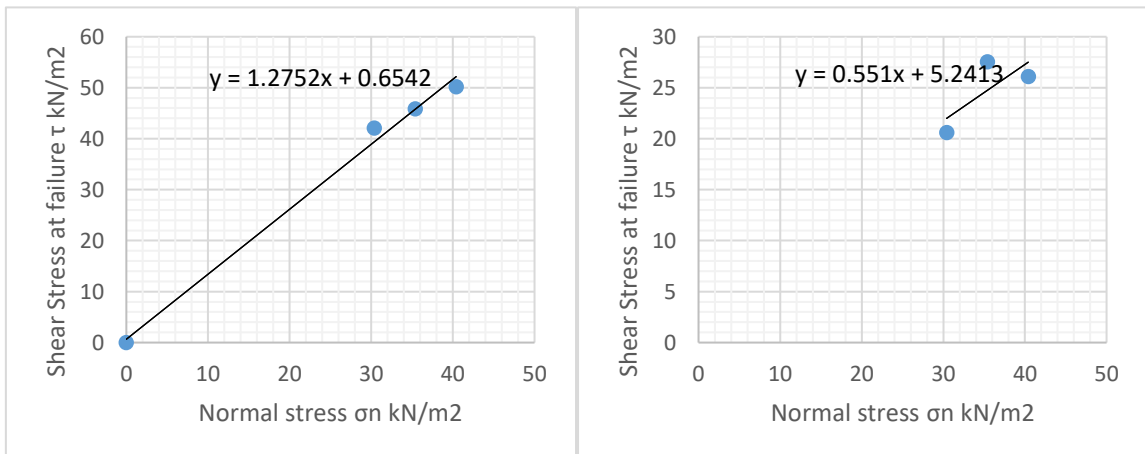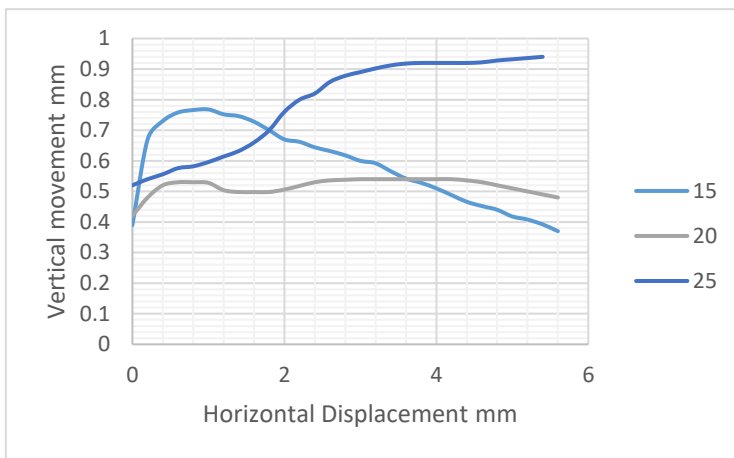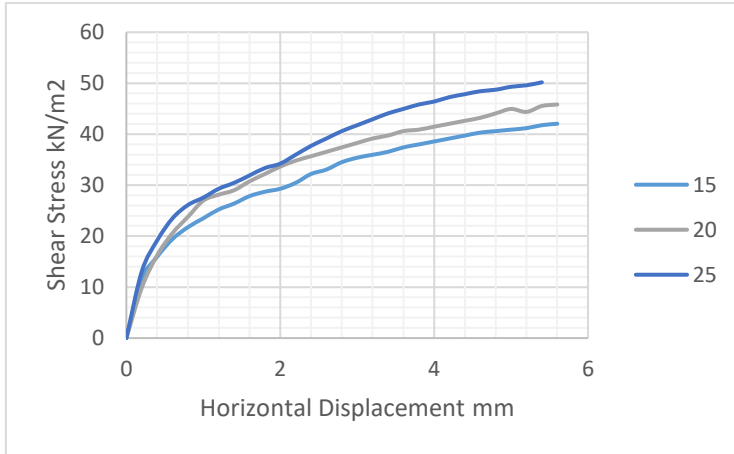
KB, water content 18%, rate of testing 2mm/min

B.1 Shear box testing for Soil sample W2 and O2 from the 2017 soil sampling.
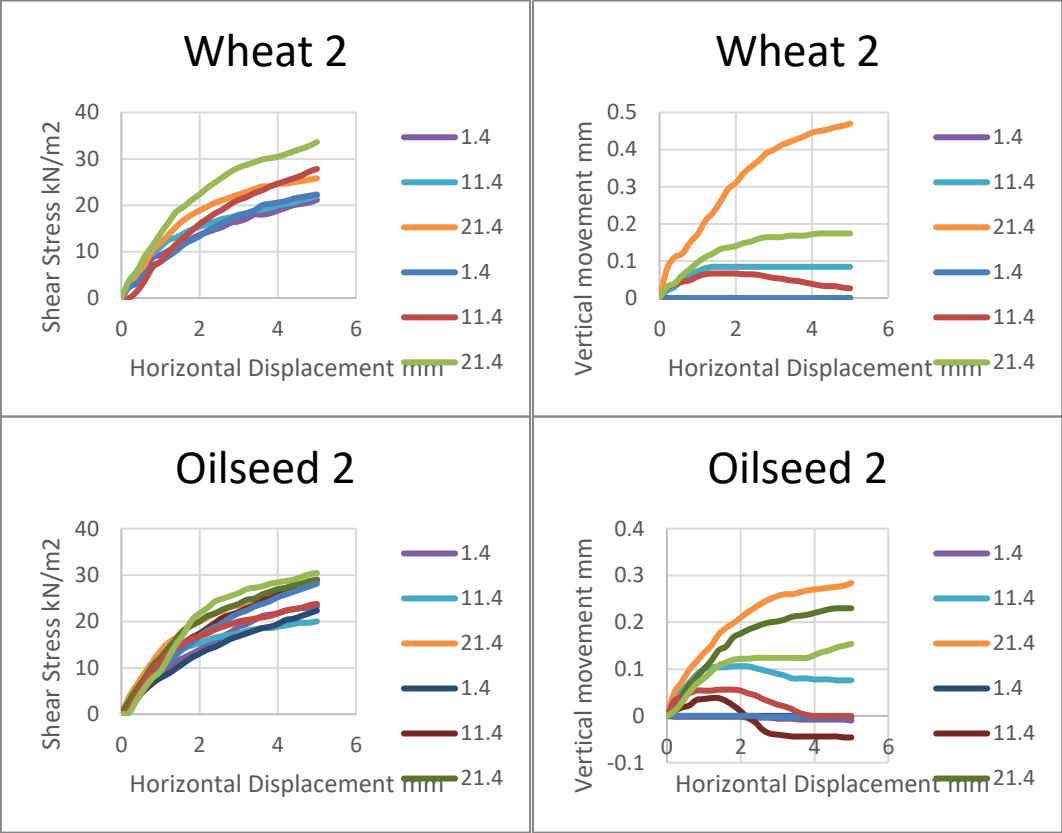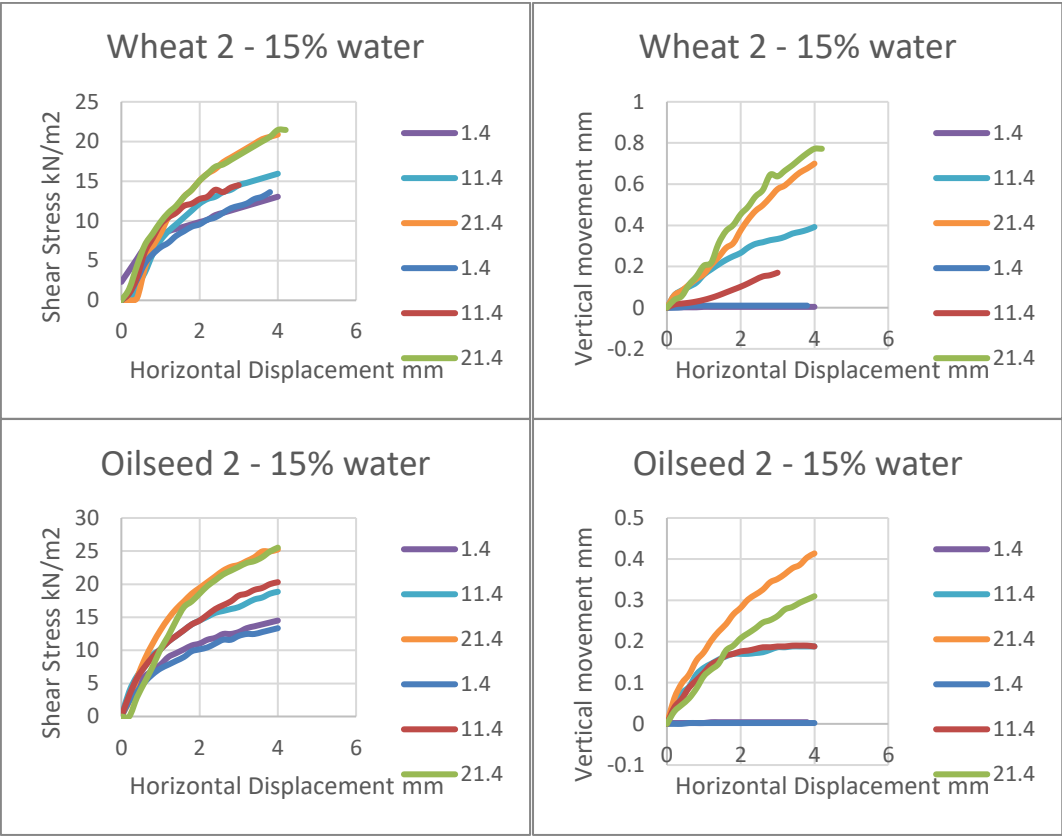
Figure Shear box results for repeated soil samples
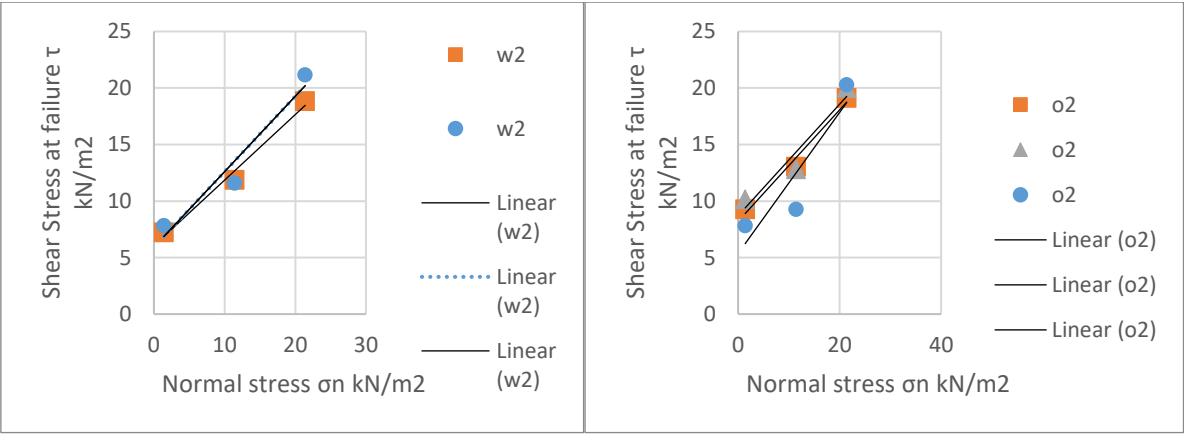
Figure 10% water content
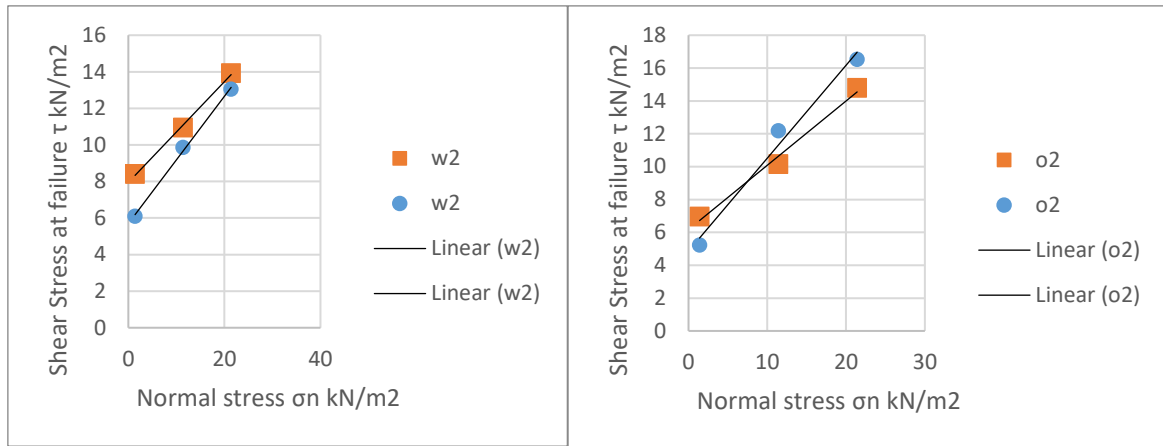
Figure 15% water content

C.1 Arduino code to run the new lodging instrument created during this research.

```
#include "I2Cdev.h"
#include "MPU6050.h"
#if I2CDEV_IMPLEMENTATION == I2CDEV_ARDUINO_WIRE
    #include "Wire.h"
#endif
#include <Servo.h>
#define OUTPUT_READABLE_ACCELGYRO
#include "HX711.h"
#define calibration_factor -454000
#define DOUT  5
#define CLK  4
MPU6050 accelgyro;
int16_t ax, ay, az;
int16_t gx, gy, gz;
HX711 scale(DOUT, CLK);
Servo myservo;
int var = 0;

void setup() {
// join I2C bus (I2Cdev library doesn't do this automatically)
    #if I2CDEV_IMPLEMENTATION == I2CDEV_ARDUINO_WIRE
        Wire.begin();
    #elif I2CDEV_IMPLEMENTATION == I2CDEV_BUILTIN_FASTWIRE
        Fastwire::setup(400, true);
    #endif

    Serial.begin(9600);

  myservo.attach(9);  // attaches the servo on pin 9 to the servo object
  //Serial.begin(9600);
  Serial.print("ResistanceNm,TimeMillis,ServoAngle,ax,ay,az,gx,gy,gz"); //removed strain readings
```

288

```
  Serial.println();
  scale.set_scale(calibration_factor);
  scale.tare();
}

void loop() {

  while (var < 1){
   for (int i = 98; i >= 0; i -= 1){  // goes from 98 degrees to 0 degrees // in steps of 1 degree
   myservo.write(i);            // tell servo to go to position in variable 'pos'
   Serial.print(scale.get_units(), 6); Serial.print(',');
   Serial.print(millis());Serial.print(',');
   Serial.print(myservo.read());Serial.print(',');

   accelgyro.getMotion6(&ax, &ay, &az, &gx, &gy, &gz);
   #ifdef OUTPUT_READABLE_ACCELGYRO
      Serial.print(ax); Serial.print(',');
      Serial.print(ay); Serial.print(',');
      Serial.print(az); Serial.print(',');
      Serial.print(gx); Serial.print(',');
      Serial.print(gy); Serial.print(',');
      Serial.println(gz);
   #endif
   delay(1);
   }
  myservo.write(98);
  var++;
  }
}
```

D.1Shear box testing for laboratory tests

Sand 1

Sand 1

Sand 1 (10%)

Sand 1 (10%)

Sand 2 — Shear Stress kN/m2 vs Horizontal Displacement mm (series 1.4, 11.4, 21.4)

Sand 2 — Vertical movement mm vs Horizontal Displacement mm (series 1.4, 11.4, 21.4)

Sand 2 (10%) — Shear Stress kN/m2 vs Horizontal Displacement mm (series 1.4, 11.4, 21.4)

Sand 2 (10%) — Vertical movement mm vs Horizontal Displacement mm (series 1.4, 11.4, 21.4)

Mix 1 (water content 10%) — Shear Stress kN/m2 vs Horizontal Displacement mm (series 1.4, 11.4, 21.4)

Mix 1 (water content 10%) — Vertical movement mm vs Horizontal Displacement mm (series 1.4, 11.4, 21.4)

Mix 1 (water content 15%)

Mix 2 (water content 10%)

Mix 3 (water content 10%)

Mix 2 (water content 15%) — Shear Stress kN/m2 vs Horizontal Displacement mm

Mix 2 (water content 15%) — Vertical movement mm vs Horizontal Displacement mm

Mix 3 (water content 15%) — Shear Stress kN/m2 vs Horizontal Displacement mm

Mix 3 (water content 15%) — Vertical movement mm vs Horizontal Displacement mm

Hereford — Shear Stress kN/m2 vs Horizontal Displacement mm

Hereford — Vertical movement mm vs Horizontal Displacement mm

293

E.1 Pictures of the depth tests completed on the rigid and flexible oilseed rape models.

7cm depth, rigid oilseed rape model, coarse sand.

10cm depth, rigid oilseed rape model, coarse sand
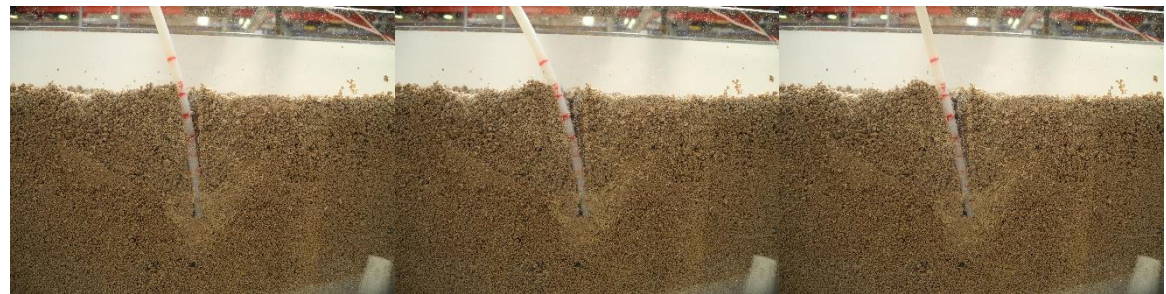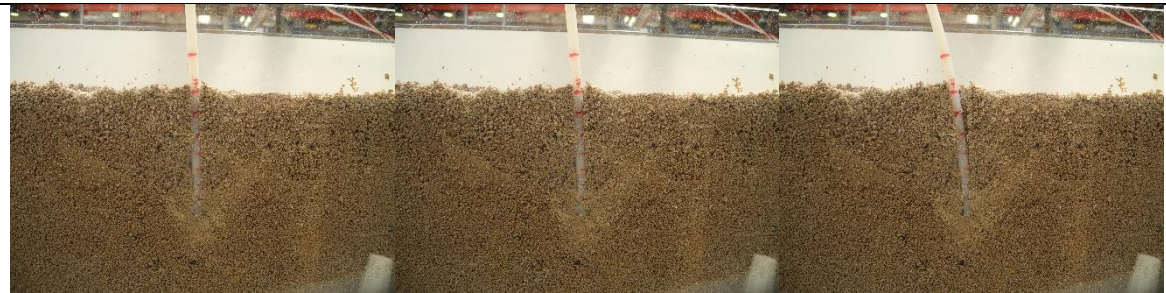
7cm, flexible oilseed rape model, Silt mix 3

6cm, flexible oilseed rape model, Silt mix 3
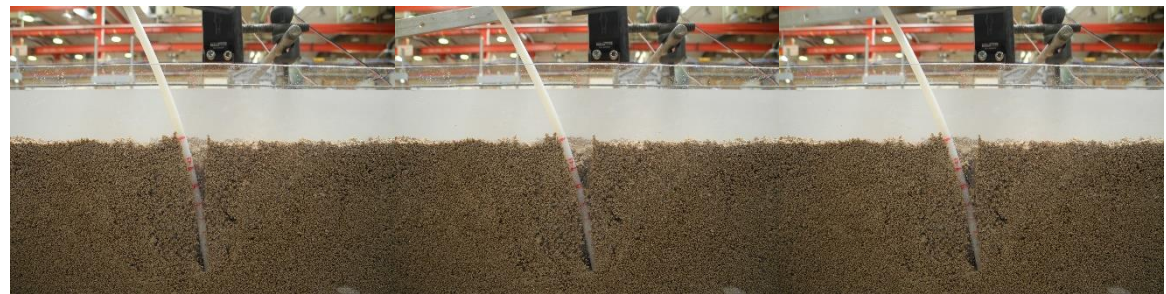
10cm, flexible oilseed rape model, Silt mix 3

7cm, rigid oilseed rape model, Silt mix 3
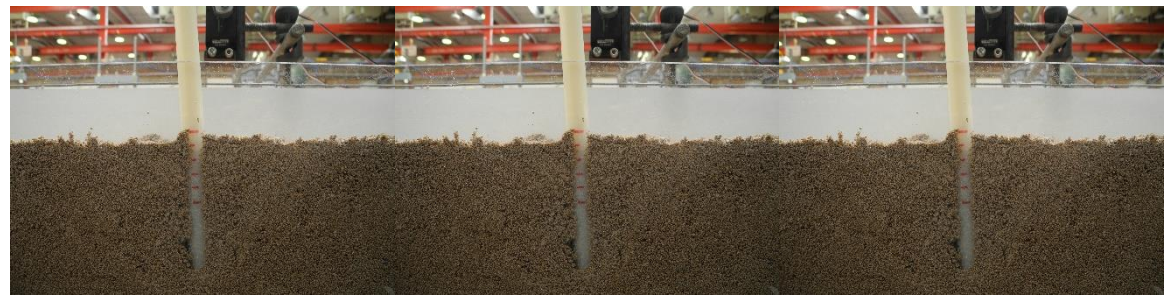
10cm, rigid oilseed rape model, Silt mix 3

F.1 Results for Sand 2, oilseed models (a) flexible, (b) rigid.
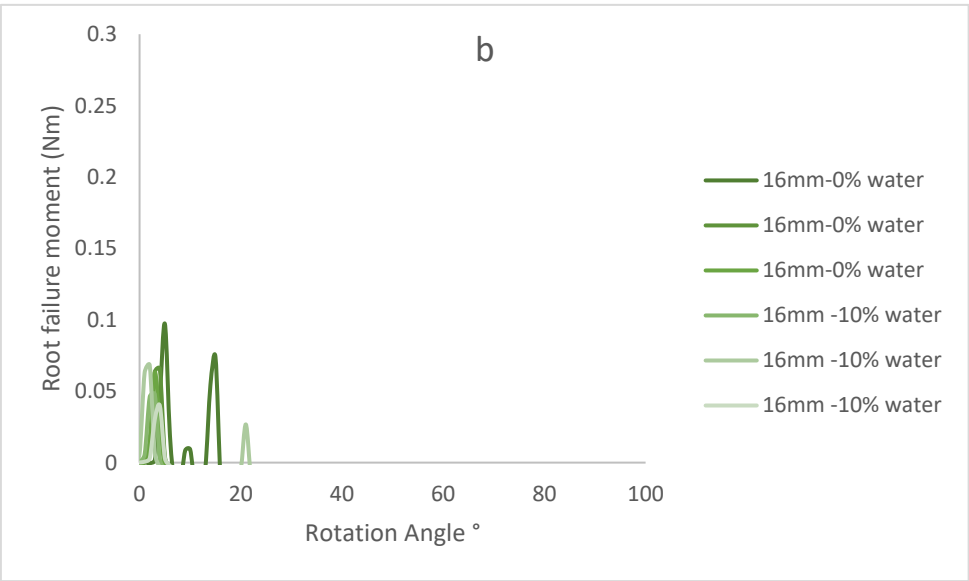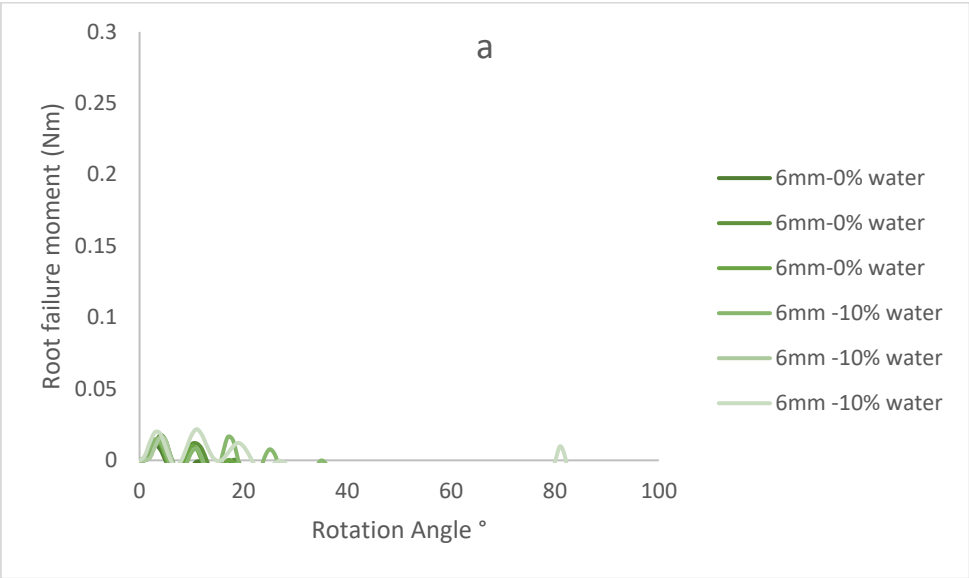
G.1 Results for Silt mix 2, oilseed models (a) flexible, (b) rigid.
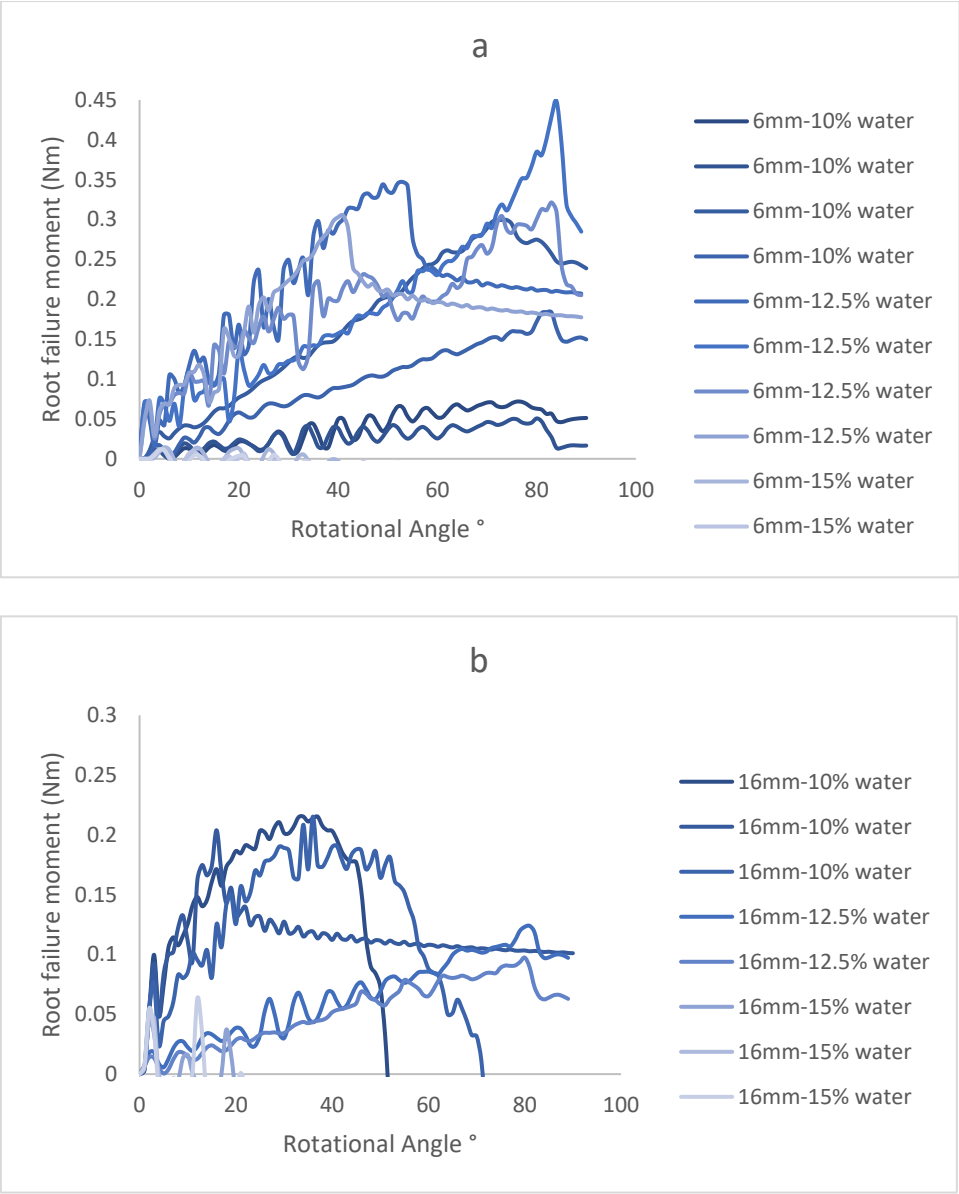
H.1 Results for Silt mix 2, wheat models (a) rigid, (b) flexible.

a

b
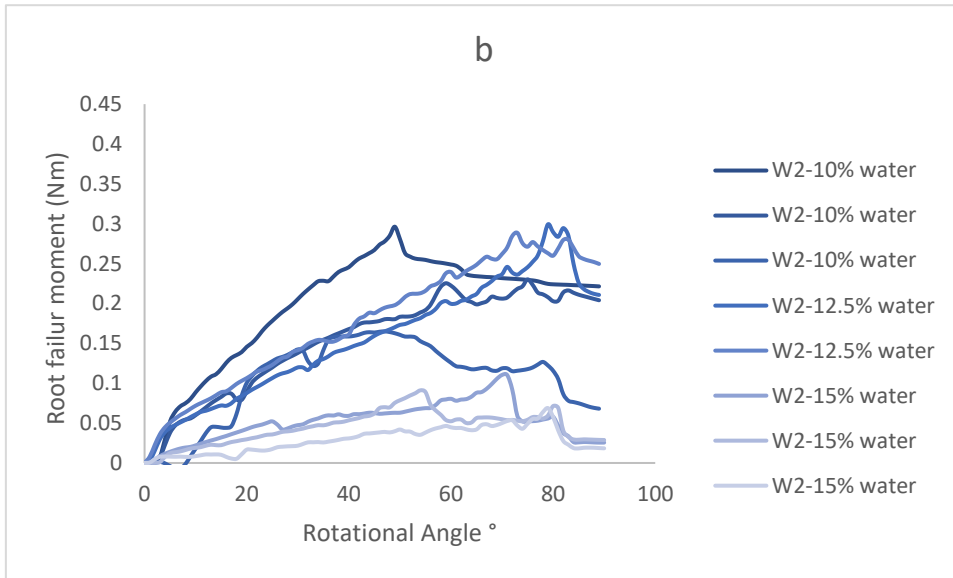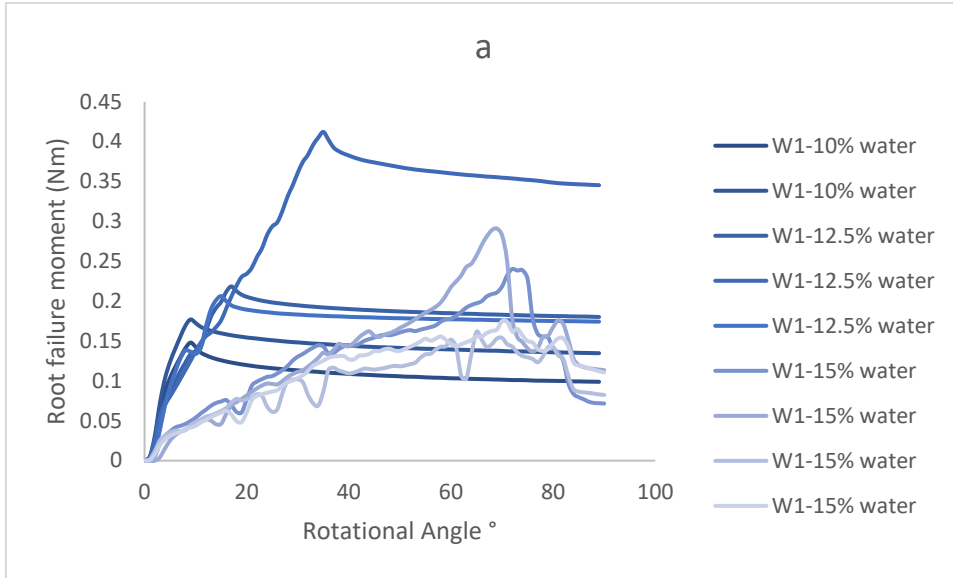
I.1 Statistical equations used in the model comparisons

The equation for the sample variance:

$$\sigma^2 = \frac{(x - \mu)^2}{n - 1}$$

3.1

Where, σ^2 is the sample variance, x is the data point, μ is the mean of the data points, and n is the number of data points.

The equation for the standard deviation, σ:

$$\sigma = \sqrt{\frac{\sum(x - \mu)^2}{n - 1}} \qquad 3.2$$

The equation for the coefficient of variance, CV:

$$CV = \frac{\sigma}{\mu} \qquad 3.3$$

The equation for the root mean squared error:

$$RMSE = \sqrt{\frac{\sum(k_{exp} - k_{mod})}{n}} \qquad 3.4$$

The equation for the normalised root mean square error:

$$NRMSE = \frac{RMSE}{k_{exp}^{max} - k_{exp}^{min}} \qquad 3.5$$

Where, k_{exp} is the measured value and k_{mod} is the predicted value, n is the number of values in the dataset, k_{exp}^{max} is the maximum measured value, k_{exp}^{min} is the minimum measured value and $\bar{k}_{exp}$ is the mean measured value.

J.1 Calculations for root failure moment model comparisons wheat and oats.

Run Prelim file for Wheat

NB: root measurements for wheat were in mm so the equations were changed

Calculations
```
MaxResist = MaxResistance - 0.05;
%the shear strength instrument is calibrated so the calculation including the
blade geometry is not needed in this case
```
Crook
```
tau = AvgShear*1000; %shear strength kPa
D = PlateDiameter/1000; %root plate diameter m (35, 10-80)
k = 1; %constant k was later modified to 0.43 by Baker et al. (1998) using
data from Griffin (1998).
Crook = k.*tau.*D.^3

RMSECrook = sqrt(mean((MaxResist - Crook).^2))
NRMSE = RMSECrook/(max(MaxResist) - min(MaxResist))
CVRMSE = RMSECrook/mean(MaxResist)
stats = [RMSECrook NRMSE CVRMSE]'
```

Goodman
```
l = RootLength/1000;
Goodman = k.*tau.*D.*l.^2

RMSEGoodman= sqrt(mean((MaxResist - Goodman).^2))
NRMSE = RMSEGoodman/(max(MaxResist) - min(MaxResist))
CVRMSE = RMSEGoodman/mean(MaxResist)
stats = [RMSEGoodman NRMSE CVRMSE]'
```

Niklas

D is being used instead of per metre run
```
Niklas = k.*tau.*((pi.*D.^2)./4).*l

RMSENiklas = sqrt(mean((MaxResist - Niklas).^2))
NRMSE = RMSENiklas/(max(MaxResist) - min(MaxResist))
CVRMSE = RMSENiklas/mean(MaxResist)
stats = [RMSENiklas NRMSE CVRMSE]'
```

Cantilever Model
For Sand
```
A = (StemDiameter/1000).*(PlantHeight/100); %area of wind force m^2
v = 4; %wind speed ms^-1
P = (0.5*1.2*v^2*A); %force on the sheet pile kN/m (1.2 = density of air
kg/m^3)
gamma = 12; %effective unit weight of soil kN/m^3
phi = [34 28 37 31 31]; %angle of internal friction degrees
```

```
L = PlantHeight/100; %length of the sheet pile above ground m
% sigma = []; %effective stress kN/m^2
% D = []; %depth of penetration m
kp = tand(45+phi/2).^2 %Rankine passive earth pressure coeff
ka = tand(45-phi/2).^2 %Rankine active earth pressure coeff
z = sqrt(2.*P./(gamma.*(kp-ka)));
part1 = P.*(L+z);
part2 = (gamma.*z.^3.*(kp-ka))/6;
CantiS = part1-part2
part2 = part2*1000
CantiS = CantiS*1000

RMSEpart2 = sqrt(mean((MaxResist - part2).^2))
RMSECantiS = sqrt(mean((MaxResist - CantiS).^2))

NRMSE = RMSEpart2/(max(MaxResist) - min(MaxResist))
CVRMSE = RMSEpart2/mean(MaxResist)
stats = [RMSEpart2 NRMSE CVRMSE]'

NRMSE = RMSECantiS/(max(MaxResist) - min(MaxResist))
CVRMSE = RMSECantiS/mean(MaxResist)
stats = [RMSECantiS NRMSE CVRMSE]'
```

For Clay
```
%P = 0.004; %force on the sheet pile kN/m
c = [6.6 7.4 5.8 5.3 9.7]; %cohesive strength
%L = 0.5; %length of the sheet pile above ground m
z2 = P./(4.*c);
part3 = P.*(L+z2);
part4 = ((4.*c.*(z2).^2)/2);
CantiC = part3 - part4
part4 = part4*1000
CantiC = CantiC*1000

RMSEpart4 = sqrt(mean((MaxResist - part4).^2))
RMSECantiC = sqrt(mean((MaxResist - CantiC).^2))

NRMSE = RMSEpart4/(max(MaxResist) - min(MaxResist))
CVRMSE = RMSEpart4/mean(MaxResist)
stats = [RMSEpart4 NRMSE CVRMSE]'

NRMSE = RMSECantiC/(max(MaxResist) - min(MaxResist))
CVRMSE = RMSECantiC/mean(MaxResist)
stats = [RMSECantiC NRMSE CVRMSE]'
```

Rahardjo - With this model we need to compare the soil strength to the 3 measures of root strength. Whichever one is the smallest is the limiting factor. We can compare 3 different soil types to see how they compare. This model gives a simple output but could be very useful.
```
%Soil
cu = tau/1000; %undrained shear strength kPa
```

```matlab
b = 1; % width of slice
h = 1; % height of the slice
gamma = 12; % unit weighht of soil kN/m^3
alpha = 1; %angle to horizontal of slice
W = gamma*b*h; % weight of the slice
%Fsoil = sum(cu*b*sec(alpha)) % or
Fsoil = (D./2).*deg2rad(Angle).*cu
%Root
A = (2.*pi.*(RootDia./1000).*(RootLength./1000)) +
(2.*pi.*(RootDia./1000).^2) % surface area of each root m^2
shear = ((11.4/9)/1000)/((pi*5^2/4)/1000)/1 % shear strength of the root kPa
(converting from Nm to kPa) Using a diameter of 3 mm and a length of 1m to
convert to kPa, 9 is the number of roots used to get 11.4 x 10-3Nm in Crook
and Ennos, (1993) work, the shear/bending stress is a sum of all the roots
measured.
K = pi*RootDia/1000 % circumference of each root m
Lslip = RootLength/1000 % length of horizontal root providing the slippage
resistance m
slip = (481/(pi*0.9.^2/4))/1000.*0.009806 % slippage strength between the soil
and root (converting from g/mm2 to kPa) using 481g Breaking load and diameter
of 0.9 mm
tensile = (582)/1000*0.009806 % tensile strength of root kPa (converting from
g to kN) using 582g breaking stress (g/mm2)
Fshear = (A.*shear.*RootNumber)*1000
Fslip = (K.*Lslip.*slip.*RootNumber)*1000
Ftensile = (A.*tensile.*RootNumber)*1000

RMSEFsoil = sqrt(mean((MaxResist - Fsoil).^2))
RMSEFshear = sqrt(mean((MaxResist - Fshear).^2))
RMSEFslip = sqrt(mean((MaxResist - Fslip).^2))
RMSEFtensile = sqrt(mean((MaxResist - Ftensile).^2))

NRMSE = RMSEFsoil/(max(MaxResist) - min(MaxResist))
CVRMSE = RMSEFsoil/mean(MaxResist)
stats = [RMSEFsoil NRMSE CVRMSE]'

NRMSE = RMSEFshear/(max(MaxResist) - min(MaxResist))
CVRMSE = RMSEFshear/mean(MaxResist)
stats = [RMSEFshear NRMSE CVRMSE]'

NRMSE = RMSEFslip/(max(MaxResist) - min(MaxResist))
CVRMSE = RMSEFslip/mean(MaxResist)
stats = [RMSEFslip NRMSE CVRMSE]'

NRMSE = RMSEFtensile/(max(MaxResist) - min(MaxResist))
CVRMSE = RMSEFtensile/mean(MaxResist)
stats = [RMSEFtensile NRMSE CVRMSE]'


Coutts = (PlantWeight/1000*9.81).*(PlateDiameter/2000)
Fourcaud = (RootSoilMass/1000*9.81).*(PlateDiameter/2000)
```

```
RMSECoutts = sqrt(mean((MaxResist - Coutts).^2))
RMSEFourcaud = sqrt(mean((MaxResist - Fourcaud).^2))


NRMSE = RMSECoutts/(max(MaxResist) - min(MaxResist))
CVRMSE = RMSECoutts/mean(MaxResist)
stats = [RMSECoutts NRMSE CVRMSE]'

NRMSE = RMSEFourcaud/(max(MaxResist) - min(MaxResist))
CVRMSE = RMSEFourcaud/mean(MaxResist)
stats = [RMSEFourcaud NRMSE CVRMSE]'
```

K.1 Calculations for root failure moment model comparisons oilseed rape.

Run Prelim file for Oilseed

NB: root measurements for oilseed were in cm so the equations were changed

Calculations
```
MaxResist = MaxResistance - 0.05;
%the shear strength instrument is calibrated so the calculation including the
blade geometry is not needed in this case
```

Crook
```
tau = AvgShear*1000; %shear strength kPa
D = RootDia/1000; %root plate diameter m (35, 10-80)
k = 1; %constant k was later modified to 0.43 by Baker et al. (1998) using
data from Griffin (1998).
Crook = k.*tau.*D.^3

RMSECrook = sqrt(mean((MaxResist - Crook).^2))
NRMSE = RMSECrook/(max(MaxResist) - min(MaxResist))
CVRMSE = RMSECrook/mean(MaxResist)
stats = [RMSECrook NRMSE CVRMSE]'
```

Goodman
```
l = RootLength/100;
Goodman = k.*tau.*D.*l.^2

RMSEGoodman = sqrt(mean((MaxResist - Goodman).^2))
NRMSE = RMSEGoodman/(max(MaxResist) - min(MaxResist))
CVRMSE = RMSEGoodman/mean(MaxResist)
stats = [RMSEGoodman NRMSE CVRMSE]'
```

Limit Equilibrium
D is being used instead of per metre run
```
Niklas = k.*tau.*((pi.*D.^2)./4).*l
```

```
RMSENiklas = sqrt(mean((MaxResist - Niklas).^2))
NRMSE = RMSENiklas/(max(MaxResist) - min(MaxResist))
CVRMSE = RMSENiklas/mean(MaxResist)
stats = [RMSENiklas NRMSE CVRMSE]'
```

L.1 The analytical model for the rigid under-reamed pile

This section describes the calculations required for the rigid under-reamed pile model. There are a series of steps to derive the equations. Each stage of the analysis has options for coarse and fine-grained soils (Prakash and Ramakrishna, (2004), used c-soils (fine) and ϕ-soils (coarse)). This will be represented as Equations (a) and (b). The model for under-reamed piles requires the point of rotation to be calculated from the combination of passive resistance of the uniform shaft of the pile, additional resistance on the surface of the bulb, as well as the bearing and uplift resistances, for the final equilibrium equations to be valid, i.e. through force equilibrium and the moment equilibrium equations.

The passive resistance is assumed to be the same as Broms, (1964a) with a modification of the equation for c-soils. Broms, (1964a) removed the top 1.5 times the pile diameter of the soil to remove the area that might be disturbed and undergo softening effects. However, in their research, Prakash and Ramakrishna, (2004) were constructing this analytical solution for soils in India, where alluvial soils are present. Alluvial soil is loose, unconsolidated soil or sediment that has been eroded, reshaped by water and redeposited in a non-marine setting, and it is typically made up of a variety of materials, including fine particles of silt or clay and larger particles of sand and gravel (Young, 1976)). Therefore, they assumed that no disturbance of the soil would occur and hence, the model uses a uniform resistance of $9c_u$ for c-soils and $3K_p\gamma L$ for ϕ-soils, from the ground surface.

The net passive pressure is calculated using Equations (4.1) and (4.2) Prakash and Ramakrishna:

$$R_p = 9c_u D(2x - L) \ (c \ soils) \hspace{4cm} 1$$

$$R_p = 3K_p \gamma D(x^2 - 0.5L^2) \ (\varphi \ soils) \hspace{3cm} 2$$

Where, R_p is the net passive resistance or the ultimate lateral resistance of a straight shafted pile, c_u is the undrained shear strength (for fine-grained soils), D is the diameter of the pile, x is the location of the point of rotation, L is the length of the pile, K_p is the coefficient of passive earth pressure = $\tan^2(45 + \frac{\varphi}{2})$ and γ is the unit weight of sand (for coarse-grained soils).

The additional resistance on the surface of the bulb is calculated for the top and bottom surfaces of the cylindrical bulb (root-soil cone). The interface between the pile (root) and the soil has to be considered in this equation. This interface interaction is described using a single factor called the adhesion factor. In pile engineering, the adhesion is related to the reduction in skin friction occurring around the pile as it moves through the soil. The skin friction depends on the vertical effective stress in a given layer of soil, the angle of wall friction, based on the pile material and phi and K_s the earth pressure coefficient (Das, 2011). The adhesion factor will be related to the root-soil interface, the rhizosheath and the root hairs. The resistance at the top of the bulb is described by Equations (4.3) and (4.4):

$$[R_s]_{top} = A_a(\alpha_h \ c_u) \quad (c \ soils) \hspace{3cm} 4.3$$

$$[R_s]_{top} = A_a(\gamma \ tan\delta)L_i \quad (\varphi \ soils) \hspace{2.5cm} 4.4$$

Where, A_a = projected area of the bulb = $\frac{\pi}{4}(D_u^2 - D^2)$, α_h is the adhesion factor in the horizontal direction in the case of c-soils, c_u is the undrained shear strength, γ is the unit

weight of sand and δ is the angle of wall friction in the case of φ-soils, L_i = location of the bulb below the ground surface.

In their work, Prakash and Ramakrishna, (2004) equate the adhesion factor in the horizontal direction to 40% of the adhesion factor in the vertical direction for a pile in c-soils (after Smith et al., (1987)). The angle of wall friction was assumed to be equivalent to the angle of internal friction, φ for φ-soils.

The resistance at the bottom of the bulb can be calculated using Equations (4.5) and (4.6):

$$[R_s]_{bottom} = A_a(\alpha_h\, c_u) \quad (c\ soils) \qquad 4.5$$

$$[R_s]_{bottom} = A_a(\gamma\, tan\delta)L_i + L_b \quad (\varphi\ soils) \qquad 4.6$$

Where, L_b is the length of the bulb.

The total resistance of the bulb (root-soil cone) is given by:

$$[R_{si}] = [R_s]_{bottom} + [R_s]_{top} = 2A_a(\alpha_h\, c_u) \quad (c\ soils) \qquad 4.7$$

$$[R_{si}] = [R_s]_{bottom} + [R_s]_{top} = A_a(\gamma\, tan\delta)(2L_i + L_b) \quad (\varphi\ soils) \qquad 4.8$$

A variation of the additional resistance incorporating the inclined surface of the bulb is given by Equations (4.9) to (4.14):

$$[R_s]_{top} = A_a(\alpha_h\, c_u)cos\theta_1 \quad (c\ soils) \qquad 4.9$$

$$[R_s]_{top} = A_a(\gamma\, tan\delta)L\, cos\theta_1 \quad (\varphi\ soils) \qquad 4.10$$

$$[R_s]_{bottom} = A_a(\alpha_h\, c_u)\, cos\theta_2 \quad (c\ soils) \qquad 4.11$$

$$[R_s]_{bottom} = A_a(\gamma\, tan\delta)L_i + L_b\, cos\theta_2 \quad (\varphi\ soils) \qquad 4.12$$

$$[R_{si}] = [R_s]_{bottom} + [R_s]_{top} = A_a(\alpha_h\, c_u)\, cos(\theta_1 + \theta_2) \quad (c\ soils) \qquad 4.13$$

$$[R_{si}] = [R_s]_{bottom} + [R_s]_{top} = A_a(\gamma\, tan\delta)[(L_i\{cos\theta_1 + cos\theta_2\} + L_b cos\theta_2) \quad (\varphi\ soils)\ 4.$$

Where, θ_1 is the upper angle of the inclined surface (Prakash and Ramakrishna, (2004) assume a value of 45°) and θ_2 is the lower angle of the inclined surface.

According to Prakash and Ramakrishna, (2004), an under-reamed pile foundation with portions of bulb projecting on either side would cause the soil underneath to be pushed down on one side and the soil on top to be pushed up on the other (shown in **Error! Reference source not found.** as p_u and p_b) creating resistances, which are called bearing and uplift, respectively. In the under-reamed pile model, the bearing resistance is assumed to be in the vertical direction on the front half of the bulb and the uplift on the back half of the bulb. These resistances would not be included in the force equilibrium, but the moment equilibrium is indirectly affected because these forces can cause the point of rotation to be shifted up or down. The bearing and uplift resistances are calculated as follows:

$$p_b = c_u N_c \ (c \ soils) \qquad\qquad 4.15$$

$$p_b = \gamma N_q L + 0.5\gamma \ \frac{D_u - D}{2} N_y \ (\varphi \ soils) \qquad\qquad 4.16$$

$$p_u = 0.5(p_b) \qquad\qquad 4.17$$

$$M_{bu} = A_2 \sum_{i=1}^{n} [(p_b) + (p_u)] \qquad\qquad 4.18$$

Where, p_b is the unit bearing resistance, p_u is the uplift resistance, N_q, N_c, N_y are bearing capacity factors and are functions of ϕ, M_{bu} is the moment of the bearing and uplift resistances, A_2 is the coefficient representing the lever arm between the centre of gravities of these forces and the pile shaft $= \left[\left(\frac{D_u^3}{12} - \frac{D^3}{12} \right) \right]$. A_2 changes to $\frac{1}{D_u - D} \left[\left(\frac{D_u^4}{16} - \frac{D^4}{16} \right) - \left(\frac{DD_u^3}{12} - \frac{D^4}{12} \right) \right]$ when the inclined surface of the bulb is considered. These pressures may not be suitable for the small scale root systems. The equilibrium equations are derived.

For force equilibrium:

$$H_{ur} = R_p + R_s \qquad\qquad 4.19$$

Moment equilibrium:

$$H_{ur}e + \sum_{i=1}^{m} R_s L_i - \sum_{i=1}^{n} R_s L - M_{bu} + A_3 = 0 \qquad 4.20$$

Moments about ground level are derived by:

$$A_3 = 9c_u D(x^2 - 0.5L^2) \; (c \; soils) \qquad 4.21$$

$$A_3 = 3K_p \gamma D(2x^3 - L^3) \; (\varphi \; soils) \qquad 4.22$$

Values of the various resisting forces and moments are substituted into the equilibrium

Equations (4.19) and (4.20), resulting in a series of simultaneous equations. The

simultaneous equations are solved iteratively to find a value for x, which is the point of

rotation.

$$x^2 + x(2e) - C = 0 \qquad 4.23$$

$$C = C_1 + C_2 + C_3$$

$$C_1 = Le + 0.5L^2$$

$$C_2 = 0.22 \frac{A_a}{D} \alpha_h L_1$$

c-soils

$$C_3 = 0.22A_2 \frac{N_c}{D}$$

$$x^3 + x^2(1.5e) - C = 0 \qquad 4.24$$

$$C = C_1 + C_2 + C_3$$

$$C_1 = 0.75L^2 e + 0.5L^3$$

φ-soils

$$C_2 = \frac{A_a tan\varphi}{DK_p} \sum_{i=1}^{n} L_i \left(e + \sum_{i=1}^{n} L_i \right)$$

$$C_3 = \frac{N_q}{DK_p} A_2 \sum_{i=1}^{n} L_i + nA_2 \frac{N_y}{K_p}$$

Finally, the ultimate resistance of the pile can be computed and the failure moment can be calculated by adding the moment of the resistance of the bulb.

The following equations (Equation 4.23-4.28) were used to determine whether the pile was long and flexible. The effect of the length of the pile on the ultimate lateral resistance was analysed, and the limiting lengths for deciding whether the pile was rigid or flexible were calculated (Prakash and Ramakrishna, 2004). A second series of equations compute the ultimate lateral load for flexible piles. In this case, the yield moments, related to the strength of the material, mainly govern the design. The yield moment is the maximum bending moment that the section of material can resist. When this point is reached, a plastic hinge will form and any load beyond this point results in plastic deformation. A pile is deemed flexible based on criteria developed by Broms, (1964a) for c-soils and Matlock and Reese, (1960) for φ-soils.

$$\beta = \sqrt[4]{\left(\frac{K_h D}{EI_{st}}\right)} \ (c \ soils) \qquad 4.23$$

if βL > 2.5 then the pile was treated as flexible

$$Z_{max} = \frac{L}{T}; where \ T = \sqrt[5]{\left(\frac{EI_{st}}{\eta_h}\right)} \ (\varphi \ soils) \qquad 4.24$$

if $z_{max} > 4.0$ the pile was treated as flexible

$$I_{ur} = \frac{I_{st}}{L}[(L_1 + L_{end}) + (n-1)L_{int} + D_r^4 nL_b] \qquad 4.25$$

$$H_{ufl} = 4.24\sqrt{M_{yu}c_u D} \ (c \ soils) \qquad 4.26$$

$$H_{ufl} = 1.5\sqrt[3]{M_{yu}^2 K_p \gamma D} \ (\varphi \ soils) \qquad 4.27$$

$$M_{yu} = 2\sigma \frac{I_{ur}}{D} \qquad\qquad 4.28$$

Where, K_h is the modulus of subgrade reaction for c-soils and n_h is the modulus of subgrade reaction for φ-soils. For this research, the modulus of subgrade reaction was assumed to be 80 and 2600 kN/m³ for c-soils and φ-soils respectively (Skempton, (1951) and Terzaghi, (1955) cited by Prakash and Ramakirshna, (2004)). I_{st} is the moment of inertia of the pile with a uniform cross-section. In the case of under-reamed piles, the moment of inertia depends on the bulb and their location underground. Leading to I_{ur}, which was the moment of inertia of the under-reamed pile. I_{ur} takes the weighted average of diameter and length of the pile as well as the bulb and their location along the shaft (Prakash and Ramakrishna, 2004) into account. However, in this research, the oilseed rape tap root did not have a bulb and so Equation 4.25 was reduced to just the moment of inertia of $I_{st} = \frac{\pi}{64} D^4$. Once the criteria are tested and I_{ur} calculated, the ultimate lateral resistance of the under-reamed pile, H_{ufl} (Equations 4.26 and 4.27) was determined. Where, M_{yu} is the yield moment of resistance, and σ is the permissible yield stress in the root.

M.1 Matlab code for the under-reamed pile model with variations for wheat and oats

```
Crook Model

RootLength_mm = RootLength; %taken from the wheat measurements 2017
Lm = RootLength_mm/1000;
StemDiameter_mm = StemDiameter;
Dm = StemDiameter_mm/1000;
cukPa = AvgShear;
PlateDiameter_mm = PlateDiameter;
Dum = PlateDiameter_mm/1000;
cukPa = AvgShear*1000; %shear strength kPa
```

```
k = 1; %constant k was later modified to 0.43 by Baker et al. (1998) using
data from Griffin (1998).
PlateDiameter_mm = PlateDiameter;
Dum = PlateDiameter_mm/1000; %root plate diameter m (35, 10-80)
Rfm = cukPa.*Dum.^3

RMSE = sqrt(mean((MaxResistance - Rfm).^2))
NRMSE = RMSE/(max(MaxResistance) - min(MaxResistance))
CVRMSE = RMSE/mean(MaxResistance)
Result = [RMSE NRMSE CVRMSE]'
```

Prakash and Ramakrishna, (2004), under-reamed pile model

**Using the simultaneous equations to find x, the point of rotation (through the
equilibrium equations for force and moment <u>including</u> the bearing and uplift
resistances)**

```
RootLength_mm = RootLength
Lm = RootLength_mm/1000
%Lm = Lm - (Lm*1.5)
StemDiameter_mm = StemDiameter
Dm = StemDiameter_mm/1000
cukPa = AvgShear
PlateDiameter_mm = PlateDiameter
Dum = PlateDiameter_mm/1000
theta1 = Angle
em = 0.17 %the eccentricity of the lateral load above ground level.
Aam2 = (pi/4)*((Dum.^2)-(Dm.^2)) %projected area of the bulb
alphah = 0.28 %adhesion factor in the horizontal direction (can be taken as
40% of the adhesion factor in the vertical direction for pile in c-soils)
C1 = Lm.*em + 0.5*Lm.^2
C2 = 0.22.*(Aam2./Dm).*alphah.*0.001
A2 = ((Dum.^3/12)-(Dm.^3/12)) %coefficient representing the lever arm
between the centres of gravity of bearing and uplift forces and the pile
phi = 34.37 %angle of internal friction
Nq = exp((pi)*tand(phi))*(tand(45+(phi/2)))^2 %bearing capacity factors,
functions of phi
Nc = (Nq-1)*(1/tand(phi))
C3 = 0.22.*A2.*(Nc./Dm)
C = C1+C2+C3
a = 1
b = 2*em
%Solving the polynomial using the roots function in matlab
for i = 1:size(C,1)
    p = [a b -C(i)]; % creating the polynomial
    r = roots(p); %solving for roots
    rr = real(r); %getting real answers
    xm(i,1)=rr(2); %creating the vector for the point of rotation one loop
at a time using the second (positive) answer from the roots
end
```

```matlab
[xm Lm 0.6*xm] %checking x against L and x^2
% Passive Resistance on the Uniform Shaft of the Pile
RpkN = 9*cukPa.*Dm.*((2.*xm)-Lm)
A3kNm = 9*cukPa.*Dm.*((xm.^2)-(0.5*(Lm.^2)))
A3Nm = A3kNm*1000
% Additional Resistance on the Surface of Bulb
RstopkN = Aam2.*alphah.*cukPa
RsbottomkN = Aam2.*alphah.*cukPa
RskN = 2*(Aam2.*alphah.*cukPa) %+ Aam2.*alphah.*cukPa
MRskNm = RskN.*Lm
MRsNm = MRskNm*1000
FinalMomentNm = A3Nm + MRsNm %possibly multiply A3 by -1

RMSE = sqrt(mean((MaxResistance - FinalMomentNm).^2))
NRMSE = RMSE/(max(MaxResistance) - min(MaxResistance))
CVRMSE = RMSE/mean(MaxResistance)
Result = [RMSE NRMSE CVRMSE]'
```

Using the simultaneous equations to find x, the point of rotation (through the equilibrium equations for force and moment including the bearing only)

```matlab
RootLength_mm = RootLength
Lm = RootLength_mm/1000
%Lm = Lm - (Lm*1.5)
StemDiameter_mm = StemDiameter
Dm = StemDiameter_mm/1000
cukPa = AvgShear
PlateDiameter_mm = PlateDiameter
Dum = PlateDiameter_mm/1000
theta1 = Angle
em = 0.17 %the eccentricity of the lateral load above ground level.
Aam2 = (pi/4)*((Dum.^2)-(Dm.^2)) %projected area of the bulb
alphah = 0.28 %adhesion factor in the horizontal direction (can be taken as
40% of the adhesion factor in the vertical direction for pile in c-soils)
C1 = Lm.*em + 0.5*Lm.^2
C2 = 0.22.*(Aam2./Dm).*alphah.*0.001
A2 = ((Dum.^3/12)-(Dm.^3/12)) %coefficient representing the lever arm
between the centres of gravity of bearing and uplift forces and the pile
phi = 34.37 %angle of internal friction
Nq = exp((pi)*tand(phi))*(tand(45+(phi/2)))^2 %bearing capacity factors,
functions of phi
Nc = (Nq-1)*(1/tand(phi))
C3 = 0.111.*A2.*(Nc./Dm)
C = C1+C2+C3
a = 1
b = 2*em
%Solving the polynomial using the roots function in matlab
for i = 1:size(C,1)
    p = [a b -C(i)]; % creating the polynomial
    r = roots(p); %solving for roots
    rr = real(r); %getting real answers
```

```
    xm(i,1)=rr(2); %creating the vector for the point of rotation one loop
at a time using the second (positive) answer from the roots
end
[xm Lm 0.6*xm] %checking x against L and x^2
% Passive Resistance on the Uniform Shaft of the Pile
RpkN = 9*cukPa.*Dm.*((2.*xm)-Lm)
A3kNm = 9*cukPa.*Dm.*((xm.^2)-(0.5*(Lm.^2)))
A3Nm = A3kNm*1000
% Additional Resistance on the Surface of Bulb
RstopkN = Aam2.*alphah.*cukPa
RsbottomkN = Aam2.*alphah.*cukPa
RskN = 2*(Aam2.*alphah.*cukPa) %+ Aam2.*alphah.*cukPa
MRskNm = RskN.*Lm
MRsNm = MRskNm*1000
FinalMomentNm = A3Nm + MRsNm %possibly multiply A3 by -1
RMSE = sqrt(mean((MaxResistance - FinalMomentNm).^2))
NRMSE = RMSE/(max(MaxResistance) - min(MaxResistance))
CVRMSE = RMSE/mean(MaxResistance)
Result = [RMSE NRMSE CVRMSE]'
```

Using the simultaneous equations to find x, the point of rotation (through the equilibrium equations for force and moment <u>excluding</u> the bearing and uplift resistances)

C-Soils

```
RootLength_mm = RootLength
Lm = RootLength_mm/1000
StemDiameter_mm = StemDiameter
Dm = StemDiameter_mm/1000
cukPa = AvgShear
PlateDiameter_mm = PlateDiameter
Dum = PlateDiameter_mm/1000
theta1 = Angle
em = 0.17 %the eccentricity of the lateral load above ground level.
Aam2 = (pi/4)*((Dum.^2)-(Dm.^2)) %projected area of the bulb
alphah = 0.14 %adhesion factor in the horizontal direction (can be taken as
40% of the adhesion factor in the vertical direction for pile in c-soils)
C1 = Lm.*em + 0.5*Lm.^2
C2 = 0.22.*(Aam2./Dm).*alphah.*0.001
A2 = ((Dum.^3/12)-(Dm.^3/12))%coefficient representing the lever arm between
the centres of gravity of bearing and uplift forces and the pile
C = C1+C2
a = 1
b = 2*em
% %Solving the polynomial using the quadratic equation
% a = 1 %coefficient of the quadratic equation
% b = 2*em %coefficient of quadratic equation
% xm1 = (-b-sqrt((b^2)-4*a*-C))/2*a %location of the point of rotation below
ground level
% xm2 = (-b+sqrt((b^2)-4*a*-C))/2*a
%Solving the polynomial using the roots function in matlab
```

```
for i = 1:size(C,1)
    p = [a b -C(i)]; % creating the polynomial
    r = roots(p); %solving for roots
    rr = real(r); %getting real answers
    xm(i,1)=rr(2); %creating the vector for the point of rotation one loop
at a time using the second (positive) answer from the roots
end
[xm Lm xm.^2 0.5*Lm.^2] %checking x against L and x^2
% Passive Resistance on the Uniform Shaft of the Pile
RpkN = 9*cukPa.*Dm.*((2.*xm)-Lm)
A3kNm = 9*cukPa.*Dm.*((xm.^2)-(0.5*(Lm.^2)))
A3Nm = A3kNm*1000
% Additional Resistance on the Surface of Bulb
RstopkN = Aam2.*alphah.*cukPa
RsbottomkN = Aam2.*alphah.*cukPa
RskN = 2*(Aam2.*alphah.*cukPa) %+ Aam2.*alphah.*cukPa
MRskNm = RskN.*Lm
MRsNm = MRskNm*1000
FinalMomentNm = A3Nm + MRsNm %possibly multiply A3 by -1

RMSE = sqrt(mean((MaxResistance - FinalMomentNm).^2))
NRMSE = RMSE/(max(MaxResistance) - min(MaxResistance))
CVRMSE = RMSE/mean(MaxResistance)
Result = [RMSE NRMSE CVRMSE]'
```

Phi-Soils including the bearing and uplift resistances

```
RootLength_mm = RootLength
Lm = RootLength_mm/1000
StemDiameter_mm = StemDiameter
Dm = StemDiameter_mm/1000
cukPa = AvgShear
PlateDiameter_mm = PlateDiameter
Dum = PlateDiameter_mm/1000
A2 = ((Dum.^3/12)-(Dm.^3/12))
Kp = (tand(45+(phi/2)))^2  %coefficient of passive earth pressure
gamma = 12 %kN/m3 unit weight of soil
Lim = 0.001 %location of the bulb below ground level
Lbm = Lm %location of the bottom of the bulb below ground level
delta = phi %angle of wall friction equivalent to phi for phi-soils
n = 1
Ny = 2*(Nq+1)*(tand(phi))
em = 0.17 %the eccentricity of the lateral load above ground level.
C1 = (0.75*Lm.^2*em)+(0.5*Lm.^3)
C2 = ((Aam2*tand(phi))./(Dm*Kp)).*Lim.*(em+Lim)
C3 = ((Nq/Dm*Kp)*A2*Lim)+(n*A2*(Ny/Kp))
C = C1+C2+C3
%find the value of x from the cubic polynomial
%when C = 1
%then x = a, b, c
%0 = (xm^3)+((xm^2)*(1.5*em))-C
a = 1
```

```
b = 1.5*em
c = 0
for i = 1:size(C,1)
    p = [a b c -C(i)]; % creating the polynomial
    r = roots(p); %solving for roots
    rr=real(r); %getting real answers
    xm(i,1)=rr(3);
end
[xm Lm]
% Passive Resistance on the uniform shaft of pile
RpkN = 3*Kp*gamma.*Dm.*((xm.^2)-(0.5*Lim.^2))
A3kNm = Kp*gamma.*Dm.*((2*xm.^3)-Lm.^3)
A3Nm = A3kNm*1000
% Additional Resistance on the Surface of Bulb
RstopkN = Aam2*(gamma*tand(delta)).*Lim
RsbottomkN = Aam2*(gamma*tand(delta)).*(Lim+Lbm)
RskN = Aam2*(gamma*tand(delta)).*(2*Lim+Lbm)
MRskNm = RskN.*Lm
MRsNm = MRskNm*1000
% Additional Resistance on the Surface of Bulb - with cone shape
RstopkN = Aam2*(gamma*tand(delta)).*Lim
RsbottomkN = Aam2*(gamma*tand(delta)).*(Lim+Lbm)
RskN = 2*(Aam2.*alphah.*cukPa) %+ Aam2*(gamma*tand(delta)).*(Lim+Lbm)
MRskNm2 = RskN2.*Lm
MRsNm2 = MRskNm2*1000
Hur = A3Nm + MRsNm

RMSE = sqrt(mean((MaxResistance - Hur).^2))
NRMSE = RMSE/(max(MaxResistance) - min(MaxResistance))
CVRMSE = RMSE/mean(MaxResistance)
Result = [RMSE NRMSE CVRMSE]'
```

Phi-Soils excluding the bearing and uplift resistances

```
RootLength_mm = RootLength
Lm = RootLength_mm/1000
StemDiameter_mm = StemDiameter
Dm = StemDiameter_mm/1000
cukPa = AvgShear
PlateDiameter_mm = PlateDiameter
Dum = PlateDiameter_mm/1000
Kp = (tand(45+(phi/2)))^2  %coefficient of passive earth pressure
gamma = 12 %kN/m3 unit weight of soil
Lim = 0.001 %location of the bulb below ground level
Lbm = Lm %location of the bottom of the bulb below ground level
delta = phi %angle of wall friction equivalent to phi for phi-soils
n = 1
Ny = 2*(Nq+1)*(tand(phi))
em = 0.17 %the eccentricity of the lateral load above ground level.
C1 = (0.75*Lm.^2*em)+(0.5*Lm.^3)
C2 = ((Aam2*tand(phi))./(Dm*Kp)).*Lim.*(em+Lim)
C = C1+C2
a = 1
```

```
b = 1.5*em
c = 0
for i = 1:size(C,1)
    p = [a b c -C(i)]; % creating the polynomial
    r = roots(p); %solving for roots
    rr=real(r); %getting real answers
    xm(i,1)=rr(3);
end
[xm Lm]
% Passive Resistance on the uniform shaft of pile
RpkN = 3*Kp*gamma.*Dm.*((xm.^2)-(0.5*Lim.^2))
A3kNm = Kp*gamma.*Dm.*((2*xm.^3)-Lm.^3)
A3Nm = A3kNm*1000
% Additional Resistance on the Surface of Bulb
RstopkN = Aam2*(gamma*tand(delta)).*Lim
RsbottomkN = Aam2*(gamma*tand(delta)).*(Lim+Lbm)
RskN = Aam2*(gamma*tand(delta)).*(2*Lim+Lbm)
MRskNm = RskN.*Lm
MRsNm = MRskNm*1000
% Additional Resistance on the Surface of Bulb - with cone shape
RstopkN = Aam2*(gamma*tand(delta)).*Lim
RsbottomkN = Aam2*(gamma*tand(delta)).*(Lim+Lbm)
RskN2 = Aam2*(gamma*tand(delta)).*Lim.*cosd(theta1) %+
Aam2*(gamma*tand(delta)).*(Lim+Lbm)
MRskNm2 = RskN2.*Lm
MRsNm2 = MRskNm2*1000
Hur = A3Nm + MRsNm

RMSE = sqrt(mean((MaxResistance - Hur).^2))
NRMSE = RMSE/(max(MaxResistance) - min(MaxResistance))
CVRMSE = RMSE/mean(MaxResistance)
Result = [RMSE NRMSE CVRMSE]'
```

C-soils changing the fundamental assumption of 9cu to 2cu (still within ranges given by Broms 1964)

```
RootLength_mm = RootLength
Lm = RootLength_mm/1000
StemDiameter_mm = StemDiameter
Dm = StemDiameter_mm/1000
cukPa = AvgShear
PlateDiameter_mm = PlateDiameter
Dum = PlateDiameter_mm/1000
theta1 = Angle
em = 0.17 %the eccentricity of the lateral load above ground level.
Aam2 = (pi/4)*((Dum.^2)-(Dm.^2)) %projected area of the bulb
alphah = 0.28 %adhesion factor in the horizontal direction (can be taken as
40% of the adhesion factor in the vertical direction for pile in c-soils)
C1 = Lm.*em + 0.5*Lm.^2
C2 = (Aam2./Dm).*alphah.*0.001
A2 = ((Dum.^3/12)-(Dm.^3/12)) %coefficient representing the lever arm
between the centres of gravity of bearing and uplift forces and the pile
```

```
C = C1+C2
a = 1
b = 2*em
%Solving the polynomial using the roots function in matlab
for i = 1:size(C,1)
    p = [a b -C(i)]; % creating the polynomial
    r = roots(p); %solving for roots
    rr = real(r); %getting real answers
    xm(i,1)=rr(2); %creating the vector for the point of rotation one loop
at a time using the second (positive) answer from the roots
end
[xm Lm 0.6*xm] %checking x against L and x^2
% Passive Resistance on the Uniform Shaft of the Pile
RpkN = 2*cukPa.*Dm.*((2.*xm)-Lm)
A3kNm = 2*cukPa.*Dm.*((xm.^2)-(0.5*(Lm.^2)))
A3Nm = A3kNm*1000
% Additional Resistance on the Surface of Bulb
RstopkN = Aam2.*alphah.*cukPa
RsbottomkN = Aam2.*alphah.*cukPa
RskN = 2*(Aam2.*alphah.*cukPa) %+ Aam2.*alphah.*cukPa
MRskNm = RskN.*Lm
MRsNm = MRskNm*1000
FinalMomentNm = A3Nm + MRsNm %possibly multiply A3 by -1

RMSE = sqrt(mean((MaxResistance - FinalMomentNm).^2))
NRMSE = RMSE/(max(MaxResistance) - min(MaxResistance))
CVRMSE = RMSE/mean(MaxResistance)
Result = [RMSE NRMSE CVRMSE]'
```

Reducing Alpha to 0.07

```
RootLength_mm = RootLength
Lm = RootLength_mm/1000
StemDiameter_mm = StemDiameter
Dm = StemDiameter_mm/1000
cukPa = AvgShear
PlateDiameter_mm = PlateDiameter
Dum = PlateDiameter_mm/1000
theta1 = Angle
em = 0.17 %the eccentricity of the lateral load above ground level.
Aam2 = (pi/4)*((Dum.^2)-(Dm.^2)) %projected area of the bulb
alphah = [0.07] % [0.08 0.06] %adhesion factor in the horizontal direction
(can be taken as 40% of the adhesion factor in the vertical direction for
pile in c-soils)
C1 = Lm.*em + 0.5*Lm.^2
C2 = 0.22*(Aam2./Dm).*alphah.*0.001
A2 = ((Dum.^3/12)-(Dm.^3/12)) %coefficient representing the lever arm
between the centres of gravity of bearing and uplift forces and the pile
C = C1+C2
a = 1
b = 2*em
%Solving the polynomial using the roots function in matlab
```

```matlab
for i = 1:size(C,1)
    p = [a b -C(i)]; % creating the polynomial
    r = roots(p); %solving for roots
    rr = real(r); %getting real answers
    xm(i,1)=rr(2); %creating the vector for the point of rotation one loop
at a time using the second (positive) answer from the roots
end
[xm Lm 0.6*xm] %checking x against L and x^2
% Passive Resistance on the Uniform Shaft of the Pile
RpkN = 9*cukPa.*Dm.*((2.*xm)-Lm)
A3kNm = 9*cukPa.*Dm.*((xm.^2)-(0.5*(Lm.^2)))
A3Nm = A3kNm*1000
% Additional Resistance on the Surface of Bulb
RstopkN = Aam2.*alphah.*cukPa
RsbottomkN = Aam2.*alphah.*cukPa
RskN = 2*(Aam2.*alphah.*cukPa) %+ Aam2.*alphah.*cukPa
MRskNm = RskN.*Lm
MRsNm = MRskNm*1000
FinalMomentNm = A3Nm + MRsNm %possibly multiply A3 by -1

RMSE = sqrt(mean((MaxResistance - FinalMomentNm).^2))
NRMSE = RMSE/(max(MaxResistance) - min(MaxResistance))
CVRMSE = RMSE/mean(MaxResistance)
Result = [RMSE NRMSE CVRMSE]'
```

N.1   Matlab code for the sensitivity analysis for wheat.

Varying the eccentricity of the load above ground C-soils

```matlab
em = [0.17 0.33 0.5]
%em = [0.17*0.5 0.17*0.75 0.17 0.17*1.25 0.17*1.5]
RootLength_mm = mean(RootLength)
Lm = RootLength_mm/1000
StemDiameter_mm = mean(StemDiameter)
Dm = StemDiameter_mm/1000
cukPa = mean(AvgShear)
PlateDiameter_mm = mean(PlateDiameter)
Dum = PlateDiameter_mm/1000
Aam2 = (pi/4)*((Dum.^2)-(Dm.^2))
alphah = 0.06
theta1 = mean(Angle)
xm = 0
for i = 1:size(em,2)
    C1 = Lm.*em(i) + 0.5.*Lm.^2
    C2 = 2*(Aam2./Dm).*alphah.*0.001
    A2 = ((Dum.^3/12)-(Dm.^3/12))
    C = C1+C2
    a = 1
    b = 2*em(i)
```

```
    for j = 1:size(C,1)
        p = [a b -C(j)] % creating the polynomial
        r = roots(p) %solving for roots
        rr=real(r)%getting real answers
        xm(j,i) = rr(2) %creating the vector for the point of rotation one
loop at a time using the second (positive) answer from the roots
    end
end
[xm]
%xm = xm(:,4)

RpkN = cukPa.*Dm.*((2.*xm)-Lm)
A3kNm = cukPa.*Dm.*((xm.^2)-(0.5*(Lm.^2)))
A3Nm = A3kNm*1000
RskN = 2*(Aam2.*alphah.*cukPa) %+ Aam2.*alphah.*cukPa
MRskNm = RskN.*Lm
MRsNm = MRskNm*1000
FinalMomentNm = A3Nm + MRsNm
```

Varying the eccentricity of the load above ground Phi-soils

```
em = [0.17 0.33 0.5]
RootLength_mm = mean(RootLength)
Lm = RootLength_mm/1000
StemDiameter_mm = mean(StemDiameter)
Dm = StemDiameter_mm/1000
cukPa = mean(AvgShear)
PlateDiameter_mm = mean(PlateDiameter)
Dum = PlateDiameter_mm/1000
phi = 34.37
Kp = (tand(45+(phi/2))).^2  %coefficient of passive earth pressure
gamma = 12 %kN/m3 unit weight of soil
Lim = 0.001 %location of the bulb below ground level
Lbm = Lm %location of the bottom of the bulb below ground level
delta = phi %angle of wall friction equivalent to phi for phi-soils
n = 1
Nq = exp((pi)*tand(phi))*(tand(45+(phi/2)))^2 %bearing capacity factors,
functions of phi
Nc = (Nq-1)*(1/tand(phi))
Ny = 2*(Nq+1)*(tand(phi))
for i = 1:size(em,2)
    C1 = (0.75*Lm.^2*em(i))+(0.5*Lm.^3)
    C2 = ((Aam2*tand(phi))./(Dm*Kp)).*Lim.*(em(i)+Lim)
    C3 = ((Nq/Dm*Kp)*A2*Lim)+(n*A2*(Ny/Kp))
    C = C1+C2+C3
    %find the value of x from the cubic polynomial
    %when C = 1
    %then x = a, b, c
    %0 = (xm^3)+((xm^2)*(1.5*em))-C
    a = 1
    b = 1.5*em(i)
    c = 0
```

```
    for j = 1:size(C,1)
        p = [a b c -C(j)]; % creating the polynomial
        r = roots(p); %solving for roots
        rr=real(r); %getting real answers
        xm(j,i)=rr(3);
    end
end
[xm Lm]
% Passive Resistance on the uniform shaft of pile
RpkN = 3*Kp*gamma.*Dm.*((xm.^2)-(0.5*Lim.^2))
A3kNm = Kp*gamma.*Dm.*((2*xm.^3)-Lm.^3)
A3Nm = A3kNm*1000
% Additional Resistance on the Surface of Bulb
RstopkN = Aam2*(gamma*tand(delta)).*Lim
RsbottomkN = Aam2*(gamma*tand(delta)).*(Lim+Lbm)
RskN2 = Aam2*(gamma*tand(delta)).*(2*Lim+Lbm)
MRskNm2 = RskN2.*Lm
MRsNm2 = MRskNm2*1000
Hur = A3Nm + MRsNm2
%[MaxResistance A3Nm MRsNm Hur]
```

Varying the Bulb width C-soils

```
PlateDiameter_mm = mean(PlateDiameter)
Dum = PlateDiameter_mm/1000
Dum = [Dum*0.5 Dum*0.75 Dum Dum*1.25 Dum*1.5];
Aam2 = (pi/4)*((Dum.^2)-(Dm.^2)); %projected area of the bulb
theta1 = mean(Angle)
RootLength_mm = mean(RootLength)
Lm = RootLength_mm/1000
StemDiameter_mm = mean(StemDiameter)
Dm = StemDiameter_mm/1000
cukPa = mean(AvgShear)
em = 0.17 %the eccentricity of the lateral load above ground level.
alphah = 0.06 %adhesion factor in the horizontal direction (can be taken as
40% of the adhesion factor in the vertical direction for pile in c-soils)
xm = 0
for i = 1:size(Dum,2)
    C1 = Lm*em + 0.5*Lm.^2
    C2 = 2*(Aam2./Dm).*alphah.*0.001
    C = C1+C2
    a = 1
    b = 2*em
    %Solving the polynomial using the roots function in matlab
    for j = 1:size(C,1)
        p = [a b -C(j)]; % creating the polynomial
        r = roots(p); %solving for roots
        rr=real(r); %getting real answers
        xm(j,i)=rr(2); %creating the vector for the point of rotation one
loop at a time using the second (positive) answer from the roots
    end
end
```

```matlab
%[xm Lm xm.^2] %checking x against L and x^2
% Passive Resistance on the Uniform Shaft of the Pile
RpkN = cukPa.*Dm.*((2.*xm)-Lm)
A3kNm = cukPa.*Dm.*((xm.^2)-(0.5*(Lm.^2)))
A3Nm = A3kNm*1000
% Additional Resistance on the Surface of Bulb
RskN = 2*(Aam2.*alphah.*cukPa) %+ Aam2.*alphah.*cukPa
MRskNm = RskN.*Lm
MRsNm = MRskNm*1000
FinalMomentNm = A3Nm+MRsNm %possibly multiply A3 by -1
%[MaxResistance A3Nm MRsNm FinalMomentNm]
%[MaxResistance FinalMomentNm]
```

Varying the Bulb width Phi-soils

```matlab
PlateDiameter_mm = mean(PlateDiameter)
Dum = PlateDiameter_mm/1000
Dum = [Dum*0.5 Dum*0.75 Dum Dum*1.25 Dum*1.5];
Aam2 = (pi/4)*((Dum.^2)-(Dm.^2)); %projected area of the bulb
theta1 = mean(Angle)
RootLength_mm = mean(RootLength)
Lm = RootLength_mm/1000
StemDiameter_mm = mean(StemDiameter)
Dm = StemDiameter_mm/1000
cukPa = mean(AvgShear)
phi = 34.37
Aam2 = (pi/4)*((Dum.^2)-(Dm.^2)); %projected area of the bulb
em = 0.17 %the eccentricity of the lateral load above ground level.
Kp = (tand(45+(phi/2)))^2  %coefficient of passive earth pressure
gamma = 12 %kN/m3 unit weight of soil
Lim = 0.001 %location of the bulb below ground level
Lbm = Lm %location of the bottom of the bulb below ground level
delta = phi %angle of wall friction equivalent to phi for phi-soils
n = 1
Nq = exp((pi)*tand(phi))*(tand(45+(phi/2)))^2 %bearing capacity factors,
functions of phi
Nc = (Nq-1)*(1/tand(phi))
Ny = 2*(Nq+1)*(tand(phi))
xm=0
for i = 1:size(Dum,2)
    C1 = (0.75*Lm.^2*em)+(0.5*Lm.^3)
    Aam2 = (pi/4)*((Dum(i).^2)-(Dm.^2)) %projected area of the bulb
    A2 = (Dum(i).^3/12)-(Dm.^3/12) %coefficient representing the lever arm
between the centres of gravity of bearing and uplift forces and the pile
    C2 = ((Aam2*tand(phi))./(Dm*Kp)).*Lim.*(em+Lim)
    C3 = ((Nq/Dm*Kp)*A2*Lim)+(n*A2*(Ny/Kp))
    C = C1+C2+C3
    %find the value of x from the cubic polynomial
    %when C = 1
    %then x = a, b, c
    %0 = (xm^3)+((xm^2)*(1.5*em))-C
    a = 1
```

```
    b = 1.5*em
    c = 0

    for j = 1:size(C,1)
        p = [a b c -C(j)]; % creating the polynomial
        r = roots(p); %solving for roots
        rr=real(r); %getting real answers
        xm(j,i)=rr(3);
    end
end
[xm Lm]
% Passive Resistance on the uniform shaft of pile
RpkN = 3*Kp*gamma.*Dm.*((xm.^2)-(0.5*Lim.^2))
A3kNm = Kp*gamma.*Dm.*((2*xm.^3)-Lm.^3)
A3Nm = A3kNm*1000
% Additional Resistance on the Surface of Bulb
RstopkN = Aam2*(gamma*tand(delta)).*Lim
RsbottomkN = Aam2*(gamma*tand(delta)).*(Lim+Lbm)
RskN = Aam2*(gamma*tand(delta)).*(2*Lim+Lbm)
MRskNm2 = RskN2.*Lm
MRsNm2 = MRskNm2*1000
Hur = A3Nm + MRsNm
%[MaxResistance A3Nm MRsNm Hur]
```

Varying Adhesion factor for C-soils

```
alphah = [0.04 0.05 0.06 0.07 0.08] %adhesion factor in the horizontal
direction (can be taken as 40% of the adhesion factor in the vertical
direction for pile in c-soils)
RootLength_mm = mean(RootLength)
Lm = RootLength_mm/1000
StemDiameter_mm = mean(StemDiameter)
Dm = StemDiameter_mm/1000
cukPa = mean(AvgShear)
PlateDiameter_mm = mean(PlateDiameter)
Dum = PlateDiameter_mm/1000
em = 0.17 %the eccentricity of the lateral load above ground level.
Aam2 = (pi/4)*((Dum.^2)-(Dm.^2)) %projected area of the bulb
theta1 = mean(Angle)
xm = 0
for i = 1:size(alphah,2)
    C1 = Lm*em + 0.5*Lm.^2
    C2 = 2*(Aam2/Dm)*alphah(i)*0.001
    C = C1+C2
    a = 1
    b = 2*em
    %Solving the polynomial using the roots function in matlab
    for i = 1:size(C,1)
        p = [a b -C(i)]; % creating the polynomial
        r = roots(p); %solving for roots
        rr=real(r); %getting real answers
```

```matlab
        xm(i,1)=rr(2); %creating the vector for the point of rotation one
loop at a time using the second (positive) answer from the roots
    end
end
[xm Lm xm.^2] %checking x against L and x^2
% Passive Resistance on the Uniform Shaft of the Pile
RpkN = cukPa.*Dm.*((2.*xm)-Lm)
A3kNm = cukPa.*Dm.*((xm.^2)-(0.5*(Lm.^2)))
A3Nm = A3kNm*1000
% Additional Resistance on the Surface of Bulb
RskN = 2*(Aam2.*alphah.*cukPa)%+ Aam2.*alphah.*cukPa
MRskNm = RskN.*Lm
MRsNm = MRskNm*1000
FinalMomentNm = A3Nm + MRsNm %possibly multiply A3 by -1
%[MaxResistance A3Nm MRsNm FinalMomentNm]
%[MaxResistance FinalMomentNm]
```

Varying phi using values found in the field for Phi-Soils

```matlab
phi = [34.37
phi = [34.37 28.14 37.40 31.91 31.12]
phi = [0.6*phi 0.7*phi 0.8*phi 0.9*phi phi]
delta = phi
RootLength_mm = mean(RootLength)
Lm = RootLength_mm/1000
StemDiameter_mm =mean(StemDiameter)
Dm = StemDiameter_mm/1000
cukPa = mean(AvgShear)
PlateDiameter_mm = mean(PlateDiameter)
Dum = PlateDiameter_mm/1000
Aam2 = (pi/4)*((Dum.^2)-(Dm.^2)); %projected area of the bulb
em = 0.17 %the eccentricity of the lateral load above ground level.
Kp = (tand(45+(phi/2))).^2  %coefficient of passive earth pressure
gamma = 12 %kN/m3 unit weight of soil
Lim = 0.001 %location of the bulb below ground level
Lbm = Lm %location of the bottom of the bulb below ground level
n = 1
Nq = exp((pi).*tand(phi)).*(tand(45+(phi./2))).^2 %bearing capacity factors,
functions of phi
Nc = (Nq-1).*(1./tand(phi))
Ny = 2.*(Nq+1).*(tand(phi))
xm=0
for i = 1:size(phi,2)
    C1 = (0.75*Lm.^2*em)+(0.5*Lm.^3)
    Aam2 = (pi/4)*((Dum.^2)-(Dm.^2)) %projected area of the bulb
    A2 = (Dum.^3/12)-(Dm.^3/12) %coefficient representing the lever arm
between the centres of gravity of bearing and uplift forces and the pile
    C2 = ((Aam2*tand(phi(i)))./(Dm*Kp)).*Lim.*(em+Lim)
    C3 = ((Nq./Dm.*Kp).*A2.*Lim)+(n.*A2.*(Ny./Kp))
    C = C1+C2+C3
    %find the value of x from the cubic polynomial
    %when C = 1
```

```
    %then x = a, b, c
    %0 = (xm^3)+((xm^2)*(1.5*em))-C
    a = 1
    b = 1.5*em
    c = 0

    for j = 1:size(C,1)
        p = [a b c -C(j)]; % creating the polynomial
        r = roots(p); %solving for roots
        rr=real(r); %getting real answers
        xm(j,i)=rr(3);
    end
end
[xm Lm]
% Passive Resistance on the uniform shaft of pile
RpkN = 3*Kp*gamma.*Dm.*((xm.^2)-(0.5*Lim.^2))
A3kNm = Kp*gamma.*Dm.*((2*xm.^3)-Lm.^3)
A3Nm = A3kNm*1000
% Additional Resistance on the Surface of Bulb
RstopkN = Aam2*(gamma*tand(delta)).*Lim
RsbottomkN = Aam2*(gamma*tand(delta)).*(Lim+Lbm)
RskN = Aam2*(gamma*tand(delta)).*(2*Lim+Lbm) %+
Aam2*(gamma*tand(delta)).*(Lim+Lbm)
MRskNm = RskN.*Lm
MRsNm = MRskNm*1000
Hur = A3Nm + MRsNm
%[MaxResistance A3Nm MRsNm Hur]
```

Varying phi for Phi-Soils

```
phi = 34.37
phi = [0.6*phi 0.7*phi 0.8*phi 0.9*phi phi]
delta = phi
RootLength_mm = mean(RootLength)
Lm = RootLength_mm/1000
StemDiameter_mm =mean(StemDiameter)
Dm = StemDiameter_mm/1000
cukPa = mean(AvgShear)
PlateDiameter_mm = mean(PlateDiameter)
Dum = PlateDiameter_mm/1000
Aam2 = (pi/4)*((Dum.^2)-(Dm.^2)); %projected area of the bulb
em = 0.17 %the eccentricity of the lateral load above ground level.
Kp = (tand(45+(phi/2))).^2  %coefficient of passive earth pressure
gamma = 12 %kN/m3 unit weight of soil
Lim = 0.001 %location of the bulb below ground level
Lbm = Lm %location of the bottom of the bulb below ground level
n = 1
Nq = exp((pi).*tand(phi)).*(tand(45+(phi./2))).^2 %bearing capacity factors,
functions of phi
Nc = (Nq-1).*(1./tand(phi))
Ny = 2.*(Nq+1).*(tand(phi))
xm=0
```

```
for i = 1:size(phi,2)
    C1 = (0.75*Lm.^2*em)+(0.5*Lm.^3)
    Aam2 = (pi/4)*((Dum.^2)-(Dm.^2)) %projected area of the bulb
    A2 = (Dum.^3/12)-(Dm.^3/12) %coefficient representing the lever arm
between the centres of gravity of bearing and uplift forces and the pile
    C2 = ((Aam2*tand(phi(i)))./(Dm*Kp)).*Lim.*(em+Lim)
    C3 = ((Nq./Dm.*Kp).*A2.*Lim)+(n.*A2.*(Ny./Kp))
    C = C1+C2+C3
    %find the value of x from the cubic polynomial
    %when C = 1
    %then x = a, b, c
    %0 = (xm^3)+((xm^2)*(1.5*em))-C
    a = 1
    b = 1.5*em
    c = 0

    for j = 1:size(C,1)
        p = [a b c -C(j)]; % creating the polynomial
        r = roots(p); %solving for roots
        rr=real(r); %getting real answers
        xm(j,i)=rr(3);
    end
end
[xm Lm]
% Passive Resistance on the uniform shaft of pile
RpkN = 3*Kp*gamma.*Dm.*((xm.^2)-(0.5*Lim.^2))
A3kNm = Kp*gamma.*Dm.*((2*xm.^3)-Lm.^3)
A3Nm = A3kNm*1000
% Additional Resistance on the Surface of Bulb
RstopkN = Aam2*(gamma*tand(delta)).*Lim
RsbottomkN = Aam2*(gamma*tand(delta)).*(Lim+Lbm)
RskN = Aam2*(gamma*tand(delta)).*(2*Lim+Lbm) %+
Aam2*(gamma*tand(delta)).*(Lim+Lbm)
MRskNm = RskN.*Lm
MRsNm = MRskNm*1000
Hur = A3Nm + MRsNm
%[MaxResistance A3Nm MRsNm Hur]
```

Varying the Length of Root system for C-Soils

```
RootLength_mm = mean(RootLength)
Lm = RootLength_mm/1000
Lm = [Lm*0.5 Lm*0.75 Lm Lm*1.25 Lm*1.5]
PlateDiameter_mm = mean(PlateDiameter)
Dum = PlateDiameter_mm/1000
Aam2 = (pi/4)*((Dum.^2)-(Dm.^2)); %projected area of the bulb
StemDiameter_mm = mean(StemDiameter)
Dm = StemDiameter_mm/1000
cukPa = mean(AvgShear)
em = 0.17 %the eccentricity of the lateral load above ground level.
alphah = 0.06 %adhesion factor in the horizontal direction (can be taken as
40% of the adhesion factor in the vertical direction for pile in c-soils)
```

```
theta1 = mean(Angle)
xm = 0
for i = 1:size(Lm,2)
    C1 = Lm(i)*em + 0.5*Lm(i).^2
    C2 = 2*(Aam2./Dm).*alphah.*0.001
    C = C1+C2
    a = 1
    b = 2*em
    %Solving the polynomial using the roots function in matlab
    for j = 1:size(C,1)
        p = [a b -C(j)]; % creating the polynomial
        r = roots(p); %solving for roots
        rr=real(r); %getting real answers
        xm(j,i)=rr(2); %creating the vector for the point of rotation one
loop at a time using the second (positive) answer from the roots
    end
end
%[xm Lm xm.^2] %checking x against L and x^2
% Passive Resistance on the Uniform Shaft of the Pile
RpkN = cukPa.*Dm.*((2.*xm)-Lm)
A3kNm = cukPa.*Dm.*((xm.^2)-(0.5*(Lm.^2)))
A3Nm = A3kNm*1000
% Additional Resistance on the Surface of Bulb
RskN = 2*(Aam2.*alphah.*cukPa) %+ Aam2.*alphah.*cukPa
MRskNm = RskN.*Lm
MRsNm = MRskNm*1000
FinalMomentNm = A3Nm + MRsNm %possibly multiply A3 by -1
%[MaxResistance A3Nm MRsNm FinalMomentNm]
%[MaxResistance FinalMomentNm]
```

Varying the Length of Root system for Phi-Soils

```
RootLength_mm = mean(RootLength)
Lm = RootLength_mm/1000
Lm = [Lm*0.5 Lm*0.75 Lm Lm*1.25 Lm*1.5]
PlateDiameter_mm = mean(PlateDiameter)
Dum = PlateDiameter_mm/1000
Aam2 = (pi/4)*((Dum.^2)-(Dm.^2)); %projected area of the bulb
StemDiameter_mm = mean(StemDiameter)
Dm = StemDiameter_mm/1000
cukPa = mean(AvgShear)
phi = 34.37
em = 0.17 %the eccentricity of the lateral load above ground level.
Kp = (tand(45+(phi/2))).^2  %coefficient of passive earth pressure
gamma = 12 %kN/m3 unit weight of soil
Lim = 0.001 %location of the bulb below ground level
Lbm = Lm %location of the bottom of the bulb below ground level
delta = phi %angle of wall friction equivalent to phi for phi-soils
n = 1
Nq = exp((pi)*tand(phi))*(tand(45+(phi/2)))^2 %bearing capacity factors,
functions of phi
Nc = (Nq-1)*(1/tand(phi))
```

```matlab
Ny = 2*(Nq+1)*(tand(phi))
xm=0
for i = 1:size(Lm,2)
    C1 = (0.75*Lm(i).^2*em)+(0.5*Lm(i).^3)
    Aam2 = (pi/4)*((Dum.^2)-(Dm.^2)) %projected area of the bulb
    A2 = (Dum.^3/12)-(Dm.^3/12) %coefficient representing the lever arm
between the centres of gravity of bearing and uplift forces and the pile
    C2 = ((Aam2*tand(phi))./(Dm*Kp)).*Lim.*(em+Lim)
    C3 = ((Nq./Dm.*Kp).*A2.*Lim)+(n.*A2.*(Ny./Kp))
    C = C1+C2+C3
    %find the value of x from the cubic polynomial
    %when C = 1
    %then x = a, b, c
    %0 = (xm^3)+((xm^2)*(1.5*em))-C
    a = 1
    b = 1.5*em
    c = 0

    for j = 1:size(C,1)
        p = [a b c -C(j)]; % creating the polynomial
        r = roots(p); %solving for roots
        rr=real(r); %getting real answers
        xm(j,i)=rr(3);
    end
end
[xm Lm]
% Passive Resistance on the uniform shaft of pile
RpkN = 3*Kp*gamma.*Dm.*((xm.^2)-(0.5*Lim.^2))
A3kNm = Kp*gamma.*Dm.*((2*xm.^3)-Lm.^3)
A3Nm = A3kNm*1000
% Additional Resistance on the Surface of Bulb
RstopkN = Aam2*(gamma*tand(delta)).*Lim
RsbottomkN = Aam2*(gamma*tand(delta)).*(Lim+Lbm)
RskN = Aam2*(gamma*tand(delta)).*(2*Lim+Lbm) %+
Aam2*(gamma*tand(delta)).*(Lim+Lbm)
MRskNm2 = RskN2.*Lm
MRsNm2 = MRskNm2*1000
Hur = A3Nm + MRsNm
%[MaxResistance A3Nm MRsNm Hur]
```

Varying the Stem Diameter for C-Soils

```matlab
StemDiameter_mm = mean(StemDiameter)
Dm = StemDiameter_mm/1000
Dm = [Dm*0.5 Dm*0.75 Dm Dm*1.25 Dm*1.5]
RootLength_mm = mean(RootLength)
Lm = RootLength_mm/1000
PlateDiameter_mm = mean(PlateDiameter)
Dum = PlateDiameter_mm/1000
Aam2 = (pi/4)*((Dum.^2)-(Dm.^2)); %projected area of the bulb
cukPa = mean(AvgShear)
em = 0.17 %the eccentricity of the lateral load above ground level.
```

330

```matlab
alphah = 0.06 %adhesion factor in the horizontal direction (can be taken as
40% of the adhesion factor in the vertical direction for pile in c-soils)
theta1 = mean(Angle)
for i = 1:size(Dm,2)
    C1 = Lm*em + 0.5*Lm.^2
    C2 = 2*(Aam2./Dm(i)).*alphah.*0.001
    C = C1+C2
    a = 1
    b = 2*em
    %Solving the polynomial using the roots function in matlab
    for j = 1:size(C,1)
        p = [a b -C(j)]; % creating the polynomial
        r = roots(p); %solving for roots
        rr=real(r); %getting real answers
        xm(j,i)=rr(2); %creating the vector for the point of rotation one
loop at a time using the second (positive) answer from the roots
    end
end
[xm] %checking x against L and x^2
% Passive Resistance on the Uniform Shaft of the Pile
RpkN = cukPa.*Dm.*((2.*xm)-Lm)
A3kNm = cukPa.*Dm.*((xm.^2)-(0.5*(Lm.^2)))
A3Nm = A3kNm*1000
% Additional Resistance on the Surface of Bulb
RskN = 2*(Aam2.*alphah.*cukPa) %+ Aam2.*alphah.*cukPa
MRskNm = RskN.*Lm
MRsNm = MRskNm*1000
FinalMomentNm = A3Nm + MRsNm %possibly multiply A3 by -1
%[MaxResistance A3Nm MRsNm FinalMomentNm]
%[MaxResistance FinalMomentNm]
```

Varying the Stem Diameter for Phi-Soils

```matlab
StemDiameter_mm = mean(StemDiameter)
Dm = StemDiameter_mm/1000
Dm = [Dm*0.5 Dm*0.75 Dm Dm*1.25 Dm*1.5]
RootLength_mm = mean(RootLength)
Lm = RootLength_mm/1000
PlateDiameter_mm = mean(PlateDiameter)
Dum = PlateDiameter_mm/1000
Aam2 = (pi/4)*((Dum.^2)-(Dm.^2)); %projected area of the bulb
phi = 34.37
cukPa = mean(AvgShear)
em = 0.17 %the eccentricity of the lateral load above ground level.
Kp = (tand(45+(phi/2))).^2  %coefficient of passive earth pressure
gamma = 12 %kN/m3 unit weight of soil
Lim = 0.001 %location of the bulb below ground level
Lbm = Lm %location of the bottom of the bulb below ground level
delta = phi %angle of wall friction equivalent to phi for phi-soils
n = 1
Nq = exp((pi)*tand(phi))*(tand(45+(phi/2)))^2 %bearing capacity factors,
functions of phi
```

```matlab
Nc = (Nq-1)*(1/tand(phi))
Ny = 2*(Nq+1)*(tand(phi))
xm=0
for i = 1:size(Dm,2)
    C1 = (0.75*Lm.^2*em)+(0.5*Lm.^3)
    Aam2 = (pi/4)*((Dum.^2)-(Dm(i).^2)) %projected area of the bulb
    A2 = (Dum.^3/12)-(Dm(i).^3/12) %coefficient representing the lever arm
between the centres of gravity of bearing and uplift forces and the pile
    C2 = ((Aam2*tand(phi))./(Dm(i)*Kp)).*Lim.*(em+Lim)
    C3 = ((Nq./Dm(i).*Kp).*A2.*Lim)+(n.*A2.*(Ny./Kp))
    C = C1+C2+C3
    %find the value of x from the cubic polynomial
    %when C = 1
    %then x = a, b, c
    %0 = (xm^3)+((xm^2)*(1.5*em))-C
    a = 1
    b = 1.5*em
    c = 0

    for j = 1:size(C,1)
        p = [a b c -C(j)]; % creating the polynomial
        r = roots(p); %solving for roots
        rr=real(r); %getting real answers
        xm(j,i)=rr(3);
    end
end
[xm Lm]
% Passive Resistance on the uniform shaft of pile
RpkN = 3*Kp*gamma.*Dm.*((xm.^2)-(0.5*Lim.^2))
A3kNm = Kp*gamma.*Dm.*((2*xm.^3)-Lm.^3)
A3Nm = A3kNm*1000
% Additional Resistance on the Surface of Bulb
RstopkN = Aam2*(gamma*tand(delta)).*Lim
RsbottomkN = Aam2*(gamma*tand(delta)).*(Lim+Lbm)
RskN = Aam2*(gamma*tand(delta)).*(2*Lim+Lbm) %+
Aam2*(gamma*tand(delta)).*(Lim+Lbm)
MRskNm2 = RskN2.*Lm
MRsNm2 = MRskNm2*1000
Hur = A3Nm + MRsNm
%[MaxResistance A3Nm MRsNm Hur]
```

Varying the cu value

```matlab
StemDiameter_mm = mean(StemDiameter)
Dm = StemDiameter_mm/1000
RootLength_mm = mean(RootLength)
Lm = RootLength_mm/1000
PlateDiameter_mm = mean(PlateDiameter)
Dum = PlateDiameter_mm/1000
Aam2 = (pi/4)*((Dum.^2)-(Dm.^2)); %projected area of the bulb
cukPa = mean(AvgShear)
cukPa = [0.8*cukPa 0.9*cukPa cukPa 1.1*cukPa 1.2*cukPa]
```

```matlab
em = 0.17 %the eccentricity of the lateral load above ground level.
alphah = 0.06 %adhesion factor in the horizontal direction (can be taken as
40% of the adhesion factor in the vertical direction for pile in c-soils)
theta1 = mean(Angle)
xm = 0
C1 = Lm*em + 0.5*Lm.^2
C2 = 2*(Aam2./Dm).*alphah.*0.001
C = C1+C2
a = 1
b = 2*em
%Solving the polynomial using the roots function in matlab
for i = 1:size(C,1)
    p = [a b -C(i)]; % creating the polynomial
    r = roots(p); %solving for roots
    rr=real(r); %getting real answers
    xm(i,1)=rr(2); %creating the vector for the point of rotation one loop
at a time using the second (positive) answer from the roots
end
[xm Lm xm.^2] %checking x against L and x^2
% Passive Resistance on the Uniform Shaft of the Pile
RpkN = cukPa.*Dm.*((2.*xm)-Lm)
A3kNm = cukPa.*Dm.*((xm.^2)-(0.5*(Lm.^2)))
A3Nm = A3kNm*1000
% Additional Resistance on the Surface of Bulb
RskN = 2*(Aam2.*alphah.*cukPa) %+ Aam2.*alphah.*cukPa
MRskNm = RskN.*Lm
MRsNm = MRskNm*1000
FinalMomentNm = A3Nm + MRsNm %possibly multiply A3 by -1
%[MaxResistance A3Nm MRsNm FinalMomentNm]
%[MaxResistance FinalMomentNm]
```

Varying the gamma value phi-soils

```matlab
StemDiameter_mm = mean(StemDiameter)
Dm = StemDiameter_mm/1000
RootLength_mm = mean(RootLength)
Lm = RootLength_mm/1000
PlateDiameter_mm = mean(PlateDiameter)
Dum = PlateDiameter_mm/1000
Aam2 = (pi/4)*((Dum.^2)-(Dm.^2)); %projected area of the bulb
cukPa = mean(AvgShear)
cukPa = [0.8*cukPa 0.9*cukPa cukPa 1.1*cukPa 1.2*cukPa]
em = 0.17 %the eccentricity of the lateral load above ground level.
alphah = 0.28 %adhesion factor in the horizontal direction (can be taken as
40% of the adhesion factor in the vertical direction for pile in c-soils)
theta1 = mean(Angle)
phi = 34.37
xm = 0
Kp = (tand(45+(phi/2))).^2  %coefficient of passive earth pressure
gamma = [0.8*gamma 0.9*gamma gamma 1.1*gamma 1.2*gamma] %kN/m3 unit weight
of soil
Lim = 0.001 %location of the bulb below ground level
```

```matlab
Lbm = Lm %location of the bottom of the bulb below ground level
delta = phi %angle of wall friction equivalent to phi for phi-soils
n = 1
Nq = exp((pi)*tand(phi))*(tand(45+(phi/2)))^2 %bearing capacity factors,
functions of phi
Nc = (Nq-1)*(1/tand(phi))
Ny = 2*(Nq+1)*(tand(phi))
xm=0
for i = 1:size(Dm,2)
    C1 = (0.75*Lm.^2*em)+(0.5*Lm.^3)
    Aam2 = (pi/4)*((Dum.^2)-(Dm(i).^2)) %projected area of the bulb
    A2 = (Dum.^3/12)-(Dm(i).^3/12) %coefficient representing the lever arm
between the centres of gravity of bearing and uplift forces and the pile
    C2 = ((Aam2*tand(phi))./(Dm(i)*Kp)).*Lim.*(em+Lim)
    C3 = ((Nq./Dm(i).*Kp).*A2.*Lim)+(n.*A2.*(Ny./Kp))
    C = C1+C2+C3
    %find the value of x from the cubic polynomial
    %when C = 1
    %then x = a, b, c
    %0 = (xm^3)+((xm^2)*(1.5*em))-C
    a = 1
    b = 1.5*em
    c = 0

    for j = 1:size(C,1)
        p = [a b c -C(j)]; % creating the polynomial
        r = roots(p); %solving for roots
        rr=real(r); %getting real answers
        xm(j,i)=rr(3);
    end
end
[xm Lm]
% Passive Resistance on the uniform shaft of pile
RpkN = 3*Kp*gamma.*Dm.*((xm.^2)-(0.5*Lim.^2))
A3kNm = Kp*gamma.*Dm.*((2*xm.^3)-Lm.^3)
A3Nm = A3kNm*1000
% Additional Resistance on the Surface of Bulb
RstopkN = Aam2*(gamma*tand(delta)).*Lim
RsbottomkN = Aam2*(gamma*tand(delta)).*(Lim+Lbm)
RskN = Aam2*(gamma*tand(delta)).*(2*Lim+Lbm) %+
Aam2*(gamma*tand(delta)).*(Lim+Lbm)
MRskNm = RskN.*Lm
MRsNm = MRskNm*1000
Hur = A3Nm + MRsNm
%[MaxResistance A3Nm MRsNm Hur]
```

Varying the depth to the bulb Li value (0.001m)

```matlab
StemDiameter_mm = mean(StemDiameter)
Dm = StemDiameter_mm/1000
RootLength_mm = mean(RootLength)
Lm = RootLength_mm/1000
```

```
PlateDiameter_mm = mean(PlateDiameter)
Dum = PlateDiameter_mm/1000
Aam2 = (pi/4)*((Dum.^2)-(Dm.^2)); %projected area of the bulb
cukPa = mean(AvgShear)
em = 0.17 %the eccentricity of the lateral load above ground level.
alphah = 0.06 %adhesion factor in the horizontal direction (can be taken as
40% of the adhesion factor in the vertical direction for pile in c-soils)
theta1 = mean(Angle)
Lmi = 0.001
Lmi = [Lmi Lmi*1.1 Lmi*1.2 Lmi*1.3 Lmi*1.4]
xm = 0
for i = 1:size(Lmi,2)
    C1 = Lm*em + 0.5*Lm.^2
    C2 = 2*(Aam2./Dm).*alphah.*Lmi(i)
    C = C1+C2
    a = 1
    b = 2*em
    %Solving the polynomial using the roots function in matlab
    for j = 1:size(C,1)
        p = [a b -C(j)]; % creating the polynomial
        r = roots(p); %solving for roots
        rr=real(r); %getting real answers
        xm(j,i)=rr(2); %creating the vector for the point of rotation one
loop at a time using the second (positive) answer from the roots
    end
end
[xm Lm xm.^2] %checking x against L and x^2
% Passive Resistance on the Uniform Shaft of the Pile
RpkN = cukPa.*Dm.*((2.*xm)-Lm)
A3kNm = cukPa.*Dm.*((xm.^2)-(0.5*(Lm.^2)))
A3Nm = A3kNm*1000
% Additional Resistance on the Surface of Bulb
RskN = 2*(Aam2.*alphah.*cukPa) %+ Aam2.*alphah.*cukPa
MRskNm = RskN.*Lm
MRsNm = MRskNm*1000
FinalMomentNm = A3Nm + MRsNm %possibly multiply A3 by -1
%[MaxResistance A3Nm MRsNm FinalMomentNm]
%[MaxResistance FinalMomentNm]
```

Varying the depth to the bulb Li value (0.001m) phi-soils

```
StemDiameter_mm = mean(StemDiameter)
Dm = StemDiameter_mm/1000
RootLength_mm = mean(RootLength)
Lm = RootLength_mm/1000
PlateDiameter_mm = mean(PlateDiameter)
Dum = PlateDiameter_mm/1000
Aam2 = (pi/4)*((Dum.^2)-(Dm.^2)); %projected area of the bulb
cukPa = mean(AvgShear)
em = 0.17; %the eccentricity of the lateral load above ground level.
alphah = 0.28; %adhesion factor in the horizontal direction (can be taken as
40% of the adhesion factor in the vertical direction for pile in c-soils)
```

```
theta1 = mean(Angle);
Lmi = 0.001;
Lim = [Lim Lim*1.1 Lim*1.2 Lim*1.3 Lim*1.4] %location of the bulb below
ground level
phi = 34.37;
xm = 0;
Kp = (tand(45+(phi/2))).^2;  %coefficient of passive earth pressure
gamma = 12; %kN/m3 unit weight of soil
Lbm = Lm; %location of the bottom of the bulb below ground level
delta = phi; %angle of wall friction equivalent to phi for phi-soils
n = 1;
Nq = exp((pi)*tand(phi))*(tand(45+(phi/2)))^2; %bearing capacity factors,
functions of phi
Nc = (Nq-1)*(1/tand(phi)) ;
Ny = 2*(Nq+1)*(tand(phi));
xm=0;
for i = 1:size(Lim,2)
    C1 = (0.75*Lm.^2*em)+(0.5*Lm.^3);
    Aam2 = (pi/4)*((Dum.^2)-(Dm.^2)); %projected area of the bulb
    A2 = (Dum.^3/12)-(Dm.^3/12); %coefficient representing the lever arm
between the centres of gravity of bearing and uplift forces and the pile
    C2 = ((Aam2*tand(phi))./(Dm*Kp)).*Lim(i).*(em+Lim(i));
    C3 = ((Nq./Dm.*Kp).*A2.*Lim(i))+(n.*A2.*(Ny./Kp));
    C = C1+C2+C3;
    %find the value of x from the cubic polynomial
    %when C = 1
    %then x = a, b, c
    %0 = (xm^3)+((xm^2)*(1.5*em))-C
    a = 1;
    b = 1.5*em;
    c = 0;

    for j = 1:size(C,1)
        p = [a b c -C(j)]; % creating the polynomial
        r = roots(p); %solving for roots
        rr=real(r); %getting real answers
        xm(j,i)=rr(3);
    end
end
[xm Lm]
% Passive Resistance on the uniform shaft of pile
RpkN = 3*Kp*gamma.*Dm.*((xm.^2)-(0.5*Lim.^2))
A3kNm = Kp*gamma.*Dm.*((2*xm.^3)-Lm.^3)
A3Nm = A3kNm*1000
% Additional Resistance on the Surface of Bulb
RstopkN = Aam2*(gamma*tand(delta)).*Lim
RsbottomkN = Aam2*(gamma*tand(delta)).*(Lim+Lbm)
RskN = Aam2*(gamma*tand(delta)).*(2*Lim+Lbm) %+

MRskNm2 = RskN2.*Lm
MRsNm2 = MRskNm2*1000
Hur = A3Nm + MRsNm
```

O.1 Matlab code for the validation of the final models, for wheat.

Applying the model to new dataset from 2018 using old apparatus

```matlab
%% Import data from spreadsheet
% Script for importing data from the following spreadsheet:
%
%    Workbook: M:\4th Year\Lab_fieldtests.xlsx
%    Worksheet: WheatOld
%
% To extend the code for use with different selected data or a different
% spreadsheet, generate a function instead of a script.
% Auto-generated by MATLAB on 2019/01/30 20:44:10
%% Import the data
[~, ~, raw0_0] = xlsread('M:\4th
Year\Lab_fieldtests.xlsx','WheatOld','B2:B32');
[~, ~, raw0_1] = xlsread('M:\4th
Year\Lab_fieldtests.xlsx','WheatOld','G2:G32');
[~, ~, raw0_2] = xlsread('M:\4th
Year\Lab_fieldtests.xlsx','WheatOld','L2:L32');
[~, ~, raw0_3] = xlsread('M:\4th
Year\Lab_fieldtests.xlsx','WheatOld','N2:N32');
[~, ~, raw0_4] = xlsread('M:\4th
Year\Lab_fieldtests.xlsx','WheatOld','P2:P32');
raw = [raw0_0,raw0_1,raw0_2,raw0_3,raw0_4];
raw(cellfun(@(x) ~isempty(x) && isnumeric(x) && isnan(x),raw)) = {''};
%% Replace non-numeric cells with NaN
R = cellfun(@(x) ~isnumeric(x) && ~islogical(x),raw); % Find non-numeric
cells
raw(R) = {NaN}; % Replace non-numeric cells
%% Create output variable
data = reshape([raw{:}],size(raw));
%% Allocate imported array to column variable names
MaxRes = data(:,1);
AverageShearStrength = data(:,2);
StemDiameter1 = data(:,3);
RootLength1 = data(:,4);
RootWidth = data(:,5);
%% Clear temporary variables
clearvars data raw raw0_0 raw0_1 raw0_2 raw0_3 raw0_4 R;

RootLength_mm = RootLength1
Lm = RootLength_mm/1000
StemDiameter_mm = StemDiameter1
Dm = StemDiameter_mm/1000
cukPa = AverageShearStrength
PlateDiameter_mm = RootWidth
Dum = PlateDiameter_mm/1000
theta1 = mean(Angle)
```

```matlab
em = 0.17 %the eccentricity of the lateral load above ground level.
Aam2 = (pi/4)*((Dum.^2)-(Dm.^2)) %projected area of the bulb
alphah = 0.06 %adhesion factor in the horizontal direction (can be taken as
40% of the adhesion factor in the vertical direction for pile in c-soils)
xm = 0
C1 = Lm.*em + 0.5*Lm.^2
C2 = 2.*(Aam2./Dm).*alphah.*0.001
A2 = ((Dum.^3/12)-(Dm.^3/12)) %coefficient representing the lever arm
between the centres of gravity of bearing and uplift forces and the pile
C = C1+C2
a = 1
b = 2*em
%Solving the polynomial using the roots function in matlab
for i = 1:size(C,1)
    p = [a b -C(i)]; % creating the polynomial
    r = roots(p); %solving for roots
    rr = real(r); %getting real answers
    xm(i,1)=rr(2); %creating the vector for the point of rotation one loop
at a time using the second (positive) answer from the roots
end
[xm Lm] %checking x against L
% Passive Resistance on the Uniform Shaft of the Pile
RpkN = cukPa.*Dm.*((2.*xm)-Lm)
A3kNm = cukPa.*Dm.*((xm.^2)-(0.5*(Lm.^2)))
A3Nm = A3kNm*1000
% Additional Resistance on the Surface of Bulb
RstopkN = Aam2.*alphah.*cukPa
RsbottomkN = Aam2.*alphah.*cukPa
RskN = 2*(Aam2.*alphah.*cukPa) %+ Aam2.*alphah.*cukPa
MRskNm = RskN.*Lm
MRsNm = MRskNm*1000
FinalMomentNm = A3Nm + MRsNm %possibly multiply A3 by -1
FinalMomentNm = FinalMomentNm(1:30,1)
% FinalMomentNm2 = abs(A3Nm) + MRsNm
% FinalMomentNm2 = FinalMomentNm2(1:30,1)
maxRes = MaxRes(1:30,1)

RMSE = sqrt(mean((maxRes - FinalMomentNm).^2))
NRMSE = RMSE/(max(maxRes) - min(maxRes))
CVRMSE = RMSE/mean(maxRes)
Result = [RMSE NRMSE CVRMSE]'
```

Phi-Soils including the bearing and uplift resistances

```matlab
RootLength_mm = RootLength1
Lm = RootLength_mm/1000
StemDiameter_mm = StemDiameter1
Dm = StemDiameter_mm/1000
cukPa = AverageShearStrength
PlateDiameter_mm = RootWidth
Dum = PlateDiameter_mm/1000
theta1 = mean(Angle)
```

```matlab
phi = 34.37 %angle of internal friction
Kp = (tand(45+(phi/2)))^2  %coefficient of passive earth pressure
gamma = 12 %kN/m3 unit weight of soil
Lim = 0.001 %location of the bulb below ground level
Lbm = Lm %location of the bottom of the bulb below ground level
delta = phi %angle of wall friction equivalent to phi for phi-soils
n = 1
Nq = exp((pi)*tand(phi))*(tand(45+(phi/2)))^2 %bearing capacity factors,
functions of phi
Nc = (Nq-1)*(1/tand(phi))
Ny = 2*(Nq+1)*(tand(phi))
em = 0.17
C1 = (0.75*Lm.^2*em)+(0.5*Lm.^3)
C2 = ((Aam2.*tand(phi))./(Dm.*Kp)).*Lim.*(em+Lim)
C3 = ((Nq/Dm*Kp)*A2*Lim)+(n*A2*(Ny/Kp))
C = C1+C2+C3
%find the value of x from the cubic polynomial
%when C = 1
%then x = a, b, c
%0 = (xm^3)+((xm^2)*(1.5*em))-C
a = 1
b = 1.5*em
c = 0
for i = 1:size(C,1)
    p = [a b c -C(i)]; % creating the polynomial
    r = roots(p); %solving for roots
    rr=real(r); %getting real answers
    xm(i,1)=rr(3);
end
[xm Lm]
% Passive Resistance on the uniform shaft of pile
RpkN = 3*Kp*gamma.*Dm.*((xm.^2)-(0.5*Lim.^2))
A3kNm = Kp*gamma.*Dm.*((2*xm.^3)-Lm.^3)
A3Nm = A3kNm*1000
% Additional Resistance on the Surface of Bulb
RstopkN = Aam2*(gamma*tand(delta)).*Lim
RsbottomkN = Aam2*(gamma*tand(delta)).*(Lim+Lbm)
RskN = Aam2*(gamma*tand(delta)).*(2*Lim+Lbm)
MRskNm = RskN.*Lm
MRsNm = MRskNm*1000
Hur = A3Nm + MRsNm

RMSE = sqrt(mean((MaxRes - Hur).^2))
NRMSE = RMSE/(max(MaxRes) - min(MaxRes))
CVRMSE = RMSE/mean(MaxRes)
Result = [RMSE NRMSE CVRMSE]'
```

Applying the model to new dataset from 2018 using new apparatus

```matlab
%% Import data from spreadsheet
% Script for importing data from the following spreadsheet:
%
```

```matlab
%    Workbook: M:\4th Year\Lab_fieldtests.xlsx
%    Worksheet: WheatNew
%
% To extend the code for use with different selected data or a different
% spreadsheet, generate a function instead of a script.
% Auto-generated by MATLAB on 2019/01/30 20:58:26
%% Import the data
[~, ~, raw0_0] = xlsread('M:\4th
Year\Lab_fieldtests.xlsx','WheatNew','B2:B24');
[~, ~, raw0_1] = xlsread('M:\4th
Year\Lab_fieldtests.xlsx','WheatNew','D2:G24');
[~, ~, raw0_2] = xlsread('M:\4th
Year\Lab_fieldtests.xlsx','WheatNew','AE2:AE24');
raw = [raw0_0,raw0_1,raw0_2];
%% Create output variable
data = reshape([raw{:}],size(raw));
%% Allocate imported array to column variable names
MaxResNew = data(:,1);
StemDiameter2 = data(:,2);
RootWidth1 = data(:,3);
RootWidth2 = data(:,4);
RootWidth3 = (RootWidth1 + RootWidth2)/2
RootLength2 = data(:,5);
ShearStrength = data(:,6);
%% Clear temporary variables
clearvars data raw raw0_0 raw0_1 raw0_2;

RootLength_mm = RootLength2
Lm = RootLength_mm/1000
StemDiameter_mm = StemDiameter2
Dm = StemDiameter_mm/1000
cukPa = ShearStrength
PlateDiameter_mm = RootWidth3
Dum = PlateDiameter_mm/1000
theta1 = mean(Angle)
em = 0.17 %the eccentricity of the lateral load above ground level.
Aam2 = (pi/4)*((Dum.^2)-(Dm.^2)) %projected area of the bulb
alphah = 0.06 %adhesion factor in the horizontal direction (can be taken as
40% of the adhesion factor in the vertical direction for pile in c-soils)
xm = 0
C1 = Lm.*em + 0.5*Lm.^2
C2 = 2.*(Aam2./Dm).*alphah.*0.001
A2 =  ((Dum.^3/12)-(Dm.^3/12)) %coefficient representing the lever arm
between the centres of gravity of bearing and uplift forces and the pile
C = C1+C2
a = 1
b = 2*em
%Solving the polynomial using the roots function in matlab
for i = 1:size(C,1)
    p = [a b -C(i)]; % creating the polynomial
    r = roots(p); %solving for roots
    rr = real(r); %getting real answers
```

```
    xm(i,1)=rr(2); %creating the vector for the point of rotation one loop
at a time using the second (positive) answer from the roots
end
[xm Lm] %checking x against L
% Passive Resistance on the Uniform Shaft of the Pile
RpkN = cukPa.*Dm.*((2.*xm)-Lm)
A3kNm = cukPa.*Dm.*((xm.^2)-(0.5*(Lm.^2)))
A3Nm = A3kNm*1000
% Additional Resistance on the Surface of Bulb
RstopkN = Aam2.*alphah.*cukPa
RsbottomkN = Aam2.*alphah.*cukPa
RskN = 2*(Aam2.*alphah.*cukPa) %+ Aam2.*alphah.*cukPa
MRskNm = RskN.*Lm
MRsNm = MRskNm*1000
FinalMomentNm = A3Nm + MRsNm %possibly multiply A3 by -1

RMSE = sqrt(mean((MaxResNew - FinalMomentNm).^2))
NRMSE = RMSE/(max(MaxResNew) - min(MaxResNew))
CVRMSE = RMSE/mean(MaxResNew)
Result = [RMSE NRMSE CVRMSE]'
```

Phi-Soils including the bearing and uplift resistances

```
RootLength_mm = RootLength2
Lm = RootLength_mm/1000
StemDiameter_mm = StemDiameter2
Dm = StemDiameter_mm/1000
cukPa = ShearStrength
PlateDiameter_mm = RootWidth3
Dum = PlateDiameter_mm/1000
theta1 = mean(Angle)
phi = 34.37 %angle of internal friction
Kp = (tand(45+(phi/2)))^2  %coefficient of passive earth pressure
gamma = 12 %kN/m3 unit weight of soil
Lim = 0.001 %location of the bulb below ground level
Lbm = Lm %location of the bottom of the bulb below ground level
delta = phi %angle of wall friction equivalent to phi for phi-soils
n = 1
Nq = exp((pi)*tand(phi))*(tand(45+(phi/2)))^2 %bearing capacity factors,
functions of phi
Nc = (Nq-1)*(1/tand(phi))
Ny = 2*(Nq+1)*(tand(phi))
em = 0.17 %the eccentricity of the lateral load above ground level.
C1 = (0.75*Lm.^2*em)+(0.5*Lm.^3)
C2 = ((Aam2.*tand(phi))./(Dm.*Kp)).*Lim.*(em+Lim)
C3 = ((Nq/Dm*Kp)*A2*Lim)+(n*A2*(Ny/Kp))
C = C1+C2+C3
%find the value of x from the cubic polynomial
%when C = 1
%then x = a, b, c
%0 = (xm^3)+((xm^2)*(1.5*em))-C
a = 1
```

```
b = 1.5*em
c = 0
for i = 1:size(C,1)
    p = [a b c -C(i)]; % creating the polynomial
    r = roots(p); %solving for roots
    rr=real(r); %getting real answers
    xm(i,1)=rr(3);
end
[xm Lm]
% Passive Resistance on the uniform shaft of pile
RpkN = 3*Kp*gamma.*Dm.*((xm.^2)-(0.5*Lim.^2))
A3kNm = Kp*gamma.*Dm.*((2*xm.^3)-Lm.^3)
A3Nm = A3kNm*1000
% Additional Resistance on the Surface of Bulb
RstopkN = Aam2*(gamma*tand(delta)).*Lim
RsbottomkN = Aam2*(gamma*tand(delta)).*(Lim+Lbm)
RskN = Aam2*(gamma*tand(delta)).*(2*Lim+Lbm)
MRskNm = RskN.*Lm
MRsNm = MRskNm*1000
Hur = A3Nm + MRsNm

RMSE = sqrt(mean((MaxResNew - Hur).^2))
NRMSE = RMSE/(max(MaxResNew) - min(MaxResNew))
CVRMSE = RMSE/mean(MaxResNew)
Result = [RMSE NRMSE CVRMSE]'
```

P.1 Matlab code for the flexible under-reamed pile model using with oilseed rape.

Flexible Under-reamed Piles

```
%L/D limiting value which piles behave rigid or flexible
    %Broms(1964) beta/L>2.5 for c-soils
    %Matlock and Reese(1960) Zmax>4.0 for phi-soils
E = 1840 %MPa modulus of elasticity of pile material, taken as 22000MPa for
M20 mix grade concrete
%E from Goodman and Road (2001) table 2
Ist = pi/64*Dm.^4 %moment of inertia of pile shaft with uniform cross-
section
Kh = 320.*cukPa./Dm %kN/m3 modulus of sub-grade reaction value for c-soils=
80-320cu/D per Skempton,(1951)
%Kh2 = 80.*cukPa/Dm
nh = 2600 %modulus of sub-grade reaction variation for phi-soils= 2600-7800
kN/m3 equivalent 7-21t/ft3 per Terzaghi,(1955)
Dr = Dum./Dm
beta = nthroot((Kh.*Dm/E.*Ist),4)
crit = beta.*Lm
if crit >= 2.5
    disp('ok')
elseif crit < 2.5
```

```matlab
    disp('not ok')
end
T = nthroot((E.*Ist/nh),5)
Zmax = Lm./T
if Zmax >= 4.0
    disp('ok')
elseif Zmax < 4.0
    disp('not ok')
end
Iur = (Ist./Lm) %.*(Lm+(Dr.^4.*Lbm))
sigma = 100 %permissable yield stress (stress at which a member is not
expected to fail under the given loading conditions)
%sigma taken from Goodmand and Road (2001) table 2
Myu = 2*sigma*Iur./Dm
Hufl1 = 4.24*sqrt(Myu.*cukPa.*Dm) %c-soils
Hufl2 = 1.50.*nthroot(((Myu.^2).*Kp*gamma.*Dm),3) %phi-soils
Hufl3 = Hufl2.*Lm*1000
RMSE = sqrt(mean((MaxResistance - Hufl3).^2))
NRMSE = RMSE/(max(MaxResistance) - min(MaxResistance))
CVRMSE = RMSE/mean(MaxResistance)
Result = [RMSE NRMSE CVRMSE]'
final = [Hufl1 Hufl2]
```